The role of dietary composition on metabolic health of the gut-liver axis

Aleena Mushtaq, MSc

This thesis is submitted in accordance with the requirements for the degree of Doctor of Philosophy (PhD) to the University of East Anglia, Norwich.

January 30th, 2021

<u>Supervisory team:</u>

Prof Michael Müller

Dr David Vauzour

Abstract

The critical role of a disrupted gut-liver axis in the pathogenesis of many diseases has only recently been accepted. The role of diets in the related bidirectional relationship between the gut, along with its microbiota, and the liver are however poorly defined. Designing an experimental animal model to study the gut-liver axis requires the use of commercial control diets such as chow or purified low-fat (LF) diets. While chow is a whole foods grain-based diet, LF contains high amount of easily accessible refined carbohydrates together with reduced dietary fibre and resembles a low-fat Western style diet. In this thesis, we compared chow and LF diets to characterise their differential effects on the gut-liver axis with focus on the ileum in C57BL/6J mice. For the first time, we showed that the LF diet significantly increased hepatic triglycerides, ileal bile acid levels and altered the ileal microbiota compared to chow. Long-term consumption of the LF diet led to further increased hepatic triglycerides, reduced ileal expression of antimicrobial peptides and cell cycle related genes. Next, we investigated strategies to prevent the LF induced phenotype by; 1) reducing the consumption of the LF diet with calorie restriction (CR) and, 2) addition of dietary fibres to the LF diet. We found that CR was successfully able to prevent the pathophysiological effects of the LF diet on the gut-liver axis and led to a distinct ileal microbiota profile. The second prevention strategy of enriching the LF diet with dietary fibres reduced the LF induced accumulation of hepatic triglycerides in mice. Moreover, our results showed differential effects of the structurally distinct dietary fibres on the ileal immune related gene expression. Lastly, we characterised the diet induced changes in genetically identical mice obtained from different vendors, to show differential ileal microbiota and bile acid profiles. Our studies highlight that dietary composition and animal source can affect the ileal microbiota composition and function, and lead to significant phenotype variability. The novel results from this thesis indicate that dietary fibres are essential food components with mode of actions not just in the colon but also in the ileum. Our studies further confirm that even low-fat Western style diets may have a pathophysiological impact on human health if the diet is depleted in essential food components such as dietary fibres.

List of abbreviations

ACACA	Acetyl-CoA Carboxylase
ASBT	Apical sodium dependent bile acid transporter
BA	Bile acid
BSEP	Bile salt export pump
BSH	Bile salt hydrolase
CA	Cholic acid
CDCA	Chenodeoxycholic acid
CLDN3	Claudin 3
CR	Caloric restriction
CRUK	Charles river UK
CYP7A1	Cholesterol 7 alpha-hydroxylase
CYP8B1	Sterol 12-alpha-hydroxylase
DCA	Deoxycholic acid
DF	Dietary fibre
DMU	Disease modelling unit (UEA)
En%	Energy percent
FASN	Fatty Acid Synthase
FGF15/19	Fibroblast growth factor 15/19
FITC	Fluorescein isothiocyanate
FXR	Farnesoid X receptor (NR1H4)
GLUT2/5	Glucose transporter 2/5 (SLC2A2/5)
H&E	Haematoxylin and eosin
HPLC	High-performance liquid chromatograph
IBD	Inflammatory bowel disease
IECs	Intestinal epithelial cells
KHK	Ketohexokinase (fructokinase)
LCA	Lithocholic acid
LC-MS	Liquid chromatography–mass spectrometry

LF	Low-fat
LFCR	Low-fat calorie restriction
LPS	Lipopolysaccharide
MGAM	Maltase-Glucoamylase
MUC2	Mucin 2
NAFLD	Non-alcoholic fatty liver disease
NASH	Non-alcoholic steatohepatitis
OCLN	Occludin
OSTα/β	Organic solute transporter alpha/ beta (SLC51A/B)
PPARα	Peroxisome Proliferator Activated Receptor Alpha
QIIME	Quantitative Insights into Microbial Ecology
Q-PCR	Quantitative polymerase chain reaction
SCFAs	Short chain fatty acid
SHP	Small heterodimer partner (NR0B2)
SIS	Sucrase isomaltase
SREBP1	Sterol Regulatory Element-Binding Protein 1
TCA	Taurocholic acid
TCDCA	Taurochenodeoxycholic acid
TDCA	Taurodeoxycholic acid
TLR4	Toll like receptor 4
TNFα	Tumour necrosis factor alpha
TαMCA	Tauro-α-muricholic acid
TβMCA	Tauro-β-muricholic acid
UDCA	Ursodeoxycholic acid
UEA	University of East Anglia
WUR	Wageningen University and Research
ZO-1 (TJP1)	Zonula occludens 1 (or Tight junction protein 1)
αMCA	α-Muricholic acid
βMCA	β-Muricholic acid

Table of contents

List of figures

Chapter 5

Chapter 6

Chapter 7

List of tables

Chapter 1: General introduction

Our ancestor's diet comprised of whole foods and most of the consumed sugar derived from fruits. At present times, changes in lifestyle, dietary trends like veganism and increased production of ultra-processed foods has meant overconsumption of refined carbohydrates, deficiency of dietary fibres (DF) and essential micronutrients in individuals. These types of foods predispose people to a wide range of chronic illnesses including cardiovascular disease (CVD), non-alcoholic fatty liver disease (NAFLD), diabetes, and cancers of the gastrointestinal tract (O'Keefe et al., 2018). The pathophysiology of these diseases is highly complex and involves several pathways in the gut-liver axis. In this thesis, we compare different dietary interventions to counteract the effects of a highly refined diet on the gut and liver of mice. The aim of our research is to 1) characterise molecular and microbial signatures associated with highly refined diet, 2) explore dietary interventions that may counteract these pathophysiological phenotypes.

1.1 The gut- liver axis

The gut and liver communicate bidirectionally through the biliary tract and portal vein (Fig.1.1). The liver communicates with the intestine by releasing bile acids into the biliary tract. In the gut, host and microbes metabolise endogenous (e.g. bile acids, amino acids) as well as exogenous substrates (from diet and environmental exposure), to produce microbial metabolites, microbe-associated molecular patterns (MAMPs; e.g., lipopolysaccharides (LPS) and secondary bile acids which translocate to the liver through the portal vein and influence liver functions.
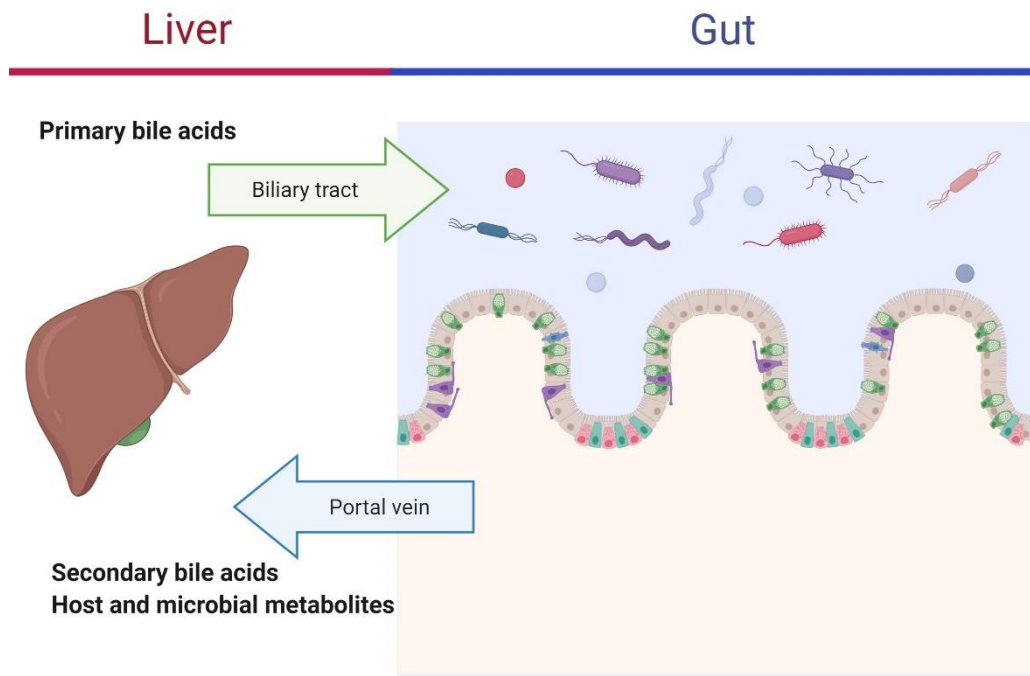
Figure 1.1 Communication between the liver and the gut.

1.1.1 Communication via bile acids

Bile acids are synthesised from cholesterol in the liver and act as detergents to facilitate the digestion and absorption of dietary fats, and fat-soluble vitamins. Bile acids are conjugated to glycine or taurine in the liver, stored in the gallbladder and from there secreted postprandially into the duodenum part of the small intestine via the biliary tract. After dietary fat is absorbed, about 95% of the bile acids are actively reabsorbed in the ileum and transported back to the liver via the portal vein. The remaining 5% of the total secreted bile acids may be lost in the faeces. The liver recycles the reabsorbed bile acids and releases them back to the small intestine and therefore, a continuous circulation of bile acids exists between the liver and the intestine, also known as the enterohepatic circulation (Ticho et al., 2019).

The bile acids that are synthesised in the hepatocytes are known as primary bile acids. These include cholic acid (CA; 3α-,7α-, and 12α-hydroxylated) and chenodeoxycholic acid (CDCA; 3α- and 7α-hydroxylated) in most mammals. In mice, next to CA and CDCA, a group of bile acids termed muricholic acids (MCAs) are the most abundant in the bile acid pool. The two major MCAs in mice are α-muricholic acid (αMCA;3α-, 6β-, and 7α- hydroxylated) and β-muricholic acid (βMCA; 3α-, 6β-, and 7β- hydroxylated). The first reaction in the bile acids synthesis pathway is catalysed by cytochrome P450 7A1 (cholesterol 7α-hydroxylase; CYP7A1) (Fig. 1.2). CYP7A1 is a rate limiting enzyme, and critical for efficient synthesis of bile acids. Indeed, deletion of CYP7A1 function by homozygous knockout of the *Cyp7a1* gene in mice reduced bile acid synthesis by approximately 60% and bile acid pool size by approximately 75%, and resulted in increased faecal fat content, hypercholesterolemia, and poor survival. The classical pathway can generate CDCA and CA, whilst the alternative pathway that involved CYP27A1 primarily produces CDCA. The ratio between CA and CDCA is determined by another enzyme in the classical bile acids synthesis pathway; cytochrome P450 8B1 (sterol 12α-hydroxylase; CYP8B1). CYP8B1 is responsible for hydroxylating the 12α carbon of the steroid ring. Therefore, CYP8B1 is involved in the synthetic routes of CA, which is 12α-hydroxylated, and not CDCA (Ticho et al., 2019). Transgenic *Cyp8b1* knockout mice were shown to have a profoundly different bile acid profile compared to wild-type animals (Li-Hawkins et al., 2002). Secondary bile acids found in mammals are deoxycholic acid (DCA; 3α- and 12α- hydroxylated) and lithocholic acid (LCA; 3α- hydroxylated), that are generated in the intestine by microbiota via 7α-dehydroxylation of CA and CDCA, respectively (Fig. 1.2). In mice specifically, ursodeoxycholic acid (UDCA; 3α- and 7β- hydroxylated) is produced from CDCA by intestinal bacteria via 7- hydroxyl epimerization.

Under physiological conditions, most of bile acids are produced via the classical pathway. However, in the event of liver injury the alternate acidic pathway may become predominant. The alternative bile acids pathway is initiated by sterol 27-hydroxylase (CYP27A1) located in the inner mitochondrial membrane (Ticho et al., 2019).
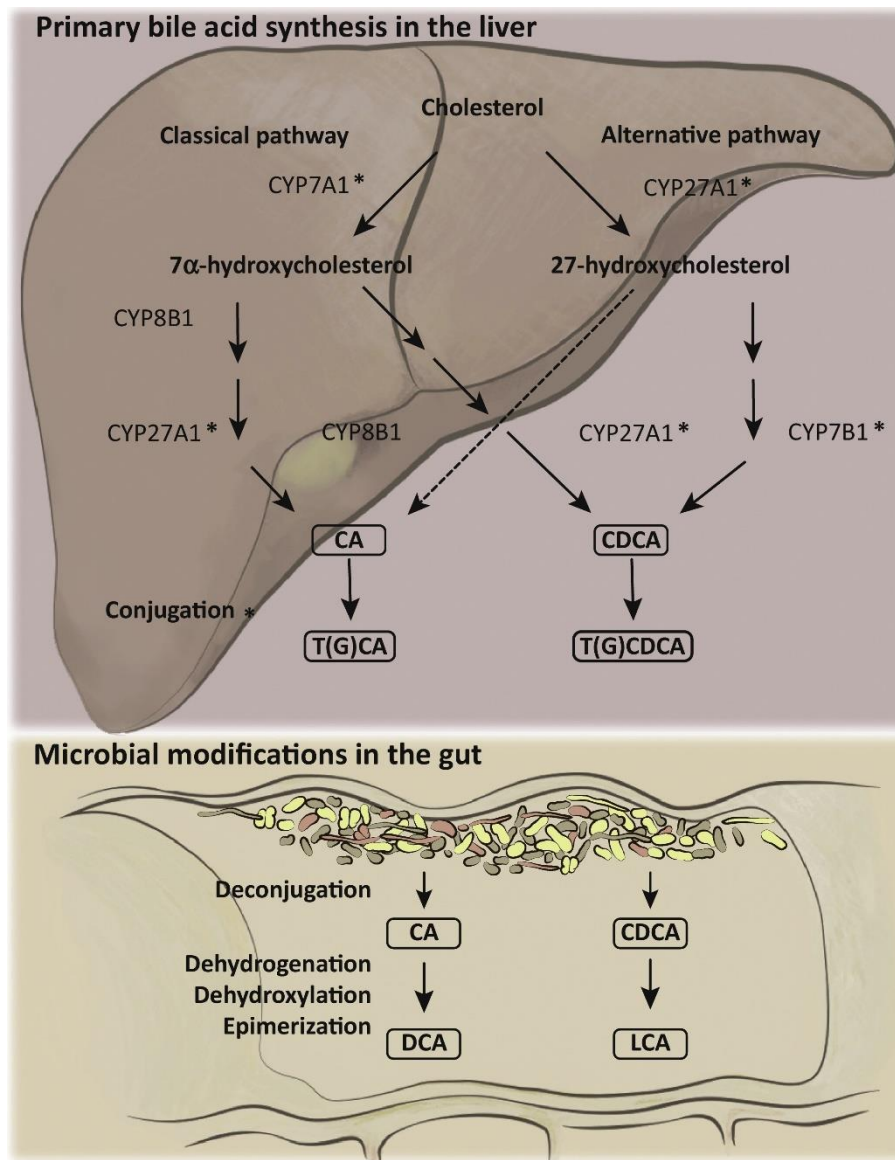
Figure 1.2 Bile acids synthesis. CYP7A1: cholesterol 7α-hydroxylase, CYP27A1: sterol-27-hydroxylase, CYP8B1: 12α-hydroxylase, CA, cholic acid; CDCA, chenodeoxycholic acid; DCA, deoxycholic acid; LCA, lithocholic acid. T and G are taurine and glycine conjugates. *CYP27A1: alternative bile acids synthesis pathway. Sourced from Molinaro et al., (2018): Trends in Endocrinology & Metabolism.

The *de novo* bile acids are released from the liver across the canalicular membrane by the bile salt export pump (BSEP/ABCB11). Biliary bile acids are stored in the gallbladder and secreted into the duodenum postprandially, where they act as detergents for lipids as well as signalling biomolecules. In the lumen bile acids travel along the length of the small intestine and are actively reabsorbed in the terminal ileum by the apical sodium-dependent bile acid transporter (ASBT/SLC10A2). Reabsorbed bile acids are shuttled from the apical to the basolateral membrane of the enterocyte and are transported into the portal circulation by the organic solute transporter alpha/beta heterodimer (OSTα/β, SLC51A/B). These bile acids are returned to the liver via the portal vein and enter hepatocytes at the sinusoidal

membrane via sodium-taurocholate co-transporting polypeptide (NTCP/SLC10A1) (Fig.1.3). In addition to their active uptake by ASBT in the ileal enterocytes, bile acids with a high enough pKa can passively diffuse through membranes in the intestine. Higher pKa means weaker bile acid, reduced water solubility and increased lipophilicity (Suga et al., 2017).

Unconjugated bile acids have a high pKa (~6) and are able to passively diffuse through membranes. Conjugation of primary bile acids with taurine and glycine in the liver decreases the pKa of bile acids, and therefore require transporter mediated uptake. In addition to producing secondary bile acids, gut microbiota can deconjugate bile acids and thus increase their pKa. However, ASBT and OSTα/β remain the critical transporters for the intestinal absorption and enterohepatic circulation of bile acids (Krag and Phillips, 1974; Ticho et al., 2019).

In the recent years, bile acids have received great attention due to their role as hormone-like signalling molecules. Bile acids interact with extra- and intracellular cellular receptors, including the nuclear receptor farnesoid X receptor (FXR/NR1H4). Several studies have reported FXR as a major regulator of bile acid homeostasis that functions to protect against bile acids induced cytotoxicity. Depending on the structure, bile acids have the ability to act as FXR agonists or antagonists. In the liver, FXR controls the expression of bile acid transporters to reduce cellular bile acids. Hepatic FXR inhibits the expression of NTCP through a Small heterodimer partner (SHP)-dependent process resulting in reduced uptake of bile acids from the portal circulation (Denson et al., 2001). Intestinal FXR plays an important role in supressing bile acid synthesis. Activation of FXR in the intestine increases the transcription of fibroblast growth factor 15 (Fgf15 in rodents, FGF19 in humans). FGF15/19 is transported to the hepatocytes in the portal blood, where it binds to the FGF receptor 4 (FGFR4)/β-klotho (KLB) complex. This complex blocks CYP7A1 transcription in a SHP dependent manner, thereby reducing bile acids synthesis (Kir et al., 2012). Studies using transgenic mouse models have helped unravel the complex mechanisms underlying FGF15/19 biological activity. Mice lacking FGF15, FGFR4 and KLB show impaired bile acids metabolism (with increased bile acids synthesis and serum bile acids levels), and exogenous FGF15 administration is unable to repress CYP7A1 in both FGFR4 and KLB knockout mice (Yu et al., 2000; Ito et al., 2005). In addition to the involvement of FGF15/19 in bile acid homeostasis, FGF15/19 is an important regulator of glucose and energy homeostasis. Kir et al. (2011) demonstrated FGF15 involvement in glucose regulation by using *Fgf15*- knockout mice. These mice were unable to maintain physiological concentrations of glucose, additionally, they displayed impaired hepatic glycogen storage and glucose intolerance. The authors suggest FGF15/19-FGFR4-KLB complex triggers an increase in hepatic glycogen synthase activity and glycogen synthesis, via activation of small guanosine triphosphatase RAS, and extracellular signal regulated protein kinase (ERK) signalling pathway (Kir et al., 2011). FGF15 is known to inhibit hepatic gluconeogenesis in an insulin independent manner via downregulation of genes involved in gluconeogenesis. The inhibition of gluconeogenesis occurs by inactivation of cAMP regulatory element–binding protein (CREB) and blunting the expression of peroxisome proliferator-activated receptor γ

coactivator-1α (PGC-1α) (Fig. 1.3). This FGF15/19-dependent pathway regulates hepatic glucose metabolism following the fall in insulin levels, thereby regulating hepatic metabolism from the fed to fasted state (Potthoff et al., 2011). Dysregulation of FGF15 has also been associated with the development of hepatocellular carcinoma (HCC) in mice, in which the *Fgf15* gene expression is increased in the ileum as well as hepatocytes (Cui et al., 2018; Gadaleta1 and Moschetta, 2019).
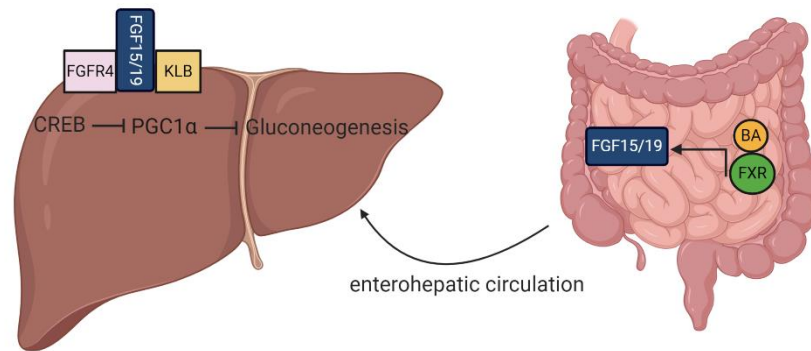
Figure 1.3 FGF15/19 effects on glucose regulation in the liver. FGF15/19: fibroblast growth factor, BA: bile acids, FXR: farnesoid X receptor, FGFR4: FGF receptor, KLB: β-klotho, CREB: cAMP regulatory element–binding protein, PGC1α: transcriptional co-regulator peroxisome proliferator-activated receptor 1α. Adapted from Kir et al., (2011).

Multiple lines of evidence indicate that bile acids and the gut microbiota closely interact and modulate each other. Bile acids exert direct control on the intestinal microbiota by activation of FXR dependent gene regulation. Inagaki et al. (2006) demonstrated that bile duct ligation (BDL) and obstructing bile flow to the intestine in mice caused bacterial overgrowth, mucosal damage, and consequent systemic inflammation. The authors also showed that the adverse effects of BDL were reversed by administration of the synthetic FXR agonist (GW4064) that induced genes related to enteroprotection, inhibited bacterial overgrowth and systemic translocation. It is becoming increasingly evident that bile acids profoundly impact the composition of the gut microbiota, and that bacterial disturbance may alter the fine balance between primary and secondary bile acids and their subsequent enterohepatic cycling. Dysregulation of enterohepatic circulation can lead to the accumulation of bile acids in the hepatocytes and enterocytes, thereby inducing bile acid toxicity and oxidative stress due to their detergent properties (Ticho et al., 2019).

Figure 1.4 Enterohepatic circulation of bile acids. BA: bile acids, CYP7A1: cholesterol 7α-hydroxylase, BSEP: bile salt export pump, ASBT: apical sodium-dependent bile acid transporter, OSTα/β: organic solute transporter α/β heterodimer, NTCP: Na+-taurocholate cotransporting polypeptide, FXR: farnesoid X receptor, FGF15/19: fibroblast growth factor. Sourced from Ticho et al., (2019): Comprehensive Physiology.

1.1.2 Intestinal barrier function

The gut barrier consists of a physical barrier, a biochemical barrier and an immune system barrier (Chu et al., 2019). The physical barrier is supported mainly by the gut microbiota, mucus layer and a single layer of intestinal epithelial cells that are linked by tight junction proteins. Molecules with antimicrobial and anti-inflammatory properties, such as bile acids and antimicrobial proteins (including α-defensins and β-defensins, C-type lectins, cathelicidin, lysozyme and intestinal alkaline phosphatase) support and mediate the highly structured biochemical barrier (Dupont et al., 2014). Secretory immunoglobulin A (IgA) and lymph node resident immune cells form the components of immune system barrier (Melo-Gonzalez et al., 2019).

The gut microbiota is comprised of thousands of microbial species including, archaea, bacteria, fungi and viruses. The gut microbiota plays a crucial role in host's physiology and is involved in various processes such as immune response, nutrition absorption and intestinal permeability. Mammalian gut bacteria mainly comprises of *Firmicutes, Bacteroidetes, Actinobacteria* and *Proteobacteria* phylum, however, their abundance may be modulated by genetic (Tran et al., 2019) and physiological factors such as age and environmental factors such as diet, medication (antibiotics) and living conditions (Phillips, 2009). The host and gut microbiota act together to

maintain tissue homeostasis and mutualism to prevent colonization by pathogenic bacteria. The gradient of microbial density in the gastrointestinal tract increases from duodenum (10^4/ml) to the distal ileum (10^8/ml), and the colon (10^{11}/ml) (Donaldson et al., 2016).

Mucus and tight junction proteins form the structure of the physical barrier between luminal bacteria and the underlying epithelial layer. Mucus is comprised of mucin proteins, mainly mucin 2 (MUC2) which is secreted by goblet cells (Van der Sluis et al., 2006). The thickness of the mucus layer is dependent on the location in the gut. The large intestine has a dense mucus layer, compared to the less dense and porous mucus layer found in the small intestine. MUC2 not only provides physical protection but has also been reported to restrict the immune response towards intestinal antigens by imprinting enteric dendritic cells (DCs) towards an anti-inflammatory state (Shan et al., 2013). The mucus is also associated with antimicrobial properties through the action of antimicrobial peptides (AMPs) such as α-defensins, β-defensins, C-type lectins, and lysozyme which are released into the mucus gel to reinforce the barrier. Hence, the mucus layer is the very first line of defence against gut bacteria and exogenous molecules in the gut lumen (Vancamelbeke and Vermeire, 2017).

Underneath the mucus layer, the intestinal epithelial cells (IECs) comprise of several distinct cell types; absorptive enterocytes, goblet cells, enteroendocrine cells, Paneth cells, microfold (M) and Tuft cells. These cells together form a continuous and polarised monolayer that separates the lumen from the lamina propria. Tight junction proteins are apical adhesives that seal the intercellular space. These junctional proteins include large families of claudins, occludins, junctional adhesion molecules (JAMs) as well as scaffolding molecules (Vancamelbeke and Vermeire, 2017). Altogether, this physical barrier functions to maintain gut epithelial integrity, epithelium polarity to allow transport of nutrients, and create a barrier against pathogens and dietary antigens by separating the lamina propria from the lumen (Odenwald and Turner, 2017). Moreover, crosstalk between the gut bacteria and immunity is represented by AMPs which are mostly produced by Paneth cells. Pattern recognition receptors (PRRs), such as Toll-like receptors (TLRs) and NOD-Like receptors (NLRs) also recognise bacterial components and release interleukins (such as IL-22) to shape the gut microbiota and maintain gut homeostasis. Innate lymphoid cells (ILCs) have recently been discovered to play a role in innate immune cell population. The population and function of the intestinal ILCs are reported to be influenced by the signals from the microbiota (Gury-Benari et al., 2016). The small intestine is the largest producer of immunoglobulins in the body. Secretory IgA plays an important role in protecting the host against pathogens and shaping the gut microbiota (Lycke et al., 2017). Palm et al. (2014) identified colitogenic (colitis promoting) intestinal bacteria to be coated with secretory IgA in a mouse model of microbiota-driven colitis. The study suggests IgA coating of these inflammatory commensal bacteria prevents bacterial dysbiosis during colitis and helps to maintain homeostatic gut microbiota. Altogether, the intestinal barrier is highly dynamic and adaptable to both internal and exogenous signals (such as cytokines, bacteria, dietary antigens). When the gut barrier function is compromised, gut bacteria and bacterial

derived products (for instance, bacteria cell wall components and microbial metabolites) can circulate to the liver via the portal vein and induced hepatic and systemic inflammation (Aron-Wisnewsky et al., 2020). Western style diets have been known to profoundly affect gut microbiota composition and adversely impact the gut barrier function (Aron-Wisnewsky et al., 2020) (More on Western diets in Paragraph 1.2.1).

<u>1.1.3 Carbohydrate metabolism</u>
Human population has thrived on diets with varying carbohydrate amounts. The basic carbohydrates that are consumed by most humans include simple sugars (glucose and fructose; fruits, honey, beverages), disaccharides (lactose; milk and dairy products and sucrose; table sugar), and complex carbohydrates (starch; potato, rice and wheat and dietary fibres (DF); grains, non-starchy vegetables, pulses). The current carbohydrate intake in humans typically comprises of 45-60% of total energy (Ludwig et al., 2018). It is becoming increasingly clear that the quality as well as the amount of carbohydrate plays an important role in population health. Increased consumption of high glycaemic load grains such as white rice, potato products, and added sugars (e.g. in beverages) are causally related to obesity, diabetes, and cardiovascular disease, whereas non-starchy vegetables, whole fruits, legumes, and whole kernel grains are associated with lower risk of metabolic diseases (Feinman et al., 2015, Ludwig et al., 2018).

In theory, dietary carbohydrates are compounds that can be metabolised directly into glucose, or that undergo oxidation into pyruvate. Glucose homeostasis involves three physiological stages: 1) intestinal glucose absorption in the fed state, 2) hepatic glucose production, and 3) extrahepatic glucose usage by the brain, skeletal muscle, and adipose tissue (Merino et al., 2019). Inside the small intestine, carbohydrates (e.g. starch, sucrose) are broken down into monosaccharides by the brush border ectoenzymes known as α-glucosidases expressed on the enterocytes. One of the brush border enzymes is maltase glucoamylase (MGAM) which hydrolyses α-1,4 glycosidic linkages between glucose molecules in maltose (from starch). Another brush border enzyme is sucrase-isomaltase (SIS), which hydrolyses α-1,2 glycosidic linkages between glucose and fructose molecules, thereby breaking down sucrose. Other brush border enzymes include lactase involved in breaking down lactose from milk into glucose and galactose (Goodman, 2010).

Although glucose and fructose share the same molecular formula ($C_6H_{12}O_6$) and caloric value (4 kcal/g), they have distinct metabolism in the intestine (Merino et al., 2019) (Fig. 1.5 and Fig. 1.6).

Glucose is absorbed into the intestinal epithelial cells by the sodium-glucose linked transporter (SGLT1/SLC5A1) that is expressed at the apical membrane, and glucose transporter 2 (GLUT2/ SLC2A2) at the basolateral membrane. SGLT1 and GLUT2 expression is regulated by luminal concentration of glucose, insulin, and caloric demand (Merino et al., 2020). Further, in response to high luminal glucose concentration, GLUT2 may be translocated to the apical membrane of the enterocyte, leading to enhanced glucose absorption (Zheng, et al., 2012).

Blood glucose enters hepatocytes via GLUT2 and is phosphorylated by glucokinase to form glucose-6-phosphate (G-6-P), which leads to decreased glucose concentration in the cell and stimulates further glucose uptake. G-6-P acts a substrate for glycogenesis in the fed state. It can also be metabolised into pyruvate, which can be used to generate ATP through the tricarboxylic acid (TCA) cycle or enter lipogenesis pathway. G-6-P can be dephosphorylated by glucose 6 phosphatase (G-6-Pase) to generate glucose for metabolic adaptation during fasting (Rui, 2014).
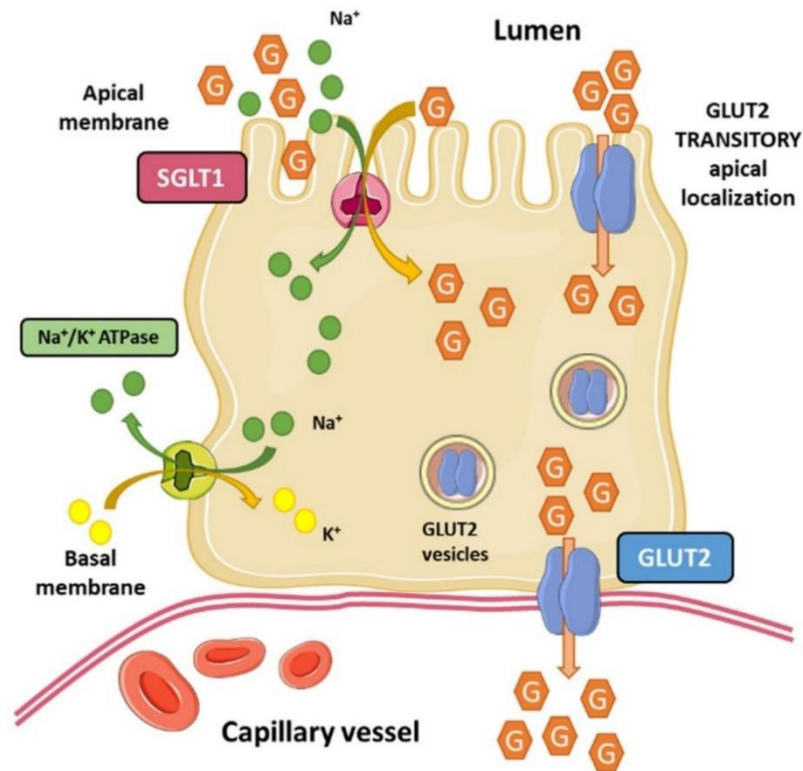
Figure 1.5 Glucose uptake in the intestine. G: glucose, SGLT1: sodium-glucose co-transporter 1, GLUT2: glucose transporter 2. Figure sourced from Merino et al., (2020): Nutrients.

The transport of fructose relies on GLUT5 (SLC2A5) as the primary transporter responsible for fructose uptake into the enterocyte at the apical side of the membrane, whereas GLUT2 transports most of fructose from the cytosol into blood circulation at the basolateral side of the enterocyte (Ferraris et al., 2018). Once fructose is transported to the cytosol, it is rapidly phosphorylated by the ketohexokinase (KHK) to fructose-1-phosphate (F1P) using ATP as a phosphate donor. The resultant F1P is further broken down into glyceraldehyde (GA) and dihydroxyacetone phosphate (DHAP) by the aldolase B (ALDOB). Finally, the triokinase (TKFC) catalyses the phosphorylation of GA by ATP to form the glycolytic intermediate glyceraldehyde-3-phosphate (GA-3-P) (Hannou et al., 2018). Traditionally, the liver has been considered as the main site of metabolism of dietary fructose, however, this concept has been challenged by Jang et al. (2018), the authors used isotopic tracing techniques and portal blood sampling to demonstrate that 90% of dietary fructose is metabolized by the small intestine in mice. While, high doses of fructose may

saturate the absorption capacity of the small intestine, leading to fructose spill over into the liver and stimulate *de novo* lipogenesis.
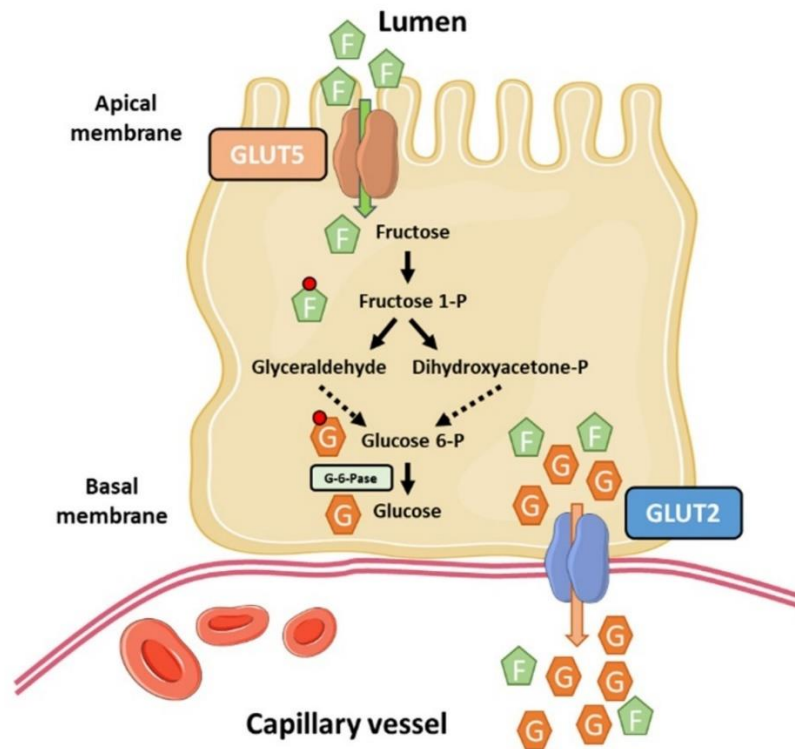
Figure 1.6 Fructose uptake in the intestine. G: glucose, F: fructose, GLUT2/5: Glucose transporter 2 or 5. Figure sourced from Merino et al., (2020): Nutrients

1.2 Influence of diet on the gut-liver axis

Several researchers have shown that dietary factors may influence the gut microbiota, enterohepatic circulation and intestinal barrier function (Zmora et al., 2018). The changes in the gut microbiota may influence the host metabolism by affecting energy balance and by producing microbial metabolites that may induce various phenotypes depending on the health of the host (Zhao et al., 2020; Koh et al., 2016).

1.2.1 Western style diet

The UK government guidelines for macronutrient composition for adults comprises of 50% of total energy as carbohydrate (no more than 5% of total energy should be derived from free sugars), 15% as protein, and 35% as fat. However, the adherence of the UK population to these guidelines is suboptimal. A UK study based on National Diet and Nutrition Survey (NDNS) 2014–2016 reported that free sugars accounted for almost 13% total energy intake (Amoutzopoulos et al., 2020). The recommended fibre intake for UK adults is generally 30g per day, whereas the average intake does not reach recommendations and stays between 16-20g per day (Stephen et al., 2017). Western style diet is generally described by increased consumption of ultra-processed and pre-packaged solid foods and beverages that are

high in saturated fat and refined carbohydrate (starch, sucrose and fructose) content. Western style diets have been associated with various metabolic diseases such as obesity, diabetes, NAFLD and gut microbial dysbiosis (Santos-Marcos, 2019). The adverse health effects of increased fat consumption have led the public to embrace a low-fat diet for heart disease prevention and weight loss. This phenomenon has encouraged the food industry to manufacture highly palatable and convenient ultra-processed food products that are low in fat and dietary fibres (DF), and enriched with highly refined carbohydrates such as high fructose corn syrup, starch and sucrose (Hall et al., 2019). During the past two decades, the consumption of calories from ultra-processed foods has almost tripled (from 11% to 32%). The ultra-processed foods are formulations of ingredients that are obtained from fractioning of whole foods by various industrial processes including, grinding, pureeing, hydrolysis, or hydrogenation. These modified foods are then assembled by using industrial techniques such as extrusion, moulding and pre-frying. Colour and additives are frequently added to make the end-product hyper-palatable and to enhance duration (Monteiro et al., 2019). The nature of the processes and ingredients used in the preparation of these foods and their displacement of whole foods containing meals make ultra-processed foods intrinsically unhealthy. In a recent French study using data from NutriNet-Santé study, Schnabel et al (2018) showed statistically significant associations between consumption of ultra-processed foods and increased risk of cancer and gastrointestinal diseases. Long-term consumption of the ultra-processed diet could lead to permanent loss of several species of the gut bacteria and possibly induce inheritable metabolic changes via the epigenome (Sonnenburg et al., 2016). Zinöcker and Lindseth (2018) reviewed the effects of high consumption of ultra-processed foods in animals to show dysbiosis in the gut, systemic inflammation and onset of metabolic disease, due to high starch, sucrose and low fibre in the ultra-processed foods.

In line with these findings, research in the recent years has focused on the promising potential of gut microbiota targeted therapies, for example, probiotics and prebiotics to tackle the health effects caused by overconsumption of processed foods (Martinez et al., 2017; Aron-Wisnewsky et al., 2020).

1.2.2 Western style diet and NAFLD
NAFLD is an epidemic liver disease, that affects approximately one third of the entire population in the world. This disease represents as a wide range of clinical phenotypes from early hepatic steatosis to non-alcoholic steatohepatitis (NASH), fibrotic NASH, advanced fibrosis, liver cirrhosis and eventually hepatocellular carcinoma (HCC) (Tilg et al., 2020).

The underlying pathophysiology of NAFLD involves various pathways including the role of dietary factors and gut microbiota as a crucial player in disease progression. In the past decade, it has been increasingly recognized that various common food components (trans-fats, fructose, choline in red meat) have proinflammatory potential and may contribute to the pathogenesis of NAFLD (Neuschwander-Tetri et al., 2012; Jang et al., 2018; Chen et al., 2016). The role of gut microbiota was confirmed by Lommba et al. (2017) that identified microbial signatures associated with different

severities of NAFLD in humans. The authors showed increased abundance of species from *Proteobacteria* (*Escherichia coli*) in fibrotic NASH patients. Endotoxins from *Proteobacteria* include proinflammatory LPS, that are found in high concentrations in the blood and hepatocytes of NASH patients (Carpino et al., 2020). LPS can induce inflammation in hepatocytes via Toll like receptor 4 (TLR4) and NF-κB signalling pathway leading to proinflammatory cytokines and chemokines; Tumour necrosis factor α, (TNFα), interleukin 1β (Il-1β) (Alexander and Rietschel, 2001). As well as the proinflammatory role of LPS, it has also been associated with promoting lipogenesis in the liver. Recently, Todoric et al. (2020) reported that microbial endotoxin (LPS) engages TLR4 to trigger TNF production by liver macrophages, which induced lipogenic enzymes, thereby driving *de novo* lipogenesis in hepatocytes.

In contrast, various prebiotics, probiotics and dietary restriction interventions have been proposed to counteract the above effects (Hu et al., 2020; Chen and Vitetta, 2020).

1.2.3 Addition of dietary fibres to Western style diet
DF are described by wide array of polysaccharides that are indigestible by the host enzyme systems. DF not only provide direct benefits to the host by increasing the faecal bulking and providing laxative effects, but they also act as a substrate for the gut microbiota. The gut microbiota contains thousands of carbohydrate active enzyme (CAZyme) families that enable them to degrade these non-digestible carbohydrates into short chain fatty acids (SCFAs). DF can be generally categorised as insoluble (e.g. cellulose) or soluble fibres (e.g. inulin, pectin and psyllium).

Most DF comprise of sugars monomers (e.g. glucose, fructose, xylose, arabinose) with α- or β- linkages, and different ring structure (pyranose or furanose) to form polysaccharides and oligosaccharides. Therefore, the structural heterogeneity between the DF may have an impact on their fermentability, microbial diversity, and differential host response (Rao et al., 2013; Singh et al., 2019). Soluble and insoluble DF originate from different food sources, such as legumes, vegetables, nuts, seeds, fruits, and cereals (Table 1.1). For example, pectins are found in fruits, such as apples and citrus fruits, whereas β-glucans and arabinoxylans are present in cereals. Due to the decreased consumption of whole foods in Western countries, fortification of processed foods or prebiotic supplements with enzymatically extracted non-digestible carbohydrates such as psyllium and inulin are popular means to increase fibre intake (Makki et al., 2018).

Pectin is a soluble fibre and its structure is a linear chain of D-galactopyranosyluronic acids linked via α-(1→4) bonds, with carboxyl groups of some residues esterified with methyl ether. One of the main properties of pectin is its ability to form gels that are stable in acidic conditions (Khotimchenko., 2020). Due to the gelling ability of pectin, it is often used in milkshake, ice cream and sauces (Cameron et al., 2018). Pectin is known to lower circulating cholesterol and glucose levels (Shtriker et al., 2018).

DF in cereals such as wheat and barley, largely comprises of cell wall polymers and include cellulose, hemicellulose, lignin and soluble fibres such as β-glucans and arabinoxylans. The β-glucans in cereals mainly exist as glucose monomers linked via β-(1→4) and β-(1→3) glycosidic bonds and its fermentation in the gut is associated with high level of propionate and butyrate. Arabinoxylans are comprised of a mixed linkage between arabinose and xylose. Diets supplemented with wheat arabinoxylans have been shown to be associated with increased viscosity of small intestine content, changes in gut microbiota composition that led to high levels of short chain fatty acids, and reduced serum triglyceride levels (Gong et al., 2018).

Psyllium is another gel forming fibre sourced from a valuable Chinese herbal plant, *Plantago ovata*. This DF is a popular ingredient for over the counter laxatives and has been reported to have a variety of biological effects, including gut immunomodulatory and blood glucose regulation (Jane et al., 2019). The structural backbone of psyllium consists of xylose units and β-(1→4)-linked D-xylopyranosyl residues (Zhang et al., 2019). Studies on the addition of psyllium to food products presents attractive strategies to allow consumers to increase their fibre intake. Psyllium has been added to biscuits, cakes and gluten-free products (Franco et al., 2020).

Inulin is a polysaccharide that mainly originates from chicory root. It belongs to a class of DF knows as fructans and their structure is a linear chain of fructose with β(2→1) linkage (Davani-Davari et al.m 2019). Salazar et al. (2015) reported consumption of inulin in obese women led to increased abundance of *Bifidobacterium* species, reduced serum LPS and improved metabolic parameters. The wide range of uses of inulin by the food industry include, sugar and fat replacement, and as a prebiotic ingredient in juice and dairy beverages (Castellino et al., 2020).

The major SCFAs produced by the gut microbiota include acetate, propionate and butyrate. SCFAs act as important energy and signalling molecules that bridge the gap between the gut microbiota and the host (Koh et al., 2016). Butyrate is the preferred energy source for colonocytes and is locally consumed, whereas other SCFAs can be absorbed by the enterocytes and enter liver via the portal vein. One of the mechanisms as to how butyrate may protect against colorectal cancer and gut inflammation is by acting as a histone deacetylation (HDAC) inhibitor (Donohoe et al., 2012). SCFAs also act as ligands for free fatty acid receptors (FFARs) which can be found in various cell types and organs including immune cells, adipose tissue, and the liver, to induce various anti-inflammatory and metabolic effects (improved glucose and lipid metabolism) (Kimura et al., 2013). However, the role of FFARs in SCFAs signalling and how SCFAs contribute to improved metabolic health needs further clarification.

Overall, DF provide as an attractive strategy to improve Western style diet induced gut microbiome. However, a better understanding of diet-microbiota interactions is required to further understand the underlying mechanisms for their beneficial effect on the gut-liver axis.

Table 1.1 Properties and source of dietary fibres (DF).

Dietary Fibre (DF)	Properties	Source
Arabinoxylans	Soluble	Most cereals
β-glucans	Viscous and soluble	Barley and Oats
Cellulose	Poor solubility	Plant foods
Inulin	Non viscous, soluble	Several plants
Pectin	Viscous and soluble	Fruits such as apples
Psyllium	Viscous and soluble	*Plantago ovata*

1.2.4 Calorie restriction (CR) to counteract the adverse effects of Western style diets

The increased consumption of Western style diets is one of the drivers for age related increased incidence of metabolic diseases such as type II diabetes and NAFLD (Fontana, 2009; Afshin et al., 2019). These diseases present a major burden not only on the individual, but also at a societal level, owing to the increased medical cost on the health sector (Bloom et al., 2016). Consequently, there is an urgent need for the development of innovative lifestyle interventions and therapeutics that can improve age-associated chronic diseases.

Calorie restriction (CR) is a dietary intervention that reduces calorie intake while preventing malnutrition or reduction in essential nutrients. Initially, CR induces weight loss and over time energy expenditure (EE) declines until it eventually matches energy intake and leads to a new stable body weight (Most and Redman, 2020). CR has been shown to induce beneficial metabolic changes and oppose age-related physiological and pathological changes, thereby extending longevity (Fontana and Klein, 2007; Colman et al., 2009). The underlying mechanisms for beneficial effects of CR have been explored in several studies to show enhanced cellular protection, reduction of inflammation and oxidative DNA damage (Qu et al., 2000; Kim et al., 2016). In the recent years, research on the effects of CR on the gut microbiome has also markedly increased. The impact of CR on gut microbiota has been studied in various models including yeast, rodents, primates and humans (Mair and Dillin, 2008; Meydani et al., 2016). CR studies in model organisms found improved multiple aspects of health and increased survival with CR dose of 30–40%. However, translation of animal CR studies to humans is not as straightforward. This was confirmed in the controlled clinical study of healthy non-obese adults with a target of 25% CR for two years (CALERIE study, Kraus et al., 2019). While, the achieved level of energy reduction over the two years was only 12% (from normal average calorie intake of 2467kcal/day to 2170kcal/day), confirming that most humans are not capable of sustained major reduction in calorie intake.

Research on ageing gut microbiota has found disturbed balance between beneficial and harmful bacteria that may drive inflammaging (Claesson et al., 2012). Some of the benefits of CR have been associated with an overall increased relative abundance of probiotic species from the *Bifidobacterium* and *Lactobacillus* genus (Zhang et al., 2013; Russo et al., 2016). The increased abundance of *Lactobacillus* and *Bifidobacterium* has been negatively correlated with total cholesterol, low-density lipoprotein (LDL), body mass index (BMI), and inflammatory markers (Sun et al.,

2015; Fraumene et al., 2018). Moreover, studies have also reported increased abundance of health associated mucin degrading bacteria, *Akkermansia* in response to CR (Fabbiano et al., 2018). Dao et al. (2016) showed individuals with a high baseline abundance of *Akkermansia* before CR had improved insulin sensitivity and overall healthier metabolic status than individual with a low *Akkermansia* baseline abundance. Increased levels of *Akkermansia* have been inversely associated with body fat mass and glucose intolerance in mice (Everard, et al., 2013).

In addition to the microbiota's response, CR has been reported to increase bile acids pool size in mice (Green et al., 2019; Fu and Klaassen, 2013). Increase in CR-induced bile acids is associated with increased expression of bile acids synthesis enzyme CYP7A1 (Fu and Klaassen et al., 2013), which indicated that under CR conditions the liver becomes increasingly efficient at metabolising lipids. Moreover, CR switches metabolism towards energy conservation by enhanced breakdown of lipids via β-oxidation, and by increased glycogenolysis and gluconeogenesis (Zheng et al., 2018), thereby, improving metabolic parameters.

CR has been shown to reduce the onset of age-related cancers by reducing oxidative stress and enhancing DNA repair (Heydari et al., 2007). Another mechanism by which CR provides protection against age related pathologies is by boosting the regenerative capacity of stem cells in the host (Mihaylova et al., 2014). Many mammalian tissues (skin, liver, neurogenic) are maintained by stem cells. For example, the intestinal crypt contains Lgr5$^+$ cells that are markers for the intestinal stem cells (ISCs), and regulate cell turnover (Barker et al., 2012). CR has been reported to increase the number of stem cells in the intestinal crypts (Yilmaz et al., 2012; Igarashi and Guarente, 2016), which has been suggested to contribute towards the cancer protecting effects of CR (Bruens et al., 2020).

The effects of CR on gut microbiota, bile acid metabolism and intestinal regeneration indicates an important role of the gut-liver axis in CR induced health and lifespan. Although, preclinical research on health-promoting potential of CR has proved to be promising, the increased availability of energy-dense foods and social behaviour towards food makes this intervention difficult and demanding to maintain in humans. Considering this, CR related changes in the gut-liver signalling may provide a unique doorway to discover novel molecules and innovative methods to optimize healthy ageing without the need for drastic food restriction.

1.3 Mouse models for studying the gut-liver axis
Studying the direct interactions between human gut microbiota and the host tissue is often challenging due to the difficulties involved with obtaining samples. Even though faecal samples can be easily obtained from humans, scientists may not be able to control several experimental variables, such as diet, and environmental factors (Seksik and Landman, 2015).

Mice models offer advantages due to their similar gastrointestinal anatomy, straightforward sample collection, and better control over diet and genetics. Therefore, mice have been extensively used to translate the knowledge on microbiota-gut-liver axis in humans.

Most research on the gut microbiota has been performed in C57BL/6J mice, however, there is no specific mouse strain that has been recommended for studying the effect of diet on microbiota. The mice that scientists often use are sourced from inhouse facilities, or those that are easily commercially available. This may not be an ideal method, as recent research has shown environmental factors and genetic background of mice to have a significant impact on their gut microbiota (Rasmussen et al., 2019).

In order to design animal experiment to study the effect of diets on the gut-liver axis, selecting the proper control diet is a crucial factor. However, the choice of control diet for mice studies is often not optimal, mostly due to lack of a robust and healthy control diet (Pellizzon and Ricci, 2018). The most commonly used control diets within the research community are the chow, and purified diets based on the American Institute of Nutrition 93 maintenance diet (AIN-93M) also known as low-fat (LF) diet. The exact formula of the chow diet is often not defined, and the amount of each ingredient used can vary widely depending on the batch, source, and season. In contrast, purified diets are composed of refined ingredients therefore, the formula of the diet is well defined, and the amount of each ingredient is openly available to researchers. The purified diet is a processed diet with highly refined ingredients, increased simple carbohydrates and reduced fibre content which may be detrimental to the health of the mice (González-Blázquez et al., 2020).

The protein in chow diet is mainly plant based (potato protein, hydrolysed wheat gluten, soya, maize gluten), whereas the purified diet contains only casein extracted from cow's milk. Several studies have comprehensively investigated the impact of dietary protein on gut microbiota composition (Kar et al., 2017; Zhao et al., 2020). Moreover, chow diet contains increased level of isoflavones from soy (daidzein and genistein) that are absent in the LF diet. Isoflavones are polyphenolic compounds that are among the most common categories of phytoestrogens. These compounds are structurally similar to 17-β-oestradiol and their metabolism involves the help of the gut microbiota (Křížová et al., 2019). Guevara-Cruz et al. (2020) showed consumption of genistein altered the gut microbiota of obese patients, followed by reduced insulin resistance and metabolic endotoxemia.

Therefore, the differences in the composition of control diets may lead to differential outcomes in studies investigating the effect of diets on mouse physiology. The choice of proper control diet in metabolic studies is extremely important for successful reproduction of the research data and calls for the development of a healthy universal control diet.

In view of these differences, the use of mouse models for translational research may be criticised, however, there is no suitable alternative present to reproduce the communication pathways involved in microbiota-gut-liver crosstalk. Although, *in vitro* models represent a strategy to overcome the mentioned limitations and recapitulate basic disease mechanisms in a controlled environment, their reduced complexity compared to *in vivo* models restricts their effectiveness to study the gut-liver axis (Pearce et al., 2018). The advent of bioengineering advances has made possible the use of 3D engineered models such as organ on a chip to research

microbiome interactions. Jalili-Firoozinezhad et al. (2019) described an *in vitro* system that mimics the host and microbiota interactions in the human intestine. The authors successfully cultured primary human intestinal cells with a diverse species of aerobic and anaerobic microbiota on the microfluid chip, by establishing an elegant oxygen gradient across the mammalian cells and the lumen. Although, this technology is in its early stages, the gut microbiome on a chip can provide ample opportunities to successfully study the microbiota-host interactions in detail in the future.

1.4 Aims and outline of the thesis

The aim of the research presented in this thesis is to study the effects of different dietary interventions on the health of the gut-liver axis in mice, by focusing on the ileum. Most of the studies that investigate the response of gastrointestinal (GI) tract to dietary interventions have mainly focused on the colon. The ileum contains the second largest microbiota population in the GI tract and has closer proximity to the gut bacteria due to the less dense mucus layer found here. Furthermore, transport of bile acids is mediated by the ileal enterocytes thus connecting the gut to the liver via the portal vein. We hypothesised that due to the aforementioned reasons, the ileum plays an important role in the dietary impact on the gut-liver axis. The limited information on the ileal response to diet prompted us to study the molecular microbiota changes in the ileum, in response to dietary interventions.

In our first experimental chapter (**Chapter 3**), we compare the response of the gut-liver axis to two diets, the plant-based high fibre chow (RM3-P, SDS Diets, UK) and low fibre purified diet (LF) (D17060802, a version of AIN93M from Research Diets, USA) that also resembles the low-fat ultra-processed foods in Western style diet. The study provides an opportunity to compare diets that are similar in calories but differ in their composition on the health of the gut-liver axis.

Chapter 3 aims and hypotheses: We hypothesised that the increased refined carbohydrates and low fibre in the LF diet may lead to an 'unhealthy' gut-liver phenotype in mice. We aimed to describe the changes in the liver phenotype, ileal gut microbiota and bile acid composition in response to the 4 weeks feeding of the LF compared to chow diet. The duration of these experiments was based on previous unpublished results from feeding mice the LF diet for 2-8 weeks. In our hands, the period of 4 weeks was shown to be the earliest timepoint where LF induced a significant gut-liver phenotype.

Furthermore, due to the lack of fibre and high content of easily metabolisable carbohydrates, we propose that the gut-liver axis of LF fed mice is more susceptible to an inflammatory challenge. To test this hypothesis, we created a model of systemic low-grade inflammation by injecting mice with low dose of lipopolysaccharide (LPS; 0.5mg/Kg body weight) once a week for 4 weeks (Raduolovic et al., 2018; López-Collazo and del Fresno, 2013).

In collaboration with Dr Steegenga at Wageningen University, ileal samples from adult and old mice fed with lifelong LF and CR (calorie restriction on LF diet

background: IDEAL study) were used to study the long-term effects of the LF diet in **Chapter 4**.

Chapter 4 aims and hypotheses: We used this opportunity to investigate whether lifelong CR protected the mice against the LF induced phenotype. We hypothesised that decreased consumption of the LF diet may prevent LF induced pathophysiological effects on the gut-liver axis. We also used the study to characterise the ileal response to lifelong CR in mice. To the best of our knowledge, this is the first study to present gene expression profiling of the ileal mucosa and microbiota composition in response to lifelong CR in adult (6 months) and aged (24 months) old mice. The age of 6 months in mice represents mature adults, whereas 24 months old mice represent old age, and this is when age-related changes (e.g., diminished lung function, kidney degeneration and impaired wound healing) can be detected (Flurkey et al., 2007).

Research on the impact of CR on mouse physiology is often performed on different background diets. In continuation of this concept and due to the differences observed between chow and LF fed mice in the previous chapters, we aimed to characterise the changes in the ileum and the liver of mice after 8 weeks of CR intervention with chow or LF diet background. We hypothesised that not only the dose of CR but also the composition of the background diet may lead to differential response of gut-liver axis. The IDEAL study showed that mice needed approximately 8-10 weeks to adapt to CR feeding schedule and reach a relatively stable weight. Therefore, we chose dietary intervention period of 8 weeks as the earliest timepoint to test the effects of 'short term' CR on the gut-liver axis.

In **Chapter 5**, we designed new rodent diets in collaboration with Research Diets Inc. (USA). **Aims and hypothesis:** The aim of this study was to describe the effects of different fibres on the ileal, liver gene expression and ileal microbiota. The mice were fed with LF and LF+fibre diets for 10 weeks. We hypothesised that the detrimental effects of the LF diet on the gut-liver axis of mice may be due to the reduced fibre content in this diet. Indeed, the addition of fibres improved the liver phenotype of mice and led to a differential ileal microbiota composition. The duration of 10 weeks was chosen to ensure experimental manipulation of gut-liver phenotype with the feeding of fibre enriched diet. We performed preliminary fibre feeding experiment of 2 weeks which did not result in a prominent improvement of the gut-liver phenotype.

Interestingly, we observed that despite the same amount of fibres used in our new diets, the composition of the fibres led to differential ileal gene expression between the fibre groups. Increased consumption of DF has been shown to have various benefits for human health (Makki et al., 2018), however, the role of structural heterogeneity of the different fibres in the gut-liver axis is largely unexplored.

The reproducibility of preclinical biomedical research using mice models is currently being scrutinised by National Institutes of Health (NIH). **Chapter 6 aims and hypotheses:** In addition to the differences observed between control diets, we also aimed to describe differences in the gut-liver axis of mice sourced from different

vendors. We investigate the variation in the gut microbiota and consequently the gut-liver axis of mice from an external vendor and inhouse animal facility. We hypothesised that mice would present different microbiota profiles based on their distinct environmental exposures. Such differences may explain in part the poor experimental reproducibility in animal research, despite using similar mouse models and strains. Finally, the general discussion, future perspective and human relevance of our work is presented in **Chapter 7**.

Chapter 2: Materials and methods

2.1 List of chemicals and reagents used for the experimental studies mentioned in this thesis.

Table 2.1 List of chemicals and reagents.

Reagents	Product number	Supplier
Ac-DEVD-AFC Caspase 3 substrate	ALX-260-032-M001	Enzo LifeSciences, Inc
CHAPS (3-[(3-Cholamidopropyl)dimethylammonio]-1-propanesulfonate) hydrate BioXtra 98%)	C5070	Sigma-Aldrich
Chloroform (99%)	372978	Sigma-Aldrich
DNase I, Amplification Grade	18068015	Invitrogen
DPX new mounting medium	100579	Merck
Eosin Y solution, alcoholic	HT110116	Sigma-Aldrich
Ethanol (BioUltra, for molecular biology, ≥99.8%)	51976	Sigma-Aldrich
FITC-dextran 4 kDa (FD4)	FD4	TdB Labs
Formalin solution, neutral buffered, 10%	HT501128	Sigma-Aldrich
Hematoxylin Solution, Harris Modified	HHS128	Sigma-Aldrich
HEPES (4-(2-Hydroxyethyl)piperazine-1-ethanesulfonic acid 99.5%)	H3375	Sigma-Aldrich
Histo-Clear II Histology Clearing Agent	NAT1334	Scientific Labs UK
IsoFlo (isoflurane, USP, 100%)	50019100	Zoetis Inc
Isopropanol (2-Propanol) 99.5%	I9516	Sigma-Aldrich
Lipopolysaccharides from Escherichia coli O111:B4	L2630	Sigma-Aldrich
Lysozyme from chicken egg white 90%	SAE0152	Sigma-Aldrich
Methanol for HPLC, ≥99.9%	34860	Sigma-Aldrich
Paraplast Plus for tissue embedding	P3683	Sigma-Aldrich
Phosphate Buffered Saline, 10X, Sterile	6506-OP	Sigma-Aldrich
PIPES (Piperazine-1,4-bis(2-ethanesulfonic acid) ≥99%	P6757	Sigma-Aldrich
QIAamp DNA Mini Kit	51306	Qiagen
QIAzol Lysis Reagent	79306	Qiagen
SuperScript III Reverse Transcriptase	18080093	Invitrogen
SYBR Green PCR Master Mix	4309155	Applied Biosystems
Triglycerides liquicolormono colorimetric test	10724	HUMAN Diagnostics
Triton™ X-100	X100	Sigma-Aldrich
Water for molecular biology, sterile filtered	95284	Sigma-Aldrich

2.2 Ethics

All experimental procedures and protocols performed were reviewed and approved by the Animal Welfare and Ethical Review Body and were conducted in accordance to the specification of the United Kingdom Animal Scientific Procedures Act, 1986 (Amendment Regulations 2012).

2.3 Animal model

For all experiments male C57BL/6J mice were used. We chose this strain as our animal model because of its popularity in studying consequences of diet on metabolic health (Wong et al., 2016).

Mice were either obtained from the Disease Modelling Unit (DMU) of the University of East Anglia (UEA) and/or Charles River UK (CRUK, Margate, UK). At the DMU, mice were maintained in Individually Ventilated Cages (IVC), controlled environment (21±2°C; 12-h light/dark cycle; light from 7:00 AM) and fed *ad libitum* on a standard chow diet (RM3-P; Special Diet Services (SDS), United Kingdom, Table 2.2). According to the experimental requirements, mice were either switched to other diets or kept under the same chow diet for the duration of the experiments. Power calculations have been undertaken to determine group sizes for all mouse experimental procedures, aiming to detect differences of 15% or more with a power of 0.85 and alpha set at 5%; calculations being informed by our previous experiments (Blokker et al, unpublished results), resulting in a minimum group size of n=6. In all cases, mice were randomized between groups and mice were divided into two cages per experimental group. All mice were aged 10-13 weeks old at the start of the experiment, to ensure stabilization of the microbiota (Laukens et al., 2016). The mice were weighed twice a week and food consumption was recorded at the same time by weighing the remaining diet. Mice were transferred to a clean cage on Monday each week. At the end of each experiment, mice were sedated with isoflurane and blood was collected by cardiac puncture under terminal anaesthesia. Sera was then isolated via centrifugation at 2000 xg for 10 minutes. Organs were collected and processed as described below.

2.4 Organ collection and processing

The small intestine of each mouse was collected, cleaned of any mesenteric fat, pancreatic tissue and Peyer's patches and then transferred to a petri dish containing ice cold phosphate buffer saline (PBS). The tissue was then divided into 3 equal parts, referring approximately to the duodenum (Part 1), jejunum (Part 2) and ileum (Part 3). The luminal content of each section was gently pushed out using a spatula and collected into separate Eppendorf tubes and snap frozen in liquid nitrogen for microbiota analysis. After pushing out the content, the ileum was further divided into 6 sections as depicted in Figure (2.1). The section 2 was collected for histology and stored immediately in 10% neutral buffer formalin (NBF) solution for 24 hours, before being transferred into 50% ethanol until embedding (See Histology, paragraph 2.7). The sections 1, 3 and 5 were collected together in an Eppendorf tube and snap frozen in liquid nitrogen. These sections were then used for gene expression analysis. The remaining two large sections (4 and 6) were collected in a cryotube and snap frozen to be used for bile acid analysis.

The liver was collected, and weight was recorded before dividing the liver into further sections as illustrated in Figure 2.2. The sections labelled H were collected for histology, the sections labelled R were collected for RNA isolation and the remaining liver pieces including pieces labelled Pr (protein), BA (bile acids) were collected into a cryotube and snap-frozen in liquid nitrogen for bile acids and caspase 3 activity analysis.
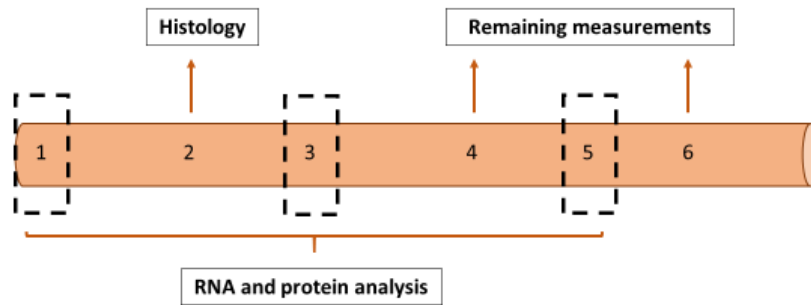
Figure 2.1 Method of sample collection from ileum at the time of sacrifice.
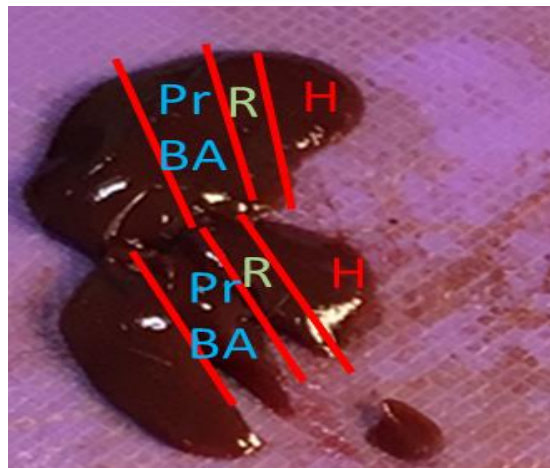
Figure 2.2 Method of sample collection from livers at the time of sacrifice.
H: Sample for histology, R: RNA, Pr: protein analysis, BA: bile acids analysis.

2.5 Experimental designs

2.5.1 Study 1: Investigating the impact of chow versus LF diet on gut-liver axis

Twelve male C57BL/6J mice were obtained from the DMU at UEA. The mice were randomly divided into two groups, 1) Chow, n=6 and 2) LF diet group, n=6. The mice were fed a standard chow diet (RM3, SDS, UK, Table 2.2) and/or a purified low-fat (LF) diet (D17060802, Research Diets, USA, Table 2.2) for a period of 4 weeks. The LF D17060802 is a variant of commonly used control diet D12450H, which slightly differs on the fat source. The fat source in D12450H comes from soybean oil and lard, while the fat source of D17060802 (our LF diet) is a mixture of soybean oil and palm oil in order to balance saturated and unsaturated fat composition. Brief description of the diets is shown in Table 2.2. A more detailed description of the diet is included in Supplement data 1. The impact of the two diets on the gut-liver axis is investigated in Chapter 3.

Table 2.2 Summary of dietary composition of chow and semi purified low-fat (LF) diet used.

	chow diet SDS diets RM3	LF diet D17060802
KJ/g	15.21	16.21
Protein (%)	26.9	20
Carbohydrate (%)	61.2	70
Fat (%)	11.5	10
Starch (g/Kg)	338.8	452.2 Corn Starch
Maltodextrin 10 (g/Kg)	0	75
Sucrose (g/Kg)	43.7	173
Fibre (g/Kg)	161.5 Soluble and insoluble	50 Cellulose

2.5.2 Study 2: The impact of chow versus LF diet feeding on mice exposed to a low dose lipopolysaccharide (LPS) challenge

Twenty-four mice were randomly divided into four groups, 1) Chow, 2) LF, 3) Chow LPS, and 4) LF LPS, n=6 per group. In the LPS group, mice were injected with low dose 0.5mg per kg of body weight of LPS intraperitoneally (i.p.) once a week for the duration of four weeks in addition to the diet treatment. The dose was chosen to induce a model of low-grade inflammation as described by Ramírez et al., (2018). The control groups received a sham i.p. injection (sterile PBS) in addition to the diets per week for four weeks. The effect of LPS on the gut-liver axis of chow and LF fed mice is investigated in Chapter 3.

The method of i.p. injections for administering substances is widely used in rodent experiments. This technique allows for LPS to be administered and rapidly absorbed systemically (Baek et al., 2015).

Mice were restrained and head of the mouse was tilted downwards, and the needle inserted at an angle of approximately 30° to the lower quadrant of the abdominal

wall. A new 26-27 gauge, 3/4-inch needle was used for each mouse and the injected volume was standardized to 150µl for the sham group.

After the four weeks intervention, 44mg per 100 g body weight fluorescein isothiocyanate-conjugated dextran (FITC-dextran 4) was administered via oral gavage to measure gut permeability. Oral gavage was performed by restraining the mouse by firmly grasping the skin over the dorsal neck and with the tail held between the palm and ring finger. By using a plastic, flexible catheter (FTP-20-30 20ga x 30mm Instech Solomon) 100 -150µl of FITC-dextran dissolved in sterile PBS was dispensed into the stomach. After two hours, mice were sacrificed via exsanguination by cardiac puncture under terminal anaesthesia and whole blood was collected in an Eppendorf tube and kept on ice in the dark for 30 minutes. Sera was then isolated via centrifugation at 2000 xg for 10 minutes. The time required for FITC-dextran 4 to reach its optimum level in systemic circulation has been reported to be approximately 2 hours (Woting and Blaut, 2018).

An aliquot of 50µl of serum was diluted with 50µl of sterile PBS and added onto a 96 well microplate. Additionally, a standard serial dilution of FITC-dextran ranging from 0 to 8000 ng/ml was added to the plate. FITC fluorescence was determined by spectrophotometry on a SpectraMax M2/M2e microplate reader with an excitation of 485 nm and an emission wavelength of 528 nm. Background emission signals in serum samples of the mice receiving PBS were subtracted from those of mice treated with FITC-dextran.

2.5.3 Study 3: IDEAL ageing study performed in Wageningen University, Netherlands

The long-term calorie restriction (CR) study has been performed in Wageningen University (WUR) in accordance with the Dutch national guidelines. Male C57BL/6J mice were housed individually at the age of 9 weeks and were randomly divided into a LF and LFCR group. The control LF group were given *ad libitum* access to the purified American Institute of Nutrition 93 W (AIN-93W) diet (version of AIN-93M and similar composition to the LF (D17060802) diet) used in our previous studies. The CR mice received the same diet, however, in portions containing 70% calories of the average intake of the LF group and provided daily at 15:30. The CR diet was supplemented with added vitamins and minerals to avoid malnutrition. Body weight was recorded every week. Mice were sacrificed at 6 and 24 months of age to differentiate between the effects of CR at young and old age. The age of 6 months in mice represents mature adults, whereas in 24 months old mice the biomarkers of old age are prominently detected. Liver and colon transcriptomics data from this study has been published by Rusli et al., (2017) and Kok et al., (2018) respectively. As part of a collaboration with Dr. Wilma Steegenga at WUR, we received the ileal and ileal content samples from 6 and 24 months old mice fed with LF and LFCR diet. Analysis of the ileum samples was performed at UEA.

We performed the following measurements in the ileum samples (n=5-6 per group);

- Gene expression analysis in the ileum tissue via microarray

- Bile acids were measured in the ileum tissue samples

- 16S rRNA sequencing of the microbiota in the ileal luminal content

- Histology analysis by H&E staining on the paraffin embedded ileal tissue

Furthermore, microarray data from the liver samples was reanalysed to extract energy metabolism related genes. The effect of lifelong LF and calorie restricted LF diet on the gut-liver axis is investigated in Chapter 4.

2.5.4 Study 4: Effect of a caloric restriction intervention on chow and LF diet on the gut-liver axis

Twenty-four mice were randomly distributed into two control groups, chow (n=6) and LF (n=6) (original LF: D17060802) diet and two caloric restriction (CR) groups, chowCR (n=6) and LF CR (n=6) for 8 weeks. This duration was chosen as it's the earliest timepoint to allow the mice to adjust to the CR diet and reach stable weight. The control groups always had free access to food, whereas the CR mice received both the chow and LF diet in portions containing 70 energy percent (En%) of the mean intake of the respective control group. The CR diets were based on the same background diets, however supplemented with vitamins and minerals to avoid malnutrition at 70E% energy intake and was provided daily at 15:30 for eight weeks. The grade of 30E% CR was chosen to match previous study performed in Wageningen University (Kok et al., 2018) and studies performed by Green et al., (2019) and Fu and Klaassen (2013) that showed significant changes in global metabolomics and bile acid metabolism under 30%CR. CR mice finished their daily portions within two hours after feeding. In order to avoid drastic weight loss, a gradual decrease in food intake was provided to the mice one week before the start of CR feeding. All mice were provided with *ad libitum* access to water. The comparison of the effects of CR on the gut-liver axis of chow and LF diet fed mice is characterised in Chapter 4.

2.5.5 Study 5: Investigating the impact of dietary fibres (DF) addition to the LF diet on the gut-liver axis

In collaboration with Research Diet Inc (New Brunswick, USA), new purified diets were designed. Firstly, the LS (Low sucrose variation of the LF diet) (D12450J) was added to the experimental design, the LS diet is based on the previously used LF (D17060802), but with reduced sucrose (68.8g instead of 172.8g), in order to improve the detrimental health effects of high sucrose content. Of note, the reduced sucrose content in the LS diet was replaced with increased starch content to regulate for calorie intake (LS: 506g corn starch, LF: 452g). Additionally, 2 more diets were designed containing soluble fibres; (1) LS enriched with 75g of inulin (LS+In), (2) a combination diet comprised of; 25g inulin, 25g pectin and 25g psyllium (LS+Comb). For brief description of the diet refer to Table 2.3. Full composition of diet is described in Supplementary data 1.

Fifty mice were randomly divided into 4 groups with n=10 per group and fed with 1) chow, 2) LF, 3) LS, 4) LS+In and 5) LS+Comb diet for a duration of 10 weeks. At the end of 10 weeks, mice were sacrificed, and organs collected as described in Paragraph 2.4. The role of dietary fibres on the gut-liver axis of mice is investigated in Chapter 5.

Table 2.3 Summary of composition of fibre enriched diets. LF: Low-fat diet, LS: Low-fat diet with reduced sucrose content, LS+In: LS diet enriched with inulin, LS+Comb: LS diet enriched with inulin, pectin and psyllium.

		LF diet D17060802	LS diet D12450J	LS+In D18012101	LS+Comb D19051003
KJ/g		16.1	16.1	15.4	15.4
Protein (%)		20	20	20	20
Carbohydrate (%)		70	70	70	68
Fat (%)		10	10	10	10
Corn Starch (g)		452.2	506	478	481.3
Maltodextrin 10 (g)		75	125	125	125
Sucrose (g)		173	68.8	68.8	68.8
Fibre (g)	Cellulose	50	50	50	50
	Soluble Fibre	0	0	75 Inulin	25 + 25 + 25 In+Pec+ Psy
Total (g)		1055	1055	1101	1105

Table 2.4 Summary of amount of fibre in the fibre enriched diets.

	Chow	LF	LS+In	LS+Comb
Total Fibre gm%	16.2	4.7	11.3	11.3
Soluble Fibre gm%	Not defined	0.0	6.8	5.2
Insoluble fibre gm%	Not defined	4.7	4.5	6.1

2.5.6 Study 6: A comparative study on the effect of the source of C57BL/6J mice on their ileal microbiota

Twenty-four male C57BL/6J mice were obtained from the inhouse facility DMU and commercial vendor, Charles River Laboratories, UK (CRUK). The CRUK mice were purchased at the age of ten weeks and held for two weeks under a chow diet at the DMU in order to acclimatise to their new environment. At the age of twelve weeks, mice from CRUK and DMU were further divided into four groups; 1) CRUK chow (n=6), 2) CRUK LF (n=6), 3) DMU chow (n=6) and 4) DMU LF (n=6). The mice were fed the chow diet (RM3-P) and/or a purified LF diet (original high sucrose LF diet: D17060802, Research Diets, USA) for a period of four weeks. The effect of the source (vendor) of mice on the gut-liver axis is characterised in Chapter 6.

2.6 Gene expression analysis

Liver and ileum samples were homogenised in 1 ml Qiazol (Qiagen, UK) per 100mg of tissue for 30 seconds at 6000 rpm in a Precellys®24 (Bertin Technologies, France). After homogenization, the samples were transferred into new Eppendorf tubes and 200µl chloroform was added. Samples were then centrifuged for 15 minutes at 12,000 RPM at 4˚C and the aqueous layer was transferred to a new 2ml collection tube. Isopropanol (500µl per ml) was added and mixed by inverting the tubes, rested for 5-10 minutes on ice and then centrifuged for 10 minutes at 12,000 RPM at 4˚C. The RNA pellet that was left, was washed twice with 80% ethanol and dissolved in 100µl RNase free water. RNA concentration was measured with a Nanodrop (Thermo Scientific, Wilmington, USA). A 260/280nm ratio of ~1.8 was considered an acceptable indicator of good RNA quality. The ratio of absorbance at 260/230nm is used as a secondary measure of RNA purity. A ratio within the range 2.0 - 2.2 was considered pure. A ratio of lower than 2, may indicate contaminants in the sample.

Complementary DNA (cDNA) was synthesized from 2µg of RNA which was first treated with DNase and subsequently reverse transcription was performed using SuperScript III Reverse Transcriptase. A quantitative polymerase chain reaction (qPCR) was performed using SYBR green master mix according to the manufacturer's instructions. Reactions were performed on Applied Biosystems ViiA 7 and 384 wells plate (Applied Biosystems, Thermo Fisher Scientific, UK) using 5µL of SYBR green and primer mix (full list of the primers used, please see table 2.5) and 1.5µL of cDNA (diluted 1:20). The reaction was initialized at 50°C for 5 minutes and 95°C for 2 minutes, after which 40 cycles of denaturation (95°C; 15 seconds) and annealing/extension (59°C; 1 min) were performed. Afterwards, a melting curve was created and checked for a single product per gene. Delta CT values were calculated by subtracting the CT value of the housekeeping gene TATA-box binding protein (*Tbp*) from the target gene CT value. The delta delta CT was calculated as the difference in delta CT as described above between the target and reference samples (Equation 1). The final result of this method is then presented as the fold change of target gene expression in a target sample relative to a reference sample, normalized to a reference gene. The housekeeping gene *Tbp* was used for all gene expression analysis using qPCR because of its optimal expression stability. Housekeeping gene *Tbp* has been reported to be a constantly expressed reference gene in mouse intestine and liver tissue (Wang et al., 2010; Tatsumi et al., 2008).

Equation 2. 1 Formula used to calculate delta delta CT value

$$\Delta CT = CT \text{ (target gene)} - CT \text{ (housekeeping gene)}$$

$$\Delta\Delta CT = \Delta CT \text{ (target sample)} - \Delta CT \text{ (housekeeping gene sample)}$$

Table 2.5 Primer sequence used for gene expression analysis.

Gene	Refseq	Forward	Reverse
Acaca	NM_133360	GAGGAAGTTGGCTATCCAG	GCAGGAAGATTGACATCAGC
Asbt	NM_011388	TGGAATGCAGAACACTCAGC	GCAAAGACGAGCTGGAAAAC
Chrebp	NM_021455.5	ACAAAAAGCGGCTCCGTAAGTCC	GGGGGCGGTAATTGGTGAAGAA
Cldn3	NM_009902.4	ACCAACTGCGTACAAGACGAG	CAGAGCCGCCAACAGGAAA
Cyp7a1	NM_007824.3	GAGCGCTGTCTGGGTCACGG	GCCAGCCTTTCCCGGGCTTT
Cyp8b1	NM_010012.3	TTGCAAATGCTGCCTCAACC	TAACAGTCGCACACATGGCT
Fabp	NM_008375	CACCATTGGCAAAGAATGTG	AACTTGTCACCCACGACCTC
Fasn	NM_007988.3	AGTGCGTGGGGCGCAATCTC	CGCTCGGCTCGATGGCTCAG
Fbp1	NM_019395.3	TAGACATCGTTCCCACCGAGAT	CTTCACTTGGCTTTGTGCTTCC
Fgf15	NM_008003	CAGTCTTCCTCCGAGTAGCG	TGAAGACGATTGCCATCAAG
Fgf21	NM_020013.4	ACACAATTCCAGCTGCCTTG	TAGAGGCTTTGACACCCAGG
Fgfr4	NM_008011	CTGCCAGAGGAAGACCTCAC	GTAGTGGCCACGGATGACTT
Fxr	NM_009108	GGCCTCTGGGTACCACTACA	AAGAAACATGGCCTCCACTG
Glut2	NM_031197.2	GTCGCCTCATTCTTTGGTG	CTGATACACTTCGTCCAGC
Glut5	NM_019741.3	TCATGACCATCCTCACGATCTTT	GCGGCCGTCAGCACTAAG
Il1b	NM_008361.4	GCCTCGTGCTGTCGGACC	TGTCGTTGCTTGGTTCTCCTTG
Khk	NM_001310524.1	CCCACCGCCCCGAGTAGTAGACA	CACACCTGCCGGGGAATGG
Ocln	NM_008756.2	AGCTCATAGTTCAACACAGCCTC	TTCTTCCACAGCTGAAGGACTCA
Ostα	NM_145932	TTGTGATCAACCGCATTTGT	CTCCTCAAGCCTCCAGTGTC
Ostβ	NM_178933	ATCCTGGCAAACAGAAATCG	GGCCAAGTCTGGTTTCTCTG
Sglt1	NM_019810.4	TGGTGTACGGATCAGGTCATTG	TTCAGATAGCCACACAGGGTACA
Shp	NM_011850	TCTGCAGGTCGTCCGACTATT	AGGCAGTGGCTGTGAGATGC
Tbp	NM_013684.3	GAAGCTGCGGTACAATTCCAG	CCCCTTGTACCCTTCACCAAT
Tlr4	NM_021297.3	GCTTTCACCTCTGCCTTCAC	GAAACTGCCATGTTTGAGCA
Tnfα	NM_001278601.1	CAGGGGCCACCACGCTCTTC	CTTGGGGCAGGGGCTCTTGAC
Zo-1	NM_009386.2	GGACCCTGACCACTATGAAACAG	ATAGGTGGATATTCCCTGACCCA

RNA Sequencing

After RNA isolation as described before, selected samples from Study 3 were sent to Novogene genome sequencing company (Cambridge, UK) for Illuminia based RNASeq analysis.

Microarray analysis

Selected samples from the IDEAL Study 5 were sent for microarray analysis at WUR. RNA quality was assessed with a Bioanalyzer (Aligent 2100 Bioanalyzer, Santa Clara, USA), and microarrays were performed using the Mouse geneChip 1.1 ST arrays from Affymetrix (Thermo Fisher Scientific, Santa Clara, USA). Arrays were normalised using Robust Multiarray Average and ~22 k genes were included in the data set.

Network Analyst 3.0 (Zhou et al., 2019) a web-based software application was used to analyse and interpret the data. Log2FC of 1.5 and a P value of 0.05 were used as cut-off points and only genes with an intensity of > 20, an interquartile range (IQR) >

0.1 were selected for further analysis. Ingenuity Pathways Analysis (IPA) web-based software application was used to explore canonical pathways affected by the filtered genes in the IDEAL study 5.

2.7 Histology

After fixation in 10% NBF, tissues were stored in 50% ethanol until embedding. The samples were processed on the Leica ASP 300, program overnight no formalin and the samples were embedded in Paraplast the next morning. Tissue sections were cut at 5μm thickness using a HistoCore BIOCUT - Manual Rotary Microtome and secured on SuperFrost Plus™ Adhesion slides (Thermo Scientific, UK) and mounted with DPX mounting medium. The next morning the slides were stained with haematoxylin and eosin (H&E) following the protocol from Feldman and Wolfe, (2014) and photographs were taken with an Olympus BX60 microscope at 4X and 10X magnification. Procedure for staining with H&E is detailed below.

Deparaffinize the slides as follows.

2 x 5 minutes Histoclear

2 minutes 100% ethanol

2 minutes 80% ethanol

2 minutes 70% ethanol

5 minutes Wash slides in distilled water

4 minutes Harris Haematoxylin

5 minutes wash under running distilled water

15 seconds 1% HCl/70% ethanol

15 seconds brief rinse with distilled water

1 minute 0.1% sodium bicarbonate

5 minutes distilled water

2 minutes Eosin

Rehydrate the slides as follows:

2 minutes 70% ethanol

2 minutes 80% ethanol

2 minutes 100% ethanol

5 minutes Histoclear I

5 minutes Histoclear II

Mount slides using DPX mounting medium.

2.8 Caspase 3 activity

This assay works with a Caspase-3 specific tetrapeptide substrate DEVD and a fluorochrome 7-Amino-4-trifluoromethylcoumarin (AFC). Active caspase specifically hydrolyses the substrate DEVD-AFC resulting in the release of fluorogenic AFC which can be quantified by a spectrophotometer at 400 nm excitation, 505 nm emission wavelength.

Proteins from 30mg of liver samples were extracted using the AFC lysis buffer (Table 2.6) and prepared for the Caspase 3 assay following the manufacturer's instructions.

Table 2.6 AFC lysis buffer composition for caspase 3 activity assay.

AFC-Lysis buffer	Volume	Final concentration
Hepes 1M pH 7.4	100µL	10mM
Chaps 10%	100µL	0.1%
EDTA 0.5mM pH 8	40µL	2mM
DTT 1M	50µL	5mM
dH2O	9.71ml	

2.9 Hepatic triglycerides measurement

The triglycerides were extracted following an adjusted version of the Bligh and Dyer method (Bligh and Dyer, 1959). Approximately 50mg of liver tissue was homogenized in 200µl of chloroform and 400µl of 100% methanol. To this solution, 160µl distilled water was added, and the sample was homogenized again after which the sample was centrifuged for 10 minutes at 12,000 RPM at 4°C. The organic lower layer was subsequently transferred to clean Eppendorf tubes and the chloroform was evaporated overnight in the fume hood. The dried pellet was dissolved in 250µl of 2% Triton X-100 (Laboratory grade, Sigma-Aldrich) and this solution was used to perform the colorimetric assay by using the triglycerides liquicolor kit following the manufacturer's protocol.

2.10 Bile acids analysis

Bile acids were measured in the liver and ileal tissue samples. Ileal tissue was used instead of ileal content because of limited content sample. Approximately 25mg of tissue was homogenised in 1ml of ice cold 70% methanol for 30 seconds and 6000 RPM in a Precellys®24 (Bertin Technologies, France). After centrifugation (5 min, 12,000 RPM, 4°C) the supernatant was transferred to a new collection tube and methanol content was removed by using Speed-Vac vacuum concentrator (70 min, 50°C). Volume was restored to 1ml by adding 5% methanol. The samples were loaded onto OASIS PRIME HLB-1 30mg SPE cartridges (Waters, UK), washed twice with 5% methanol and eluted in 500µl 100% methanol.

Internal standards (d4) were added at the following time points: before homogenisation, before rotary evaporation, before loading onto cartridges, after elusion (for information on standards please refer to Supplementary data 2). Cleaned-up extracts were analysed using High-performance liquid chromatography (HPLC) – mass spectrometry operated in multiple reaction monitoring (MRM) mode.

The mass spectrometer was operated in electrospray negative mode with capillary voltage of -4500V at 550˚C. Instrument specific gas flow rates were 25ml/min curtain gas, GS1: 40ml/min and GS2: 50ml/min. Please see supplementary data 2 for Liquid chromatography–mass spectrometry (LC-MS) conditions and mass fragmentation monitoring values. Quantification was applied using Analyst 1.6.2 online tool (SCIEX, 2020 DH Tech. Dev. Pte. Ltd) to integrate detected peak areas relative to the deuterated internal standards.

2.11 Microbiota analysis

Microbial DNA was isolated from approximately 50mg ileal luminal content with the Qiagen DNA mini kit. Additional steps were added to the DNA mini kit protocol to ensure breakage of all bacterial samples. Briefly, the samples were homogenised using silica glass beads for 4x 30 seconds at 6000 rpm in a Precellys®24 (Bertin Technologies, France) and heated to 95°C for 5 minutes. Additionally, samples were incubated with a lysis buffer containing 20mg/ml lysozyme (Lysozyme from chicken egg white, Sigma-Aldrich) after which the homogenising was repeated. The lysozyme was used to help effectively capture usually difficult to lyse taxa, such as gram-positive bacteria. Consequently, DNA was isolated using the Qiagen DNA mini kit following instructions from the manufacturer. DNA quantity was assessed using a Nanodrop 2000 Spectrophotometer (Fisher Scientific, UK).

A minimum of 50ng of DNA was sent to Novogene (Cambridge, UK). Quality assessment was performed by agarose gel electrophoresis to detect DNA integrity, purity, fragment size and concentration. The 16S rRNA amplicon sequencing of the V4 region was performed with an Illumina MiSeq (paired-end 250 bp; San Diego, CA). Alpha and beta diversity were calculated by QIIME and displayed with R software (Novogene, Cambridge). Comprehensive statistical and meta-analysis including differential analysis of taxa abundance was completed with the online tool Microbiome Analyst 5.0 (Chong et al., 2020). More information on sequencing data processing in supplementary data 2.

2.12 Statistics

Statistician analysis has been performed using Graphpad Prism (Version 8). The statistical tests used are indicated in each figure legend. When diet groups were compared over time or LPS as a variable, a 2-way ANOVA with Bonferroni post-hoc test was used, when three or more groups were compared at a single time point a 1-way ANOVA was used with Tukey's multiple comparison. Lastly, when two groups were compared at one time point, an unpaired t-test was used to test for significance. $p < 0.05$ was considered overall as statistically significant and indicated as ***= $p < 0.001$ **= $p < 0.01$ *= $p < 0.05$. Data not following a normal distribution detected by the Kolmogorov-Smirnov test were assessed by nonparametric tests.

Chapter 3: Choice of control diet profoundly influences the gut-liver axis

3.1 Introduction

Animal models are invaluable for biomedical research. Factors such as genetic background and environmental conditions are given importance when designing experiments to ensure reproducibility. However, the choice of diet is often overlooked, especially if the diet is not the focus of the study. Several research studies have drawn conclusions about dietary effects on metabolism, pathophysiology or immunology from comparing the standard chow diet with purified diets (Warden and Fisler, 2008).

The choice of experimental diet is typically selected based on the quantity of carbohydrates or fats to best induce the condition being investigated. However, the qualitative composition of the diet is also of great importance. For example, standard chow diet is based on a variety of grains and cereals such as wheat, wheatfeed, soya, barley (SDS diet, UK). The exact formula of the chow diet is often not defined, furthermore, the amount of each ingredient used can vary widely depending on the batch, source and season. In contrast, purified diets are composed of refined ingredients and the formula of the diet is well defined and shared with researchers. The main source of carbohydrates in purified diet comes from corn starch, casein for protein, soybean oil for fat and cellulose for fibre (e.g. low-fat diet (LF), American Institute of Nutrition 93 maintenance, AIN-93M, Research Diets, USA). The use of refined ingredients allows the researchers to report the exact formula of the diet used in their study, replicate the composition of the diet or modify the individual components to meet the experimental needs of the study.

It is widely accepted that choice of diet can impact the overall health of the host (Santos-Marcos et al., 2019). The relationship between diet and the gut microbiota can have an influence on the absorption of nutrients, metabolism, immune system and behavioural outcomes (Gentile and Weir, 2018; Almeida-Suhett et al., 2019). The dietary fibres (DF) from wheat and barley in the chow diet can be degraded by the host's gut microbiota thereby, influencing the bacterial population. Whereas, the purified diet contains refined carbohydrates (sucrose and starch) that are readily digested by the host. The LF diet contains reduced DF content compared to chow, and DF in the LF diet solely comes from cellulose, which is an insoluble fibre, and does not interact with the gut microbiota (Soliman, 2019).

In this chapter we aimed to characterise the effects of the two diets, the grain based chow (RM3-P, SDS Diets, UK) and a highly refined low-fat diet (LF) (D17060802, based on the AIN-93M, Research Diets, USA) on the gut-liver axis of mice. The study provides an opportunity to compare diets that are similar in calories but differ in macronutrient composition. It is widely reported that long-term consumption of high refined carbohydrate diet can lead to sustained hyperglycaemia that can contribute to non-alcoholic fatty liver disease (NAFLD) (Jegatheesan and De Bandt., 2017). We hypothesised that the difference in the carbohydrate composition of the chow and LF diet may lead to an 'unhealthy' gut-liver phenotype in mice. Further, due to the lack of fibre and high content of easily metabolizable carbohydrates, we hypothesised that the gut-liver axis of LF fed mice is more susceptible to an inflammatory challenge. To test this hypothesis, we aimed to create a model of

episodic systemic inflammation by injecting the mice with low dose of lipopolysaccharide (LPS) once a week for 4 weeks (Raduolovic et al., 2018; López-Collazo and del Fresno, 2013). This model was chosen to mimic recurrent systemic inflammation that is observed during ageing and may give us an insight into the long-term effect of the LF diet on the functioning of the gut and liver of mice.

3.2 Results

3.2.1 Body composition of mice fed with chow and LF diet

Standard chow diet and a purified LF diet were compared over a period of four weeks. Figure 3.1 shows compositional profile of chow and LF diet. Full composition of the diet is available in supplementary data 1.
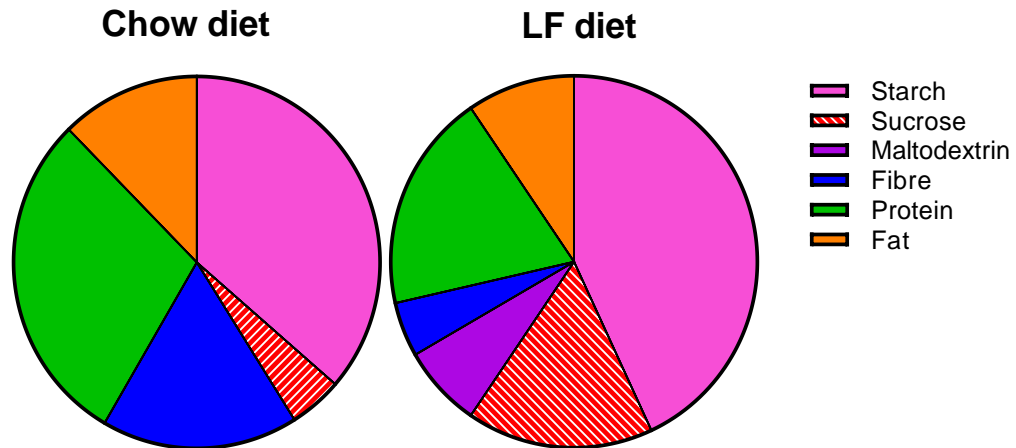
Figure 3.1 Summary of the composition of chow and LF diet per kilogram. The LF diet contains decreased fibre and increased sucrose and starch compared to the chow diet.

As shown in Figure 3.2, body weight and average calorie intake was similar between chow and LF fed mice after 4 weeks intervention (Fig. 3.2A and B). We analysed the length of small intestine and weight of liver to show no difference between the diet groups (Fig. 3.2C and D). To get a further insight into the metabolic phenotype induced by the LF diet, we quantified the triglycerides content in the liver to show increased levels in the LF fed group ($60\pm0.1\%$, $P=0.004$) (Fig. 3.2E). Furthermore, histological analysis showed hepatocyte ballooning and lipid droplet accumulation in the livers of mice fed with the LF diet compared to chow (Fig.3.2 F and G).
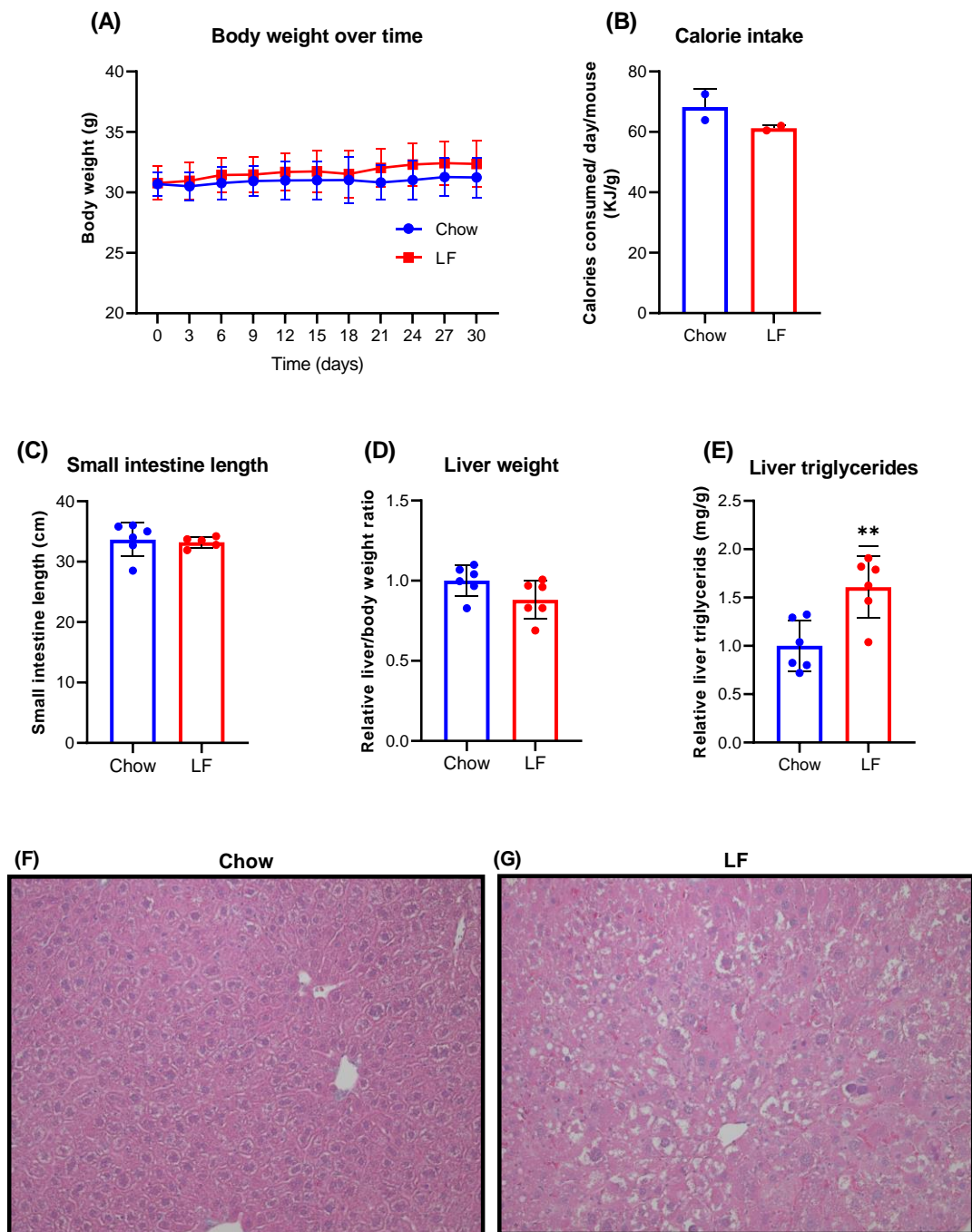
Figure 3.2 Mice were fed a standard chow diet or a purified low-fat (LF) diet for 4 weeks. During this time, no differences in either body weight (A) or calorie intake (B) were observed. Small intestinal length (C), and liver weight (g) to body weight (g) ratio (D) were recorded after sacrifice and did not show difference between the two diet groups. Triglyceride content in the liver (E) and histological analysis with haematoxylin and eosin (H&E) staining of the liver sections from the chow (F) and LF group (G) showed accumulation of lipid droplets in the LF fed mice. Significance was tested using 2-way ANOVA with Bonferroni post-hoc test (A) and unpaired t-test for B, C, D, and E (***=p<0.001, **= p<0.01, *= p<0.05). Values are the means ± SEM of n=6 mice in each group. Mice per group were divided into two cages (as 3 mice per cage), calorie intake was measured per cage and divided by 3 to calculate the intake of one mouse.

3.2.2 Increased expression of lipogenic genes in the livers of the LF group

The increase in fat accumulation observed through histological and triglyceride analyses was also reflected on gene expression level in the liver. We examined the gene expression of sterol regulatory-element binding protein 1 (*Srebp1*) transcription factor involved in *de novo* lipogenesis to show increasing trend in response to the LF diet (55±0.2% P=0.05). While SREBP1 target genes; acetyl-CoA carboxylase alpha (*Acaca*) and fatty acid synthase (*Fasn*) were shown to be significantly increased in response to the LF diet (110±0.3%, 160±0.6%, P<0.05 respectively). Gene expression analysis of fibroblast growth factor 21 (*Fgf21*) suggested an increasing trend in the LF group (P=0.08). FGF21 is a peroxisome proliferator-activated receptor α (PPARα) target and PPARα is a regulator in *de novo* lipogenesis pathway (Rusli et al., 2016) (Fig. 3.3 A, B, C, and D).

The gene expression levels of hepatic fructokinase *Khk* was found to have an increasing trend in the LF compared to chow diet group (55±0.2%, P=0.08), whereas the glucose transporter 5 (*Glut5* also known as *Slc2a5*) mainly involved in the transport of fructose was not changed between the two groups (Fig. 3.3 E and F).

The gene expression of toll like receptor 4 (*Tlr4*) a pattern recognition receptor that recognizes pathogens to induce innate immune system, and pro-inflammatory cytokines interleukin 1 beta (*Il1β*) were found to have increasing trends in the liver of mice fed with the LF diet (*Tlr4* 56±0.2% P=0.06 and *Il1β* 70±0.3%, P=0.07) (Fig. 3.3 G and H). Altogether, assessment of liver lipid content, histological and gene expression analysis showed that LF diet fed mice presented increased fat deposition in parallel with increased triglycerides levels without liver weight differences when compared to chow fed mice.
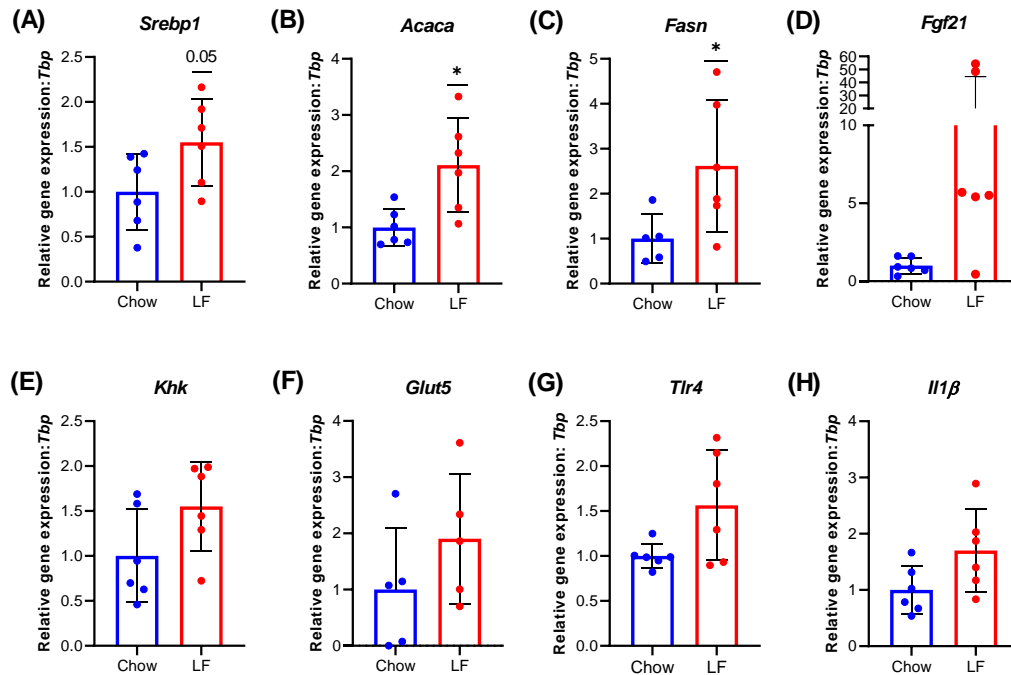
Figure 3.3 Liver expression profiles of lipid, carbohydrate metabolism genes. *Srebp1* (A), *Acaca* (B), *Fasn* (C), *Fgf21* (D), *Khk* (E) were found to be increased in response to the low-fat (LF) diet. Fructose transporter *Glut5* (F) was not changed between the two diet groups. The expression levels of inflammation related genes *Tlr4* (G) and *Il1β* (H) showed an increasing trend in the LF diet group. Significance was tested using unpaired t-test method (***=p<0.001, **= p<0.01, *= p<0.05). Values are the means ± SEM of n=5-6 mice in each group.

3.2.3 Sequencing of 16S rRNA from the ileum microbiota in response to the chow and LF diet

Shannon diversity relates both operational taxonomic unit (OUT) richness and evenness while, observed species is the total number of species in the community (only richness) (Kim et al., 2017). Figure (3.4 A and B) shows a trend towards decreasing Shannon index (26±0.3%, P =0.05) and significantly increased observed species (17±10%, P=0.04) in the LF diet group. Beta diversity compares microbial communities between samples based on their composition. To compare the microbial communities between samples, the distance or dissimilarity between each sample is calculated and then an ordination-based method such as principal coordinates of analysis (PCoA) is used for visual representation at low-dimensional space (Microbiome Analyst; Chong et al., 2020). To measure the dissimilarity between microbial communities in chow and LF fed mice, PCoA was performed with Bray-Curtis dissimilarity (Fig. 3.4 C). The percentage on each axis indicates the contribution value to discrepancy among samples. PCoA plot showed that after four weeks feeding of the diets, there was a clear clustering of ileal microbiota from chow samples compared to LF diet. Samples from chow fed mice (blue dots) are clustered to the left, which indicates compositional differences, and is confirmed by a significant result in the ANOSIM (analysis of group similarities, P value ANOSIM = 0.003). Analysis of the relative abundance at the phylum level revealed decreased

abundance of *Bacteroidetes* by 82±0.1% (P<0.0001) in ileum of LF fed mice, whereas relative abundance of *Firmicutes* was significantly increased by 52±0.1% (P<0.0001) in the LF group (Fig. 3.4 D). Figure 3.4 E shows altered microbial profiles at the genus level in the individual mice in each group. Relative abundance of *Bacteroidetes S247* group is consistently increased in the chow fed mice, while, *Romboutsia* and *Lactococcus* from *Firmicutes* phylum is prevalent in the LF fed mice. Moreover, Table 3.1 shows genera that were significantly different between chow and LF diet group. Our results show differential ileal microbiota composition in response to chow and LF feeding in mice.
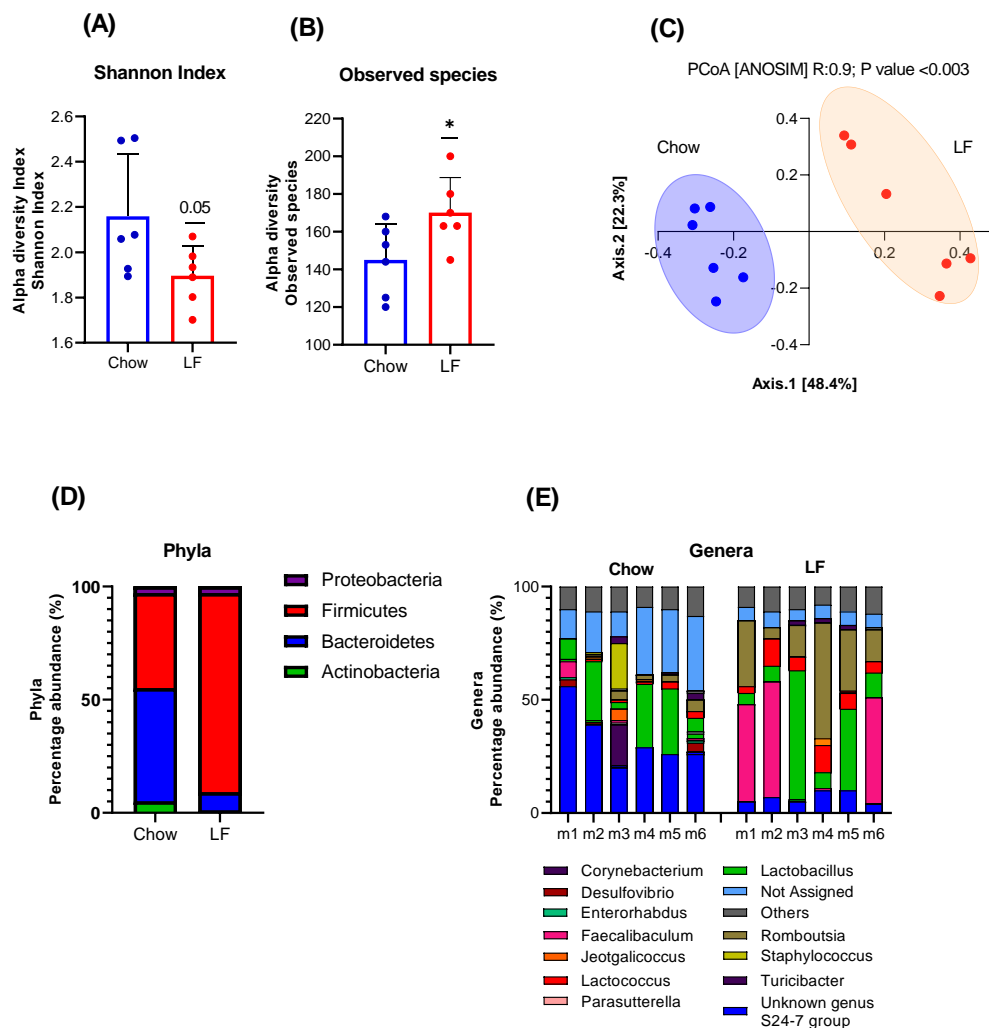
Figure 3.4 Ileal microbial composition in chow and low-fat (LF) fed mice. Alpha diversity for chow and LF diet groups (A). Beta diversity profiling of chow and LF ileal microbiota. Principal coordinates of analysis (PCoA) was carried out at the genus level. Chow samples are plotted as blue dots, and LF are represented as red dots. The groups show significant differences in similarity tested by ANOSIM (P value = 0.003) (B). At the phylum level the *Firmicutes: Bacteroidetes* ratio was increased in LF fed mice (C). Genera profiles of individual mice in the chow and LF group (E). Significance was tested by performing Kruskal-Wallis test for alpha diversity measures (*= p<0.05). Values are the means ± SEM of n=6 mice in each group.

Table 3.1 Genera that were different in the ileum of chow and low-fat (LF) fed mice. Values are based on absolute abundance. Significance was calculated using unpaired t-test, (**= p<0.01, *= p<0.05). Values are the means of n=6 mice in each group.

Genera	Phyla	Mean Chow	Mean LF	SE of difference	P value
Faecalibaculum	*Firmicutes*	1336	15476	6728	0.062
Lactococcus	*Firmicutes*	1236	5138	1014	0.003**
Romboutsia	*Firmicutes*	1925	15410	4243	0.010*
Unknown genus S24-7 group	*Bacteroidetes*	21365	4776	3496	0.001**
Cronobacter	*Proteobacteria*	30.2	154.6	57.2	0.04*
Stenotrophomonas	*Proteobacteria*	9.7	232.3	76.4	0.015*

3.2.4 The effect of diets on ileal bile acids profile and gene expression

The interaction between the microbiota and the liver is linked through the portal vein, which carries gut-derived products to the liver, and the feedback of bile acids from the liver to the small intestine. Alterations in the gut microbiota are also associated with changes in the bile acid homeostasis (Molinaro et al., 2018). Therefore, to further investigate the effects of the altered microbiota between the two diets, bile acids present in the ileal tissue at the time of sacrifice were analysed via liquid chromatography–mass spectrometry (LC-MS) as described in Chapter 2 of this thesis. Cholesterol in the serum was quantified to show no difference between the two diet groups (Fig. 3.5A). The total bile acids were shown to be significantly increased by 72±0.2% (P=0.03) in response to the LF diet (Fig. 3.5B). Further analysis of the individual bile acids revealed primary bile acids to be significantly enhanced by 67±0.2%, P=0.03 in the LF group (Fig. 3.5B). Taurine conjugated primary bile acid TβMCA and taurine conjugated secondary bile acids TUDCA were significantly increased by 196±338% and 975±48% (P=0.003, 0.03 respectively) in the ileum of LF compared to chow fed mice (Table 3.2). The gene expression levels of bile acid uptake transporter *Asbt* and the gut enterokine, fibroblast growth factor 15 (*Fgf15*) showed a trend towards increased expression in the LF fed mice (P>0.05). However, the expression levels of farnesoid X receptor, *Fxr* and bile acid organic solute transporter alpha, (*Ostα*) were not altered in the ileum (Fig. 3.5C). Moreover, in the liver, the gene expression levels of bile acid synthesis enzyme, cholesterol 7α-hydroxylase (*Cyp7a1*), *Fxr*, and its targets; fibroblast growth factor receptor 4 (*Fgfr4*) and small heterodimer partner (*Shp*) also remained unchanged in chow and LF fed mice (Fig. 3.5D).
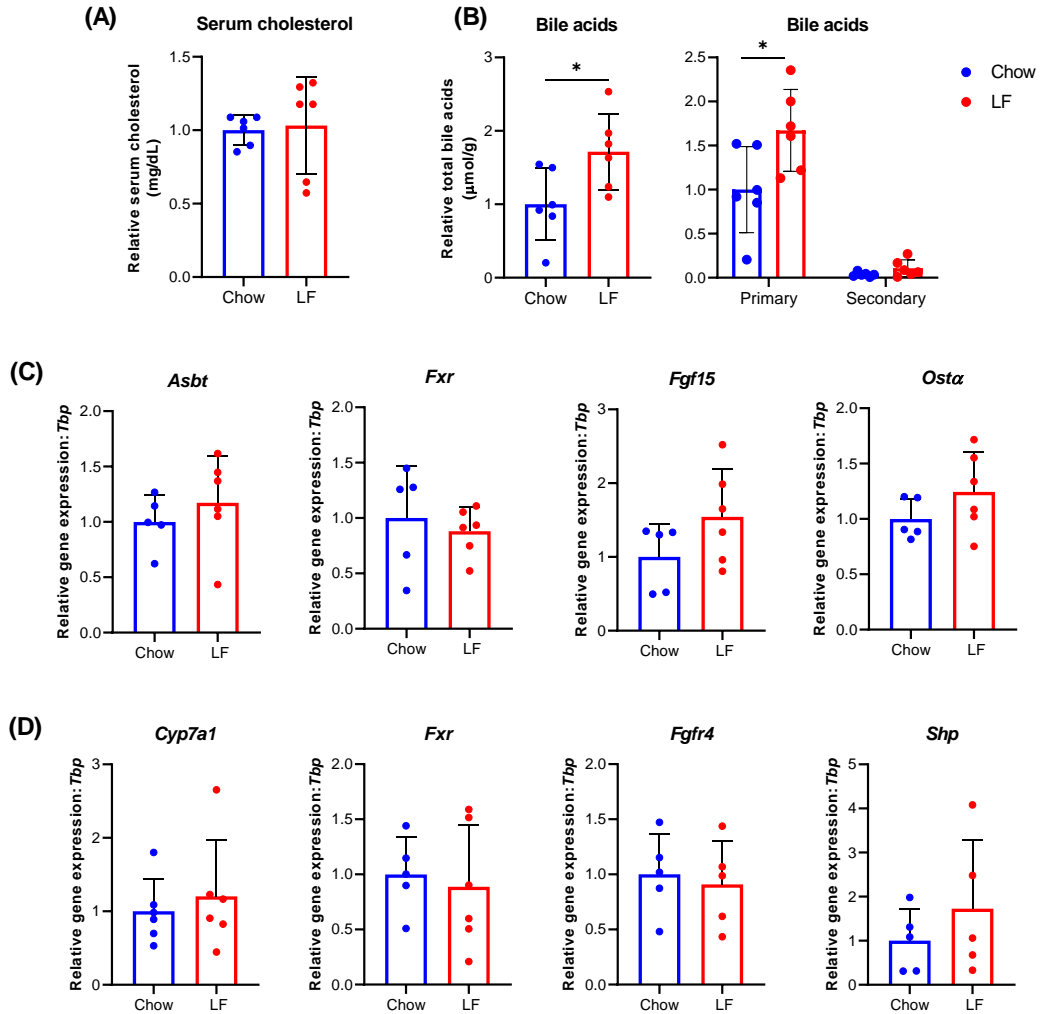
Figure 3.5 Bile acids profile and gene expression in the ileum and liver in response to the low-fat (LF) diet. Serum cholesterol levels were not significantly different between the diet groups (A). In the ileum total and primary bile acid levels were significantly increased in response to LF diet (B). Bile acid related genes were tested to show a trend towards an increase in the expression levels of *Asbt* and *Fgf15*, in the ileum of LF mice (C). Bile acid related genes in the liver were not altered between the diet groups (D). Significance was calculated using unpaired t-test (*= p<0.05). Values are the means ± SEM of n=5-6 mice in each group.

Table 3.2 Ileal bile acids profile show increased levels in mice fed the low-fat (LF) diet compared to chow. Bile acid were quantified in ileal tissue by liquid chromatography–mass spectrometry (LC-MS) and are given in µmol/g tissue. Significance was calculated using unpaired t-test (**= p<0.01, *= p<0.05). Values are the means of n=5-6 mice in each group.

	Mean chow	Mean LF	SE of difference	P value
αMCA	103.2	169.5	49.8	0.2
βMCA	554.1	692.2	152.7	0.4
CA	405.5	494.4	74.3	0.3
CDCA	10.1	12.2	3.8	0.6
MCA	6.6	11.7	3.0	0.1
TαMCA	366.1	680.6	212.8	0.2
TβMCA	666.8	1979	338.2	0.003**
TCA	665.2	603.9	202.4	0.8
TCDCA	13.8	35.7	11.3	0.1
DCA	29.2	22.0	12.0	0.6
HDCA	6.1	7.2	3.8	0.8
LCA	3.0	2.4	0.5	0.2
TDCA	26.7	72.1	32.3	0.2
TUDCA	12.2	131.2	48.7	0.034*
UDCA	11.2	13.9	5.1	0.6

3.2.5 Impact of diets on the ileum villus and crypt morphometry and barrier function genes

Due to the nutrient compositional changes in the chow and LF diet, we hypothesized alterations of the small intestinal physiology. H&E analysis of the ileal samples of mice fed the experimental diets showed no changes in villus height or crypt depth (Fig. 3.6A, B and C). Next, we tested the gene expression related to ileal barrier function in response to the two diets. Figure 3.6D shows LF diet led to decreasing trend in levels of mucin 2 (*Muc2*) (by 32±0.1% P= 0.08), and significantly decreased expression levels of claudin 3 (*Cldn3*) (by 35±0.1%, P= 0.04) and zonula occluden protein (*Zo-1*) (also known as tight junction protein 1, *Tjp1*) (40±0.1% ,P=0.01). Altogether, the barrier function genes were found to be downregulated in the ileum of LF fed mice.
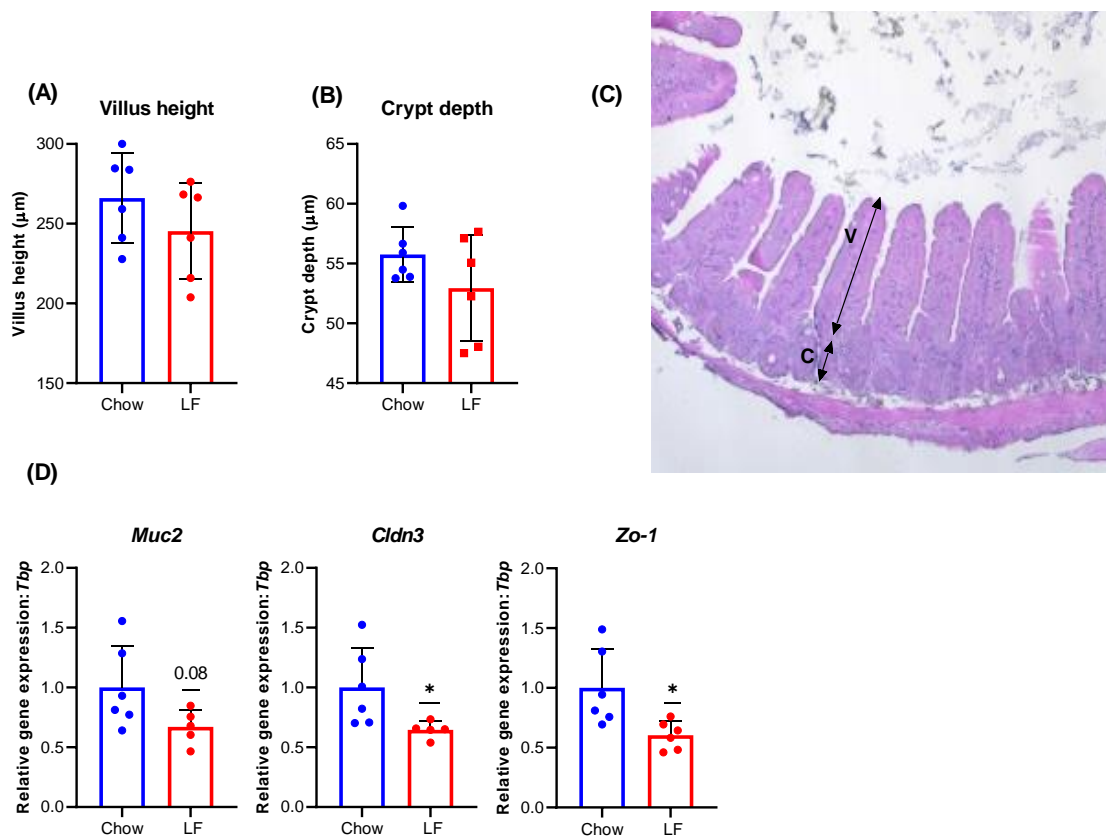
Figure 3.6 Changes in ileal physiology in response to the low-fat (LF) diet. Ileal physiology was analysed by haematoxylin and eosin (H&E) staining and barrier function genes were measured in response to the LF diet. Villus height (A) and crypt depth (B), Photomicrograph showing villi and crypts in section of ileum (Images were taken at 4x magnification) (C) Gene expression of *Muc2*, *Cldn3* and tight junction protein *Zo-1* in the ileum were tested with qPCR (D). Significance was tested by using unpaired t-test (*= p<0.05). Values are the means of n=5-6 mice in each group. qPCR: Quantitative polymerase chain reaction.

3.2.6 Increased expression of carbohydrate metabolism related genes in the ileum of LF diet fed mice

We analysed the gene expression of two α-glucosidases, maltase-glucoamylase (*Mgam*) for starch and sucrase-isomaltase (*Sis*) for sucrose hydrolysis. The gene expression levels of *Mgam* and *Sis* were shown to be significantly increased in the LF diet compared to the chow group (*Mgam*: 99±0.2%; *Sis*:68±0.1%, P<0.001) (Fig. 3.7A and B). After hydrolysis, the released monosaccharides (glucose and fructose) are transported by the epithelial cells into the bloodstream via sodium-dependent glucose cotransporter (SGLT1) and glucose transporters found in the membrane of enterocytes, GLUT2 for glucose and GLUT5 for fructose (Goodman, 2010). Gene expression levels for *Sglt1* and *Glut2* were found to show a significant increase in the ileum of mice fed the LF diet (*Sglt1*: 58±0.1%; *Glut2*: 350±0.7%, P<0.001) (Fig. 3.7C and D). The expression levels of fructose metabolism genes, *Glut5* and *Khk* showed a trend towards an increase in the LF fed mice, however it did not reach significance (P= 0.1) (Fig. 3.7E and F). Glucose 6-phosphatase (*G6pc*), a key

gluconeogenic gene was tested to show significant increase in the LF group (182±0.4%, P=0.003) (Fig. 3.7G). Whereas, triokinase (*Tkfc*) that converts glyceraldehyde to glycolytic/gluconeogenic intermediate glyceraldehyde 3-phosphate (GA3P) did not change between the two diet groups (Fig. 3.7H).
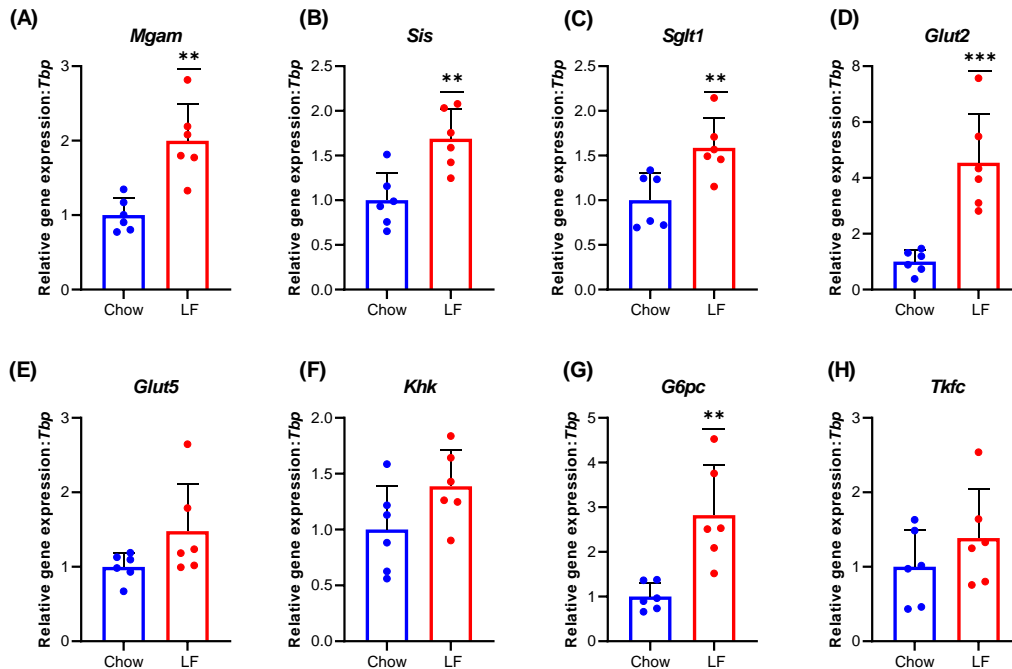
Figure 3.7 Genes related to carbohydrate metabolism are increased in the ileum of mice fed the low-fat (LF) diet compared to chow. Significance was tested using unpaired t-test (***= p<0.001, **= p<0.01). Significance was calculated using unpaired t-test (*= p<0.05). Values are the means ± SEM of n=6 mice in each group.

3.2.7 LPS administration in mice enhances the LF diet induced detrimental effects on the liver

The low dose LPS challenge provided an experimental model of periodic systemic low-grade inflammation that is a typical feature of ageing (Howcroft et al., 2013; d'Avila et al., 2018). This experiment aimed to investigate the response of the gut-liver axis to the high fibre chow and low-fibre, high refined carbohydrate purified (LF) diet in a state of mild systemic inflammation induced by an intraperitoneal dose of 0.5mg LPS per kg body weight per week for 4 weeks (Raduolovic et al., 2018). The control group received equal amount of sterile phosphate buffered saline (PBS) (Fig. 3.8).
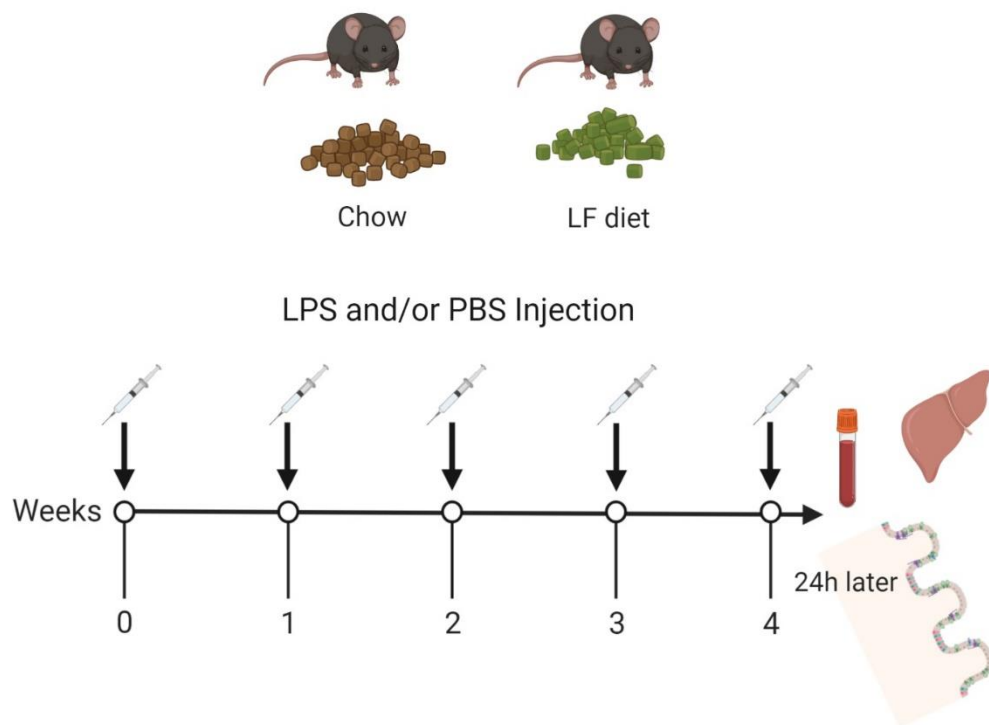
Figure 3.8 Summary of the LPS challenge experiment. Mice were divided into four groups: chow + PBS, LF + PBS, chow + LPS and LF + LPS. During the feeding experiment, mice were administered with LPS or sterile PBS per week for four weeks. At the time of sacrifice, blood, liver and ileum samples were collected. Low-fat diet: LF, PBS: Phosphate buffered saline, LPS: Lipopolysaccharide

We did not observe a significant difference between the weight gain of chow and chow LPS group, whereas LF LPS mice showed decreasing weight gain compared to the LF control group ($36\pm0.4\%$, P=0.04) (Fig. 3.9A and B). There was no difference observed in calorie intake between the groups (Fig. 3.9C). The liver weight of mice did not change in response to diets or the LPS challenge (Fig. 3.9D). Increased liver stress was quantified by measuring caspase 3 activity as an indication of apoptotic cells and showed a significant increase in the LF LPS group compared to LF control ($90\pm0.1\%$, P<0.0001). Moreover, the caspase 3 activity was also increased in LF LPS compared to chow LPS group ($50\pm0.1\%$, P=0.001) (Fig. 3.9E). Similar to the first study, liver histology showed hepatocyte ballooning and accumulation of lipid droplets in the livers of mice fed with LF diet (Fig.3.10B). Livers from the LF LPS group showed hepatocyte ballooning as well as increased inflammation illustrated by the large number of monocytes around the vein (Fig.3.10D).
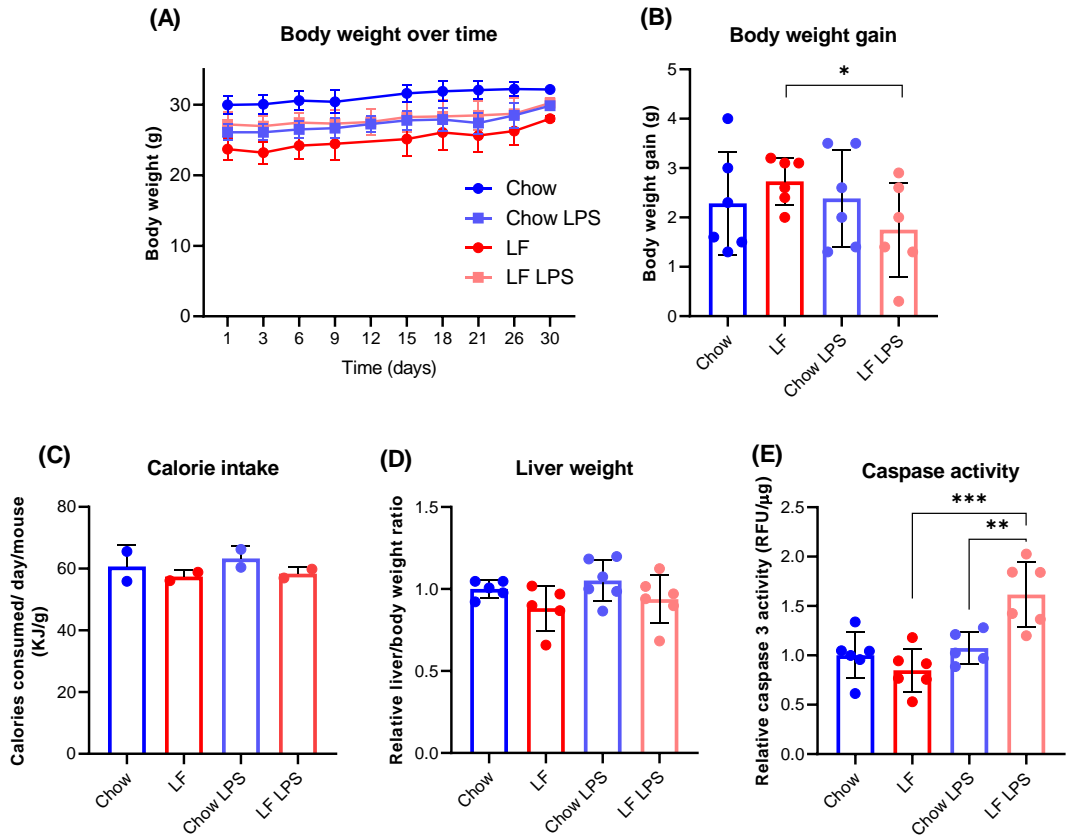
Figure 3.9 Body weight, calorie intake and liver phenotype were analysed in response to the LPS challenge. Body weight changes during the experiment (A), Body weight gain at the end of 4 weeks (B), and average calorie intake of mice in the different groups (C). Liver weight (g) relative to body weight (g) ratio showed no difference between the groups (D). Apoptosis was measured in the liver by caspase 3 activity (C3) assay and the LF LPS group C3 activity was significantly increased compared to LF control and chow LPS group. Significance was tested using 2-way ANOVA with Tukey's multiple comparison test between the groups (***= p<0.001, *= p<0.05). Values are the means ± SEM of n=5-6 mice in each group. Mice per group were divided into two cages (as 3 mice per cage), calorie intake was measured per cage and divided by 3 to calculate the intake of one mouse. Low-fat diet: LF, LPS: Lipopolysaccharide.
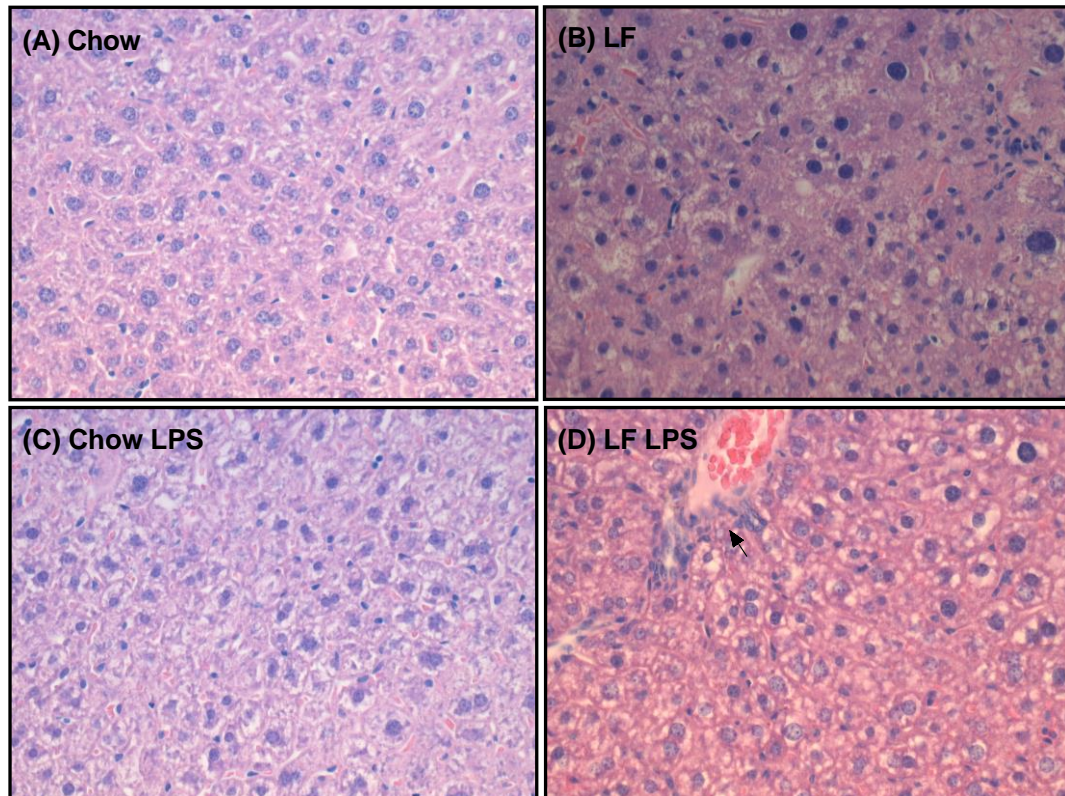
Figure 3.10 Histological analysis of livers. Liver sections were stained with haematoxylin and eosin (H&E) and micrographs taken at 20x magnification, chow (A), Low-fat (LF) (B), chow LPS (C), and LF LPS (D). Arrow on the LF LPS micrograph denotes accumulation of monocytes. LPS: Lipopolysaccharide.

Expression of lipogenic gene *Fasn* was observed to be increased in the liver in response to the LF compared to chow fed mice (169±0.4%, P=0.01). The gene expression of *Fgf21* showed an increasing trend by 548±3%, P=0.1 in the livers of LF mice. This LF induced effect was observed regardless of LPS treatment (chow LPS vs LF LPS 124±0.4%, P=0.03; 753±3%, P=0.1, *Fasn* and *Fgf21* respectively) (Fig. 3.11A and B).

Treatment with LPS led to increased expression of inflammation related genes, serum amyloid 1 (*Saa1*) (Fig. 3.11C), tumour necrosis factor alpha (*Tnfα*) (Fig. 3.11D), macrophage marker; mouse epidermal growth factor-like module-containing mucin-like hormone receptor-like 1 (*F4/80*) (Fig. 3.11E), and nucleotide-binding domain-like receptor (*Nlrp3*) (Fig. 3.11F), in chow LPS compared to chow control (*Saa1*: 412±0.9%, P=0.001; *Tnfα*: 350±1%, P=0.0007; F4/80: 140±0.5%, P= 0.001; *Nlrp3*: 112±0.3%, P=0.0008), and in LF LPS compared to LF control (*Saa1*: 315±0.9%, P=0.001; *Tnfα* 178±1% P=0.01; *F4/80*: 132±0.5%, P=0.002; *Nlrp3*: 48.5±0.3%, P=0.04). The increased expression of the inflammation related genes confirms that the LPS injections successfully induced an inflammation response in the liver. We observed a trend towards increased expression of *Saa1*, *Tnfα, F4/80* and

Nlrp3 in LF LPS compared to chow LPS group, however the difference did not reach significance due to the variability in responses in the group (P>0.1).
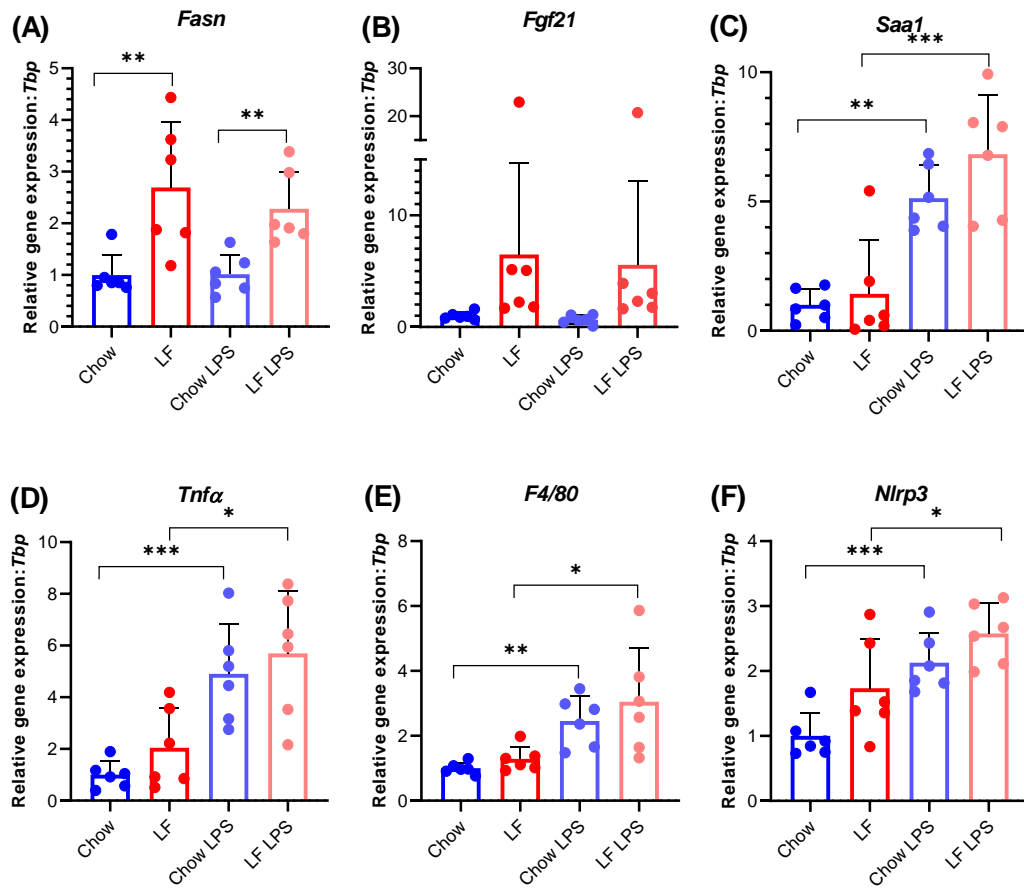
Figure 3.11 Gene expression analysis of liver. Increased expression of lipid metabolism related genes; *Fasn* (A) in the liver of low-fat (LF) (control and LPS) group compared to chow counterparts. The gene expression levels of *Fgf21* showed an increasing trend with LF diet independent of LPS treatment (B). Expression of inflammation related genes, *Saa1, Tnfα, F4/80* and *Nlrp3* was increased in mice injected with LPS regardless of diet (C, D, E, and F). Significance was tested using 2-way ANOVA with Tukey's multiple comparison test (***= p<0.001, **= p<0.01, *= p<0.05). Values are the means ± SEM of n=5-6 mice in each group. LPS: Lipopolysaccharide.

3.2.8 The response of ileum to the LPS challenge in mice fed with chow and LF diet
Due to the previously observed differences in the expression of barrier function
genes, intestinal permeability was tested using fluorescein isothiocyanate, FITC-
dextran. FITC-dextran was administered via oral gavage two hours before sacrifice
and the appearance of fluorescence was measured in the serum. A higher
fluorescence indicates an increase in gut permeability, as FITC-dextran crosses the
intestinal epithelium. Increased concentrations of FITC-dextran were observed in
mice fed the LF diet and increasing trend was observed for the LF LPS treatment
group (chow vs LF: 265±1%, P=0.04; chow LPS vs LF LPS: 352±1%, P=0.08) (Fig.
3.12A). In line with FITC-dextran concentrations, barrier function genes were tested
to suggest decreased *Cldn3* and occludin, (*Ocln*) expression in groups fed the LF diet
(Fig. 3.12B). The barrier function gene expression showed decreasing trend in the LF
fed mice independent of the LPS challenge (chow vs LF: *Cldn3*: 30±0.04%, P<0.01;
Ocln: 18±0.1%, P=0.08 and, chow LPS vs LF LPS: *Cldn3*: 33±0.1%, P=0.02; *Ocln*:
42±0.2%, P=0.05). Inflammation related genes were tested to show a significant
increase in expression of interleukin 1 β (*Il1β*) and *Tnfα* in the LF LPS compared to
LF control group (Fig. 3.12C). The expression of myeloid differentiation primary
response gene 88, (*Myd88*) showed an increasing trend in LF LPS mice (P>0.1). The
gene expressions of *Il1β* and *Tnfα* were also shown to be increased in LF LPS
compared to chow LPS mice. While no difference in inflammation related gene
expression was observed between chow and chow LPS group. Our previous findings
showed the expression of carbohydrate related genes, *Mgam*, *Sis* and *Glut2* to be
increased in the ileum of LF mice. The current study reproduced this effect in the
control as well as LPS treated LF fed mice. However, the carbohydrate metabolism
genes were not affected by LPS treatment (Fig. 3.12D). Summary of statistics in
Table 3.3.
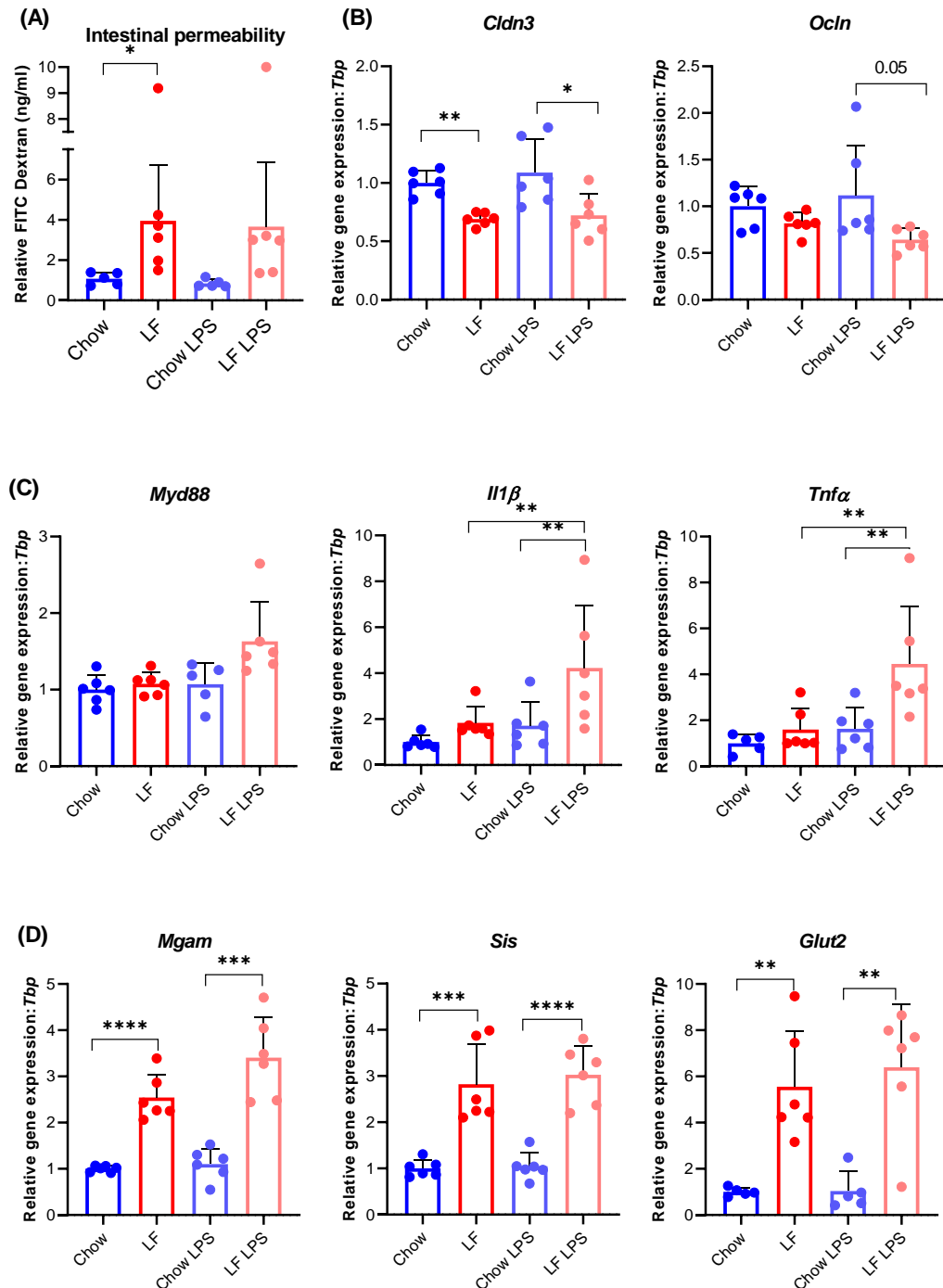
Figure 3.12 Intestinal permeability and gene expression changes in response to diet and LPS challenge. Low-fat (LF) fed mice had increased intestinal permeability measured by FITC-dextran independent of LPS treatment (A), Barrier function gene expression levels were decreased in the ileum of LF fed mice (B), Inflammation related genes had increased expression in response to LF LPS compared to chow LPS (C), Carbohydrate metabolism related gene expression increased in LF fed mice independent of LPS treatment (D). Significance was tested using 2-way ANOVA with Tukey's multiple comparison test (***= p<0.001, **= p<0.01, *= p<0.05). Values are the means ± SEM of n=5-6 mice in each group. LPS: Lipopolysaccharide.

Table 3.3 Summary of statistics for ileal gene expression analysis. Significance was tested using 2-way ANOVA with Tukey's multiple comparison test (*= p<0.001, **= p<0.01, *= p<0.05). Values are the means of n=5-6 mice in each group. LPS: Lipopolysaccharide. LF: Low-fat diet.**

	Percentage increase %	SE of diff.	P value
Myd88			
chow vs. LF	7.0	0.7	1.0
chow vs. chow LPS	7.0	0.7	1.0
LF vs. LF LPS	51	0.7	0.9
chow LPS vs. LF LPS	52	0.7	0.9
Il1β			
chow vs. LF	83	0.7	0.6
chow vs. chow LPS	71	0.7	0.7
LF vs. LF LPS	130	0.7	0.007**
chow LPS vs. LF LPS	146	0.7	0.004**
Tnfα			
chow vs. LF	59	0.7	0.9
chow vs. chow LPS	62	0.7	0.8
LF vs. LF LPS	179	0.7	0.001**
chow LPS vs. LF LPS	173	0.7	0.001**
Mgam			
chow vs. LF	154	0.6	0.00001****
chow LPS vs. LF LPS	209	0.6	0.0001***
Sis			
chow vs. LF	182	0.6	0.0005***
chow LPS vs. LF LPS	189	0.6	0.00003****
Glut2			
chow vs. LF	455	0.7	0.002**
chow LPS vs. LF LPS	513	0.7	0.002**

3.3 Discussion

The studies performed in this chapter demonstrated that the purified LF diet compared to the chow has differential effects on the gut-liver axis independent of weight gain. The LF diet leads to significant changes in 1) liver phenotype of mice, 2) ileal gene expression related to carbohydrate metabolism and barrier function, 3) ileal microbiota and 4) ileal bile acid composition. Moreover, our data showed LF fed mice had increased sensitivity to the LPS challenge compared to chow.

No changes in body weight or calorie intake of mice were observed during the four weeks feeding of the two diets, which indicates that the significant changes observed in the gut and liver of mice in response to the diet are independent of weight gain. We show that the LF diet feeding of 4 weeks, led to increased hepatic triglycerides in mice compared to the chow fed group, which was confirmed by upregulation of genes related to *de novo* lipogenesis, *Acaca* and *Fasn*. We observed increased expression of PPARα target gene *Fgf21* in the livers of LF fed mice. Maekawa et al. (2017) has reported increased hepatic *Fgf21* mRNA expression in mice fed a high refined carbohydrate diet that led to increased energy expenditure, thus attenuating weight gain. Moreover, Rusli et al. (2016) found upregulation of PPARα targets including *Fgf21* gene expression in the livers of mice with NAFLD and suggest a protective role of FGF21 against fatty acid induced lipotoxicity and oxidative stress in NAFLD.

Diet is an important external factor that affects the gut microbiota (Gentile and Weir, 2018), therefore, we next examined the influence of chow and LF diet on the ileal microbiota of mice. We observed changes in α diversity between the diet groups and the shifting of the ileal microbiota induced by the different diets as indicated by the β diversity. Although, the count of observed species was higher in the LF compared to chow diet, the evenness (Shannon index) was decreased in the LF group, which suggests uniformity of the population size of each of the species (Wagner et al., 2018). Microbial analysis at the phylum level indicated that the LF diet group exhibited an increased proportion of *Firmicutes* and reduced proportion of *Bacteroidetes*. Dalby et al (2017) reported increased *Firmicutes: Bacteroidetes* ratio to in mice fed the purified LF and high fat diets relative to standard chow, which may suggest that differences in fat content between the diets was not the main driver of the change in *Bacteroidetes and Firmicute* quantity, but the lack of fibre in the purified diets compared to chow diet. Further examination at the genus level showed an increased population of the genus from *Bacteroidales S24-7* family in the chow compared to the LF diet fed mice. Ormerod et al. (2016) proposed the name *Ca. Homeothermaceae* for this genus which contains increased abundance of enzymes involved in the degradation of complex plant cell wall glycans (hemicellulose and pectin) as are present in the chow diet. Although, *Bacteroidales S24-7* family of bacteria has been well described in the murine gut, its importance on long-term health is still unclear. LF group showed a significantly increased proportion of *Romboutsia*, *Faecalibaculum*, and *Lactococcus* belonging to the *Firmicutes* phylum. *Romboutsia* is an obesity-related genus that is positively associated with lipogenesis in the liver (Zhao et al., 2018). *Faecalibaculum* and *Lactococcus* are lactic acid producing bacteria and their role in metabolic disease has been studied to some

extent (Lim et al., 2016 and Yu et al., 2017). Furthermore Yu et al. assessed the genomic characteristics of ten *Lactococcus* species to reveal the ability of most of the strains to hydrolyse sucrose to d-glucose-6P and d-fructose. The authors also found that all the strains of *Lactococcus* have genes encoding fructokinase, a key enzyme in fructose metabolism. Therefore, increased presence of refined carbohydrates in the LF diet may explain the higher abundance of *Lactococcus* observed in the LF fed mice. Although, the relative abundance of *Proteobacteria* phylum was not different between the two diets, the relative abundance of pathogenic genera *Cronobacter* and *Stenotrophomonas* within the *Gamma Proteobacteria* group was increased in the LF fed mice (Trifonova and Strateva, 2019).

LPS is a product of gram-negative bacteria that are mostly found in the *Bacteroidetes* and *Proteobacteria* phylum. However, the endotoxin activity of LPS in *Bacteroidetes* is less effective compared with that of *Proteobacteria*. Studies have reported that bacteria in the *Enterobacteriaceae* family (*Gamma Proteobacteria*) possess markedly increased LPS endotoxin activity than LPS extracted from the envelope of bacteria of the *Bacteroidetes* phylum which can inhibit the host immune response (Salguero et al., 2019). We observed increased proportions of *Enterobacteriaceae* family in the LF compared to chow group in the first study (Supplementary Fig. 3.1). Altogether, our study shows that ileal microbiota composition is significantly influenced by the chow and LF diet. However, it remains unclear if the microbiota also contributes to the 'unhealthy state' of the LF fed mice, or if it itself was shaped by metabolic dysregulation as a result of the LF diet.

The gut microbiota and bile acids interaction play an important role in regulating enterohepatic bile acid metabolism. Primary bile acids are synthesised from cholesterol in the liver, conjugated with glycine or taurine and further metabolised by the gut microbiota into secondary bile acids (Ticho et al., 2019). We determined ileal bile acid profiles of the chow and LF fed mice by liquid chromatography-mass spectrometry. The total bile acids were shown to be significantly enhanced in the ileum of LF fed mice. We observed an increase in ileal primary bile acids in response to the LF diet, while, the secondary bile acids were not changed between the diet groups. Analysis of the bile acids at the individual level showed primary conjugated bile acid; TβMCA and conjugated secondary bile acid; TUDCA to be significantly increased in the LF group. Removal of glycine/taurine conjugates by the microbiota relies on their bile salt hydrolase (BSH) activity. BSH is expressed in some strains of *Lactobacillus*, *Bacteroides*, *Clostridium*, and *Bifidobacterium* (Song et al., 2018). Although, the abundance of *Lactobacillus* varied among the groups, we observed a consistent increased abundance of *Bacteroidales* S24-7 from *Bacteroides* group in the chow fed mice. The increased levels of taurine conjugated bile acids might be due to the decreased abundance of BSH containing bacteria in the LF mice. Further experiments to measure BSH enzyme activity in the ileal content of chow and LF fed mice can help confirm this hypothesis. Sayin et al. (2013) proposed TβMCA to be an antagonist of FXR, however, we did not observe difference in the ileal *Fxr* expression between the diet groups. In contrast, the gene expression of FXR target, the enterokine *Fgf15* showed an increasing trend in LF diet fed mice. These contrasting results could be due to the fact that concentration of TβMCA in LF group

was not enough to function as FXR antagonist. Sayin et al. used ileal explants and germ-free mice to show the FXR inhibition by TβMCA, which eliminates the competition that exists between bile acid agonist and antagonist for the activation or suppression of FXR expression in ileum. Moreover, our previous studies have demonstrated increased ileal glucose concentration to be associated with upregulation of *Fgf15,* possibly by GlcNAcylation of ileal FXR independent of bile acids. FGF15 binds to its hepatic membrane receptor FGFR4 to suppress the expression of CYP7A1, the rate limiting enzyme in the bile acid synthesis pathway in the liver. The LF diet did not alter the gene expression of *Fgfr4* and *Cyp7a1*. Moreover, we did not observe changes in the gene expression levels of bile acid transporters in the ileum.

Quantity and the quality of macronutrients has been shown to influence the ileum morphology in several animal models (Kieffer et al., 2016; Alonso and Yilmaz, 2018). In the current study we observed the expression levels of barrier function genes *Muc2*, *Cldn3* and *Zo-1* to be decreased in response to the LF diet. Mucin gel-forming glycoprotein (MUC2) is secreted by goblet cells and serves to physically segregate the microbiota from gut epithelium. Further, Claudins and Zonula occludens control the diffusion of water, ions, and nutrients, and restrict the entry of pathogens and pathogen derived endotoxins such as LPS, that can lead to chronic inflammation observed in metabolic syndromes (Chu et al., 2019). The downregulation of barrier function genes may be linked to reduced fibre content and/or the higher starch and sucrose present in the LF diet. The association of improved barrier function with a high fibre diet has been attributed to the microbial production of SCFAs in the gut (Hung et al., 2016). We have previously observed decreased concentrations of SCFAs in the ileal luminal content in response to 2 weeks LF feeding compared to chow (Supplementary Fig. 3.2). Moreover, Thaiss et al. (2018) showed hyperglycaemia could drive alterations in tight junction and leading to immune-stimulatory microbial products and systemic inflammation. Although, the study focused on the impact of systemic hyperglycaemia on the intestinal barrier, similar effects may be observed by a high refined carbohydrate diet resulting in high glucose concentrations in the ileum and thus induce changes in the intestinal permeability. Recent study by Jang et al. (2018) has shown that the small intestine plays a crucial role in controlling fructose that enters the liver by converting fructose into glucose and other metabolites and thus shielding the liver from fructose exposure. Due to the increased amount of simple carbohydrates present in the LF diet, we measured the expression of ileal genes related to carbohydrate metabolism to show increased expression of carbohydrate digesting enzymes *Mgam*, *Sis* and glucose transporters *Sglt1* and *Glut2* and gluconeogenesis enzyme *G6pc*. Our data suggests, the increase in the expression of carbohydrate metabolism related genes in the ileum of LF fed mice could be a result of the increased amount of starch and sucrose present in the LF compared to the chow diet.

The increased accumulation of triglycerides, abundance of pathogenic bacteria and decreased expression of barrier function genes in LF group led us to hypothesise that these mice may be more susceptible to a proinflammatory challenge compared to chow fed mice. To test this hypothesis, we administered low dose LPS via i.p. injections in addition to the chow and LF diet, to induce low-grade inflammation

state in mice. We observed decreased weight gain in LF LPS compared to other groups, although no difference in calorie intake was observed. Histological analysis of the liver sections reproduced our previous findings to show increased lipid deposition in LF group, which was confirmed by increased *Fasn* gene expression. Apoptosis plays an important role in inflammation. Therefore, we quantified the amount of apoptosis by caspase 3 assay in the liver, to reveal increased caspase 3 activity in the livers of LF LPS group compared to the other groups. Apoptosis by caspase 3 activation in hepatocytes plays a key role in non-alcoholic steatohepatitis (NASH) pathogenesis (Thapaliya et al., 2014). The increased levels of caspase 3 activity in the LF LPS mice compared to chow LPS group suggests increased sensitivity of the LF compared to chow fed mice. The exogenous administration of LPS is associated with the activation of TLR4 complex. Although, we did not observe difference in the gene expression of *Tlr4* in the liver (Supplementary Fig. 3.3), its downstream genes, *Saa1*, *Tnfα*, *F4/80* and *Nlrp3* were found to be upregulated in the liver of both diet + LPS groups. Upon analysing the expression of inflammation related genes, no significant difference was observed between chow LPS and LF LPS group, however, the response of LF liver was more pronounced to the LPS challenge compared to chow LPS. The increased trend in the expression of proinflammatory genes coincides with infiltration of monocytes observed in the histological analysis of the LF LPS group. The increased inflammation response in the LF LPS mice as indicated by hepatic caspase 3 activity may be a factor in the decreased weight gain observed in these mice, as increased inflammation response has been associated with weight loss (Seemann et al., 2017).

To confirm the LF diet effect on the barrier function genes, we measured intestinal permeability by quantifying FITC-dextran in the serum of mice. LF fed mice (control and LPS treated) showed increased FITC-dextran serum concentration compared to chow counterparts. The FITC-dextran assay results agreed with *Cldn3* and *Ocln* gene expression of the ileum, which suggested a stronger diet effect than low dose LPS treatment. Next, we questioned if the LPS treatment influenced nutrient uptake in the ileum. In agreement with our first study we observed increased gene expression levels of *Mgam, Sis* and *Glut2* in the ileum of LF fed mice and LPS treatment did not affect the expression levels of these genes. The ileal expression levels of LPS-TLR4 driven genes *Myd88, Il1b* and *Tnfα* were found to be significantly increased in LF LPS compared to chow LPS. Our results suggest that the LPS treatment in LF fed mice caused significant intestinal inflammation, which was not observed in chow LPS mice. Increased consumption of DF has been reported to reduce the concentrations of proinflammatory cytokines associated with age or model of endotoxemia, possibly by the anti-inflammatory properties of SCFAs (Matt et al., 2018; Zhang et al., 2019). However, more work is needed to understand the mode of action of SCFAs in the ileal enterocytes. Altogether, our data suggests LPS elicited a stronger response in LF fed compared to chow fed mice. The decreased weight gain together with greater inflammation response in the liver and ileum of LF group to LPS challenge could be attributed to the scarce amount of fibre and increased starch and sucrose present in the LF diet.

Chapter 4: The response of the ileum to lifelong calorie restriction of purified low-fat diet feeding

4.1 Introduction

Calorie restriction (CR) is a dietary regimen that reduces food intake without incurring malnutrition. CR has been shown to increase lifespan in a number of species ranging from single-celled organisms to mammals (Mair and Dillinas, 2008), as well as improve general health and decrease the onset of age-related diseases including cardiovascular and neurodegenerative diseases, diabetes and cancer (Most et al., 2017). Potential mechanisms associated with metabolic reprogramming may contribute to the beneficial health outcomes of CR. Several studies have suggested a complex network of signalling pathways, including SIRT1, mTOR, AMPK, IGF-1, to contribute towards health benefits of CR (Pan and Finkel, 2017; Komatsu et al., 2019). Previous studies have provided knowledge into the effects of CR on individual organs such as white adipose tissue (Fujii et al., 2019), liver (Rusli et al., 2017) and colon (Kok et al.,2018).

Although, the small intestine is a major responsive organ to food, it has not been well studied in the context of CR. The ileum is an important part of the small intestine because of its crucial homeostatic interactions with a diverse population of microbiota and its role in utilising the macro- and micronutrients. CR has been shown to alter the level of bile acids in the plasma, liver and small intestine of mice (Fu and Klaassen, 2013), which may also be associated with changes in the ileal microbiota. Therefore, the limited information on the impact of CR in the ileum prompted us to characterise the changes in the ileal microbiota, gene expression and bile acid levels in response to short- and long-term CR. In collaboration with the group of Dr Wilma Steegenga (Wageningen University, NL), we aimed to investigate ileal morphology, ileal gene expression via microarrays, bile acid metabolism and the ileal microbiota composition in response to lifelong CR in 6 and 24 months old mice. This project is known as the IDEAL study (Integrated Research on Developmental Determinants of Ageing and Longevity). The mice in the IDEAL study were fed the purified American Institute of Nutrition 93W (AIN-93W) diet which is variant of AIN-93M and is similar to the low-fat (LF) diet used in the previous chapter (composition of the diet is shown in Methods Table 2.2). The ileal samples from 6 and 24 months of age gave us the opportunity to differentiate the effects of CR at young and old age. The study also provided us with an opportunity to describe the long-term effects of LF diet on the ileal microbiota and gene expression during ageing.

In Chapter 3 of this thesis, we have shown differential effects of the two control diets on the gut-liver. In line with this, we hypothesised that the compositional differences in the chow and LF diet may result in altered gut and liver response to CR. We designed a short-term (8 weeks) CR study to compare the effects of CR on two different background diets (chow and LF). The study aimed to characterise differences in the gut-liver gene expression and bile acids levels in response to CR of the chow and LF diet. IDEAL study showed that mice needed approximately 8-10 weeks to adapt to CR feeding schedule and reach a relatively stable weight. Therefore, we chose dietary intervention period of 8 weeks to test the effects of 'short term' CR on the gut-liver axis.

4.2 Results

<u>4.2.1 Physiological effects of long-term CR on the gut and liver of mice</u>

Adaptations to the CR diet were observed in the weekly body weight measurements. At the time of sacrifice lifelong LFCR fed mice showed lower body weight (by 40±1%, P< 0.0001) compared to the LF control group (Fig. 4.1A). Fat deposition in the liver was examined by quantification of the hepatic triglycerides content and showed decreased triglycerides levels in the livers of mice exposed to CR compared to control diet at 6 and 24 months of age (37.9±0.1%, P=0.01 and 65±0.4%, P<0.0001 respectively). Furthermore, we observed 73±0.3% (P=0.001) increase in the triglycerides content with age in the control group, whereas, triglycerides content was not significantly different between CR6m and CR24m mice (P= 0.2) (Fig. 4.1B).

Histological analysis with haematoxylin and eosin (H&E) staining of ileum from LF and LFCR, 6- and 24 months old mice was performed, and the villi height and crypt depth were measured using the Image J software. Our data showed shrinkage of villi height by 19±0.04% and 8±0.03% (P= 0.01, 0.04) in CR exposed 6 and 24 months old mice compared to respective control group (Fig. 4.1C). Analysis of the crypt depth showed expansion by 23±0.04% (P<0.001) in 6m and 36±0.05% (P< 0.0001) in 24m old CR fed mice compared to control (Fig. 4.1D). The crypt depth was also increased with age in the CR group (15±0.04%, P=0.001), whereas no difference in crypt depth was observed with age in the control LF group.
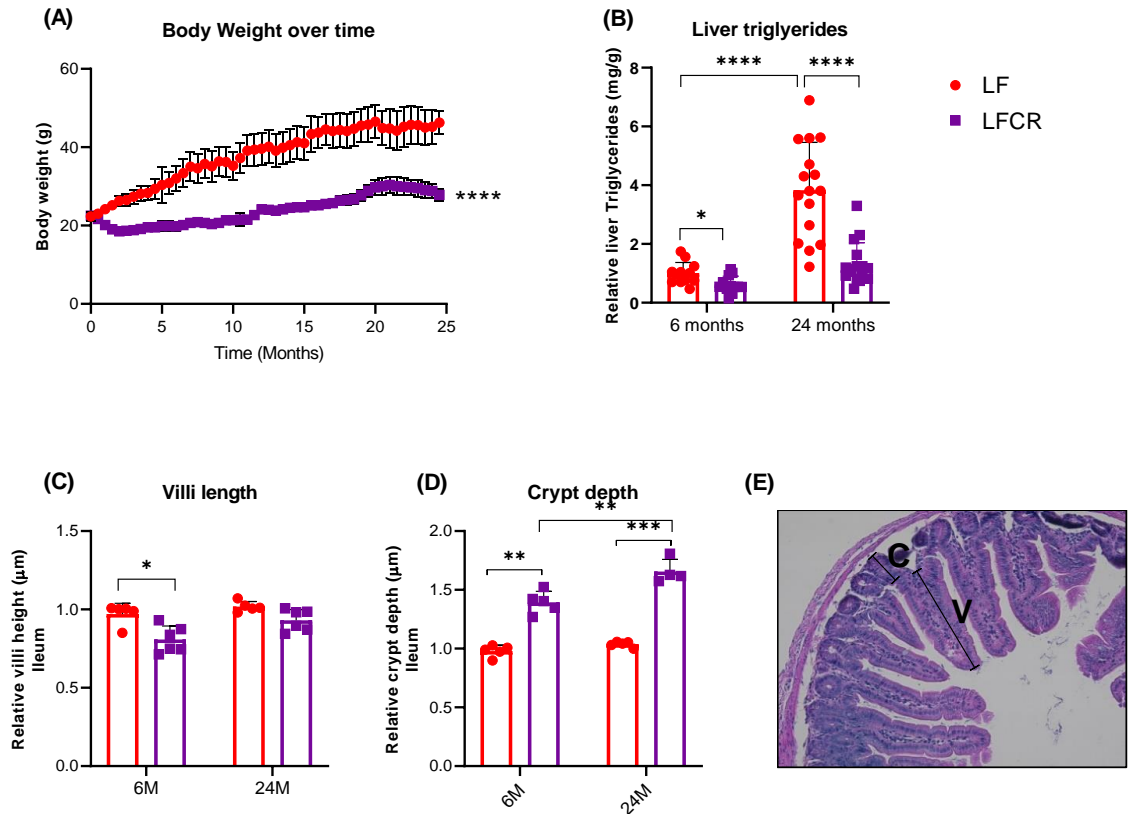
Figure 4.1 Body composition of mice in response to lifelong CR. Weekly measurements of body weight showed reduction in body weight in the lifelong CR mice (A). CR exposure led to decrease in the liver triglycerides content in 6- and 24-months old mice (B). Analysis of villi and crypt lengths in the ileum of mice revealed modifications in response to the diet and age (C, D). Micrograph shows haematoxylin and eosin (H&E) stained ileum section at magnification 4x and the distance used to measure v=villus height and c=crypt depth (E). Significance was tested using 2-way ANOVA with Bonferroni post-hoc test for both diet and time (*** = p<0.001, **= p<0.01, *= p<0.05). Values are the means ± SEM of n=13-16 mice (Body weight and IHTG) and n=5-6 mice (ileal histological analysis) in each group. LF: low-fat diet *ad libitum*, LFCR: Calorie restriction of LF diet.

4.2.2 Ileal gene expression of lifelong CR exposed mice resembles that of young mice

Gene expression profiles were measured in ileal samples (n=4 per group) to identify biological pathways regulated between the diets. A sample from LF24m group was excluded due to adipose tissue contamination. At 6 and 24 months, microarray analysis revealed 153 and 135 significantly differentially expressed genes (P<0.05) between the LFCR and LF control diet exposed mice (Fig. 4.2A). Ingenuity pathway analysis (IPA) revealed that affected canonical pathways for the comparison between LFCR against LF control were predominantly related to immune responses at 6 months and cell cycle regulation at 24 months of age. In the top canonical pathways B cell development was the major difference between the two diets at 6 months, while 'mitotic roles of Polo-Like kinase', 'cell cycle' and 'ATM signalling' were mostly affected in 24 months old mice (Fig. 4.2B).
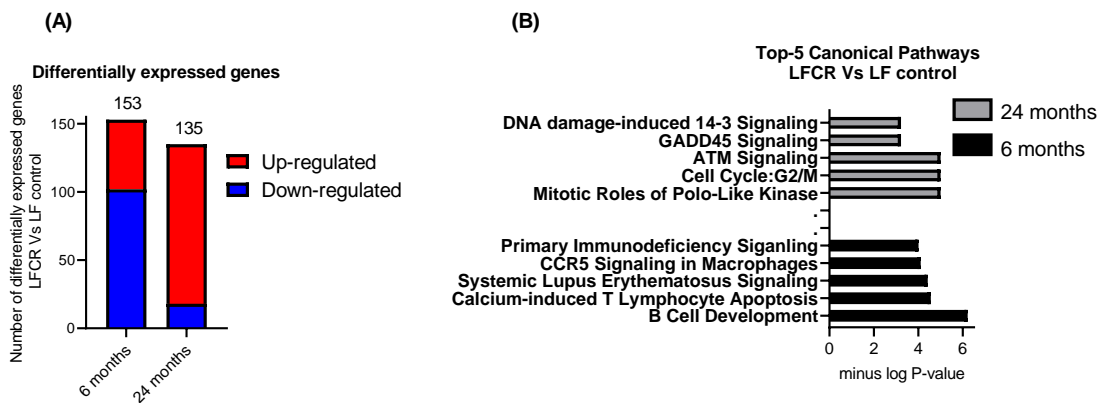
Figure 4.2 Gene expression in the ileum of 6- and 24-months old mice fed with LF control and LFCR diet. The number of differentially expressed genes at 6 and 24 months based on an intensity based moderated (IBMT) P value=0.05 (A). The top 5 canonical pathways revealed by Ingenuity pathway analysis (IPA), that were differentially regulated in mice fed the LFCR versus LF control diet at 6 (black) and 24 months (grey) of age (B). For microarrays analysis n=3-4 in each group. LF: Low-fat diet *ad libitum*, LFCR: Calorie restriction of LF diet.

IPA revealed inhibited activation state (negative Z score) for pathways involved in T lymphocytes signalling for comparison of LFCR Vs LF control at 6 months. Consistent with the IPA results we observed attenuation of gene expression related to inflammation in the ileum of mice exposed to CR diet (various T cell antigen and receptor genes, and lymphotoxin beta, *Ltb*) (Table 4.1). Top 10 genes upregulated with 6 months CR diet included; genes involved with inhibition of immune response (*Nt5e*) (Kordaß et al., 2018), B cell development related genes (immunoglobulins *Iglv1* and *2*) (Spencer and Sollid, 2016), cell proliferation related gene (*Tppp*), *Lingo4*, *Col6a3* , *Ly96* and lipid metabolism related genes (*Acsl3, Lpcat4 and Scd2*) (GeneCards, 2020). At 24 months, genes related to antimicrobial peptides and cell cycle regulation (e.g. *Mptx2*, *Cdca3*) were among the most upregulated genes (Table 4.2). Top downregulated gene included bile acid related gene *Fgf15*, inflammation

related gene *Dusp1* (also known as MAPK phosphatase 1, *Mkp1*), *Slfn8*, member of the epidermal growth factor (EGF) ligand family, *Areg* (Chen et al., 2018), cancer associated gene *Sprr1a* (Deng et al., 2020), *Phlda1* (Kastrati et al., 2015), extracellular matrix related gene *Fras1* (Beck et al., 2013), microRNA *mir1247*, Sodium/phosphate co-transporter, *Slc34a2* and olfactory related gene *Vmn2r29*. The importance of *miR-1247*, *Slc34a2* and *Vmn2r29a* in the intestine has not yet been explored. Full names of the genes in Table 4.1 and 4.2.

Table 4.1 Differentially regulated genes in the ileum for the comparison of LFCR and LF control diet at 6 months. The genes were selected based on the most pronounced differential expression (fold change of >1.5 from CR6m to LF6m). Significance of change was calculated from the mean signal intensities and difference between diet groups was analysed using IBMT statistics implementing Bayes correction. N=3-4 per group. LF: Low-fat diet *ad libitum*, LFCR: Calorie restriction of LF diet.

Gene	Description	Fold Change	Adjusted P value
Top up-regulated genes			
Iglv2	immunoglobulin lambda variable 2	2.5	0.0159
Nt5e	5' nucleotidase, ecto	2.2	0.0092
Iglv1	immunoglobulin lambda variable 1	2.1	0.0087
Tppp	tubulin polymerization promoting protein	2.0	0.0066
Lingo4	leucine rich repeat and Ig domain containing 4	1.9	0.0006
Col6a3	collagen, type VI, alpha 3	1.9	0.0347
Ly96	lymphocyte antigen 96	1.9	0.0067
Acsl3	acyl-CoA synthetase long-chain family member 3	1.9	0.0051
Lpcat4	lysophosphatidylcholine acyltransferase 4	1.7	0.0069
Scd2	stearoyl-Coenzyme A desaturase 2	1.7	0.0018
Top down-regulated genes			
Trgj2	T Cell Receptor Gamma Joining 2	-2.6	0.00125
Dio1	Deiodinase, Iodothyronine Type I	-2.1	0.00318
Cd79b	B-Cell Antigen Receptor Complex-Associated Protein Beta Chain	-2.1	0.00227
Trgj4	T Cell Receptor Gamma Joining 4	-2.0	0.00009
Tcrg-C4	T cell receptor gamma, constant 4	-1.9	0.00011
Cd7	CD7 antigen	-1.9	0.00060
Tcrg-C2	T cell receptor beta, constant region 1	-1.9	0.00207
Trbc1	T cell receptor beta, constant region 1	-1.9	0.00186
Cd3g	CD3 antigen, gamma polypeptide	-1.9	0.00024
Ltb	lymphotoxin B	-1.8	0.00228

Table 4.2 Differentially regulated genes in the ileum for the comparison of LFCR and LF control diet at 24 months. The genes were selected based on the most pronounced differential expression (fold change of >1.5 from CR24m to LF24m). Significance of change was calculated from the mean signal intensities and difference between diet groups was analysed using IBMT statistics implementing Bayes correction. N=3-4 per group. LF: Low-fat diet *ad libitum*, LFCR: Calorie restriction of LF diet.

Gene	Description	Fold change	Adjusted P value
Top up-regulated genes			
Mptx2	Mucosal pentraxin 2	3.9	5.96E-05
Defa-rs1	Defensin, alpha, related sequence 1	2.0	0.000366
Cdca3	Cell division cycle associated 3	1.9	0.000591
Cdca5	Cell division cycle associated 5	1.8	0.000797
Utp14b	UTP14, U3 small nucleolar ribonucleoprotein, homolog B	1.8	0.004697
Mmp7	Matrix metallopeptidase 7	1.7	0.003251
Ang4	Angiogenin, ribonuclease A family, member 4	1.7	0.001653
Prr11	Proline rich 11	1.7	0.002233
Aurkb	Aurora kinase B	1.7	0.001837
Ccna2	Cyclin A2	1.7	0.000712
Top down-regulated genes			
Fgf15	fibroblast growth factor 15	-3.9	0.0097
Dusp1	dual specificity phosphatase 1	-2.3	0.0028
Sprr1a	small proline-rich protein 1A	-2.1	0.0073
Areg	amphiregulin	-1.9	0.0088
Phlda1	pleckstrin homology-like domain, family A, member 1	-1.8	0.0173
Fras1	Fraser syndrome 1 homolog (human)	-1.8	0.0007
Mir1247	microRNA 1247	-1.8	0.0016
Slfn8	schlafen 8	-1.7	0.0153
Slc34a2	solute carrier family 34 (sodium phosphate), member 2	-1.6	0.0117
Vmn2r29	vomeronasal 2, receptor 29	-1.5	0.0128

Figure 4.3 shows various ileal genes implicated in the immune response, cell cycle regulation and energy metabolism that were modulated between the diet groups of 6- and 24-months old mice. Genes related to Paneth cells (*Mptx2, Defa-rs1, defa3, Dmbt1*) (Fig. 4.3A), cell cycle regulation (*Cdca3, Cdca8, Cenpe, Prr1*) (Fig. 4.3B) were observed to be decreased with age in the LF control group, whereas, no significant difference was observed in their gene expression levels between CR6m and CR24m old mice.

Lipid metabolism genes (*Acsl3, Scd2, Lpcat4, Elovl6*) are suggested to be increased in response to CR compared to LF control at both 6m and 24m of age (Fig. 4.3C). Genes involved in carbohydrate metabolism (*Chrebp, Sis, Khk, Fbp1, Sglt1, Glut2* and *Glut5*) were upregulated in the ileum of CR24m compared to CR6m group (Fig. 4.3D) (Full names of the genes in Table 4.3). Whereas, no such effect on carbohydrate metabolism genes was observed between the ages in LF control group. Genes related to bile acid metabolism, *Fgf15*, *Asbt* and *Ostα* show a decreasing trend with age in CR exposed mice (Fig. 4.3E). Although no difference was observed in the gene expression of ileal *Fxr*, its downstream regulator *Fgf15* was significantly downregulated in CR24m compared to LF24m old mice. Taken together, 6 and 24m CR intervention modulated gene expression of various pathways, however, most differences in gene expression were observed in CR24m old mice. Summary of statistics in supplementary table 4.1.
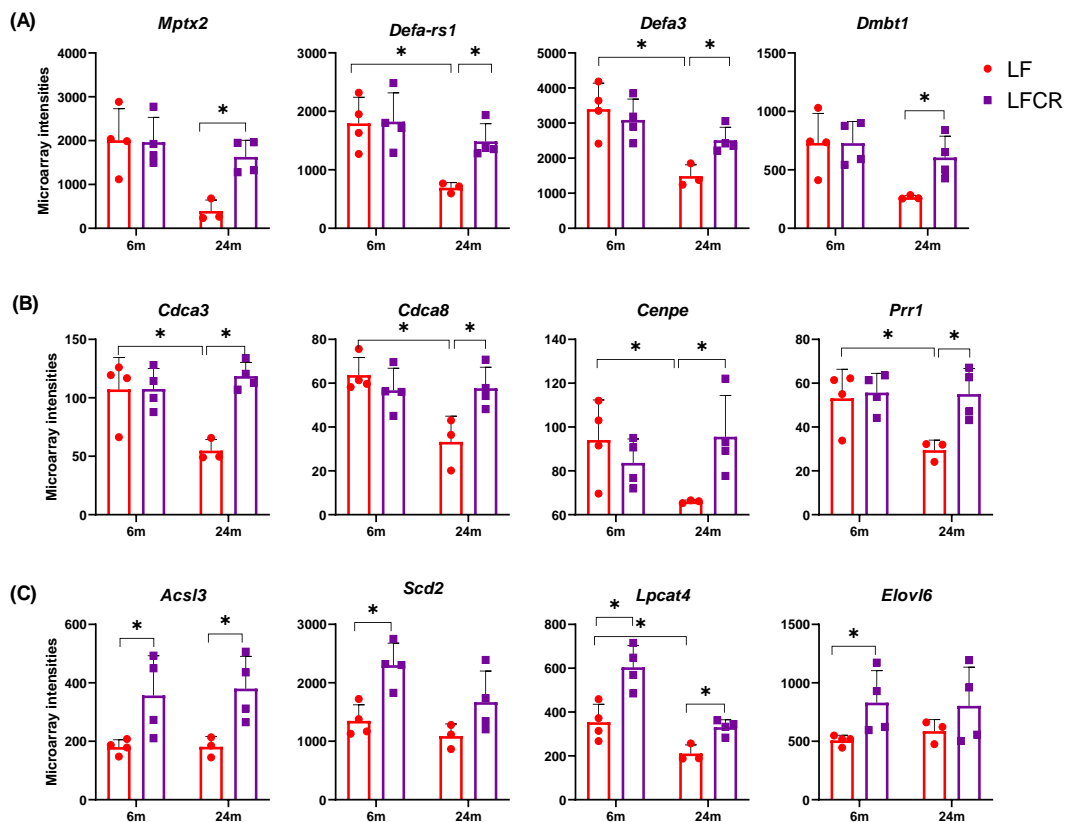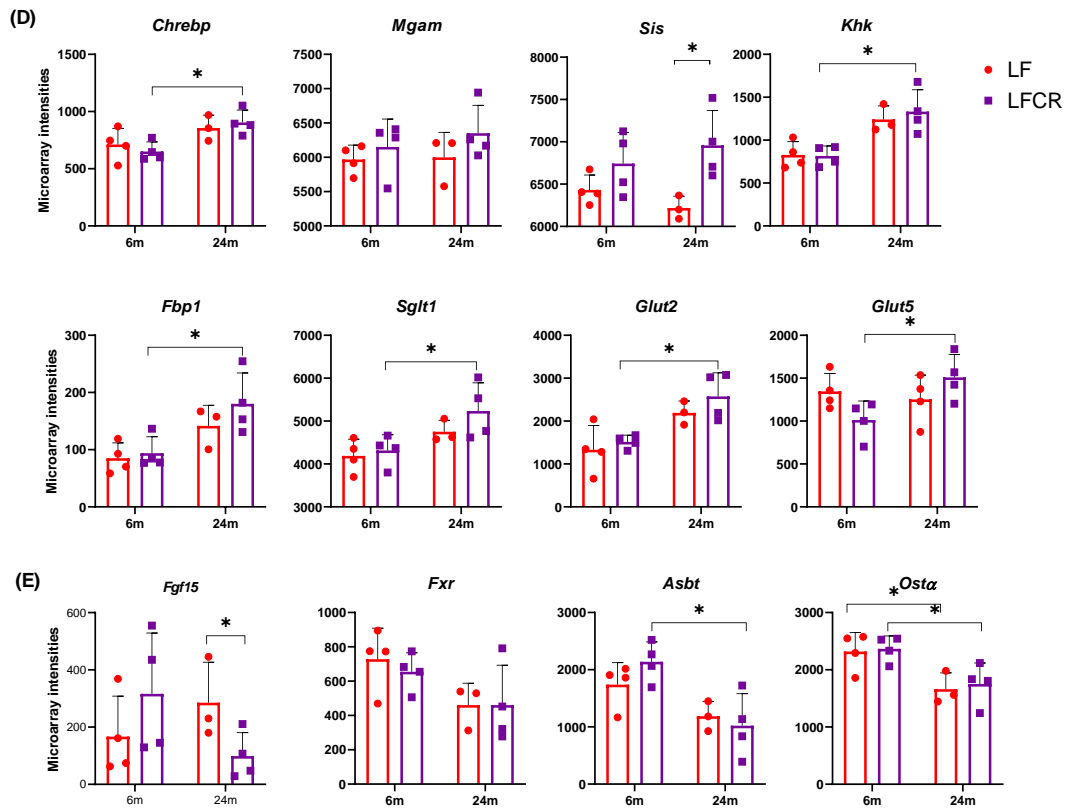
Figure 4.3 Microarray profiles of differentially regulated genes between diet and age. Genes related to Paneth cells (A), cell cycle regulation (B) lipid metabolism (C) carbohydrate metabolism (D) and bile acids metabolism (E) in the ileum. Significance was tested using 2-way ANOVA with Bonferroni post-hoc test for both diet and time (**= $p<0.01$, *= $p<0.05$). Values are the means ± SEM of n=3-4 mice in each group. LF: Low-fat diet *ad libitum*, LFCR: Calorie restriction of LF diet.

Table 4.3 Full names of the carbohydrate and bile acid metabolism genes regulated during CR.

Gene abbreviation	Full name
Chrebp	Carbohydrate response element binding protein
Mgam	Maltase-Glucoamylase
Sis	Sucrase isomaltase
Khk	Ketohexokinase
Fbp1	Fructose-1,6-bisphosphatase 1
Sglt1	Sodium/glucose cotransporter protein 1
Glut2/5	Glucose transporter 2/5
Fxr	Farnesoid X receptor
Asbt	Apical sodium–bile acid transporter
Ostα	Organic solute transporter alpha

4.2.3 Bile acids in the ileum are decreased as a result of lifelong CR diet

Since we observed modulation in the expression of genes involved in bile acid metabolism, we next measured levels of bile acids in the ileum samples from the diet groups at 6 and 24 months of age. We did not observe a significant difference in total bile acid levels between LF and CR mice at both timepoints (P= 0.5 and P=0.1 at 6 and 24 months respectively). The total bile acid levels were significantly decreased with age (by 74±591%, P= 0.005) in CR24m compared to CR6m mice (Fig. 4.4A). Deeper analysis of individual bile acids revealed significant decrease in most major bile acids, primary bile acids: βMCA (P= 0.04), CA (P= 0.03), TβMCA (P= 0.01), TCA (P= 0.01), and secondary bile acids: TDCA (P= 0.02), and TUDCA (P= 0.04) in response to 24m CR (Fig. 4.4B).
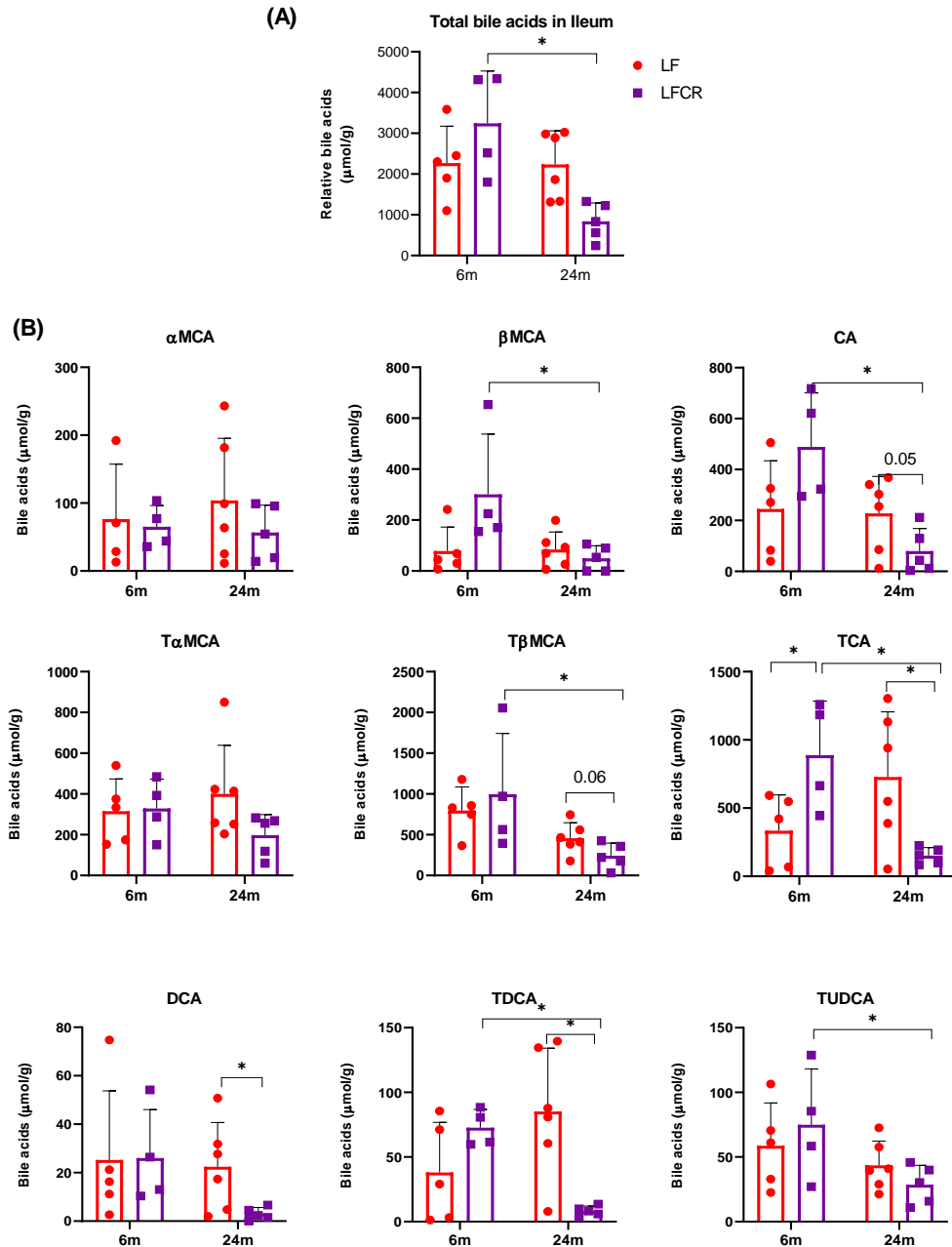
Figure 4.4 Bile acids were measured in ileal tissue samples from LF and LFCR diet fed mice at 6 and 24 months. Total bile acids (A), Individual bile acid profiles, Primary bile acids: αMCA, βMCA and CA, taurine conjugated primary bile acids: TαMCA, TβMCA and TCA, secondary conjugated bile acids: TDCA and TUDCA, secondary unconjugated bile acid: DCA (B). Significance was tested using 2-way ANOVA with Bonferroni post-hoc test (*= p<0.05). Values are the means ± SEM of n=4-6 mice in each group. LF: Low-fat diet *ad libitum*, LFCR: Calorie restriction of LF diet.

<u>4.2.4 Calorie restriction of the LF diet alters the microbiota profile in the ileum</u>
The microbial 16S rRNA sequencing analysis was performed on samples from the ileal content of mice. The groups contained sample size of n=4-6. A sample from CR24m (m6) was excluded from the analysis by performing the Grubbs' outliers test at the genera level. Differences in overall microbiota communities (β diversity) were determined by Bray-Curtis Index. Permutational multivariate analysis of variance (PERMANOVA) test found that microbiota communities differed significantly between LF and CR condition (R: 0.83; P < 0.003) in 6 months old mice. However, the microbiota differences by diet are not as pronounced in 24 months old mice (PERMANOVA, R:0.16; P<0.2) (Fig. 4.5A and B). Examination of α diversity by observed species and Shannon index showed similar diversity between the groups (Fig. 4.5C).

We identified specific taxa (at the phylum to genus level) that changed with CR at the different time points (Fig. 4.5D). Mice were individually housed throughout the course of the study to eliminate cage effects and coprophagy. The abundance of *Firmicutes* and *Bacteroidetes* was observed to be similar among the diet and age groups (P >0.1). We observed an increase in the abundance of *Actinobacteria* (80±1.3%, P= 0.01) in CR6m compared to LF6m mice. The levels of *Actinobacteria* were decreased with age in CR exposed mice (91±1%, P=0.007), whereas no difference was observed in *Actinobacteria* levels between LF6m and LF24m mice. A decrease in the abundance of *Proteobacteria* (70±0.2%, P= 0.02) was observed in CR6m compared to LF6m mice, while the levels of *Proteobacteria* were not changed with age in control LF or CR exposed mice.

The different genera present in the ileum of each mouse was examined to provide a more in-depth observation into the ileum microbiota. The profiles of genera present are shown for each individual mouse and show clear differences between LF and CR fed mice (Fig. 4.5E). At 6 months, genera within *Firmicutes* including *Allobaculum* (99% similar to *Faecalibaculum*) and *unknown Clostridiaceae* (similar to *Romboutsia*) were shown to be highly abundant in the LF compared to CR fed mice (P= 0.004 and P=0.02 respectively). Within the CR6m group, there was an increasing trend in the abundance of *Lactobacillus* (phylum *Firmicutes*) and *Bifidobacterium* (phylum *Actinobacteria*) in the ileum (P= 0.001 and P=0.05 respectively) (Table 4.4). At the age of 24 months, we observed an increasing trend in the abundance of *Lactobacillus* in the CR mice, although it did not reach significance (P= 0.1) (Table 4.5).
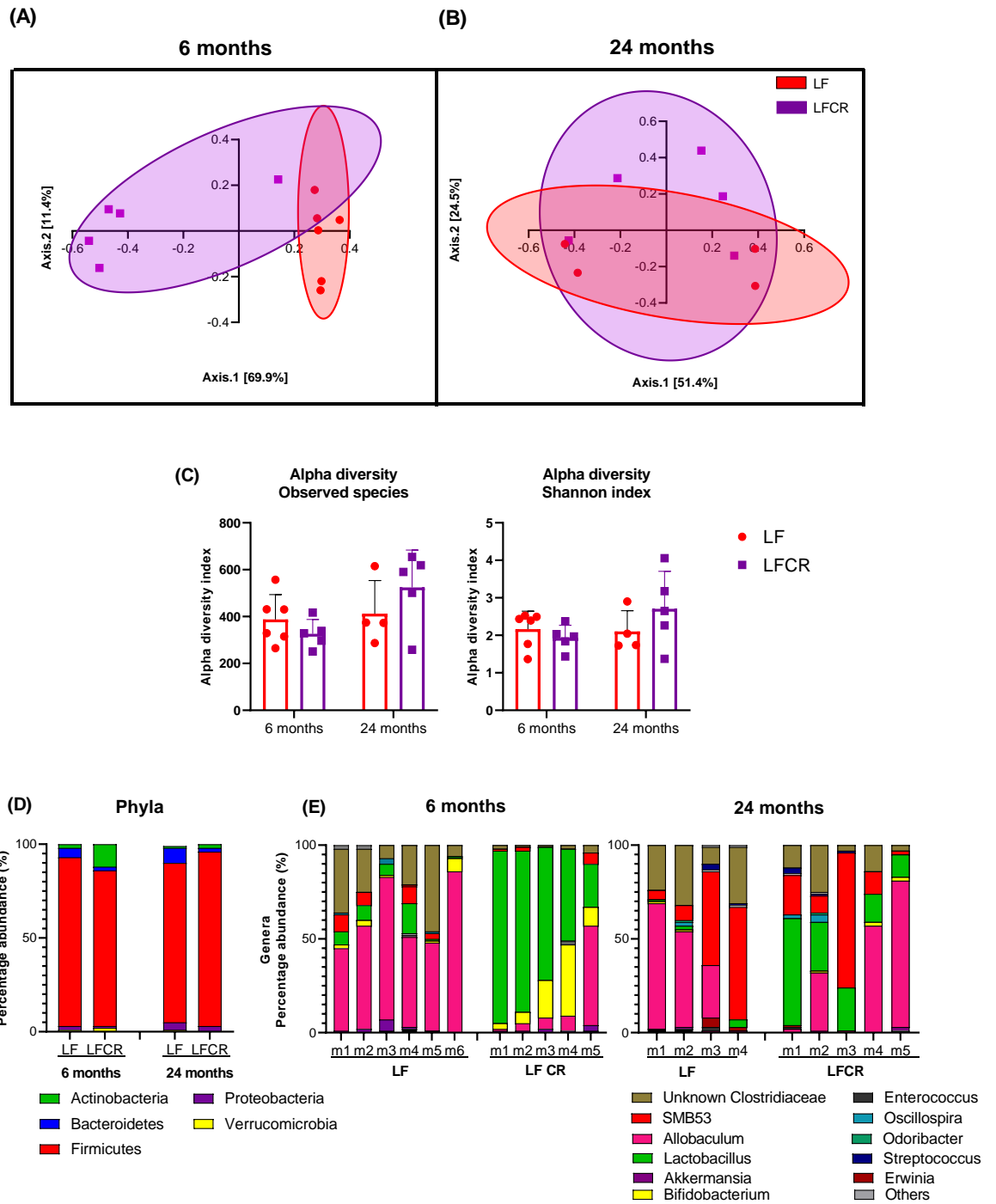
Figure 4.5 Microbiota composition in the ileum is different between LF and CR fed mice. PCoA plots show the separation of the two diet groups (β diversity) which is most prominent at 6 months of age (A and B). Alpha diversity was calculated by observed species and Shannon diversity score (C). Phylum levels show differentially distinct profiles with more *Actinobacteria* in the CR fed mice (D). Genera abundance in the ileum are presented for each individual mouse, showing a clear difference between the diets (E). Significance in β diversity was calculated by PERMANOVA tests. Significance for α diversity measures was tested using Kruskal-Wallis statistical test. N= 4-6 for each group. LF: Low-fat diet *ad libitum*, LFCR: Calorie restriction of LF diet.

Table 4.4 Summary of changes in the abundance at the genus level between LF and LFCR at 6 months. Significant difference between the groups was calculated by unpaired t-test. Values are the means of n=5-6 mice in each group. LF: Low-fat diet *ad libitum*, LFCR: Calorie restriction of LF diet.

Genera	Mean LF	Mean LFCR	SE of difference	P value
Akkermansia	1.67	1.60	1.08	0.95
Allobaculum	59.3	14.40	11.79	**0.004
Bifidobacterium	2.33	15.40	5.83	0.05
Lactobacillus	6.50	64.20	11.73	**0.001
Unknown Clostridiaceae	22.8	2.00	7.01	*0.02

Table 4.5 Summary of changes in the abundance at the genus level between LF and LFCR at 24 months. Significant difference between the groups was calculated by unpaired t-test. Values are the means of n=4-5 mice in each group. LF: Low-fat diet *ad libitum*, LFCR: Calorie restriction of LF diet.

Genera	Mean LF	Mean LFCR	SE of difference	P value
Akkermansia	0.25	0.50	0.47	0.61
Allobaculum	30.00	29.33	21.26	0.98
Bifidobacterium	0.50	0.83	0.55	0.56
Lactobacillus	8.75	26.6	10.7	0.13
Unknown Clostridiaceae	23.8	20.5	12.8	0.8

4.2.5 Impact of short-term CR on the gut-liver axis of mice under chow and LF diet

Next, we performed a short term (8 weeks) study to observe the initial effects of CR on the gut-liver axis. In addition to CR on the purified LF diet (LFCR), we included a group of chow calorie restriction (chowCR) to investigate the response to CR on different diet background on the gut-liver axis. To determine the physiological features of mice after exposure to the CR diet, body weight was recorded twice a week. As expected, the average body weight of CR mice was lower than control mice in both diet groups. At the end of 8 weeks, the body weights of chowCR mice was $20\pm0.8\%$ lower (P< 0.0001) compared to chow *ad libitum* fed mice, and the average body weight of LFCR mice at the time of sacrifice was $16\pm0.4\%$ (P< 0.0001) lower than the control LF fed mice (Fig. 4.6A). Figure (4.6B) shows the calculated average daily caloric intake of one mouse per day, which was reduced by $30\pm0.4\%$ in the CR mice compared to their control counterparts. Triglyceride content levels in the liver showed a decreasing trend in chowCR mice (reduced by $27\pm0.1\%$, P=0.1) compared to chow control, whereas this effect was more pronounced in the LFCR group when compared to LF control (decreased by $67\pm0.1\%$, P= 0.005) (Fig. 4.6C). We did not observe changes in the ileal villi height and crypt depth in response to CR in chow or LF diet groups (Fig. 4.6D and E).
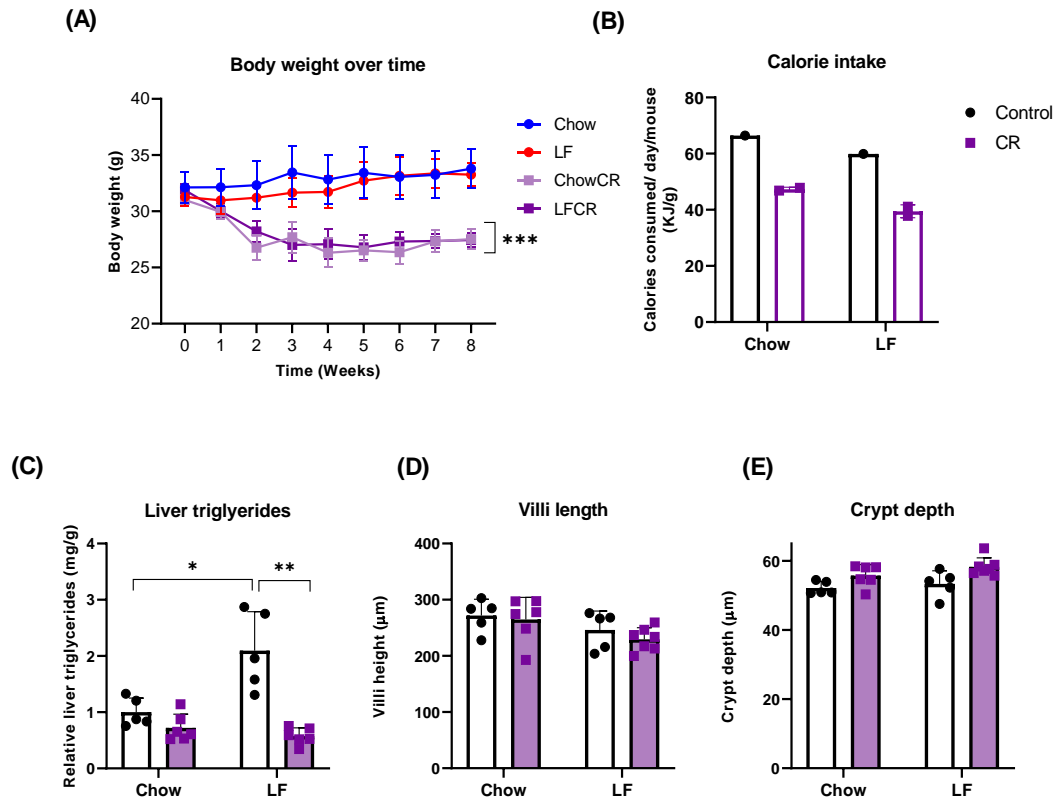
Figure 4.6 Effects of CR intervention on physiological parameters under chow and LF conditions.
Weekly measurement of body weight (A). Calorie intake measurements of chow and LF and their
calorie restricted groups (B). Liver triglycerides content is reduced in CR groups (C). Villi height and
crypt depth was measured in the ileum of mice (D and E). Significance was tested using 2-way
ANOVA with Bonferroni post-hoc test (**= p<0.01, *= p<0.05). Values are the means ± SEM of n=5
(control group) and 6-7 (CR group) mice in each group. Mice in the CR group were divided into two
cages (as 3-4 mice per cage), calorie intake was measured per cage and divided by 3-4 to calculate
the intake of one mouse. LF: Low-fat diet *ad libitum***, CR: Calorie restriction.**

4.2.6 Effect of CR on total bile acid levels in different compartments of the enterohepatic circulation

Due to the difference in ileal bile acids observed in the long-term CR study, we next examined the changes in bile acid levels in the organs involved in enterohepatic circulation (ileum and liver) in the present study. Total bile acids were measured in the ileum and liver samples from the mice in all the diet groups (Fig. 4.7A). In the ileum, we observed increased total bile acid levels in LF compared to chow mice ($49\pm0.2\%$, P= 0.04), and increased levels of total bile acids in LFCR compared to chowCR mice ($44\pm0.3\%$, P= 0.03). We did not observe changes in the total ileal bile acid levels between control and their CR counterpart for both chow and LF group (P>0.5). In the liver, total bile acid levels were similar among chow and chowCR groups (P >0.5), whereas, the LFCR showed a trend towards increased total liver bile acids compared to LF control diet fed mice ($27\pm0.4\%$, P= 0.1).

The expression of genes related to bile acid metabolism in the ileum and liver samples from mice was quantified by quantitative polymerase chain reaction (q-PCR). In the chow fed mice, CR intervention did not change the gene expression levels of *Fgf15, Fxr* and bile acid transporter, fatty acid binding protein 6, (*Fabp6*) in the ileum (Fig. 4.7B). Whereas CR on the LF diet significantly reduced the expression of *Fgf15* in the ileum (by $74\pm0.6\%$, P= 0.004). The gene expression of *Fxr* and *Fabp6* was not altered in response to the LFCR intervention (Fig. 4.7B).

In the liver, the gene expression of rate limiting bile acid synthesis enzyme cholesterol 7 alpha-hydroxylase, (*Cyp7a1*) was significantly increased in mice fed with chowCR (by $53\pm0.4\%$, P= 0.04). Whereas, the gene expression of bile acid receptor *Fxr*, its target, small heterodimer partner (*Shp*), and fibroblast growth factor receptor 4 (*Fgfr4*) the receptor for FGF15 were not changed in the liver of chow fed mice exposed to CR (Fig. 4.7C). The bile acid transporters, Na+-taurocholate cotransporting polypeptide and bile salt export pump (*Ntcp* and *Bsep*) were not altered in the livers of chowCR compared to chow control diet fed mice. In the LF group, the gene expression levels of *Cyp7a1*, *Fxr, Shp, Fgfr4, Ntcp and Bsep* were not observed to be different between the CR and control LF diet group (Fig. 4.7C).
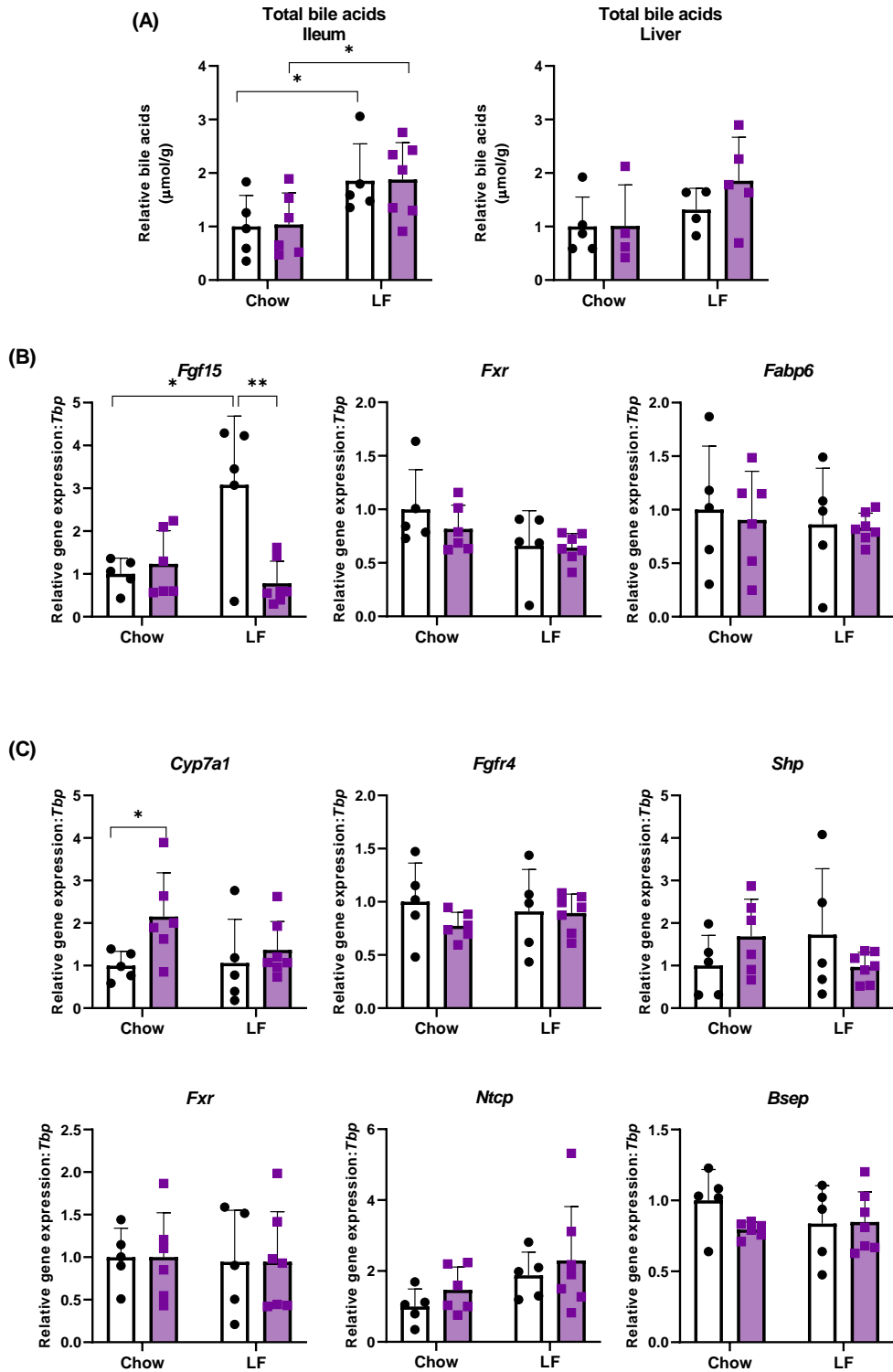
Figure 4.7 Bile acid metabolism in response to CR on chow and LF background diet. Total bile acids were measured in the ileum and liver of mice from all diet groups (A). Expression levels of bile acid metabolism related genes in the ileum (B) and liver of mice (C). Significance was tested using 2-way ANOVA with Bonferroni post-hoc test (**= p<0.01, *= p<0.05). Values are the means ± SEM of n=5-7 mice in each group. LF: Low-fat diet *ad libitum*, CR: Calorie restriction.

4.2.7 Response of metabolic homeostasis related genes to CR differed in chow and LF conditions

CR resulted in increased gene expression of ileal glucose transporters *Glut2* ($83\pm1.2\%$, P= 0.003), *Glut5* ($33\pm0.1\%$, P= 0.01), and carbohydrate enzyme *Sis* ($54\pm0.6\%$, P= 0.04) in the ileum of chowCR mice compared to chow control. CR under the LF diet condition, also resulted in an increasing trend for the expression of ileal carbohydrate metabolism genes, however this increase did not reach significance (P values for *Glut2*: 0.1, *Glut5*:0.1, *Mgam*:0.5 and *Sis* 0.5) (Fig. 4.8A).

Under the chow diet condition, genes in the liver related to lipogenesis were not altered by CR (P > 0.5) (Fig 4.8B). While, the gene expression of peroxisome proliferator activated receptor alpha (*Ppara*) which is the main controlling factor for fatty acid oxidation and its target, cluster of differentiation 36 (*Cd36*) were found to be increased in the livers of chowCR compared to chow control diet fed mice ($42\pm0.2\%$, P=0.03 and $50\pm0.3\%$, P=0.03 respectively). LFCR diet led to an increase in the lipogenic gene expression in the liver, fatty acid synthase (*Fasn*) and acetyl-coA carboxylase (*Acaca*) were increased in the LFCR compared to LF control fed mice (by $75\pm0.5\%$, P= 0.01 and $67\pm0.2\%$, P=0.0002). In agreement with our 4 weeks chow Vs LF study, the gene expression of liver *Fgf21* was increased in response to the LF compared to chow diet ($79\pm0.7\%$, P= 0.001). Whereas, *Fgf21* levels were significantly decreased in response to CR under the LF diet condition ($65\pm0.7\%$, P=0.001). Furthermore, the gene expression of sirtuin 1 (*Sirt1*) ($35\pm0.8\%$, P= 0.0007), *Ppara* ($45\pm0.3\%$, P=0.01) was significantly increased in LFCR fed mice. The gene expression of *Cd36* was not altered in response to LFCR compared to LF control diet fed mice (P >0.5).
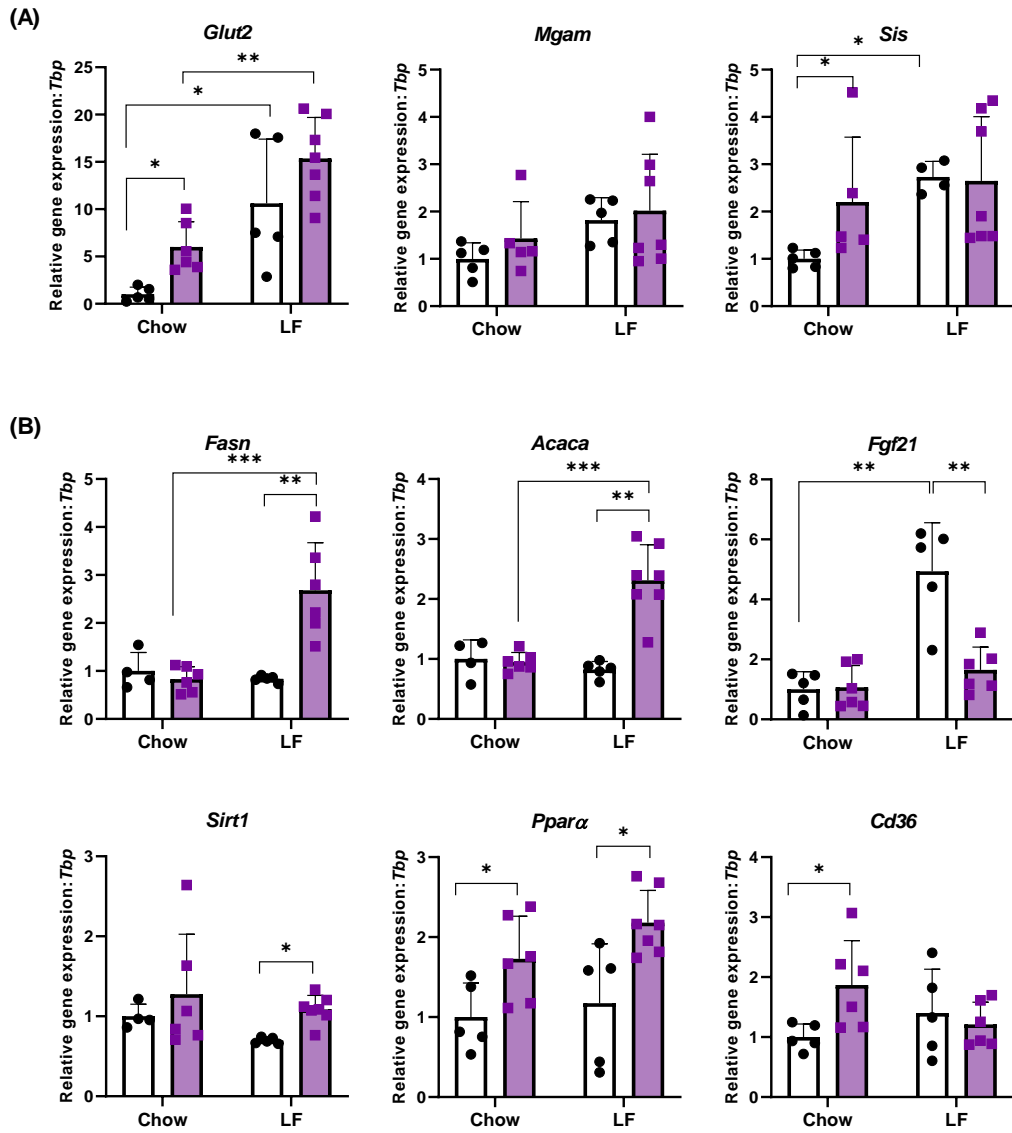
Figure 4.8 Differential effect of CR on the energy metabolism gene expression in chow and LF fed mice. Carbohydrate metabolism genes in the ileum (A), and lipid metabolism genes in the liver (B) were tested by qPCR. Significance was tested using 2-way ANOVA with Bonferroni post-hoc test (**= p<0.01, *= p<0.05). Values are the means ± SEM of n=5-7 mice in each group. Qpcr: Quantitative polymerase chain reaction. LF: Low-fat diet *ad libitum*, CR: Calorie restriction.

4.3 Discussion

In this chapter we have presented changes in the gene expression profile and microbiota composition of the ileum in response to long-term feeding of the LF diet. We also show that CR intervention on the LF diet background prevented these age-related changes induced by purified diet.

Fasting and feeding may induce structural alterations in the intestine, such as changes in villi height and crypt depth. Our results showed increased crypt depth in the ileum in response to 6 and 24 months intervention of CR. These results are consistent with research carried out by Yilmaz et al. (2012) that report crypt expansion in the small intestine of mice that were subjected to CR for 7 months, the authors propose increased crypt size resulted from increased number of stem cells per crypt in response to CR.

Gene expression profiling of ileum samples showed decreased expression of Paneth cells and cell cycle regulation related genes in LF24m compared to LF6m mice, whereas expression of these genes remained unaffected with age, between CR6m and CR24m mice. Paneth cells release stimulatory factors for intestinal stem cells growth and secrete antimicrobial peptides to provide host defence against pathogens (Yilmaz et al., 2012). Our results suggest reduced function of Paneth cells in aged mice may be due to age associated decline in intestinal regenerative capacity and organ maintenance (Nalapareddy, et al., 2018). Moreover, research has shown changes in gut microbiota with age (Langille et al., 2014; Kok et al., 2018), therefore the decrease in the expression of antimicrobial peptides (*Mptx2, Defars1, Defa3,* and *Dmbt1*) may be an adaptive response to the age-associated changes in microbiota described in this chapter. Further analysis to quantify the number of Paneth cells per crypt by lysozyme or MMP7 staining in the aged ileum on control and CR diet will provide more information on the effect of age and CR intervention. We were unable to perform lysozyme immunohistochemistry analysis due to the limited ileum tissue available for this study.

We observed decreased expression of cell cycle regulatory genes (*Cdca3, Cdca8, Cenpe* and *Prr1*) upon ageing under control LF diet, whereas long-term CR resisted this decline in cell cycle genes and resembled the gene expression levels of young 6 months old mice. Nalapareddy et al. (2018) reported downregulation of cell proliferation genes as a consequence of reduced canonical Wnt signalling in intestinal stem cells during ageing. CR has been shown to increase the number of proliferating stem cells in the intestinal crypt base, in response to signals sent from neighbouring Paneth cells that sense nutrient availability (Igarashi and Guarente, 2016; Yilmaz et al., 2012). Therefore, the increase in cell cycle regulation gene expression levels indicates enhanced regenerative capacity of the aged CR epithelium. CR has been shown to reduce the accumulation of DNA damage that occurs during ageing and thus prevent diseases such as age-related cancer. Bruens et al. (2020) has recently shown that damaged and less fit cells in the intestinal epithelium have reduced chance of survival under CR conditions due to competition by CR-induced stem cells which promote the elimination of mutated and weak cells. In line with the studies mentioned, we also observed increased gene expression of

cell regulators, which might be one of the mechanisms that drives intestinal tissue health and increased lifespan of CR mice as observed in the IDEAL study (Rusli et al., 2015; Kok et al., 2018).

Interestingly, we observed increased expression of genes involved in lipid and carbohydrate metabolism under long-term CR. A possible explanation for this effect is that the limited access to food during CR conditions can enhance the capacity of the ileum to uptake nutrients leading to increased gene expression of glucose sensing transcription factor *Chrebp,* disaccharidase *Sis,* fructose metabolism *Khk* and *Fbp1*, and glucose transporters *Sglt1, Glut2* and *Glut5* (Peña-Villalobos et al., 2019). The gene expression of PPARγ and PPARα targets involved in lipid metabolism *Acsl3, Scd2, Lpcat4* and *Elovl6* was increased in response to CR. Similar to our findings, Duszka, et al. (2016) showed increased expression of PPARγ target genes in the intestine of mice exposed to two weeks, 25% CR. These data suggest mechanisms through which PPARs may contribute to energy mobilization during metabolically stressful conditions as CR.

Bile acid metabolism has been previously shown to be influenced by CR (Fu and Klaassen, 2013; Green et al., 2018) which may directly impact lipid, glucose, and energy metabolism, however the effect of CR on bile acid levels and metabolism in the ageing ileum is still scarcely known. Our results show a significant decrease in the gene expression of *Fgf15, Asbt* and *Ostα* with age in the CR mice. In line with this, we also observed decreased total and major individual bile acids including secondary bile acid DCA in CR24m mice compared to LF24m mice. Secondary bile acid, DCA is generated by the gut microbiota, increased DCA in intestine may induce inflammatory signalling that is associated with the development of cancer, therefore reduction in DCA levels may be one of the mechanisms that promotes healthy gut ageing under CR conditions (Wang et al., 2020). In agreement with previous research on the impact of CR on enterohepatic circulation (Fu and Klaassen, 2013; Green et al., 2018), our results showed that CR6m mice tended to have increased levels of primary bile acids, βMCA, CA and TCA in the ileum compared to 6 months old mice on the control diet. Bile acids in the ileum are known to promote lipid breakdown and therefore increased levels of bile acids may promote enhanced lipid absorption and metabolism from the limited nutrients present under CR conditions. Ageing is associated with decreased activity of enzymes related to bile acid synthesis pathway (De Guzman et al., 2013). Although, we observed decreased levels of ileal bile acids in response to 24 months of CR feeding, microarrays data from the liver samples of this study showed significantly increased gene expression of *Cyp7a1* and *Cyp8b1* enzymes (Supplementary Fig. 3.4) involved in bile acid synthesis pathway in CR24m compared to LF24m mice, indicating that CR prevents the decline of the bile acid synthesis pathway with age.

We observed distinct microbial profiles in the ileum of young mice exposed to CR compared to the control group. Intervention with 6 months of CR resulted in increased abundance of beneficial bacteria, *Bifidobacterium* and *Lactobacillus.* The difference in ileal microbiota composition of old mice in response to CR was not as profound as that noticed in young mice, and we observed substantial variation among

the mice. Despite variation, we observed increased presence of *Lactobacillus* in the CR24m group compared to LF24m, wherein the *Lactobacillus* seemed to be absent. The effects of increased abundance of *Lactobacilli* and *Bifidobacteria* have been extensively researched to show associated improvement of intestine mucosal physiology and regulation of the host innate and adaptive immunity (Pyclik et al., 2020).

Research on the impact of CR on mouse physiology is often performed on different background diets, for instance, Green et al. (2018) used high carbohydrate purified control diet (based on the LF diet) to assess the role of CR on the body composition and global metabolomic changes, whereas, Gibbs et al. (2018) used a background chow diet to investigate the metabolomic profiles of C57BL/6J mice exposed to CR. The compositional differences in the diet may result in differential effects of CR on the metabolomics profiles, other factors such as length of time and grade of CR should also be considered.

To test our hypothesis, we performed a preliminary 8 weeks CR study based on chow and LF diet background in order to characterise differences in the gene expression and bile acids levels in the gut and the liver. Under CR conditions, the mice from both diet groups lost weight in the first 2 weeks, and the body weight seemed to plateau in the remaining weeks, which may indicate a state of energy balance in the CR mice (Guijas et al., 2020). We have previously observed increased liver triglyceride levels in response to 4 weeks feeding with the LF compared to chow diet. This effect was reproduced in the current study with 8 weeks LF feeding, while, intervention with LFCR successfully decreased liver triglyceride levels. One of the reasons for this may be the reduced amount of refined carbohydrates presented during CR feeding.

We observed an increase in the total ileal bile acids in LF and LFCR fed mice compared to chow and chowCR respectively, which indicates a stronger LF effect rather than CR. We did not observe differences in the total bile acids in the liver among the diet groups. However, we observed a decrease in *Fgf15* gene expression in the ileum of LFCR compared to LF mice, whereas no difference in its gene expression was observed between chow and chowCR. Blokker et al. (2019, PhD thesis) has indicated that the induction of *Fgf15* expression may be associated with increased glucose concentration in the ileum, in the context of high carbohydrate diet. Therefore, the reduced expression of *Fgf15* in LFCR mice may be a result of low glucose concentration present in the ileum during CR conditions.

Although, we did not observe changes in the total bile acid levels in the liver of chow and chowCR mice, the expression of *Cyp7a1* was increased in response to chowCR diet. While, this effect was not observed in LFCR compared to LF fed mice. The increased expression of liver *Cyp7a1* in the LF mice despite increased *Fgf15* expression in the ileum might be due to the possible fasted state of LF mice as fasting of mice has been known to induce *Cyp7a1* expression in the liver (Ikeda et al., 2014). On the morning of the sacrifice day, we found the food hopper of the LF group to be empty. We are uncertain on the duration of fasting for the LF mice, as the hopper contained some food on the eve of the sacrifice day. We also observed large variation

in the expression of ileal *Fgf15* and liver *Cyp7a1* in the LF group, although, the mice with low expression of ileal *Fgf15* negatively correlated with liver *Cyp7a1* expression. The variation maybe explained by dominance hierarchies within the cage, when mice compete for access to limited food (Varholick et al., 2019).

Similar to our previous 6 and 24 months CR study, we observed increased expression of ileal carbohydrate metabolism genes in response to chowCR and LFCR, which may be an adapting mechanism to low nutritional state of these mice. In agreement with research that shows increased fatty acid β oxidation under CR condition (Green et al., 2018), we observed an increase in the hepatic expression of *Sirt1, Ppara* and *Cd36* in response to the CR intervention. Increased β oxidation of fatty acids in CR mice indicate increased breakdown of lipids for energy to maintain stable weight. Surprisingly, we observed increased expression of lipogenic genes *Fasn*, and *Acaca* in the liver of LFCR mice compared to LF. This effect was not observed between chow and chowCR mice. We believe that the increased expression of liver lipogenic genes may be LF diet exclusive effect, since we also observed increased expression of *Srebp1, Fasn* and *Acaca* in the liver of CR6m, and CR24m mice (Microarrays data from IDEAL, Supplementary Fig. 3.4). The increase in the hepatic lipogenic gene expression did not correlate with the triglyceride levels in the liver. Therefore, we are unsure if the increased hepatic lipogenic gene expression is an adaptive effect of LFCR.

We did not take into account the role of circadian rhythm during the CR studies. The CR mice were fed at 15:30 every day, which may be a different feeding time compared to control mice, as *ad libitum* fed mice have been known to become active in the dark cycle after 19:30 (Ellacott et al., 2010). Changes in the diet intake pattern due to the fact that the CR mice received their daily food at one timepoint, that was rapidly consumed may also have an effect on the metabolic genes in the gut and the liver (Yamamuro et al., 2020). Therefore, a repetition of this experiment with controlled environmental factors, such as feeding of CR mice at night time (20:00 or 21:00) and well stocked food hoppers for control groups, is required to further understand the changes in nutrient metabolism gene expression as well as bile acid metabolism.

Chapter 5: Addition of dietary fibres (DF) improves the low-fat diet induced liver phenotype

5.1 Introduction

Increased *de novo* lipogenesis in hepatocytes is a typical feature of non-alcoholic fatty liver disease (NAFLD). The pathology of NAFLD can be negatively influenced by dietary components such as higher intake of refined carbohydrates (starch, sucrose), and decreased consumption of dietary fibres (DF) (Romero-Gómez et al., 2017; Worm, 2020). Preclinical studies report microbiota disturbances and increased intestinal permeability to be associated with NAFLD (Luther et al., 2015). Indeed, in our previous chapters we have reported that 4 and 8 weeks feeding of mice with the purified high refined carbohydrate LF diet resulted in hepatic lipid deposition and changes in the ileal microbiota composition compared to a fibre rich chow diet. The liver and the ileum are connected via the enterohepatic circulation of bile acids, therefore, any disturbance in the ileal microbiota are likely to influence the functioning of the liver. The pathophysiology of NAFLD is highly complex and involves numerous pathways including the inflammation of the adipose tissue and gastrointestinal dysbiosis (Tilg et al., 2020). In the recent years, the technological advancement for microbiome analysis has driven researchers to study the interactions between the gut microbiota and dietary factors that influence NAFLD (Aron-Wisnewsky et al., 2020).

DF are known to improve metabolic diseases such as NAFLD through regulation of glucose and cholesterol metabolism and decreased gut and systemic inflammation (Hamaker and Cantu-Jungles, 2020, Shtriker et al., 2018). The underlying mechanisms for these health effects have been suggested to be associated with decreased gastric emptying, altered composition of the gut microbiota and SCFAs (Makki et al., 2018; Canfora et al., 2019). Consumption of DF alters the niche environment in the gut lumen by providing substrates for microbial growth, thereby, enhancing the abundance of bacterial species that are able to utilize these DF (Deehan et al., 2017). For example, inulin has been known to induce the abundance of *Bifidobacteria* levels that possess enzymes to efficiently utilise this substrate. Increased abundance of *Bifidobacteria* is strongly correlated with reduced endotoxemia and improved glucose tolerance (Cani et al., 2007). Further, DF have been reported to play a part in regulating and maintaining host immune system via SCFAs as well as microbiota independent effects (Makki et al., 2018). Despite the abundant research on the beneficial effects of DF, the mode of action of structurally different DF on the gut-liver axis (specifically the ileum) remains unclear.

In the current study we fed mice five different diets with varying types of DF for the duration of 10 weeks. The mice were fed with chow (16% fibre), LF (5% non-soluble fibre), LS (LF diet with reduced sucrose content, 5% fibre), LS enriched with inulin (LS+In, 11.3% fibre) and LS enriched with a combination of inulin, pectin and psyllium (LS+Comb, 11.3% fibre). We hypothesised that a higher sucrose content was one of the major drivers for LF induced liver phenotype (Jang et al., 2018). Hence, we aimed to prevent the detrimental effects of the LF diet by reducing the content of sucrose from 17% in LF to 7% in the new LS diet (sucrose was compensated with starch). Further, we enriched the LS diet with DF to investigate their effect on the gut-liver axis. The fibres were chosen due to their popularity as prebiotic supplements and applications in modern food products such as dessert pots,

milkshakes, and readymade meals (Capuano, 2017). The first aim of this study was to investigate the effects of reduced sucrose and addition of DF in the LS diet on the pathophysiology of gut-liver axis. Secondly, we hypothesised that the varying structure of DF used in our new diets may result in different gut microbiome outcomes due to bacteria having distinct specificities to different chemical and physical structures (Singh and Vijay-Kumar, 2020). Therefore, we also aimed to describe the effects of different DF on the ileal gene expression and microbiota profile. To fulfil this aim, we performed RNA sequencing and 16S rRNA sequencing on ileal tissue and luminal content samples from chow, LS, LS+In and LS+Comb groups.

5.2 Results

5.2.1 Addition of DF mitigates LF induced triglyceride accumulation in the liver

At the end of the experiment the LF fed mice showed increased trend in weight gain compared to chow (26± 0.9%, P=0.1), LS, LS+In and LS+Comb fed mice (30± 0.9%, P=0.05; 41 ±0.8, P=0.002; 55 ±0.8%, P=0.001 respectively) (Fig. 5.1A and B). The food intake did not differ between the diet groups (Fig 5.1C). To investigate the morphological differences between the diet groups, we measured the small intestine length of mice immediately after sacrifice to show increased length in the LS+In and LS+Comb group compared to LS (9 ±1%, P=0.01; 16.6 ±1%, P=0.01 respectively) (Fig. 5.1D). We did not observe a significant difference between the liver to body weight ratio of mice in the different diet groups (Fig. 5.1E).

Due to the previously observed effects of the LF diet on the liver phenotype, we investigated if reduced sucrose content and addition of fibres prevented the development of this pathophysiological phenotype. We observed an increase in the liver triglycerides content of mice fed with the LF and an increasing trend for the LS diet (68 ±0.7%, P=0.001 for LF and 55 ±0.3%, P=0.1 for LS) compared to the chow group (Fig. 5.2A). The reduced sucrose content in the LS diet resulted in decreasing trend of liver triglycerides levels compared to LF diet (28±0.5%), however, the difference was not significant P>0.5. The reduced sucrose content and addition of fibres resulted in a significant decrease in liver triglycerides content in LS+In and LS+Comb compared to LF diet group (59 ±0.5%, P=0.01, similar percentage decrease in both fibre groups). Moreover, the analysis of livers in LS+In and LS+Comb groups suggested lower triglycerides levels compared to the LS diet (43±0.5%, P=0.2) (Fig. 5.2A). The expression analysis of lipogenic genes sterol regulatory element-binding protein 1 (*Srebp1*) and acetyl-coA carboxylase (*Acaca*) in the liver coincided with triglyceride levels to show significantly increased expression in the LF and LS group compared to chow (*Srebp1*: 78±0.6%, 41 ±0.3%, P<0.001; *Acaca*: 124±0.6% ,70±1%, P<0.001, LF and LS respectively). The gene expression of *Srebp1* was significantly decreased with the LS enrichment of fibres by 44 ±0.2% P<0.001 for LS+In and 52 ±0.2%, P<0.001 in LS+Comb compared to LS group (Fig. 5.2B). While, the gene expression of *Acaca* was decreased by 49 ±0.3%, P=0.01 for both LS+In and LS+Comb groups compared to LS. The gene expression of ketohexokinase (*Khk*) was measured to show a trend towards increase in the LF compared to other groups, although, it did not reach significance (P=0.3). The expression of *Khk* was found to be decreased in the LS+Comb group compared to LF (71±0.2%, P=0.02). Figure 5.2 C ,D, E and F shows haematoxylin and eosin (H&E) stained liver samples of mice fed the different diets, although LF and LS diet both revealed accumulation of lipid droplets, the histology of LF liver sections shows presence of monocytes which indicates inflammation in the liver. In agreement with the triglycerides content and lipogenic gene expression, the reduced sucrose content with addition of fibres in the LS diet showed improved liver morphology.
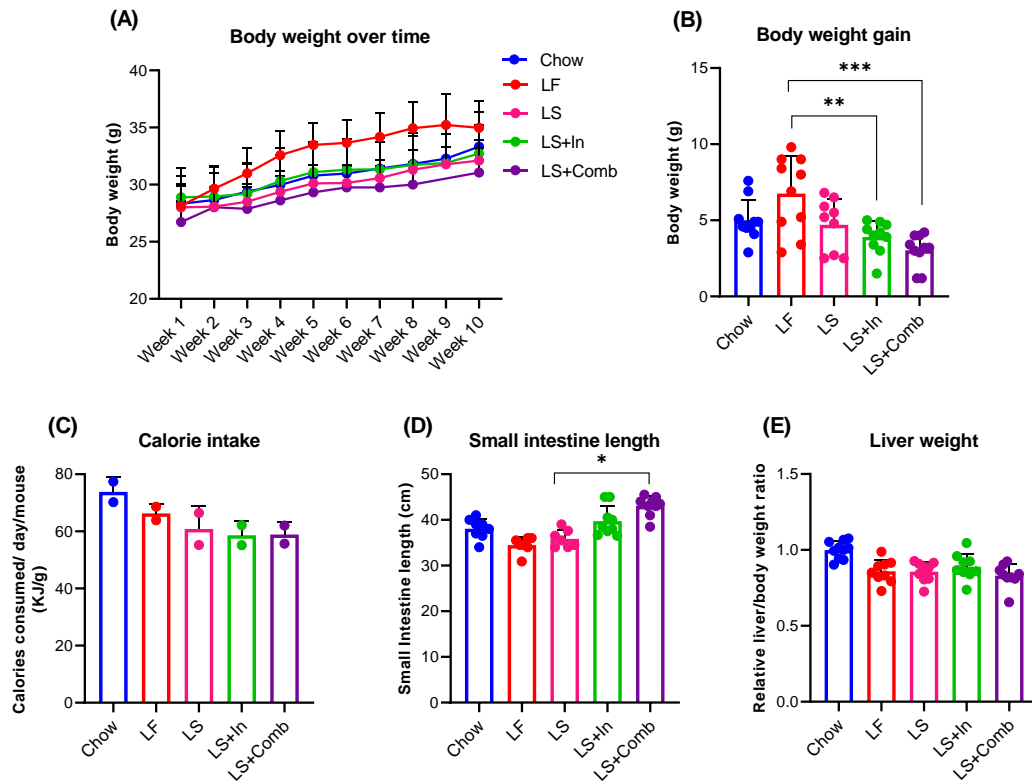
Figure 5.1 The effect of diets on body composition. Mice were fed with chow, LF, LS, LS+In and LS+Comb diet, body weight was measured every week for 10 weeks (A). After 10 weeks feeding, we analysed, body weight gain (B) the amount of calories consumed per day per mouse (C), small intestine length (D), and liver weight (g) relative to body weight (g) ratio of mice (E). Significance was tested using 1-way ANOVA with Tukey's multiple comparison test (*** = p<0.001, **= p<0.01, *= p<0.05). Values are the means ± SEM of n=10 mice in each group. Mice per group were divided into two cages (as 5 mice per cage), calorie intake was measured per cage and divided by 5 to calculate the intake of one mouse. LF: Low-fat diet, LS: Low sucrose version of LF diet, LS+In: LS diet enriched with inulin, LS+Comb: LS diet enriched with a combination of fibres.
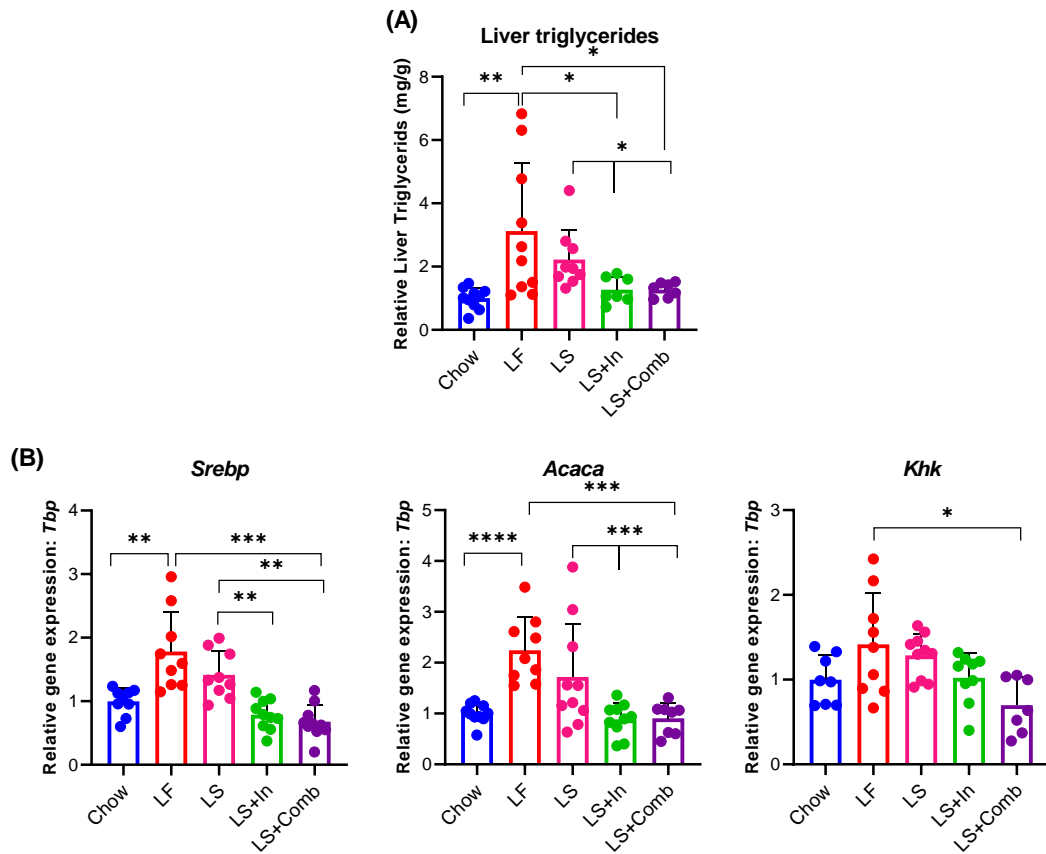
Figure 5.2 The effect of diets on the liver phenotype of mice. Liver phenotype was examined by quantification of liver triglyceride levels (A), expression analysis of lipogenic gene in the liver (B). Significance was tested using 1-way ANOVA with Tukey's multiple comparison test (*** = $p<0.001$, **= $p<0.01$, *= $p<0.05$). Values are the means ± SEM of n=9-10 mice in each group. LF: Low-fat diet, LS: Low sucrose version of LF diet, LS+In: LS diet enriched with inulin, LS+Comb: LS diet enriched with a combination of fibres.
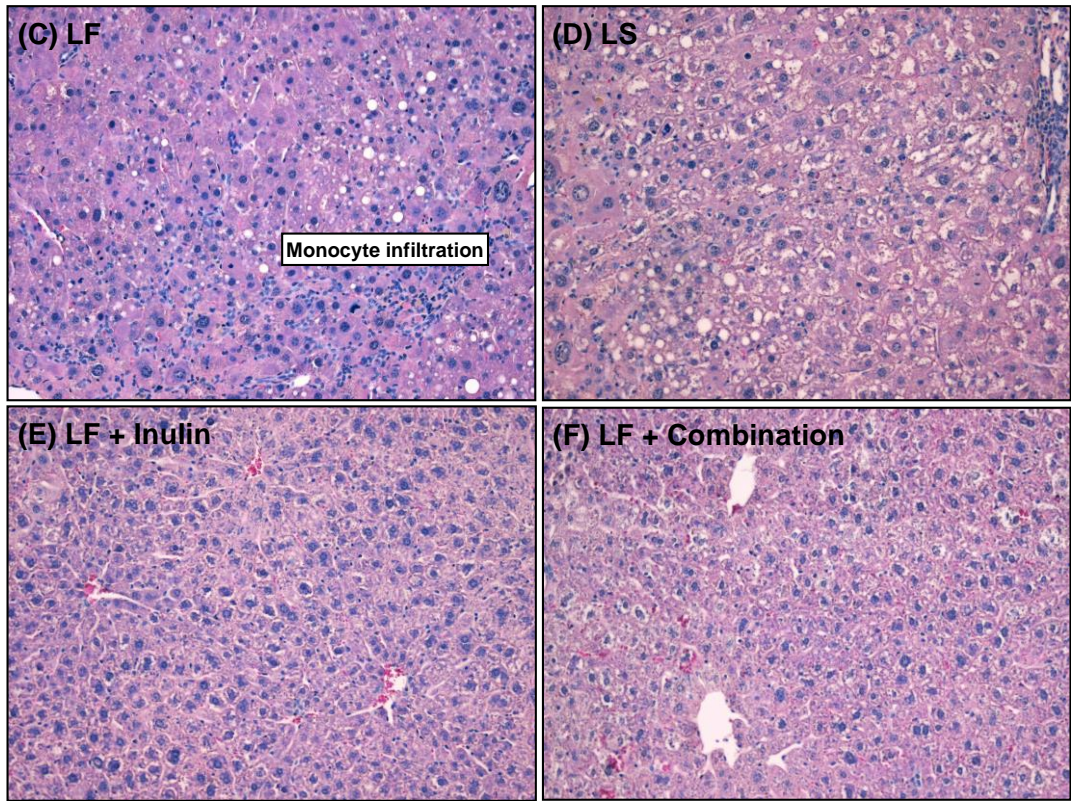
Figure 5.2 (Cont.) The effects of diets on the liver phenotype of mice. Liver phenotype was examined by histological analysis via haematoxylin and eosin (H&E) staining of livers from mice fed the LF (C), LS (D), LS+In (E) and LS+Comb (F) diets (Magnification 10x). LF: Low-fat diet, LS: Low sucrose version of LF diet, LS+In: LS diet enriched with inulin, LS+Comb: LS diet enriched with a combination of fibres.

5.2.2 Addition of DF upregulates the expression of ileal carbohydrate metabolism genes

Ileal gene expression was quantified by quantitative polymerase chain reaction (qPCR) (Fig. 5.3A). Both LF and LS diet led to an increase in the expression of maltase-glucoamylase (*Mgam*), sucrase-isomaltase (*Sis*) and glucose transporter 2 (*Glut2*) compared to chow (P<0.05). The reduced sucrose content in the LS diet, did not affect the expression levels of carbohydrate related genes compared to the LF diet. Interestingly, we observed an increase in the carbohydrate metabolism genes in the fibre groups compared to chow fed groups (P<0.001) and an increasing trend compared to the LS group (P=0.1 for *Mgam* and *Sis*, P=0.01 for *Glut2*) (Summary of statistics in Table 5.1). The barrier function was analysed by testing the gene expression of claudin 3 and occludin (*Cldn3* and *Ocln*) (Fig. 5.3B). LF and LS diet led to decreased *Cldn3* and *Ocln* expression compared to chow (33 and 27±0.1, LF and LS respectively, P<0.03). Addition of fibres in LS+In and LS+Comb diet did not significantly improve *Cldn3* gene expression. We noticed an increasing trend in *Ocln* gene expression in the fibre groups, however, the difference did not reach significance compared to LF and LS diet groups (P>0.05). We observed increased gene expression of *Fgf15* in both LF and LS diet groups (P<0.02). Whereas, the *Fgf15* gene expression was significantly decreased with the addition of fibres to the LS group in both LS+In and LS+Comb (Summary of statistics in Table 5.1).
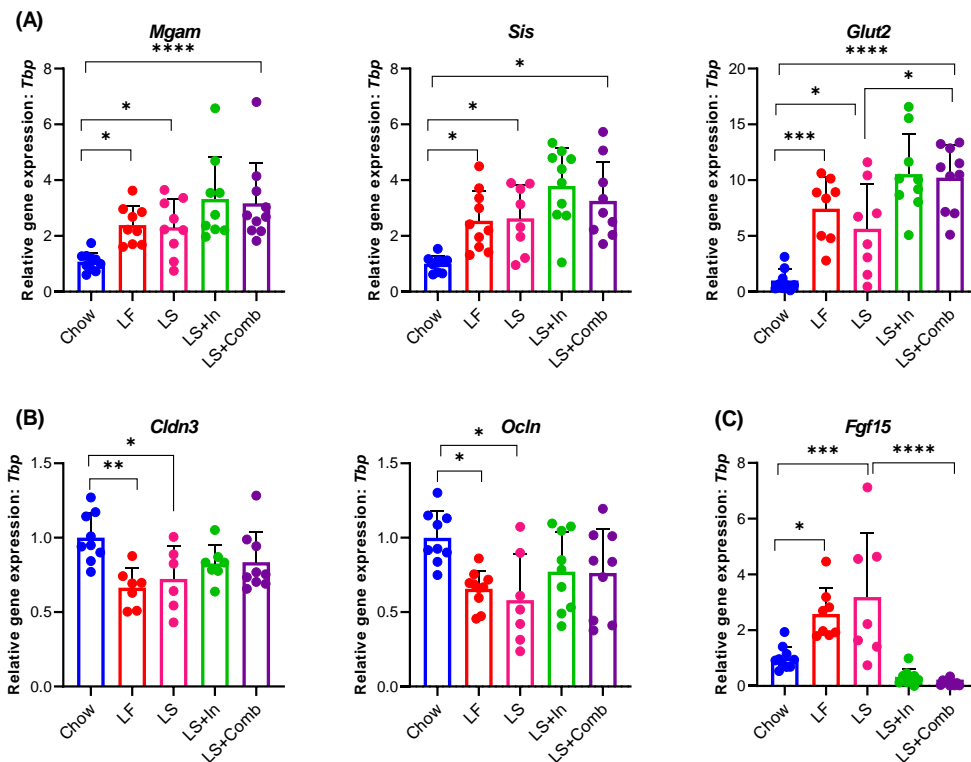
Figure 5.3 Qpcr gene expression analysis of ileum. Significance was tested using 1-way ANOVA with Tukey's multiple comparison test (*** = p<0.001, **= p<0.01, *= p<0.05). Values are the means ± SEM of n=9-10 mice in each group. Qpcr: Quantitative polymerase chain reaction. LF: Low-fat diet, LS: Low sucrose version of LF diet, LS+In: LS diet enriched with inulin, LS+Comb: LS diet enriched with a combination of fibres.

Table 5.1 Summary of statistics for ileal gene expression analysis. Significance was tested using 1-way ANOVA with Tukey's multiple comparison test. Values are the means of n=9-10 mice in each group. LF: Low-fat diet, LS: Low sucrose version of LF diet, LS+In: LS diet enriched with inulin, LS+Comb: LS diet enriched with a combination of fibres.

Test details	Mean 1	Mean 2	SE of diff.		P Value
Mgam					
chow vs. LF	1.0	2.4	0.5	*	0.05
chow vs. LS	1.0	2.3	0.5	*	0.05
chow vs. LS+In	1.0	3.3	0.5	***	0.0005
chow vs. LS+Comb	1.0	3.2	0.5	***	0.0009
LS vs. LS+In	2.3	3.3	0.5	ns	0.1
LS vs. LS+Comb	2.3	3.2	0.5	ns	0.1
Sis					
chow vs. LF	1.0	2.5	0.5	*	0.04
chow vs. LS	1.0	2.6	0.6	*	0.04
chow vs. LS+In	1.0	3.8	0.5	****	0.0001
chow vs. LS+Comb	1.0	3.3	0.5	**	0.001
LS vs. LS+In	2.6	3.8	0.5	ns	0.07
LS vs. LS+Comb	2.6	3.3	0.6	ns	0.1
Glut2					
chow vs. LF	1.0	7.4	1.5	***	0.0008
chow vs. LS	1.0	5.6	1.5	*	0.02
chow vs. LS+In	1.0	10.6	1.4	****	0.0001
chow vs. LS+Comb	1.0	10.2	1.4	****	0.0001
LS vs. LS+In	5.6	10.6	1.5	*	0.02
LS vs. LS+Comb	5.6	10.2	1.4	*	0.02
Cldn3					
chow vs. LF	1.0	0.7	0.1	**	0.004
chow vs. LS	1.0	0.7	0.1	*	0.01
Ocln					
chow vs. LF	1.0	0.7	0.1	*	0.03
chow vs. LS	1.0	0.6	0.1	*	0.01
Fgf15					
chow vs. LF	1.0	2.6	0.5	*	0.02
chow vs. LS	1.0	3.2	0.5	***	0.0008
LF vs. LS+In	2.6	0.3	0.5	***	0.0004
LF vs. LS+Comb	2.6	0.1	0.5	****	0.0001
LS vs. LS+In	3.2	0.3	0.5	****	0.0001
LS vs. LS+Comb	3.2	0.1	0.5	****	0.0001

5.2.3 RNA sequencing analysis revealed differential gene regulation between fibres

RNA sequencing analysis was performed on ileum samples from chow, LS, LS+In and LS+Comb fed mice. Sequences were mapped using the HISAT2 software to the reference genome. HTSeq software was used to analyse gene expression levels using the union mode. Expression values were calculated as FPKM (Fragments Per Kilobase of transcript sequence per Millions base pairs sequenced). Further analysis on the RNA sequencing data was performed on Network Analyst 3.0 (Zhou et al., 2019). The data was filtered for low variance (variance genes based on IQR <15) and low relative abundance (average expression signal < 15) and unannotated genes, and normalization was selected for Log2-counts per million, which resulted in 45, 9 and 58 differentially expressed genes (DEGs) (EdgeR based method, FDR adjusted P value cut-off: 0.05; logFC ≥1.0) between chow Vs LS, LS+In Vs LS and LS+Comb Vs LS diet groups (Fig. 5.4A). Next, we compared the chow and LS fibre enriched groups together against LS to reveal 61 DEGs (adjusted P value cut-off :0.05; logFC ≥1.0). We performed gene set enrichment analysis (GSEA) on the 61 DEGs to find out the biological functions or pathways associated with the genes by using Kyoto Encyclopedia of Genes and Genomes (KEGG) database that annotates genes to pathway level. The KEGG pathway analysis revealed that the 61 DEGs were significantly enriched in immune related pathways (Herpes simplex infection, Epstein-Barr virus infection, Influenza A, Antigen processing and presentation, Allograft rejection, Toxoplasmosis, Graft-versus-host disease, Type I diabetes mellitus, Autoimmune thyroid disease) and metabolic pathways. Figure 5.4B shows the top 10 KEGG pathways.
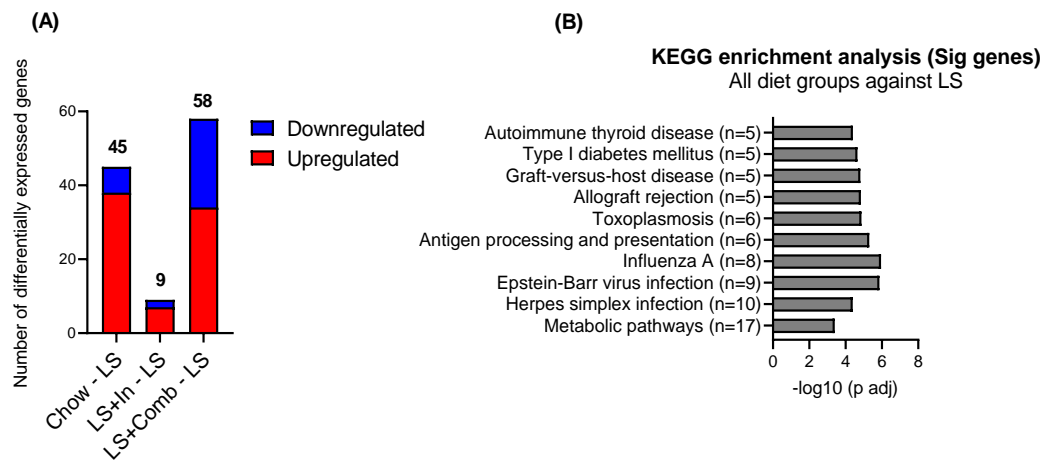
Figure 5.4 RNA sequencing analysis on ileal samples (n=5 per group) from chow, LS, LS+In and LS+Comb fed mice. RNA sequencing analysis revealed 45, 9, and 58 differentially expressed genes when chow, LS+In and LS+Comb were compared against LS diet group (A). KEGG pathway analysis of differentially expressed genes revealed significant enrichment of genes related to immune and metabolic pathways (B). Differential analysis was performed by EdgeR method, FDR adjusted P value cut-off of 0.05; logFC ≥1.0). LF: Low-fat diet, LS: Low sucrose version of LF diet, LS+In: LS diet enriched with inulin, LS+Comb: LS diet enriched with a combination of fibres.

Figure 5.5A shows the immune related genes that were altered between the diets. Interferon induced oligoadenylate synthetases (*Oas1g, Oas3* and *Osal2*), interferon induced protein with tetratricopeptide repeats 1(*Ifit1*) were shown to be upregulated in chow and LS+Comb diet groups. Adaptive immune response, major histocompatibility complex class II genes (*H2-aa, H2-ab1,* and *H2-dmb1*) were increased in fibre rich groups, however the significance was limited to LS+Comb group. Other genes related to immunity such as lipopolysaccharide (LPS) induced ubiquitin D (*Ubd*), gene involved in transport of antigens, T cell specific gene, granzyme B (*Gzmb*) and Z DNA binding protein, a cytosolic bacterial DNA sensor and activator of interferon (IFN)-regulatory factors (*Zbp1*) were also increased in chow and LS+Comb groups, however significantly in the latter. Gene coding for interferons such as *Ifn-α*, *Ifn-γ* and interferon alpha and beta receptor subunit 1 *Ifnar1* were not altered between the diets (Shulzhenko et al., 2011).

The changes in the expression levels of genes involved in carbohydrate digestion and absorption in the ileum are shown in Figure 5.5B. Similar to our results from the qPCR gene expression analysis, significant upregulation in the expression levels of carbohydrate metabolism genes, *Mgam*, *Sis* and *Khk* was observed after 10 weeks of LS diet feeding. While, the addition of fibre groups (LS+In and LS+Comb), further enhanced the gene expression of *Mgam, Sis, Khk* (only in LS+In), aldolase B (*Aldob*), and fructose-bisphosphatase 1 (*Fbp1*) compared to chow and LS diet groups. The absorption of the resultant glucose in the small intestine is primarily driven by two separate transport proteins, sodium-dependent glucose cotransporter (SGLT1) and glucose transporter 2 (GLUT2). The expression levels of *Sglt1* and *Glut2* gene in the ileum were significantly increased in mice fed the LS and LS+In compared to chow diet group. The gene expression levels of *Sglt1* and *Glut2* were decreased in the LS+Comb when compared to LS and LS+In groups. We have previously shown that LF and LS induced the expression of *Fgf15* in the ileum. While, the addition of fibres blunted the LS induced expression of *Fgf15* (Fig. 5.5B) (Summary of statistics in supplementary table 4.2).
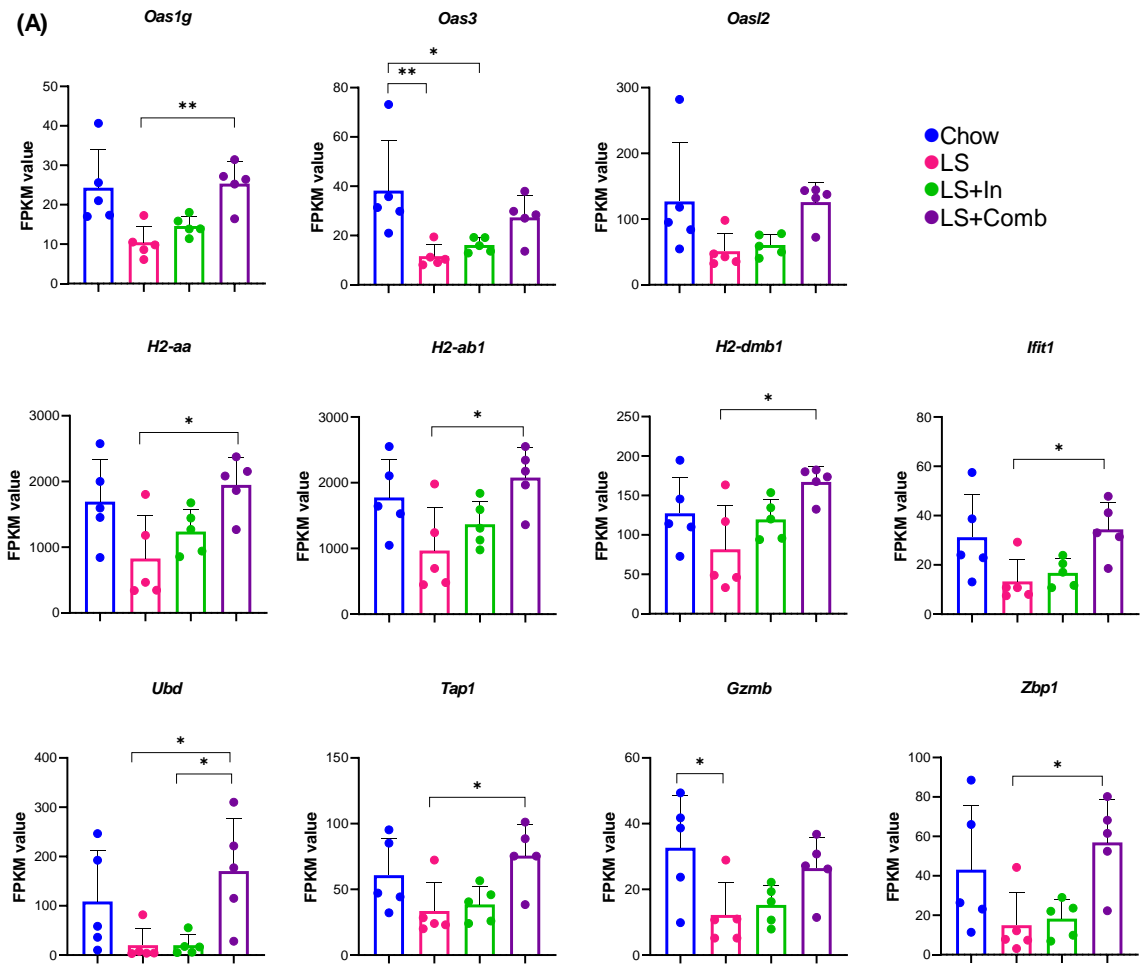
Figure 5.5 Ileal expression profiles of immune related genes in response to the different diets. **Significance was tested using 1-way ANOVA with Tukey's multiple comparison test (*** = p<0.001,** ****= p<0.01, *= p<0.05). Values are the means ± SEM of n=5 mice in each group. LF: Low-fat diet, LS:** **Low sucrose version of LF diet, LS+In: LS diet enriched with inulin, LS+Comb: LS diet enriched with a** **combination of fibres.**

(B)
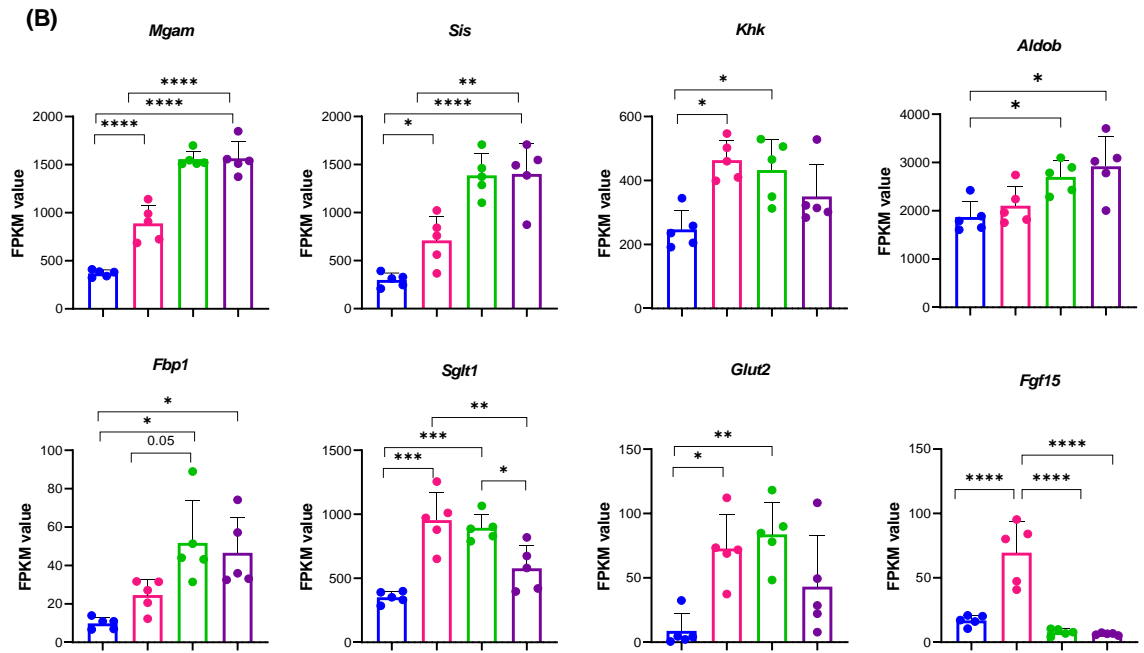
Figure 5.5 (Cont.) Ileal expression profiles of carbohydrate related genes in response to the different diets. Significance was tested using 1-way ANOVA with Tukey's multiple comparison test (* = p<0.001, **= p<0.01, *= p<0.05). Values are the means ± SEM of n=5 mice in each group. LF: Low-fat diet, LS: Low sucrose version of LF diet, LS+In: LS diet enriched with inulin, LS+Comb: LS diet enriched with a combination of fibres.**

5.2.4 DF differentially impact the composition of ileal microbiota

Considering the differential impacts of DF on ileal gene expression, we next investigated the changes in ileal microbiota composition via 16S rRNA sequencing. The alpha diversity measured by Shannon index was significantly decreased in LS based diets ($30 \pm 0.2\%$ LS, $26 \pm 0.2\%$ LS+In and $43 \pm 0.2\%$ LS+Comb, P<0.01) compared to chow diet. While, the observed species was significantly increased in the LS compared to LS+fibre groups ($16 \pm 9\%$ P<0.001 LS+In and $13\pm10\%$ P=0.02) (Fig. 5.6A) At the phylum level, we observed a significant decrease in the relative abundance of *Bacteroidetes* (by $55\pm 0.02\%$, P<0.0001) and a significant increase (by $33\pm 0.02\%$, P<0.0001) in the relative abundance of *Firmicutes* in the LS fed mice. Whereas, the addition of inulin to the LS diet resulted in increased relative abundance of *Bacteroidetes* ($34 \pm 0.02\%$, P<0.001) and a decreased relative abundance of *Firmicutes* ($28.5\pm 0.02\%$, P<0.0001) compared to LS fed mice. The LS+Comb diet also decreased the relative abundance of *Firmicutes* ($10\pm 0.02\%$, P=0.04), however, the combination of fibres did not influence the *Bacteroidetes* levels compared to LS group. Notably, the addition of inulin and fibre combination suggested enhanced levels of *Actinobacteria* by $74\pm 0.02\%$ P <0.001 and $64\pm 0.02\%$, P=0.06 respectively compared to LS fed mice (Fig. 5.6B).

Within the *Firmicutes* phylum, we observed increasing trend in the levels of *Lactobacillus* in the chow compared to LS and significantly increased levels compared to other groups (32% P=0.1 LS, 90% and 91% P<0.0001 LS+In and LS+Comb) (Fig. 5.6C and 5.7A). While, the levels of *Faecalibaculum* from the *Erysipelotrichidae* family were significantly increased in the LS, LS+In and LS+Comb compared to chow (52%, 43% and 56% respectively, P<0.01) (Fig. 5.6C and 5.7B). Levels of genus *Bacteroidales S24-7 group* from the *Bacteroidetes* phylum were increased (57%, P=0.01) in the chow compared to LS fed mice. Furthermore, the levels of the *Bacteroidales S24-7 group* suggested an increase by 33%, P=0.1 in the LS+In compared to LS diet group. The levels of *Bacteroidales S24-7 group* were not affected by LS+Comb feeding (Fig. 5.6C and 5.7C). The genus *Akkermansia* from the *Verrucomicrobia* phylum was significantly increased in LS+Comb compared to chow (84%, P=0.04) and LS diet groups (90%, P=0.006). Although the mean levels of *Akkermansia* in LS+In group suggested an increase compared to chow and LS fed mice, the difference did not reach significance (58% compared to chow, 65% compared to LS, P>0.1, due to large interindividual variation). The levels of *Akkermansia* were significantly different between the LS+In and LS+Comb diet groups (70%, P=0.03) (Fig. 5.6C and 5.7D). The addition of DF to the LS diet resulted in significantly increased levels of *Bifidobacteria* (98% in LS+In and 97% in LS+Comb, P<0.001) compared to the LS diet (Fig. 5.6C and 5.7E). Altogether, our results show modified profiles of the ileal microbiota in response to addition of DF. We also show fibre specific differences in the ileal microbiota, especially the levels of *Akkermansia* were found to be different between LS+In and LS+Comb diet groups.
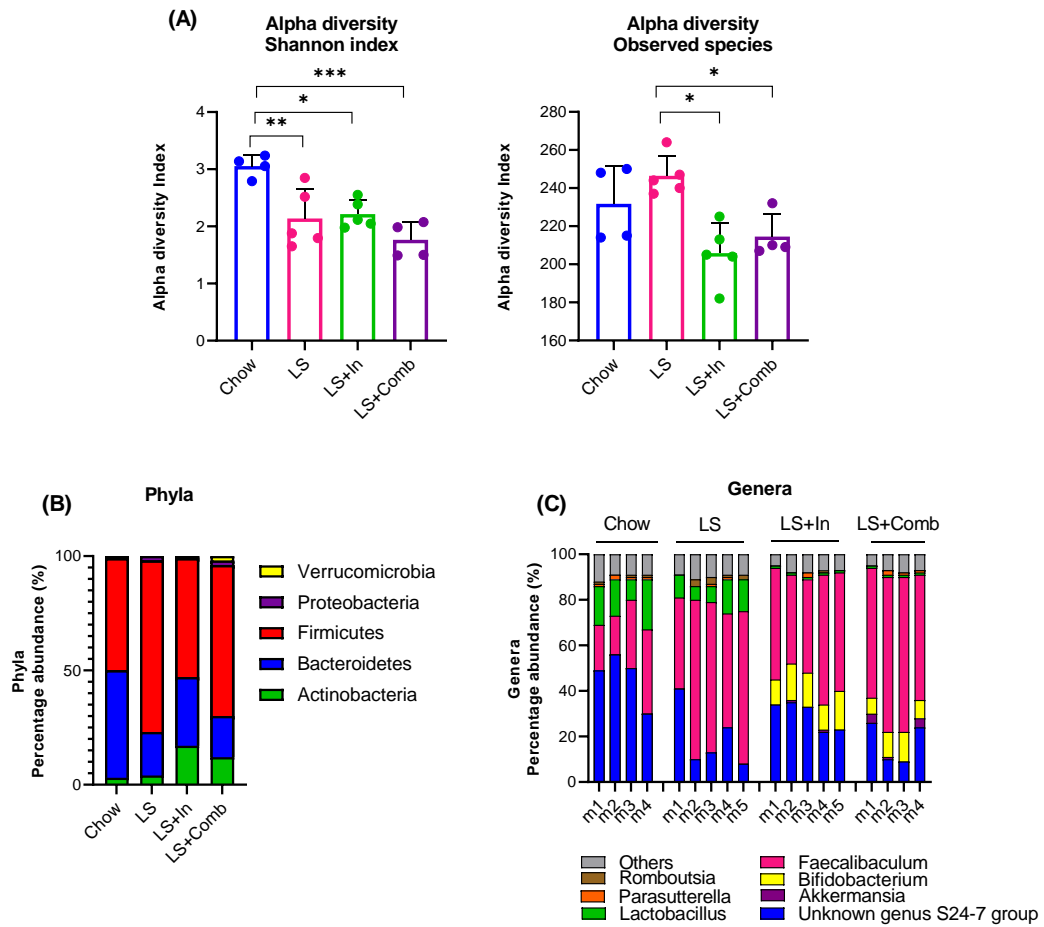
Figure 5.6 Altered profiles of the ileal microbiota in response to addition of dietary fibres (DF). Alpha diversity (Shannon index) was decreased in LS and LS+DF compared to chow fed mice (A). Summarization of the changes in bacteria at the phylum level between the different diet groups (B). Bar graph displays the relative abundance of bacteria at the genus level in the individual mice in the four diet groups (D). Significance for α diversity was tested using a Kruskal–Wallis non-parametric test (* = p<0.001, **= p<0.01, *= p<0.05). Values are the means ± SEM of n=4-5 mice in each group. LF: Low-fat diet, LS: Low sucrose version of LF diet, LS+In: LS diet enriched with inulin, LS+Comb: LS diet enriched with a combination of fibres.**
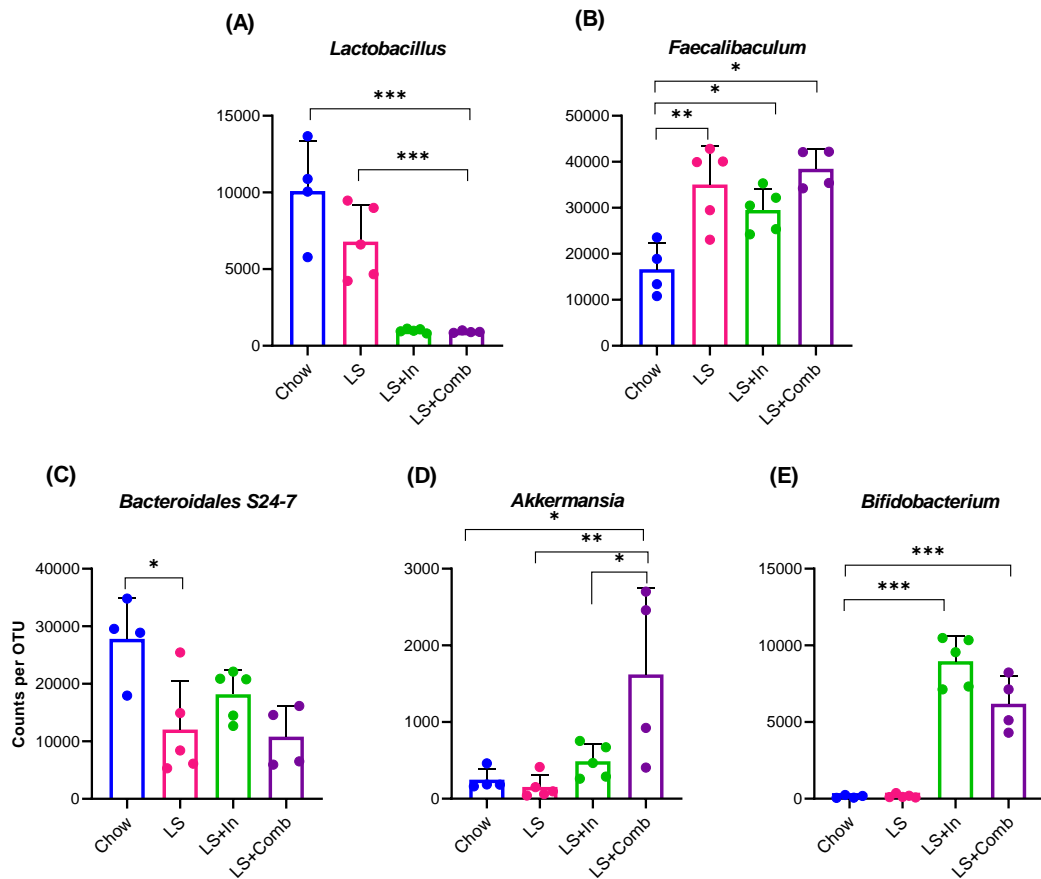
Figure 5.7 Ileal microbiota composition at the genus level that was significantly altered between the diet groups. Significance was tested using 1-way ANOVA with Tukey's multiple comparison test (* = p<0.001, **= p<0.01, *= p<0.05). Values are the means ± SEM of n=4-5 mice in each group. LF: Low-fat diet, LS: Low sucrose version of LF diet, LS+In: LS diet enriched with inulin, LS+Comb: LS diet enriched with a combination of fibres.**

5.3 Discussion

In the first part of this chapter we compared chow, LF (high sucrose), LS (LF diet with low sucrose), LS enriched with inulin and LS enriched with a combination of inulin, pectin and psyllium to investigate the effects of these diets on the liver phenotype of mice. In the second part, we compared the effects of the fibre groups on the ileal gene expression and microbiota composition to show differential effects of the fibres.

We observed a decrease of body weight gain in LS fibre enriched groups compared to the LF group. The decreased weight gain in these groups may be a result of reduced sucrose as well as high fibre intake compared to the LF group. The presence of soluble fibres as in the LS+In and LS+Comb groups, has been known to increase food viscosity and decrease appetite in mice, which may result in weight loss (Muller et al., 2018). We did not observe a difference in the calorie intake of mice in different diet groups, which may be due to the lack of sensitive methods used to measure food intake in this study. The mice were not housed individually therefore, food consumption was calculated as average intake per mouse. Moreover, a large amount of food crumbs often gets mixed with bedding in the cage, which makes food intake difficult to be measured accurately (Ellacott et al., 2010). It is worth noting that we have not observed difference in weight gain between chow and LF feeding experiments performed for 4 and 8 weeks. The difference in weight gain (although did not reach significance) between chow and LF groups in this study, may have been affected by the source of the mice (Charles River UK) used in this experiment, as previously our studies have been conducted on mice sourced from inhouse Disease Modelling Unit (DMU) facility. This has been further discussed in Chapter 6.

We observed an increase in the small intestinal length in response to the fibre enriched LS diets. Several studies have found inulin supplementation to increase the small intestine length in poultry animals (Bucław et al., 2016). Further morphological analysis on the villi length can provide information on this adaptive response of the small intestine.

The liver triglyceride levels were found to be increased in LF and LS groups compared to the high fibre group, chow, LS+In and LS+Comb. Our results showed that reduction of sucrose content of the LF diet did not improve the liver triglyceride levels in the LS group (possibly due to high levels of refined starch present in the LS diet). Whereas, the addition of fibres to the LS diet prevented lipid accumulation in the liver, and matched liver triglyceride levels to that of the chow fed mice. We were able to confirm these results by quantifying *Srebp1*, *Acaca* gene expression and haematoxylin and eosin (H&E) stained histology of liver samples. Our results suggest a protective role of soluble fibres to early signs of liver steatosis observed in purified LS diet feeding. Soluble DF are able to form gels in the presence of water which may impact intestinal motility and absorption rates of glucose and fructose (breakdown products of sucrose and starch) from the LS diet leading to reduced *de novo* lipogenesis in the liver (Muller et al., 2018).

We observed increased gene expression of the brush border enzymes responsible for hydrolysis of dietary carbohydrates, *Mgam* and *Sis* and glucose uptake transporter

Glut2 in LS+In and LS+Comb compared to the LF and LS diet fed mice. Neyrinck et al (2016) has demonstrated an inhibitory action on the intestinal sucrase activity for the inulin extract from chicory root *in vitro* and proposed a mixed non-competitive inhibitory mode for inulin. This may be an inulin or purified fibres specific effect, since the gene expression of *Sis* and *Mgam* was not upregulated by the grain-based crude fibres in the chow diet. In line with the glucosidase inhibitory effect of refined fibres, we observed a significant decrease in the *Fgf15* gene expression in the fibre rich diets compared to the LF and LS diet. Our results are in agreement with findings from Blokker et al. (2019, PhD thesis) that suggested high intracellular glucose concentration in the epithelial cells to induce *Fgf15* expression in the ileum. We did not observe a difference between the ileal gene expression levels of *Fgf15* between LF (high sucrose) and LS (low sucrose) fed mice, which fits with Blokker et al.'s hypothesis that *Fgf15* induction is due to increased glucose concentration from starch in the ileum of LF fed mice. The *Fgf15* ileal expression is decreased in the added fibre diets possibly due to inhibition of MGAM, thereby, reducing the glucose absorption from starch in the LS diet. Altogether, the decreased absorption of glucose in the ileum may be the reason for reduced triglycerides levels and lipogenic gene expression in the liver of LS+fibre groups.

The gene expression of *Cldn3* and *Ocln* was decreased in response to the LF as well as the LS diet compared to chow, which suggests that the reduced sucrose content of the LS did not improve the barrier function in mice. Although, we observed some improvement in the gene expression of *Cldn3* and *Ocln* with the addition of fibres to the LS diet, the increase did not reach significance. These results indicate that there may be other components lacking in the LS+In and LS+Comb, compared to the chow diet. Postal et al. (2020) showed that aryl hydrocarbon receptor (AHR) activation protected barrier integrity in the intestinal epithelium of diet induced obesity (DIO) mice models. Thus, the absence of AHR ligands in the purified diets compared to chow may be one of the factors for reduced expression of barrier function genes. We observed significantly decreased expression of duodenal cytochrome P450, family 1, subfamily A, polypeptide 1 (*Cyp1a1* target gene for AHR), in the LF, LS and LS+fibre groups compared to chow (Supplementary Fig. 3.5).

RNA sequencing analysis of ileum samples suggested an increase in the interferon induced genes (*Oas1g, Oas3 and Osal2, Ifit1, Zbp1*) and immune related genes (*H2-aa, H2-ab1, H2-dmb1, Ubd, Gzmb*) in mice fed with chow and LS+Comb diet. The MHC class II molecules, H2-AA, H2-AB1, H2-DMB1 are distinctive markers for ILC3e (Type III Innate lymphoid cells) (Hepworth et al., 2015). Activation of antigen-presenting ILC3e subset have been shown to inhibit commensal bacteria associated T cell responses rather than inducing T-cell proliferation (Hepworth et al., 2015). These findings are indicative of the role of ILCs in maintaining intestinal homeostasis through MHC II-dependent interactions with T cells to inhibit pathological adaptive immune responses to gut microbiota. Our data suggests that the activity of ILCs might be influenced by complex fibres present in LS+Comb and chow diet. Recent research has shown that that in addition to the fibre's effect on the gut microbiota composition, fibres can also directly impact signalling in the intestinal mucosa (Wu et al., 2017). Chow and the LS+Comb group contains a variety of

complex structured soluble fibres with increased branching, whereas the LS+In diet solely contains chicory inulin, a long-chain linear fructan. The presence of the variety of polysaccharides in the chow and LS+Comb diet may differentially interact with the intestinal epithelial cells (IECs) compared to LS+In and thus causing the differential expression of immune related genes (Tiwari et al., 2020).

Similar to our Q-PCR results, RNA sequencing analysis of the ileal samples showed increase in the gene expression *Mgam* and *Sis*, in the LS group compared to chow. The gene expression of *Mgam Sis*, *Khk Aldob* and *Fbp1* was further increased in the added fibre groups compared to LS. The structure of inulin is made up of a chain of fructose monomers, which may bind to enzymes involved in fructose metabolism (KHK, ALDOB, FBP) and thus affect their activity. Further experiments are required to measure the activity of enzymes involved in carbohydrate metabolism to draw firm conclusions on their interaction with different fibres.

We have previously reported differences in the ileal microbiota composition of mice fed with chow and purified LF diet. In the current chapter, we described the effects of purified LS and LS diet supplemented with different soluble fibres on the ileal microbial composition. We observed a decrease in the Shannon α diversity index in the LS group compared to chow. In contrast to literature, the addition of fibres did not increase the microbiota α diversity in the LS+In and LS+Comb fed mice (Deehan et al., 2017). Further, we found increased observed species (another measure of α diversity) in the LS compared to other groups. The observed species represent the amount of unique OTUs present in a sample (Novogene, 2020). The increased observed species may be due to increased abundance of various sugar degrading microbes (*Faecalibaculum* and *Romboutsia* species) present in the ileum of LS fed mice. Therefore, we counter the notion that gut microbiota with lower diversity is less resilient to environmental challenges, and is less beneficial for the host, as the unique OTUs present within a sample may not always have beneficial effects for the host (Canfora et al., 2019). At the phylum level, we observed a decreased *Bacteroidetes: Firmicutes* ratio in the LS diet. While, LS+In decreased the levels of *Firmicutes* and increased the levels of *Bacteroidetes*, LS+Comb did not have a significant effect on the levels of *Bacteroidetes* compared to the LS diet. We noticed an increase in the abundance of *Actinobacteria* in both LS+In and LS+Comb group. The beneficial genus *Bifidobacterium* belongs to the *Actinobacteria* phylum and the levels of *Bifidobacteria* were significantly increased in the mice fed with LS+In and LS+Comb diet fed mice. Furthermore, we also observed increased levels of *Akkermansia* in the LS+Comb fed mice. Although, *Akkermansia* has been investigated for its effects on host metabolism, Ansaldo et al. (2019) has recently reported *Akkermansia* to induce adaptive immune and antigen specific T cell responses in mice during homeostasis. The study supports the hypothesis that T follicular helper (TfH) cell responses against physiological microbiota can be context-dependent, and not just in the setting of gastrointestinal infection by pathogens or inflammation. Melo-Gonzalex et al. (2019) demonstrated interactions of multiple immune cell types within the interfollicular niche of the intestinal mesenteric lymph nodes including TfH, B cells, and ILC3 that may regulate IgA responses and mutualism with the commensal microbiota to maintain intestinal

health. Accordingly, the upregulation of MHC II molecules (ILC3e markers) may be associated with the increased abundance of *Akkermansia* in the LS+Comb group. Similar to *Akkermansia,* Ansaldo et al also reported *Bacteroidales S24-7* to induce T cell-dependent IgA response in mice, however this response was not further characterised. The genus *Bacteroidales S24-7* was significantly increased in chow compared to other groups. The functionality of *Bacteroidales S24-7* has been associated with degrading complex dietary carbohydrates. Similarly, reports have shown decreased abundance of this genus in the rodent feeding trials using high refined carbohydrate diets (Lagkouvardos et al., 2019).

Taken together we report prevention of a pathophysiological liver phenotype as a result of addition of fibres to the purified LS diet. We propose that DF cause slow uptake of simple carbohydrates and regulate the glucose that enters the liver via the portal vein and hence prevent steatosis in liver. Moreover, we report increased expression of ileal immune related genes in chow and LS+Comb groups which may be linked to microbiota composition or the direct effect of complex fibres present in the chow and fibre combination diet. Further experiments are required to determine which variable, structure or the amount of fibre is more important in context of liver disease. Our results support the notion that immune responses against microbial and environmental (such as dietary) signal can be context-dependent and does not necessary translate to gastrointestinal abnormality. The differential effect of fibre rich diets on the ileal immune response highlight that consideration should be given to the composition of fibre diets when consumed as therapeutics.

Chapter 6: Differential effect of sourcing locations on the gut-liver axis of C57BL/6J mice

6.1 Introduction

Inbred mice strains such as C57BL/6J and controlled environments are often applied to minimize inter-individual differences in phenotypes. However, recent data questions whether inbred mice have lower inter-individual differences compared to outbred mice, and traits previously thought to be caused by genetics have been reported to be also partly related to the gut microbiota composition (Franklin and Ericsson 2017). It is well known that the genetic background of mice has a considerable impact on the composition of the gut microbiota (Hufeldt et al., 2010; Tran et al., 2019). In the recent years, studies have shown that the composition of gut microbiota can vary between the same mice strain obtained from different vendors, which may directly influence the mouse phenotype (Hansen et al., 2014; Hilbert et al., 2017; Sadler et al., 2017). Differences in the colonising gut microbiota can lead to variation in not only the phenotype but also, susceptibility to disease, and responsiveness to drug therapy (Alegre et al., 2019). For example, presence of segmented filamentous bacteria (SFB) in mice from some vendors was reported to stimulate T-helper 17 (Th17) cells in the small intestine (Ivanov et al., 2008). Presence of SFB has been suggested to provide protection against the development of autoimmune type 1 diabetes (T1D) in SFB-positive female non-obese diabetic (NOD) mice (Kriegel et al., 2011). Therefore, such differences of individual commensal bacteria can influence results for labs that use NOD mice for diabetes research, as reported in a preclinical immunotherapy study by Gill et al. 2016.

The research on the influence of environmental variables on the composition of the gut microbiota and their functionality remains incomplete. Studies have suggested the potential of husbandry-induced changes in the gut microbiota that could contribute to a lack of reproducibility between mice models from different research institutes. The gut microbiota of a mouse has been shown to be influenced by various factors; place of birth, (Korte et al., 2020), shipping and acclimatisation (Montonye et al., 2018), differences in bedding (compressed paper and aspen chips) and caging ventilation (static microisolators or individually ventilated caging) (Ericsson et al., 2018).

In the current study, we aimed to characterise the differences in the gut-liver axis of mice sourced from different locations. We performed 16S rRNA sequencing analysis on ileal content of mice from external vendor Charles River, UK (CRUK) and inhouse animal facility, Disease Modelling Unit (DMU) at University of East Anglia (UEA) fed with chow and/or LF diet. We also aimed to study the ileal gene expression and bile acid profile of mice. We hypothesised that mice from different locations may contain distinct ileal microbiota composition, which may result in differential response of the gut-liver axis to the chow and LF diets.

6.2 Results

6.2.1 Physiological changes in CRUK and DMU mice in response to different diets

Body weight analysis at the end of the experiment revealed significantly increased weight gain in CRUK LF compared to CRUK chow fed mice (weight difference: 2.7g, 212±0.8%, P=0.01) (Fig. 6.1A and B). The mice from CRUK and DMU were fed the same LF diet, however, the CRUK LF mice gained more weight compared to DMU LF (weight difference 2.4g, 155±0.9%, P=0.03) (Fig. 6.1B). The average starting weight of CRUK LF group was slightly lower than the DMU LF group, 29.53g and 30.78g respectively (Mean difference -1.25g SE of diff. ±0.9), however, this difference was not statistically significant. We did not observe any statistical difference in food intake between the groups (P=0.5).

There was no statistical difference observed in the liver weight to body weight ratio of mice between the groups (P> 0.9) (Fig. 6.1D). As observed in the previous experiments, the mice fed with the LF diet had increased levels of liver triglyceride content (CRUK: 81±238%, P=0.009; DMU: 60±189%, P=0.004) compared to chow fed mice, regardless of the vendor (Fig. 6.1E).
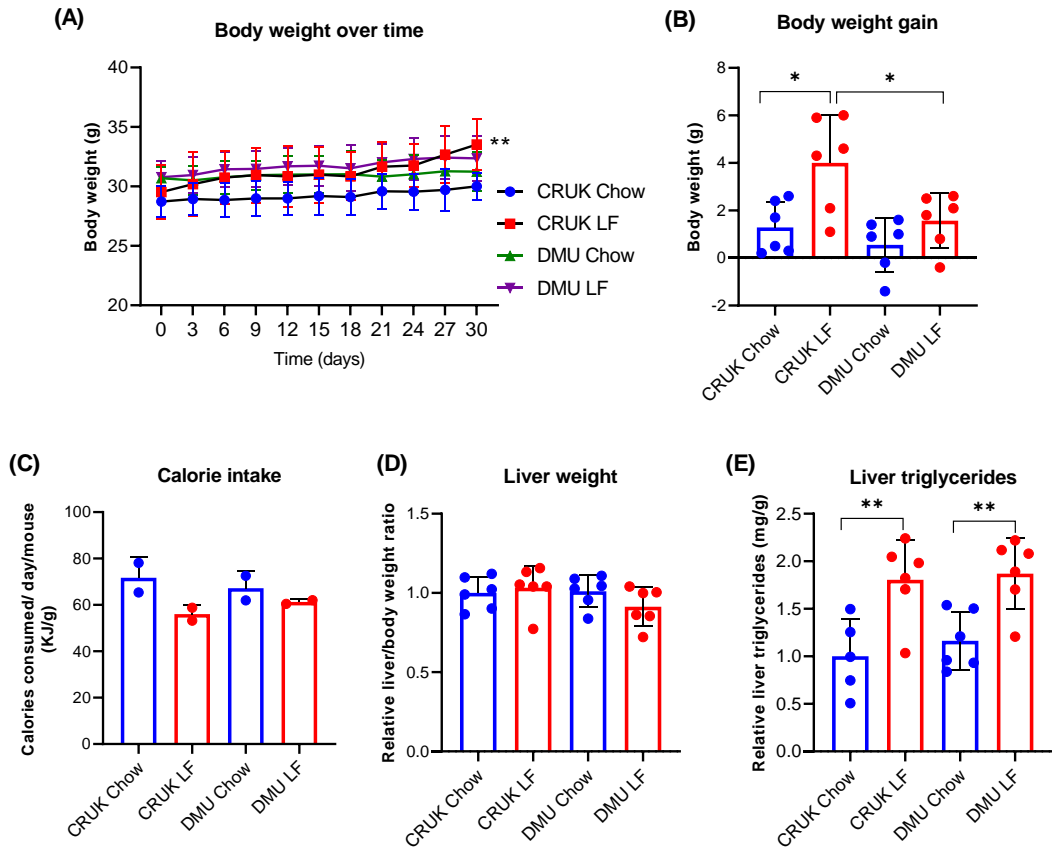
Figure 6.1 Comparison of physiological changes in mice from different vendors. C57BL/6J mice from CRUK and DMU were fed with chow and LF diet for 4 weeks. Weekly body weight of mice during the 4 weeks experiment (A), body weight gain of individual mice in different groups (B), calorie intake per mouse per day (C), liver weight (g) relative to body weight (g) ratio (D), and levels of liver triglycerides (E). Significance was tested by using 2-way ANOVA with Tukey's multiple comparison test (***=p<0.001, **= p<0.01, *= p<0.05). Values are the means ± SEM of n=6 mice in each group. Mice per group were divided into two cages (as 3 mice per cage), calorie intake was measured per cage and divided by 3 to calculate the intake of one mouse. LF: Low-fat diet, Charles River Laboratories (CRUK) and inhouse Disease Modelling Unit (DMU).

6.2.2 Differential gut microbiota composition of C57BL/6J mice from two vendors
To assess the effect of vendors and dietary intervention, we generated amplicon libraries from V3-V4 region of 16S rRNA gene in bacterial DNA from ileal content of mice. Each group contained sample size of n=6. The microbial DNA from mouse 3 in CRUK LF group was excluded from the analysis due to low DNA yield and integrity quantified on Nanodrop. Sequencing data processed resulted in total read counts of 1,474,281 and average counts per sample of 64,099.

Alpha diversity of the ileal bacterial communities did not differ between the diet groups in CRUK and DMU mice (Shannon diversity index, P=0.4, Fig. 6.2A). Further, the bacterial richness (number of observed species) was found to be similar between the two diet treatments in CRUK mice (P= 0.9) (Fig. 6.2B). Whereas, the observed species were significantly increased in ileal gut microbiota of DMU LF compared to DMU chow mice (17±11%, P= 0.04). Principal coordinate of analysis (PCoA) plot of the bacterial community structure based on Bray–Curtis distances at the genus level showed distinct separation between CRUK and DMU chow groups, whereas the LF fed mice from both vendors are clustered closer together. In agreement with our previous report we found distinct separation between chow and LF fed microbiota profile in DMU mice, whereas the distance between CRUK chow and LF microbiota was not as pronounced (Permutational multivariate analysis of variance, PERMANOVA, R Squared:0.47, P <0.001).

In all groups, bacterial communities at the phylum level were predominantly composed of *Bacteroidetes* and *Firmicutes* (Fig. 6.3A and Table 6.1). Analysis of the phyla shows increased abundance of *Firmicutes* (68±7.7% and 102±4% CRUK and DMU respectively) and decreased abundance of *Bacteroidetes* (percentage decrease by 68.5±5% and 82.7±5% CRUK and DMU respectively) in the ileum of LF fed mice from both vendors. Comparison of ileal microbial profiles between the mice from the different groups suggested increased levels of *Verrucomicrobia* in the CRUK chow mice compared to other groups (6.2 mean relative abundance in CRUK chow compared to relative abundance of approximately 1.5 in other groups) (Fig. 6.3A and summary of statistics in Table 6.1).

We analysed raw OTU counts per samples to gain a deeper knowledge of the microbiota composition and their abundance among different samples. Within the *Firmicutes* phylum (Fig. 6.4A) average levels of genus *Faecalibaculum* were higher in DMU LF mice compared to CRUK LF, although the increase was not significant due to high interindividual differences (P=0.1). Similarly, levels of *Lactobacillus* showed high heterogeneity between the samples within the LF groups. Overall, analysis of ileal microbiota from CRUK mice suggested increased levels of *Lactobacillus* compared to DMU mice (Difference between CRUK chow and DMU chow *Lactobacillus* levels: 37±4773% P= 0.1, and difference between CRUK LF and DMU LF: 48±9975%, P=0.2). Levels of *Lactococcus* were increased in LF compared to chow fed mice in both vendors (P value for difference between chow and LF; CRUK: P=0.05 and DMU: P= 0.003). Levels of *Turicibacter* were similar in all groups (around 1000 counts per OTU), except that the microbiota composition of 2 out of 6 mice in CRUK LF group contained very high levels of *Turicibacter* (15,000

and 16,000 counts). Two genera from the *Lachnospiraceae* family, *Lachnoclostridium* and *Lachnospiraceae NK4A136 group* were observed to be present at high levels in CRUK chow compared to CRUK LF group (P value for *Lachnoclostridium* and *Lachnospiraceae NK4A136 group*: P=0.04 and P=0.002 respectively). The levels of *Lachnospiraceae NK4A136 group* were significantly higher in CRUK chow and LF fed mice compared to their DMU counterparts (P value CRUK chow Vs DMU chow: P=0.0006 and CRUK LF Vs DMU LF: P=0.01). The levels of an unknown genus from *Peptostreptococcaceae* family were increased in CRUK LF compared to CRUK chow (P=0.004) and DMU LF mice (P=0.04). The levels of *Romboutsia*, also from the *Peptostreptococcaceae* family were increased in LF compared to chow fed mice in both vendors (P value for chow Vs LF in CRUK: P=0.04 and DMU: P=0.01).

The unknown genus from the *Bacteroidales S24-7* family within the *Bacteroidetes* phylum was found to be highly abundant in chow compared to LF fed mice, regardless of the vendors (P value for chow Vs LF in CRUK: P=0.0002 and DMU: P<0.0001) (Fig. 6.4B). We did not observe a difference in the levels of genus from *Bacteroidales S24-7* family between CRUK and DMU chow fed mice (P=0.3). Whereas, the levels of *Bacteroidales S24-7* were found to be significantly increased in the CRUK LF compared to DMU LF mice (P=0.02). Within the *Verrucomicrobia* phylum, the levels of *Akkermansia* showed an increasing trend in the CRUK chow and LF groups compared to its DMU counterparts (P value for CRUK chow Vs DMU chow: P=0.07 and CRUK LF Vs DMU LF: P=0.008) (Fig. 6.4C). The mean value of *Akkermansia* levels in CRUK chow mice was higher compared to CRUK LF group, 3938 and 944.8 counts respectively, however the difference did not reach significance. The mean value of *Akkermansia* counts in DMU chow and LF mice was found to be below 60 counts and the levels of *Akkermansia* between the two diet groups were not found to be significantly different (P= 0.2). We did not observe a difference in the levels of genus *Pseudomonas* and *Enterobacteriaceae* from the *Proteobacteria* phylum between chow and LF diet groups in both CRUK and DMU mice. However, the DMU LF mice showed increased levels of these genera compared to CRUK LF mice (P= 0.01 and 0.03 for *Pseudomonas* and *Enterobacteriaceae* respectively). The CRUK chow group suggested decreased levels of *Pseudomonas* and *Enterobacteriaceae* compared to DMU chow, however, the difference did not reach significance (P=0.2 and 0.07 respectively) (Fig. 6.4D).

Altogether, we observed distinct differences in the microbiota composition between the mice from the two sources: CRUK and DMU. We also demonstrate that while there were no clear patterns of variation in the *Firmicutes* between the vendors, there appeared to be OTUs that differed in abundance between CRUK chow compared to DMU chow, and CRUK LF compared to DMU LF.

(A)
Shannon Index

(B)
Observed species

(C)
PCoA Bray–Curtis dissimilarity

[PERMANOVA] R-squared: 0.49785; p-value < 0.001
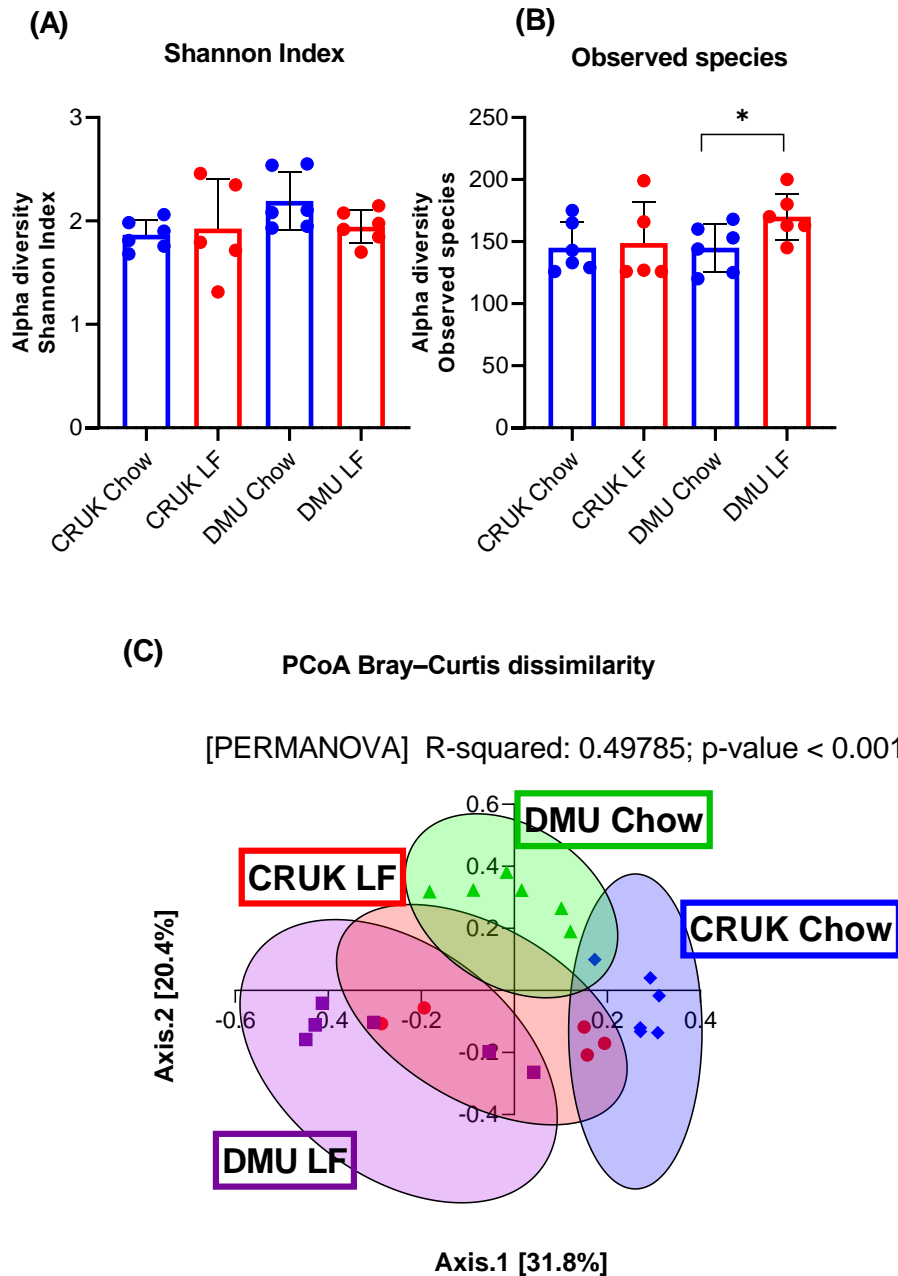
Figure 6.2 Diversity and richness of gut microbiota. Alpha diversity was measured via Shannon index (A) and observed species (B) and Principal coordinate analysis of the ileal microbiota in chow and LF fed C57BL/6J mice purchased from CRUK and DMU facility. Data points are coloured to indicate vendor and diet: CRUK chow: blue, CRUK LF: red, DMU chow: green and DMU LF: purple (C). Significance was determined by Kruskal-Wallis test for Shannon index and observed species. PERMANOVA statistical method with Bray-Curtis index for distance was used for PCoA. (***=p<0.001, **= p<0.01, *= p<0.05). Values are the means ± SEM of n=5-6 mice in each group. Mouse 3 from CRUK LF group was excluded due to low DNA yield. LF: Low-fat diet, Charles River Laboratories (CRUK) and inhouse Disease Modelling Unit (DMU).
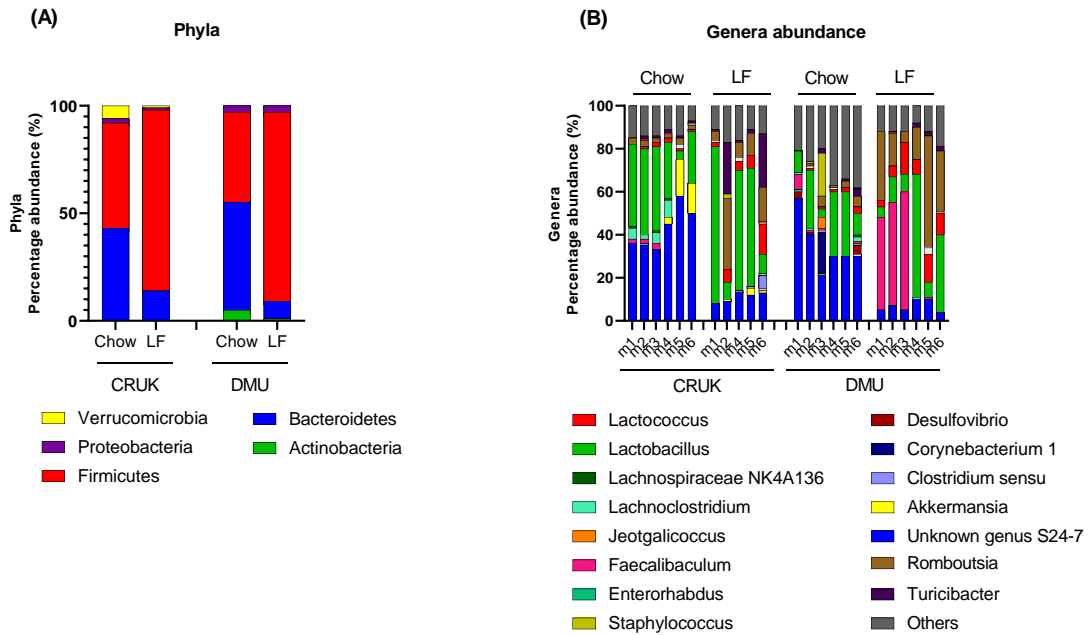
Figure 6.3 Composition of the ileal microbiota at phylum and genus levels (n=5-6 per group). Relative abundance at taxonomic level of phylum (A) and genus (B) in the ileum content of chow and LF fed mice from two vendors (CRUK and DMU). Mouse 3 from CRUK LF group was excluded due to low DNA yield. LF: Low-fat diet, Charles River Laboratories (CRUK) and inhouse Disease Modelling Unit (DMU).

Table 6.1 Summary of phyla that were significantly different between the four groups. Significance was tested by using 2-way ANOVA with Tukey's multiple comparison test (***=p<0.001, **= p<0.01, *= p<0.05). Values are the means of n=5-6 mice in each group. Mouse 3 from CRUK LF group was excluded due to low DNA yield. LF: Low-fat diet, Charles River Laboratories (CRUK) and inhouse Disease Modelling Unit (DMU).

Phyla	Mean 1	Mean 2	SE of diff.	Summary	P value
Bacteroidetes					
CRUK chow vs. CRUK LF	41.6	13.1	2.0	****	0.0001
CRUK chow vs. DMU chow	41.6	48.1	1.9	**	0.004
CRUK LF vs. DMU LF	13.1	8.3	2.0	ns	0.08
DMU chow vs. DMU LF	48.1	8.3	1.9	****	0.0001
Firmicutes					
CRUK chow vs. CRUK LF	49.2	82.6	2.0	****	0.0001
CRUK chow vs. DMU chow	49.2	42.7	1.9	**	0.004
CRUK LF vs. DMU LF	82.6	86.1	2.0	ns	0.3
DMU chow vs. DMU LF	42.7	86.1	1.9	****	0.0001
Verrucomicrobia					
CRUK chow vs. CRUK LF	6.2	1.5	2.0	ns	0.09
CRUK chow vs. DMU chow	6.2	0.0	1.9	**	0.008
CRUK LF vs. DMU LF	1.5	0.1	2.0	ns	0.9
DMU chow vs. DMU LF	0.0	0.1	1.9	ns	1.0

(A)

(B) **(C)** **(D)**
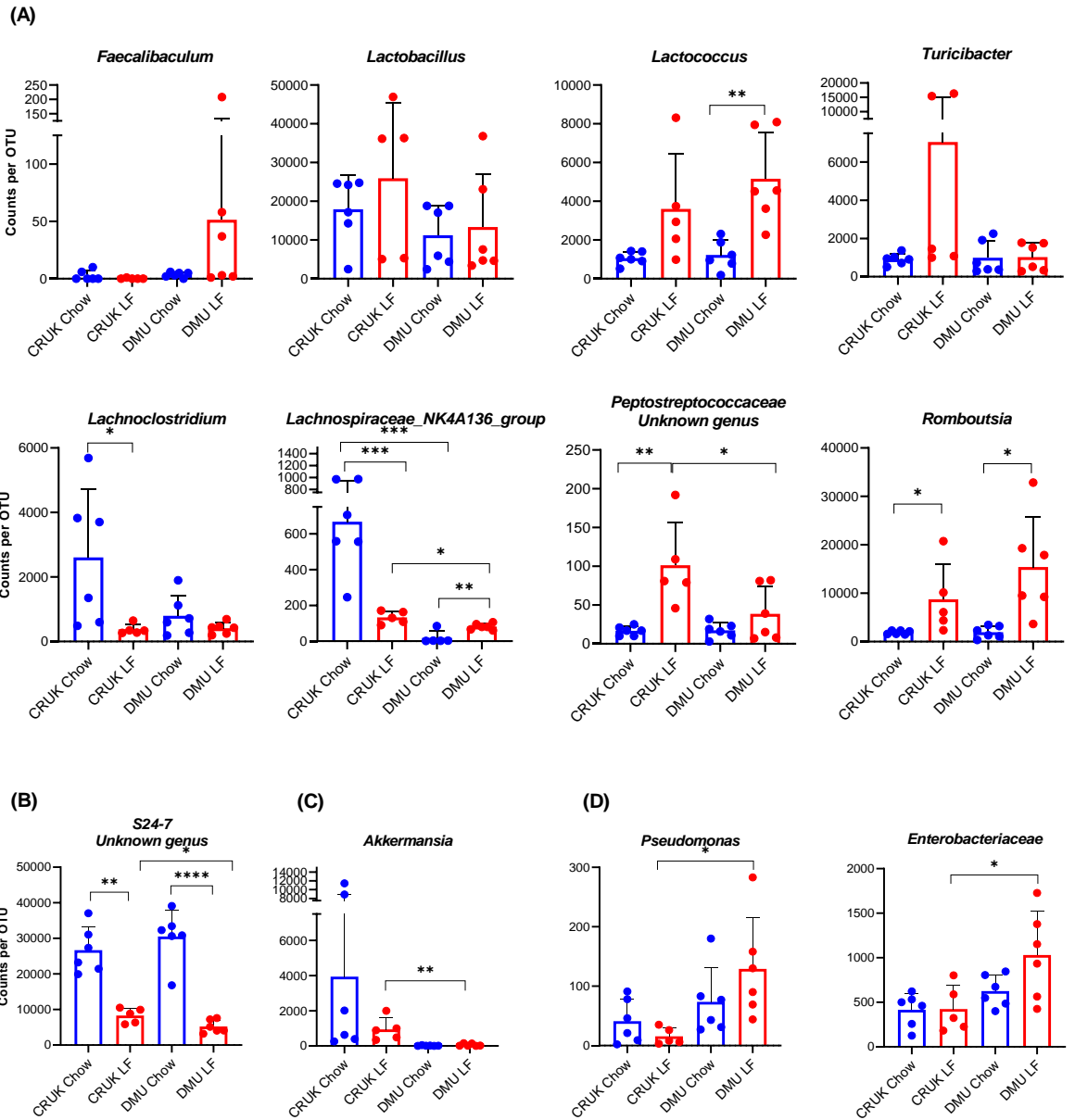
Figure 6.4 Differences in the composition of the gut microbiota at the genus level between diet and vendor. Significance was tested by using 2-way ANOVA with Tukey's multiple comparison test (*=p<0.001, **= p<0.01, *= p<0.05). Values are the means ± SEM of n=5-6 mice in each group. Mouse 3 from CRUK LF group was excluded due to low DNA yield. LF: Low-fat diet, Charles River Laboratories (CRUK) and inhouse Disease Modelling Unit (DMU).**

6.2.3 Differential expression of ileal barrier function and inflammation related genes in response to diet and vendor

Expression of barrier function genes mucin 2 (*Muc2*), claudin 3 (*Cldn3*) and zonula occludens-1 (*Zo-1*) was suggested to be downregulated in response to LF feeding in mice from both vendors, (*Muc2*: 32±0.1%, P=0.05; *Cldn3*: 43±0.1, P=0.02; *Zo-1*: 39±0.1%, P=0.01) (Fig. 6.5A). The gene expression of *Muc2* and *Cldn3* was observed to be significantly decreased in DMU LF compared to CRUK LF mice 28±0.1%, P=0.02 and 25±0.1%, P=0.03 respectively. Inflammation related genes in the ileum were not changed between the diets or vendors, although a trend towards increased Serum Amyloid A1 (*Saa1*) gene expression was observed in LF fed mice independent of the vendors (Fig. 6.5B).
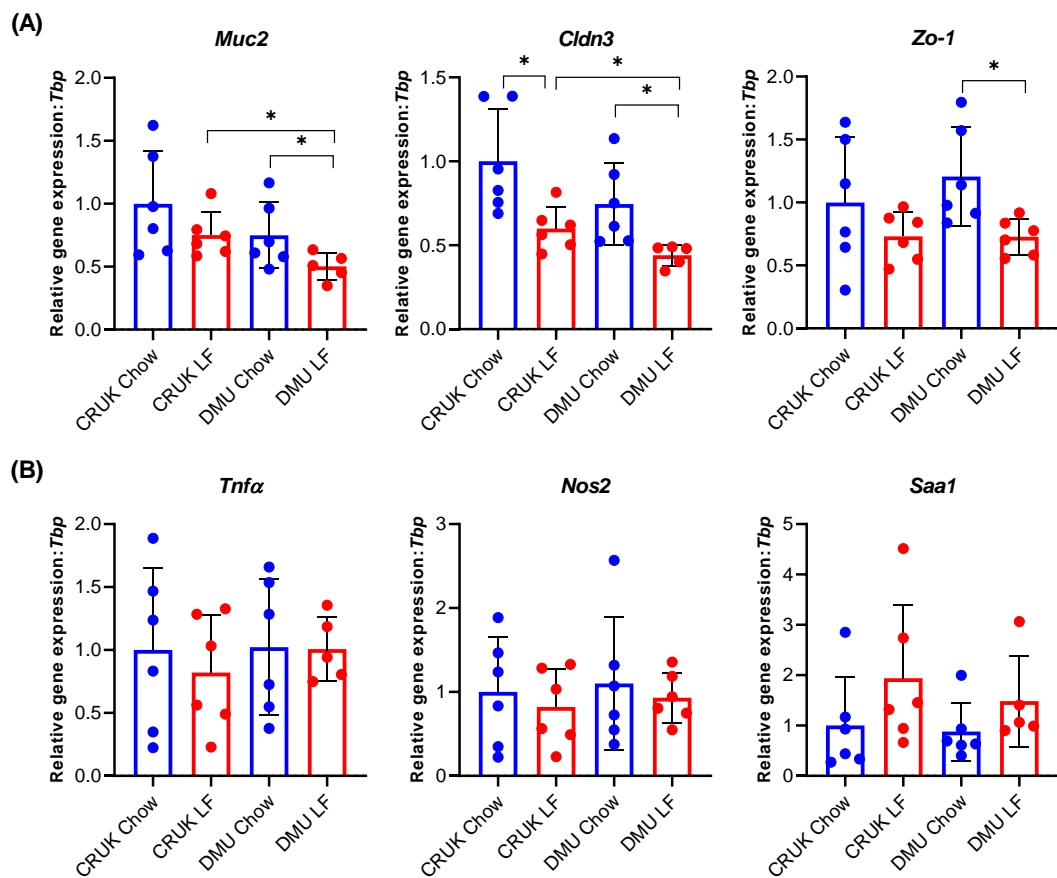
Figure 6.5 Ileal gene expression in response to the different diet and vendors. Barrier function (A) and inflammation related (B) gene expression in the ileum of mice from CRUK and DMU. Significance was tested by using 2-way ANOVA with Tukey's multiple comparison test (***=p<0.001, **= p<0.01, *= p<0.05). Values are the means ± SEM of n=5-6 mice in each group. LF: Low-fat diet, Charles River Laboratories (CRUK) and inhouse Disease Modelling Unit (DMU).

6.2.4 Bile acid metabolism in the ileum reveals vendor-associated differences

The gene expression analysis revealed significantly increased fibroblast growth factor 15 (*Fgf15*) expression in the CRUK LF compared to CRUK chow group (84±0.3%, P=0.02), whereas the increase in *Fgf15* expression did not reach significance in the DMU LF compared to DMU chow fed mice (54±0.3%, P= 0.1) (Fig 6.6A). We did not observe a difference in the expression of ileal basolateral transporter, organic solute transporter alpha (*Ostα*) between the diet and vendor groups. In line with the increase in ileal *Fgf15* expression, we observed a significant decrease in the expression of cytochrome P450 7A1 (*Cyp7a1*) in the livers of CRUK LF compared to CRUK chow fed mice (66±0.2%, P=0.01). The hepatic expression of *Cyp7a1* was not changed between chow and LF fed DMU mice (20±0.3%, P= 0.5) (Fig. 6.6C).

We observed increasing trends in the levels of total bile acids in the ileum of CRUK LF (by 21.5±7185%, P=0.4) and significant increased bile acid levels in the DMU LF (by 41.7±851%, P=0.03) compared to chow fed CRUK and DMU mice respectively (Fig. 6.6B). We also observed a trend towards increased bile acid levels in CRUK chow compared to DMU chow mice (29.5±662%, P=0.09), whereas no vendor difference was observed between the CRUK and DMU mice fed with LF diet (P=0.7).

Further examination of the individual bile acids revealed differential bile acids profile between mice from different groups (Fig. 6.7A, B, C, and D). In the ileum of CRUK mice, we observed significantly increased levels of primary unconjugated bile acids αMCA (by 240±52%, P=0.01), βMCA (by 179±119%, P=0.007) in the CRUK LF compared to CRUK chow mice (Fig. 6.7A). Interestingly, the levels of secondary bile acid, DCA were found to have an increasing trend in DMU chow compared to CRUK chow (207±10%, P= 0.06). The difference in the DCA levels between LF fed CRUK and DMU mice did not reach significance (P= 0.2) despite the mean of DMU LF (22µmol/g) being higher than CRUK LF group (11µmol/g) (Fig. 6.7B).

The levels of taurine conjugated bile acids TαMCA, TβMCA, TCA, TCDCA, and TUDCA were significantly increased in CRUK chow compared to DMU chow (115±111%, 108±207%, 72±215%, 165±5% and 177±% respectively, P <0.05) (Fig. 6.7C and D).

Although the levels of TβMCA showed an increasing trend in CRUK LF compared to CRUK chow, this increase did not reach significance (40±296%, P= 0.1). Whereas the levels of TβMCA were observed to be significantly higher in DMU LF compared to DMU chow (196±338%, P= 0.003). The subtle difference observed in the levels of TβMCA between diets in CRUK group is possibly due to already high levels of TβMCA levels found in the CRUK chow fed mice. Lastly, we observed increased levels of TUDCA in LF fed mice from both vendors (386±45%, P=0.02 and 991±48%, P=0.03, in CRUK and DMU respectively) compared to chow fed mice (Fig. 6.7C).

(A) Ileum
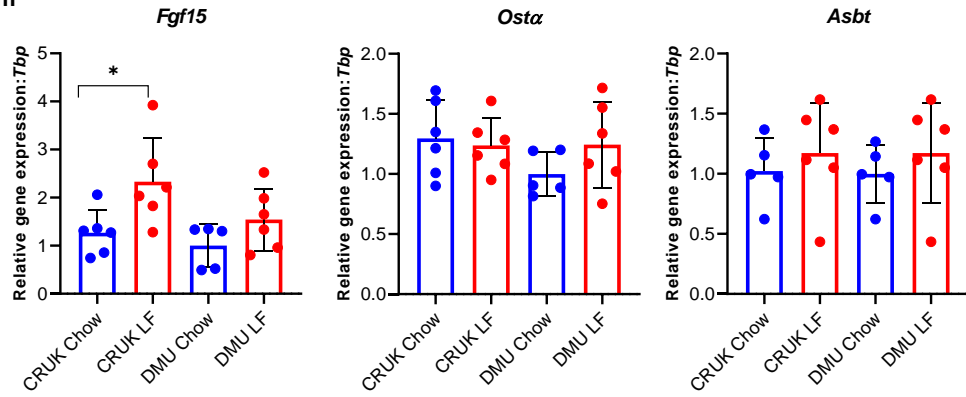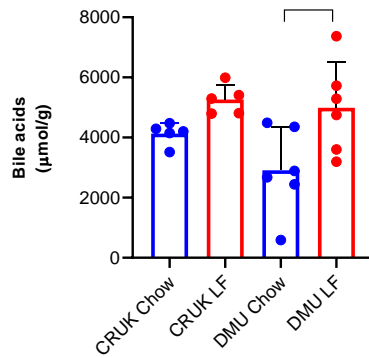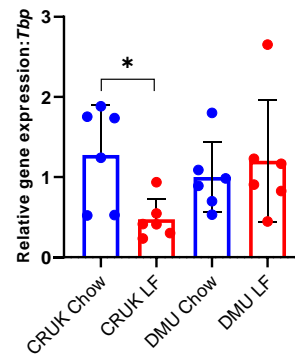
Figure 6.6 Bile acid metabolism in CRUK and DMU diet groups. Expression of genes involved in bile acids signalling in ileum (A), total bile acids in the ileum (B), gene expression of *Cyp7a1* in the liver (C). Significance was tested by using 2-way ANOVA with Tukey's multiple comparison test (***=p<0.001, **= p<0.01, *= p<0.05). Values are the means ± SEM of n=5-6 mice in each group. LF: Low-fat diet, Charles River Laboratories (CRUK) and inhouse Disease Modelling Unit (DMU).
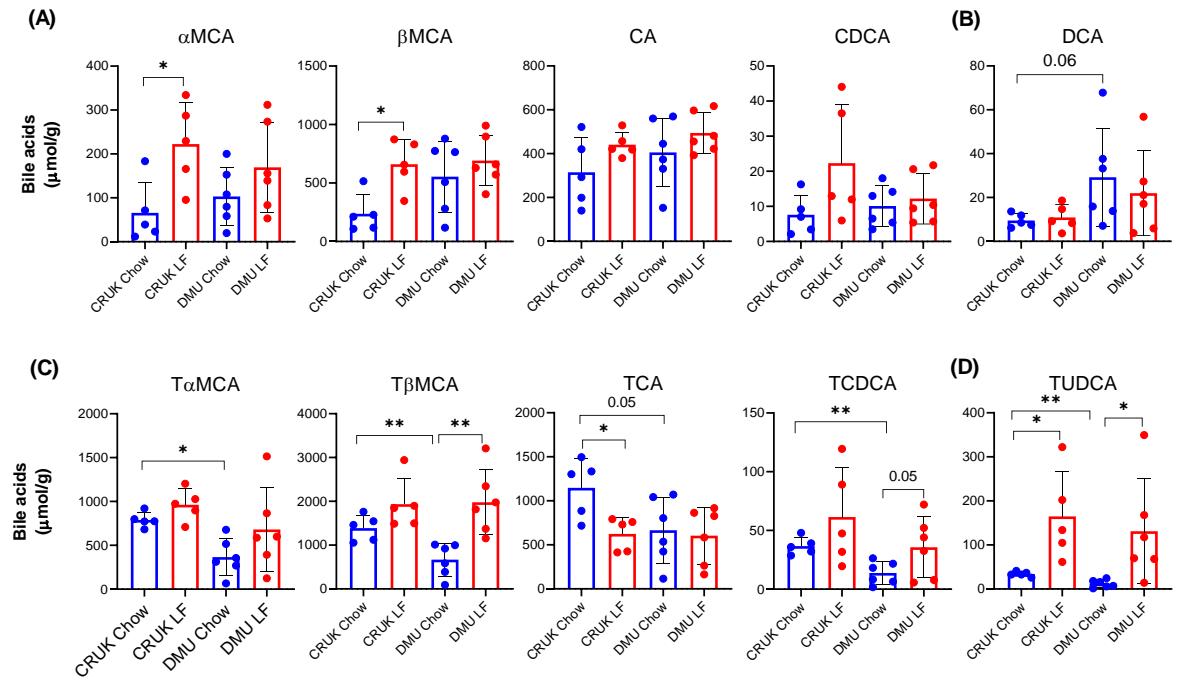
Figure 6.7 Ileal composition of individual bile acids. Primary unconjugated bile acids αMCA, βMCA, CA, CDCA (A), secondary unconjugated bile acid DCA (B), Taurine conjugated primary bile acids TαMCA, TβMCA, TA, TCDCA (C) and secondary taurine conjugated bile acid TUDCA (D). Significance was tested by using 2-way ANOVA with Tukey's multiple comparison test (***=p<0.001, **= p<0.01, *= p<0.05). Values are the means ± SEM of n=5-6 mice in each group. LF: Low-fat diet, Charles River Laboratories (CRUK) and inhouse Disease Modelling Unit (DMU).

6.3 Discussion

The reproducibility of preclinical biomedical research using mice models is currently being scrutinised by the National Institutes of Health (NIH). Several possibilities for lack of reproducibility have been discussed including randomisation, sex differences, poor experimental power, and environmental differences between animal facilities (Ericsson, 2015). In the previous chapters of this thesis, we have investigated the effects of commonly used control diets (chow and purified LF diet) which may be a major factor for lack of reproducibility in preclinical research, and highlighted some major differences of these diets on the gut-liver axis.

In the current chapter, we investigated the variation in the gut microbiota and consequently the gut-liver axis of mice from an external vendor CRUK and inhouse animal facility, DMU. We propose that the differences observed in the gut microbiota of mice between animal facilities may be one of the environmental factors contributing to poor reproducibility of research using mice models.

Four weeks feeding of the LF diet resulted in increased weight gain compared to chow fed mice in the CRUK group. Whereas, no difference in weight gain was observed in the DMU mice between the two diet groups. We did not observe a difference between the average calorie intake in the LF fed mice from CRUK and DMU. We were unable to access metabolic chambers to measure precise daily calorie intake and energy expenditure in mice; therefore, we cannot assess the direct calorimetry for metabolic rate of the CRUK LF mice which may provide the reasoning for weight gain.

Previous literature has highlighted substantial differences between the gut microbiota of mice purchased from different vendors (Ericsson et al., 2015; Franklin and Ericsson, 2017). In the current study, PCoA plot revealed two distinct vendor specific microbiota clusters in the chow fed mice. The DMU LF microbiota cluster was distinctly separate from DMU chow cluster with no overlap between the groups. Whereas, CRUK LF cluster had some overlapping microbiota composition with CRUK chow. These data show that there was complete division of the composition of microbiota between samples at the diet level in DMU mice. However, the effect of diet on cluster separation did not seem as distinct as in the CRUK mice. Further analysis at the genus level showed mice from CRUK LF group harboured increased levels of *Unknown genus S24-7* from *Bacteroidales* family and *Lactobacillus* compared to the DMU LF mice. Both these genera are highly prevalent in homeothermic animals; however, their differential abundance suggests the ability of the surrounding microbial milieu and other environmental factors that may affect the gut microbiota (Ng et al., 2019).

The level of *Firmicutes* did not differ between the CRUK and DMU LF fed mice. However, the analysis of the genera within the *Firmicutes* phylum revealed increased *Faecalibaculum* and *Romboutsia* in the DMU LF, while, increased levels of *Lactobacillus* and *Peptostreptococcus* were found in the CRUK LF group. The high abundance of *Lactobacillus* in the CRUK mice may provide resistance to colonization by *Faecalibaculum* and *Romboutsia* in response to LF diet. The genus *Faecalibaculum* is an obligate anaerobe that has been shown to replace *Lactobacilli*

from young to adult age (Ke et al., 2019). The CRUK mice were 10 weeks old when they arrived at the animal facility, after 2 weeks quarantine period, the feeding experiment was started at the age of 12 weeks for all mice from CRUK and DMU. Therefore, the increased levels of *Lactobacillus* and decreased levels of *Faecalibaculum* found in the CRUK mice is not due to the age differences and may be due to the stronger vendor effect than diet.

We observed increased levels of *Enterobacteriaceae* and *Pseudomonas* from the *Gamma Proteobacteria* group in DMU LF mice. The average of *Enterobacteriaceae* and *Pseudomonas* in DMU chow mice was also observed to be higher than CRUK chow and CRUK LF group. Our results suggest that the abundance of these pathogenic bacteria is higher in DMU mice compared to CRUK mice and the exposure of the DMU mice to a low fibre and high refined carbohydrate (LF) diet promoted the abundance of these pathogenic bacteria. Under high fibre chow diet conditions, this effect may be supressed by the increased levels of SCFAs (butyrate) that promote consumption of oxygen in the intestine, leading to anaerobic milieu which prevents the growth of facultative anaerobe and optimises conditions for anaerobic commensal strains. Whereas, under the decreased SCFAs conditions with LF diet, anaerobic glycolysis in the intestine leads to increased oxygen levels in the gut lumen that promote the growth of facultative anaerobes such as *Enterobacteriaceae* and *Pseudomonas* (Byndloss et al., 2017). Tennoune et al. (2014) identified Clp heat-shock disaggregation chaperone protein in the *Enterobacteriaceae* strain to decrease body weight in mice via production of anti-Clp immunoglobulins (Igs). Both *Enterobacteriaceae* and *Pseudomonas* express Clp (Lee et al., 2018), which may be associated with reduced weight gain observed in the DMU LF fed mice.

We observed decreased ileal expression levels of barrier function genes *Cldn3*, *Zo-1* and *Muc2* in response to the LF diet in both vendors. In addition, the ileal gene expression levels of *Cldn3* and *Muc2* in DMU LF fed mice were significantly decreased compared to CRUK LF group. The ileal expression of inflammation related genes such as Tumour necrosis factor alpha (*Tnfα*), Serum amyloid A1 (*Saa1*) and Nitric oxide synthase (*Nos2*) did not differ between groups, which suggests that the colonisation of the gut with *Enterobacteriaceae and Pseudomonas* did not induce an inflammatory response. Low levels of *Enterobacteriaceae* have been known to inhabit healthy murine gut (Velazquez et al., 2019), however, further studies are required to ascertain whether increased colonisation of these strains in the gut of DMU mice, make the gut-liver more susceptible to an inflammatory challenge (as shown in Chapter 3) compared to CRUK mice.

We observed an increase in the genera *Lachnoclostridium* and L*achnospiraceae NK4A136 group* (Phylum: *Firmicutes*) and *Akkermansia* from phylum *Verrucomicrobia* in the CRUK chow compared to other groups. A possible explanation for differences in microbiota could be the maintenance diet used in the CRUK facility before their arrival at the DMU. The mice at CRUK were fed VRF1 chow diet (SDS diets,UK), whereas the maintenance diet used at the DMU is RM3-P

(SDS diets, UK). The summary composition of the diets is shown in the Table 6.2 below.

Table 6.2 Summary composition of RM3 diet fed to mice at the DMU and VRF1 diet fed to mice at the CRUK facility. RM3: Rat and mouse number 3, VRF1: Very high nutrient rodent diet.

	RM3 (DMU)	VRF1 (CRUK)
Fat (kcal%)	11.5	13
Protein (kcal%)	26.9	22
Carbohydrate (kcal%)	61.2	65
Total Dietary Fibre(g/Kg)	161.5	151.4
Pectin(g/Kg)	15.3	13.7
Hemicellulose(g/Kg)	96.1	87.6
Cellulose(g/Kg)	41.3	39.5
Lignin(g/Kg)	15.4	10.6
Starch(g/Kg)	338.8	354.1
Sugar(g/Kg)	43.7	46.4
Ingredients	Wheat, Wheatfeed, De-hulled Extracted Toasted Soya, Barley, Macro Minerals, Yeast, Potato Protein, Hydrolised Wheat Gluten, Full Fat Soya, Soya Oil, Maize Gluten Meal, Dextrose Monohydrate, Vitamins, Micro Minerals, Amino Acids.	Wheat, Dehulled Extracted Toasted Soya, Wheatfeed, Barley, Dehulled Cooked Soya, Soya Oil, Vitamins, Micro Minerals

Although, the RM3 and VRF1 diets vary slightly in terms of level of energy from macronutrients, the amount and source of dietary fibre (DF) in both diets is very similar. One of the major differences between the diets is the source of protein. Dietary protein in the RM3 diet is sourced from soya, potato protein, wheat and maize gluten meal, whereas, the VRF1 dietary protein source is derived solely from soya. The same amount of protein but different digestibility may lead differential gut microbiota. Further, the microbes in the gut have been shown to synthesise proteases and are also known to catabolise amino acids (Zhao et al., 2020; Gentile and Weir, 2018). Kar et al. (2017) investigated the effects of different dietary protein sources on the ileal microbiota composition to show increased levels of *Erysipelotrichaceae* family (genus *Faecalibaculum*) and decreased levels of *Lactobacillaceae* (genus *Lactobacillus*) in mice fed a diet enriched with wheat gluten meal compared to soybean meal. These results agree with the differential genera profile observed in the DMU and CRUK mice and suggest that early life dietary composition may be the reason for these differences.

Analysis of ileal bile acids showed differential profiles between the mice from different vendors and diet groups. In CRUK mice, we observed significant increased levels of αMCA and βMCA in response to LF feeding. Whereas, in agreement with our previous experiments (Chapter 3 and 4), TβMCA was significantly increased in

the LF fed DMU mice. While, CRUK chow fed mice displayed increased levels of taurine conjugated bile acids such as, TαMCA, TβMCA, TCA, TCDCA, and TUDCA compared to DMU chow fed mice. The significant increase in taurine conjugated bile acids suggests decreased bile salt hydrolases (BSH: involved in removal of amino acid group from bile acids) activity within the gut microbiota of the CRUK chow mice. Although, *Lactobacillus* species have been shown to express increased BSH enzymes (Song et al., 2019), the increase in taurine conjugated bile acids did not correlate with increased abundance of *Lactobacillus* in the CRUK chow group. We also observed increased levels of secondary bile acid DCA in the ileum of DMU mice, whereas its primary bile acid CA was generally unaffected between the groups. Certain species of *Clostridium* can carry out 7α-dehydroxylation of cholic acid to produce DCA which has potential pro-carcinogenic and pro-inflammatory actions (Xu et al., 2020). However, deeper analysis at the species level with shotgun metagenomic techniques are required to identify the species responsible for CA modifications to DCA by 7α-dehydroxylation reactions. Metagenomics analysis can also identify the *Lactobacillus* species present in the CRUK mice and the abundance of BSH encoding genes expressed in these species. Different species of *Lactobacilli* have been reported to contain varying number of BSH genes that may affect their enzyme activity (Horackova et al., 2020).

The gene expression of organic solute transporters, *Ostβ* and *Ostα* and intestinal bile acid transporter of apical sodium bile acid transporter, *Asbt* did not show any significant alterations between the groups. However, we found ileal *Fgf15* expression to be significantly increased in the CRUK LF compared to CRUK chow mice. In agreement with literature, the upregulation of *Fgf15* gene expression suppressed the hepatic *Cyp7a1* gene expression which leads to decrease *de novo* bile acid synthesis in the liver (Sayin et al., 2013). In the DMU group, we observed a slight increase in the ileal *Fgf15* expression (not significant) in the LF fed mice while, the gene expression of liver *Cyp7a1* remained unchanged between the diets. The sustained expression of *Cyp7a1* in the liver suggests maintained synthesis of bile acids in DMU LF compared to CRUK LF fed mice. These results are in line with significantly reduced serum cholesterol observed in the DMU LF compared to CRUK LF group (Supplementary Fig. 3.6).

Our results highlight the need to acknowledge vendor associated differences in the gut microbiota composition and their effects on the gut-liver axis. Further studies that utilise metagenomics can enhance our knowledge on species differences which may be involved in modulating the metabolic health. To the best of our knowledge, this is the first study to investigate the differential effect of diets in mice from different vendors, on the composition of gut microbiota and subsequent gut-liver axis of C57BL/6J mice.

Chapter 7: General discussion

7.1 Discussion

The interactions within the gut-liver axis play a crucial role in regulating the host response to diet. The diet-gut-liver axis in the context of microbiota has been shown to be involved in the development of type II diabetes (Qin et al., 2012), liver cholestasis (Isaacs-Ten et al., 2020) and more recently several studies have explored the contribution of the gut microbiome to the pathophysiology of non-alcoholic fatty liver disease (NAFLD) (Roychowdhury et al., 2018; Aron-Wisnewsky, 2020). Most of the studies investigating the diet-gut-liver axis during NAFLD have focused on the colon due to its highest microbiota density. Although, the ileum has the second largest microbiota population to colon, and it provides a direct link to the liver via the enterohepatic circulation of bile acids (Ticho et al., 2019), it has not been well studied in the context of diet-gut-liver axis. The scarce literature on the effects of diet on the ileum-liver axis prompted us to explore this part of the gastrointestinal (GI) tract to investigate its role on metabolic health and prevention of disease.

Our results have highlighted the negative effects of a high refined carbohydrate, low fibre diet on the liver compared to a high fibre grain-based diet. We used two control diets, chow and LF to investigate the effects of 1) increased easily metabolisable carbohydrates, and 2) the lack of fermentable soluble fibres in the LF diet. We showed that mice fed with LF diet for as short as 4 weeks exhibited early development of hepatic steatosis, a precursor of non-alcoholic steatohepatitis (NASH), compositional changes in the ileal microbiota, an increase in the gut permeability and changes in the bile acid metabolism. We also showed that LF fed mice exposed to low dose lipopolysaccharide (LPS) had increased sensitivity to this proinflammatory challenge. This was reflected by increased caspase 3 activity in the liver and upregulation of inflammatory related genes in the ileum compared to their chow counterparts. Reduced consumption of the LF diet in a calorie restricted model, protected the liver from LF induced hepatic triglycerides accumulation in short and long-term dietary intervention study. We further examined the effects of addition of soluble fibres to counteract the detrimental effects of the LF diet and revealed that the liver phenotype of LF induced early steatosis was successfully prevented, despite the same quantity of refined carbohydrates present.

7.1.1 Increased levels of easily accessible carbohydrates in LF diet drive hepatic *de novo* lipogenesis in mice

The easily accessible carbohydrates present in the LF diet are refined starch and sucrose. Sucrose is a disaccharide formed of glucose and fructose, whereas starch (amylose) is formed of a long chain of glucose monomers linked through α-(1-4) glycosidic bonds (Goodman, 2010). Under physiological conditions, glucose and fructose only reach the ileum when the small intestine is overloaded with carbohydrates (Jang et al., 2018). We found increased ileal gene expression of disaccharidases maltase-glucoamylase and sucrase-isomaltase (*Mgam* and *Sis*) and glucose transporters (*Sglt1* and *Glut2*) in response to the 4, 8 and 10 weeks feeding of the LF diet, indicating overloading of the capacity of duodenum and jejunum to digest the carbohydrates in the LF diet and leading to ileal starch/fructose exposure. The increased levels of lipogenic gene expression and levels of triglycerides

observed in response to the LF diet may be explained by the following potential mechanisms:

Under LF conditions, glucose from starch and sucrose is rapidly absorbed in the small intestine, however, some fructose may reach the liver due to either, overloading the capacity of the small intestine, or by increased gut permeability observed in LF fed mice.

LF diet contains 17% sucrose compared to experimental high sucrose (>50%) diets used to induce NAFLD in mice. However, our results show that the 17% sucrose was sufficient to induce an increased gene expression of hepatic fructokinase *Khk*, suggesting exposure of the liver to fructose. Furthermore, the increased *Glut2* expression observed in response to the LF diet suggested increased absorption of glucose in the ileal enterocytes, which may lead to high glucose concentrations in the portal circulation. We propose that increased glucose as well as fructose exposure of the liver under LF conditions contributes to *de novo* lipogenesis. As suggested by increased gene expression of *Srebp1*, that plays a major role in driving the transcription of lipogenic genes *Fasn* and *Acaca* indicating increased lipogenesis in response to the LF feeding.

Another way fructose may reach portal circulation could be through the increased gut permeability observed in the LF diet as indicated by increased serum fluorescein isothiocyanate dextran (FITC-dextran) in (Chapter 3) and consistently decreased ileal expression of barrier function genes like claudin 3 (*Cldn3*)*,* and zonula occluden 1 (*Zo-1*) in response to LF diet feeding of mice. Exposure of the liver to unmetabolised fructose can lead to production of fructose metabolism intermediate glycerol-3-phosphate (G3P) which can directly enter the lipogenesis pathway (Macdonald et al., 2016).

Exposure of intestinal microbiota to refined carbohydrates can lead to production of hepatotoxic metabolites. Although, most of the refined carbohydrates are mainly taken up by the proximal small intestine, excess unabsorbed starch and sucrose may reach the distal part of the intestine and interact with the microbiota (Howe et al., 2016; Jang et al., 2018). In line with this, we observed an increased relative abundance of *Romboutsia* and *Lactococcus* in the ileum of LF fed mice. These bacteria have been shown to encode genes related to carbohydrate transport and metabolism. *Romboutsia* can utilise a wide variety of simple carbohydrates and have good growth in high sucrose conditions to produce end products of fermentation such as, acetate, lactate and formate (Gerritsen et al., 2017). In the context of high sucrose conditions, microbial metabolism of simple carbohydrates has been shown to promote *de novo* lipogenesis in the liver by providing acetate for production of hepatic acetyl-CoA and fatty acids (Zhao et al., 2020). Although, the authors also showed that acetate is insufficient to trigger an increase in lipogenesis in the absence of the sugar-derived lipogenic transcriptional signal. In addition to acetate, dominant SCFAs from *Faecalibaculum*, butyrate has also been suggested to contribute to liver lipogenesis depending on the metabolic state of the cells. Donohoe et al. (2012) showed that butyrate can serve as a carbon source for β-oxidation and the TCA cycle and therefore increase the production of acetyl-CoA and lipid biosynthesis.

Therefore, it is possible that in the context of high carbohydrate conditions, LF diet may promote lipogenic gene expression in the liver and microbial metabolisation of starch and sucrose produce microbial metabolites such as acetate, which can act together to support *de novo* lipogenesis in the liver of LF fed mice. SCFAs have been considered beneficial for human health, however, it is becoming increasingly accepted that their precise mechanisms can differ between tissues and metabolic conditions (Koh et al., 2016).
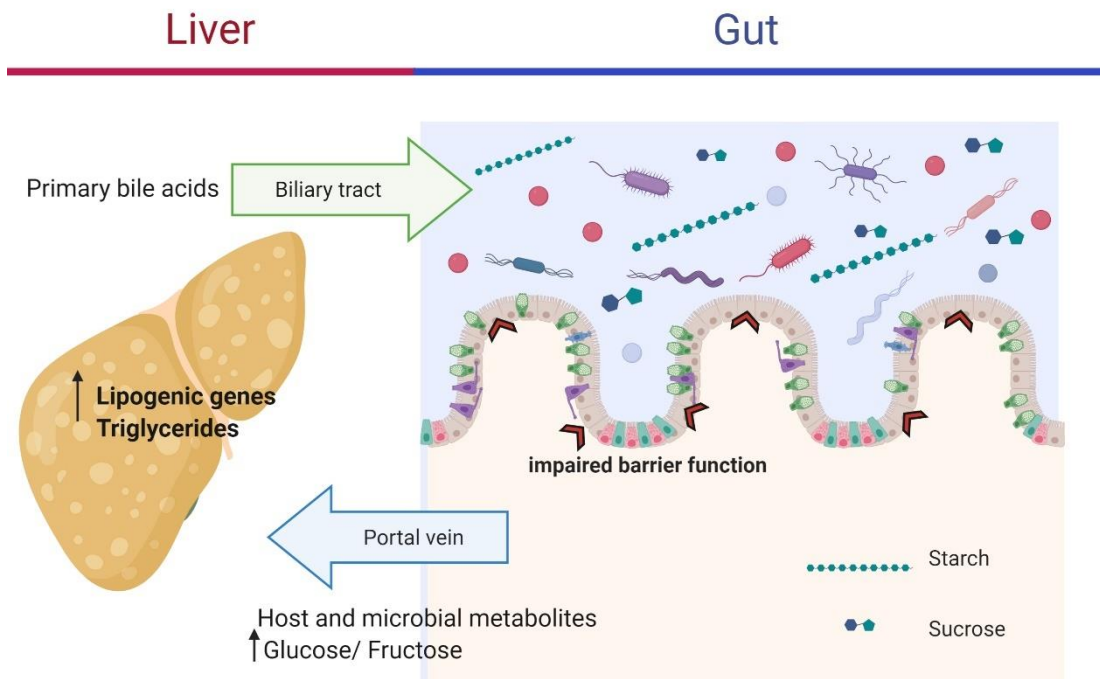
Figure 7.1 High starch and sucrose in the low-fat (LF) diet leads to a pathophysiological liver phenotype in mice.

7.1.2 Composition and amount of dietary fibres have differential ileal immunomodulatory properties

Soluble dietary fibres (DF) are a major component lacking in the LF diet, therefore, in chapter 5, we enriched the LF diet with various DF to investigate their role on the gut-liver axis. We showed that addition of the DF protected the livers from the LF induced lipid accumulation as demonstrated by lower hepatic triglyceride levels and liver histology. The amelioration of the liver phenotype may be due to fibre impacted slower starch and sucrose hydrolysis by MGAM and SIS, hence, reduced glucose/fructose passage into the intestine resulting in efficient intestinal clearance. We observed increased ileal gene expression of carbohydrate digestion enzymes (α glucosidases) *Sis*, *Mgam*, and glucose and fructose transporters *Sglt1, Glut2,* and *Glut5* in the fibre groups, that indicates increased delivery of nutrients to the ileum. Another reason for the increased expression of the α glucosidases and glucose/fructose transporters could be due to the inhibitory effect of fibres by direct

binding to digestive enzymes and transporters, thereby, delaying the digestion and uptake of carbohydrates (Grundy et al., 2016; Neyrinck et al., 2016).

The LF diet was enriched with either 6.8% inulin alone (LS+In) or a combination of 2.3% inulin, pectin and psyllium each (LS+Comb). We performed RNA sequencing on the ileal samples from this study to show differential effects of fibre enriched groups on the ileal immune related genes; interferon induced and major histocompatibility complex (MHC) class II genes were most upregulated in the fibre combination group compared to inulin alone. Our results highlight that not all DF provide similar effects on host GI health. We did not find major differences in the ileal microbial composition between the groups. However, the heterogeneity in the structures of inulin, pectin and psyllium can influence the rate of fermentation of these fibres by the microbiota and hence, lead to different concentration ratios of SCFAs; acetate, propionate and butyrate, and consequent physiological effects (Singh and Vijay-Kumar, 2020). Time-of-flight mass-spectrometry based metabolomics analysis of the caecal content from mice in this experiment can reflect the changes of the metabolome in response to the different diets. We hypothesise varying concentrations of SCFAs in the caecal content in response to the distinct fibres in our diets, may influence the gut immune response (Singh et al., 2018).

Shotgun metagenomic assessment of ileal content samples from the different diet groups can provide us with a taxonomic resolution down to the species level and identify the variety of host undigestible carbohydrate-active enzymes present in the gut microbiota of each group. The metagenomics approach can not only give us a comprehensive description of the gut microbiota, but also characterise the viruses present in the gut virome, which is highly important for the regulation of the host immunophenotype (Rampelli, et al., 2016). However, shotgun metagenomics techniques are far more expensive than the 16S rRNA analysis and were not in the scope of this PhD thesis.

Many DF can also directly interact with the gut immune cells, such as macrophages or dendritic cells independent of the microbiota (Beukema et al., 2020). Mouse studies have shown that DF are transported into the Peyer's patches through microfold (M) cells and can activate immune cells (Suh et al., 2013; De Jesus et al., 2014). Moreover, the structural characteristics such as degree of polymerisation (complexity of the structure) of the fibres also play a role in the host immune response (Beukema et al., 2020; Vogt et al., 2016). Therefore, the heterogeneity in the structure of pectin, inulin and psyllium may explain the varied immune response in the groups. This effect may be due to the complexity of these fibres which is in the order inulin < pectin < psyllium (Alexander et al., 2019). Further research on germ free mice needs to be carried out to understand the precise mechanisms through which DF affect immune response in the gut independent of the microbiota.

We performed bulk RNA sequencing on the ileum samples which reflects the average gene expression across thousands of cells. In the future, single cell RNA sequencing can allow us to identify the immune cells that are expressing genes related to interferon induction and MHC Class II molecules (Zhao et al., 2020). For instance, ILC3 (Innate lymphoid cells subset 3) are known to express MHCII and

play a critical role in maintaining gut homeostasis by supporting the mutualism with commensal bacteria (Melo-Gonzalez et al., 2019), therefore, by measuring the gene expression of *H2-aa, H2-ab1,* and *H2-dmb1* in sort-purified ILC3, we may be able to confirm if the gene signal is indeed coming from ILC3 to maintain tissue homeostasis.

7.1.3 Calorie restriction (CR) improves the LF induced phenotype in mice

In collaboration with Dr Steegenga (Wageningen University and Research), we analysed the ileal samples from the IDEAL study to describe the long-term effects of the LF diet on ileal gene expression and microbiota composition. We also used this opportunity to investigate if CR intervention can reverse these LF induced effects. Long-term (24 months) feeding of the LF diet led to increased liver triglycerides (Rusli et al., 2017), decreased Paneth cells and cell cycle related genes and altered microbiota composition in the ileum, whereas CR intervention prevented this age-related effect of purified diets fed *ad libitum*.

Various intracellular mechanisms have been proposed by which CR can reduce the age-related cell and DNA damage including decreased oxidative stress and enhanced DNA repair (Heydari et al., 2007; Bruens et al., 2020). The stable expression of genes related to Paneth cells and cell cycle regulation suggests that 1) CR provides protection against age associated dysregulation of antimicrobial peptides secretion/production in the ileum (Tremblay et al., 2017), 2) CR maintains regeneration of the intestinal tissue which can eliminate age-related mutations of weak and damaged cells through niche competition, thereby contributing to the beneficial healthy ageing effect of CR (Bruens et al., 2020).

Studies on CR have been performed on chow (Guijas et al., 2020) as well as purified diet background (Green et al., 2018). We anticipated that the difference in the composition of the background diet may have an effect on the gut-liver axis in response to CR. We showed that 8 weeks CR on the LF background successfully reduced hepatic lipid accumulation in mice, whereas no difference in hepatic triglycerides was observed between chow control and its CR counterpart. In agreement with previous CR studies (Green et al., 2018; Guijas et al., 2020), we observed upregulation of peroxisome proliferator-activated receptor alpha (*Pparα*) in the liver of chowCR and LFCR mice, which is involved in the regulation of lipid β oxidation to provide energy (Zheng et al., 2018). However, the differential expression of hepatic lipogenic genes between chowCR and LFCR requires further investigation.

Moving forward with this study, it will be important to perform longer CR experiments with controlled variables to investigate if the diets affect the circulatory and intestinal luminal metabolites (e.g. free fatty acids) profile differently. Another important factor that may contribute to the differences observed between chow and LF, is the involvement of the gut microbiota and SCFAs that may affect the host's response to CR. Determining these gut-liver related changes that take place during CR can provide us with fundamental information to develop CR mimetics to promote health span in humans.

7.1.4 Challenges of using mice as research models

In chapter 6, we compared mice that were bred in different locations to show differential effects of the chow versus LF intervention on the microbiota composition and bile acid metabolism. In brief, we found increased abundance of *Proteobacteria* in the inhouse disease modelling unit (DMU) mice, which is further enhanced when these mice were exposed to the LF diet. Furthermore, we also show differential profiles of ileal bile acids, specifically increased levels of taurine conjugated bile acids in the externally sourced CRUK mice which indicates decreased bile salt hydrolase (BSH, involved in deconjugation of bile acids) activity in the ileal microbiota of these mice. Our results did not correlate with the abundance of genus *Lactobacillus* in this group, which is known to contain high amount of BSH enzymes (Song et al., 2019). Therefore, chemoproteomic approaches for interrogating the metabolic activities of the gut microbiota may shed some light on the measure of activity of the BSH present in gut of CRUK and DMU mice.

A limitation of this study was that due to cost and time restrictions, we were unable to sequence the gut microbiota of CRUK mice before they arrived at the University of East Anglia (UEA) facility. In the future, a baseline measure of ileal microbiota of mice from different locations at timepoint zero would give us further information on the original microbiota of these mice and how the microbiota has shifted over the course of the experiment (week 1, 2, 3 and 4) under chow and LF dietary conditions.

Our results highlight that despite the mice being genetically identical and exposed to the same dietary conditions, heterogeneity in the gut microbiota composition in mice due to their source can have profound implications in the field of biomedical research. The ever-increasing research on disease mechanisms and host processes that are impacted by gut microbiota make it abundantly clear that properly controlling for gut microbiota variation is critical for reproducibility. The scientific community and commercial vendors need to work together in order to address these realities. Scientists could help facilitate clear and consistent publishing of mouse husbandry details by providing information on the vendor name, mouse strain, barrier room, and inhouse husbandry conditions such as type of water, dietary compositional details, bedding, type of cages and light cycle. Smith et al. (2017) published the PREPARE guidelines: Planning Research and Experimental Procedures on Animals: Recommendations for Excellence to address the widespread concerns about reproducing and translating animal research.

Another challenge that we faced during our mouse studies was the presence of inter-individual variation in phenotype and microbiota results between the mice from the same group or cage dependent effects. For example, in chapter 6, we found presence of the genus *Akkermansia* in all mice from cage number 2 (that contained m4, m5, m6) within the CRUK chow group. The increased abundance of this mucus degrading genus *Akkermansia* is associated with the health status of mice and a reduced body weight (Depommier et al., 2020). However, presence of *Akkermansia* within these mice lacked correlation with factors such as body weight, *Muc2* or inflammation related gene expression. We also noticed low and high body weight gainers within the same group which could be attributable to various factors such as

dominance status, social interaction and stress. Moreover, some of these environmental factors may favour inter-individual differences via early life programming of the individual mouse dependent on litter size, and induction of epigenetic modifications of the genome (such as, DNA methylation, histone acetylation, or microRNA modifications) which can have major effects on the microbiome of the mouse (De Francesco et al., 2019).

Although, we did not observe strong correlations for abundance of *Akkermansia* with other phenotype or gene expression data for the mice. It would be interesting to see whether these inter-individual variations have long-term effects, such as healthy ageing or protection against diet induced metabolic syndrome (Biagi et al., 2016).

Recently, human intestinal organoids or organ on a chip technology have been demonstrated as powerful tools to understand unresolved mechanisms underlying physiology and disease progression. For example, De Gregorio et al. (2020) utilised integrated microfluid intestine-liver device as a tool to reproduce the first-pass metabolism of ethanol. Given the rapid technological advancement in the field, the variety of organoid models and organ on a chip options available will provide a powerful platform to research host-microbiota-gut-liver interactions for preclinical studies, and help scientists produce reproducible and translatable data in the field of metabolic research.

7.2 Human relevance

The consumption of ultra-processed foods, which are high in added starch and sucrose, and low in DF, are strongly linked with a 62% increased hazard for mortality (Rico-Campà et al., 2019). Detrimental effects have also been shown in this thesis with the development of early signs of NASH when the mice were exposed to the highly refined LF diet, that resembles a high refined carbohydrate, and low-fat Western style diet. Our studies further confirm the emerging epidemiological consensus that reduced fat processed foods such as low-fat desserts, fruit juices that were once viewed as healthy because of their low-fat content, can have dangerous outcomes in the liver because of the easily accessible carbohydrates present in these foods.

To avoid these detrimental effects, recently food manufacturers have started to fortify processed foods with refined DF such as inulin and pectin in various products (baked goods, fruit yoghurts) to promote them as health foods and increase the public's fibre intake. Indeed, high intake of fibres can provide many health benefits, such as improved barrier function (as shown in Chapter 3) and abundance of beneficial *Bifidobacterium* as reported in Chapter 5 of this thesis. Moreover, we also observed increased immune response in chow and fibre combination diet, but not in solely inulin enriched LF fed mice, which suggests that not all DF effect the GI health equally. The activation of an immune response to DF may be beneficial to the host under different circumstances. During physiological conditions, mild activation of immune responses by a high fibre intake can be beneficial because it promotes intestinal immunity. However, under gut inflammatory conditions (Irritable bowel disease, IBD), the activation of the immune response may add to the injury in the gut resulting in exacerbation of the disease. Therefore, further research is required to

understand whether the different fibre products provide similar health benefits in all human population.

Numerous studies have demonstrated various benefits of microbial metabolites such as SCFAs, from serving as fuel for colonocytes to improving intestinal inflammation. However, several studies have also shown that persistent elevation of SCFAs in the gut could prove harmful to gut and metabolic health (Singh and Vijay-Kumar, 2020). An intriguing study by Zhang et al. (2016) demonstrated aggravated colitis in DSS treated mice that received butyrate producing bacteria, while no detrimental effect was observed in healthy controls. Therefore, the differential impact of fibres on the gut immune response supports the paradigm that fibres are a 'double edged sword' that could promote or deter health depending on the health status of the host. Moreover, our research also highlights the need for careful consideration when selecting prebiotic interventions to alter levels of SCFAs. As dysregulated levels of SCFAs may promote or dampen inflammation depending on the microbiota composition (healthy or dysbiotic) and level of gut inflammation in humans.

7.3 Future perspectives

7.3.1 Susceptibility of LF mice to infection

In Chapter 3, we demonstrated that the gut and liver of LF fed mice were more sensitive to the LPS challenge compared to chow fed mice. In order to confirm this hypothesis future mouse studies with *Clostridium difficile* infection can further explain health effects of the two control diets. *C. difficile* is known to cause gastrointestinal infections, with symptoms ranging from diarrhoea in mild infections to ulcerative colitis in severe cases (Magill et al., 2014). The infection model rather than dextran sulfate sodium (DSS) colitis or LPS model, will allow us to study the normal host immune and gut microbiota response to the pathogen.

Four weeks chow and LF fed mice can be challenged with *C. difficile* strain such as R20291 (known to be enhanced in conditions of high simple sugars) and monitored daily for a further 4 weeks for signs of *C. difficile* infection (such as weight loss, temperature). Mice will be sacrificed at the end of the experiment, or if the infection symptoms reached a severity endpoint as described by Chrisabelle et al. (2020), so that no mice experienced severe distress. After sacrifice, the effect of diet on the outcome of C. *difficile* infections would be assessed by analysing changes in gut permeability by FITC-dextran in the serum, microbiota composition by shotgun metagenomics, metabolomics of luminal content and portal vein, caspase 3 activity in the liver, and gene expression analysis in the liver and gut for inflammatory markers.

7.3.2 The impact of dietary fibres on the gut-liver axis

Based on the results presented in chapter 5 of this thesis, the addition of DF inulin, and a combination of inulin, pectin and psyllium improves the lipid accumulation in the liver induced by the LF diet. In order to understand the 1) microbiota independent and 2) microbiota dependent mechanisms by which fibres have these beneficial effects we propose the following experiments;

1. To elucidate microbiota independent mechanisms
   Firstly, we could assess how glucose/fructose under the LF diet reaches the liver, and the possible mechanisms by which addition of inulin and fibre combination could prevent it. We could utilise isotope tracer experiments and administer mice with a solution of 1g sucrose (comprised of 1:1 mixture of labelled [U-^{13}C] glucose and [U-^{13}C] fructose) via oral gavage and quantify the levels of labelled sugars in the portal circulation at different time points (30 and 60 minutes) in mice. The mice will be fed a variant of the LF diet with 0g of sucrose. The amount of 1g per mouse is similar to the amount consumed on the LF diet per mouse per day. Additional groups with labelled sucrose solution with supplementation of inulin and/or combination fibres can demonstrate whether the fibres aid slower fructose/glucose uptake in the liver by measuring the levels of labelled glucose and fructose in the portal blood.

2. To elucidate microbiota dependent mechanisms
   Feeding experiments with the LF and LF + Fibre diets to mice with depleted gut microbiota (by using antibiotics treatment or germ-free mice) can give us further information about the role of microbiota in the development of the detriment liver phenotype in LF fed mice.

   Furthermore, lifelong studies of feeding with the LF diet, and LF diet enriched with different fibres will give us deeper knowledge on the long-term effect of these diets. Liver phenotype via histology, intestinal permeability measurements via FITC-dextran, bile acids in the ileum and serum, metabolomics in the portal vein blood, serum and the intestine, microbiota composition analysis via shot gun metagenomics sequencing and transcriptomics in both the intestine and liver could give us comprehensive data to form robust conclusions on the role of DF in the gut-liver axis. Within this experiment, time point analysis of all the above measures at 6, 12 and 24 months can also provide us information on the effects of different fibres during ageing and if some fibre via microbiota mechanisms are better than others in increasing health in aged mice (or life expectancy).

   FMT techniques can be used to inoculate mice with faecal human microbiota from healthy adults to assess the effects of different DF in improving diet induced NASH phenotype. Furthermore, inoculation of mice with faecal microbiota from NASH patients, could provide us with information on the role that the original (preintervention) microbiota may play in the effectiveness of DF in improving NASH phenotype. These strategies can help explain why some adults respond more positively to a dietary intervention than others and pave the way towards personalised dietary strategies (personalised fibre products) to tackle NASH and various metabolic diseases.

7.4 Further Limitations

Chow and LF diet have major differences in their carbohydrate composition. Another difference between the diets is in terms of their protein content and source. Chow diet contains slightly more protein (26.9 kcal%) compared to the LF diet (20 kcal%). Protein in the chow diet comes from a plant-based source (soya, potato protein, hydrolysed wheat gluten and maize gluten meal) and the protein in the LF diet comes from casein alone, which is mainly sourced from dairy. Protein source and amino acid balance has been known to influence gut microbiota and its metabolites. For example, plant proteins such as soy protein has been linked to a greater abundance of *Bacteroidetes*, and decreased circulating LPS levels compared to meat, dairy, and casein-protein consumption (Prokopidis et al., 2020). Furthermore, chow diet contains dietary aryl hydrocarbon receptor (AhR) ligands from phytochemicals (daidzein and genistein) in grains and soya oil, whereas the LF diet lacks such phytochemicals. Schanz et al. (2020) has demonstrated that dietary AhR ligands have a profound influence on intestinal immune cells as well as gut microbiota composition. Therefore, the lack of DF as well as AhR ligands in the LF diet may be one of the reasons underlying the 'unhealthy' phenotype caused by the LF diet. The target gene of AhR, cytochrome P450, family 1, subfamily A, polypeptide 1 (*Cyp1a1*) is highest in the proximal parts of the small intestine and almost none in the ileum. We have analysed gene expression of *Cyp1a1* in the duodenum of chow vs LF study to show downregulation of *Cyp1a1* in the LF groups (Supplementary Fig. 3.5). Therefore, the quality of the diet is just as important as the quantity, in order to achieve metabolic health.

List of communications

The role of diet on the gut-liver axis

Aleena Mushtaq, David Vauzour, Michael Müller

Bitesize seminar series, University of East Anglia, Norwich, United Kingdom February 2020

Source of genetically identical mice may affect the gut microbiota and bile acids profile

Aleena Mushtaq, Ildefonso Romero Rodriguez, David Vauzour, Michael Müller

NuGO Week, Agroscope, Bern, Switzerland, September 2019

Impact strategy for research of calorie restriction mimetics

Aleena Mushtaq, Benedikt Fecher, Michael Müller

Impact School Berlin, Germany, September 2019

The hunger gains

Aleena Mushtaq, Ildefonso Romero Rodriguez, David Vauzour, Michael Müller

Pint of Science, Norwich, United Kingdom, May 2019

PhD in the field of molecular nutrition

Aleena Mushtaq

Royal Society of Biology School Fair, London, United Kingdom, January 2019

The role of calorie restriction (CR) on the ileum-liver axis of mice

Aleena Mushtaq, David Vauzour, Wilma Steegenga, Michael Müller

Knowledge exchange trip: Parma University, Italy, September 2018

Acknowledgements

References

Afshin A, Sur PJ, Fay KA, et al. Health effects of dietary risks in 195 countries, 1990-2017: a systematic analysis for the Global Burden of Disease Study 2017. Lancet. 2019;393(10184):1958-1972. doi:10.1016/S0140-6736(19)30041-8

Alegre M-L. Mouse microbiomes: overlooked culprits of experimental variability. Genome Biol. 2019;20(1):108. doi:10.1186/s13059-019-1723-2

Alexander C, Rietschel ET. Bacterial lipopolysaccharides and innate immunity. J Endotoxin Res. 2001;7(3):167-202.

Alexander C, Swanson KS, Fahey Jr GC, Garleb KA. Perspective: Physiologic Importance of Short-Chain Fatty Acids from Nondigestible Carbohydrate Fermentation. Adv Nutr. 2019;10(4):576-589. doi:10.1093/advances/nmz004

Almeida-Suhett CP, Scott JM, Graham A, Chen Y, Deuster PA. Control diet in a high-fat diet study in mice: Regular chow and purified low-fat diet have similar effects on phenotypic, metabolic, and behavioral outcomes. Nutr Neurosci. 2019;22(1):19-28. doi:10.1080/1028415X.2017.1349359

Amorim JC, Vriesmann LC, Petkowicz CLO, Martinez GR, Noleto GR. Modified pectin from Theobroma cacao induces potent pro-inflammatory activity in murine peritoneal macrophage. Int J Biol Macromol. 2016;92:1040-1048. doi:https://doi.org/10.1016/j.ijbiomac.2016.08.015

Amoutzopoulos B, Steer T, Roberts C, Collins D, Page P. Free and Added Sugar Consumption and Adherence to Guidelines: The UK National Diet and Nutrition Survey (2014/15-2015/16). Nutrients. 2020;12(2). doi:10.3390/nu12020393

Ansaldo E, Slayden LC, Ching KL, et al. Akkermansia muciniphila induces intestinal adaptive immune responses during homeostasis. Science. 2019;364(6446):1179-1184. doi:10.1126/science.aaw7479

Aron-Wisnewsky J, Vigliotti C, Witjes J, et al. Gut microbiota and human NAFLD: disentangling microbial signatures from metabolic disorders. Nat Rev Gastroenterol Hepatol. 2020;17(5):279-297. doi:10.1038/s41575-020-0269-9

Aron-Wisnewsky J, Warmbrunn M V, Nieuwdorp M, Clément K. Nonalcoholic Fatty Liver Disease: Modulating Gut Microbiota to Improve Severity? Gastroenterology. 2020;158(7):1881-1898. doi:https://doi.org/10.1053/j.gastro.2020.01.049

Austad SN, Hoffman JM. Beyond calorie restriction: aging as a biological target for nutrient therapies. Curr Opin Biotechnol. 2021;70:56-60. doi:https://doi.org/10.1016/j.copbio.2020.11.008

Baek JM, Kwak SC, Kim J-Y, et al. Evaluation of a novel technique for intraperitoneal injections in mice. Lab Anim (NY). 2015;44(11):440-444. doi:10.1038/laban.880

Barker N, van Oudenaarden A, Clevers H. Identifying the stem cell of the intestinal crypt: strategies and pitfalls. Cell Stem Cell. 2012;11(4):452-460. doi:10.1016/j.stem.2012.09.009

Baur JA, Pearson KJ, Price NL, et al. Resveratrol improves health and survival of mice on a high-calorie diet. Nature. 2006;444(7117):337-342. doi:10.1038/nature05354

Beck TF, Shchelochkov OA, Yu Z, et al. Novel frem1-related mouse phenotypes and evidence of genetic interactions with gata4 and slit3. PLoS One. 2013;8(3):e58830-e58830. doi:10.1371/journal.pone.0058830

Bellono NW, Bayrer JR, Leitch DB, et al. Enterochromaffin Cells Are Gut Chemosensors that Couple to Sensory Neural Pathways. Cell. 2017;170(1):185-198.e16. doi:10.1016/j.cell.2017.05.034

Beukema M, Faas MM, de Vos P. The effects of different dietary fiber pectin structures on the gastrointestinal immune barrier: impact via gut microbiota and direct effects on immune cells. Exp Mol Med. Published online 2020. doi:10.1038/s12276-020-0449-2

Biagi E, Franceschi C, Rampelli S, et al. Gut Microbiota and Extreme Longevity. Curr Biol. 2016;26(11):1480-1485. doi:10.1016/j.cub.2016.04.016

Bindels LB, Porporato P, Dewulf EM, et al. Gut microbiota-derived propionate reduces cancer cell proliferation in the liver. Br J Cancer. 2012;107(8):1337-1344. doi:10.1038/bjc.2012.409

Bligh, EG., Dyer, W.J. A RAPID METHOD OF TOTAL LIPID EXTRACTION AND PURIFICATION. Can. J. Biochem. Physiol. 1959, 37(8): 911–17. doi:10.1139/o59-099.

Bloom DE, Chatterji S, Kowal P, et al. Macroeconomic implications of population ageing and selected policy responses. Lancet (London, England). 2015;385(9968):649-657. doi:10.1016/S0140-6736(14)61464-1

Bruens L, Ellenbroek SIJ, Suijkerbuijk SJE, et al. Calorie Restriction Increases the Number of Competing Stem Cells and Decreases Mutation Retention in the Intestine. Cell Rep. 2020;32(3):107937. doi:https://doi.org/10.1016/j.celrep.2020.107937

Bruss MD, Khambatta CF, Ruby MA, Aggarwal I, Hellerstein MK. Calorie restriction increases fatty acid synthesis and whole body fat oxidation rates. Am J Physiol Metab. 2009;298(1):E108-E116. doi:10.1152/ajpendo.00524.2009

Bucław M. The use of inulin in poultry feeding: a review. J Anim Physiol Anim Nutr (Berl). 2016;100(6):1015-1022. doi:10.1111/jpn.12484

Byndloss MX, Olsan EE, Rivera-Chávez F, et al. Microbiota-activated PPAR-γ signaling inhibits dysbiotic Enterobacteriaceae expansion. Science (80-). 2017;357(6351):570 LP - 575. doi:10.1126/science.aam9949

Cai Y, Folkerts J, Folkerts G, Maurer M, Braber S. Microbiota-dependent and - independent effects of dietary fibre on human health. Br J Pharmacol. 2020;177(6):1363-1381. doi:10.1111/bph.14871

Cameron RG. Pectin in Foods. In: Melton L, Shahidi F, Varelis PBT-E of FC, eds. Academic Press; 2019:208-213. doi:https://doi.org/10.1016/B978-0-08-100596-5.21590-4

Camilleri M, Lyle BJ, Madsen KL, Sonnenburg J, Verbeke K, Wu GD. Role for diet in normal gut barrier function: developing guidance within the framework of food-labeling regulations. Am J Physiol Gastrointest Liver Physiol. 2019;317(1):G17-G39. doi:10.1152/ajpgi.00063.2019

Canesso MCC, Lemos L, Neves TC, et al. The cytosolic sensor STING is required for intestinal homeostasis and control of inflammation. Mucosal Immunol. 2018;11(3):820-834. doi:10.1038/mi.2017.88

Cani PD, Amar J, Iglesias MA, et al. Metabolic Endotoxemia Initiates Obesity and Insulin Resistance. Diabetes. 2007;56(7):1761 LP - 1772. doi:10.2337/db06-1491

Cani PD, Neyrinck AM, Fava F, et al. Selective increases of bifidobacteria in gut microflora improve high-fat-diet-induced diabetes in mice through a mechanism associated with endotoxaemia. Diabetologia. 2007;50(11):2374-2383. doi:10.1007/s00125-007-0791-0

Caporaso JG, Lauber CL, Walters WA, et al. Global patterns of 16S rRNA diversity at a depth of millions of sequences per sample. Proc Natl Acad Sci. 2011;108(Supplement 1):4516 LP - 4522. doi:10.1073/pnas.1000080107

Capuano E. The behavior of dietary fiber in the gastrointestinal tract determines its physiological effect. Crit Rev Food Sci Nutr. 2017;57(16):3543-3564. doi:10.1080/10408398.2016.1180501

Carpino G, Del Ben M, Pastori D, et al. Increased Liver Localization of Lipopolysaccharides in Human and Experimental NAFLD. Hepatology. 2020;72(2):470-485. doi:10.1002/hep.31056

Castellino M, Renna M, Leoni B, et al. Conventional and unconventional recovery of inulin rich extracts for food use from the roots of globe artichoke. Food Hydrocoll. 2020;107:105975. doi:https://doi.org/10.1016/j.foodhyd.2020.105975

Chen F, Yang W, Huang X, et al. Neutrophils Promote Amphiregulin Production in Intestinal Epithelial Cells through TGF-β and Contribute to Intestinal Homeostasis. J Immunol. 2018;201(8):2492 LP - 2501. doi:10.4049/jimmunol.1800003

Chen J, Vitetta L. Gut Microbiota Metabolites in NAFLD Pathogenesis and Therapeutic Implications. Int J Mol Sci . 2020;21(15). doi:10.3390/ijms21155214

Chen M, Fan B, Liu S, et al. The in vitro Effect of Fibers With Different Degrees of Polymerization on Human Gut Bacteria . Front Microbiol. 2020;11:819. https://www.frontiersin.org/article/10.3389/fmicb.2020.00819

Chen Y, Liu Y, Zhou R, et al. Associations of gut-flora-dependent metabolite trimethylamine-N-oxide, betaine and choline with non-alcoholic fatty liver disease in adults. Sci Rep. 2016;6:19076. doi:10.1038/srep19076

Chong J, Liu P, Zhou G, Xia J. Using MicrobiomeAnalyst for comprehensive statistical, functional, and meta-analysis of microbiome data. Nat Protoc. 2020;15(3):799-821. doi:10.1038/s41596-019-0264-1

Chu H, Duan Y, Yang L, Schnabl B. Small metabolites, possible big changes: a microbiota-centered view of non-alcoholic fatty liver disease. Gut. 2019;68(2):359 LP - 370. doi:10.1136/gutjnl-2018-316307

Claesson MJ, Jeffery IB, Conde S, et al. Gut microbiota composition correlates with diet and health in the elderly. Nature. 2012;488(7410):178-184. doi:10.1038/nature11319

Colman RJ, Anderson RM, Johnson SC, et al. Caloric restriction delays disease onset and mortality in rhesus monkeys. Science. 2009;325(5937):201-204. doi:10.1126/science.1173635

Crovesy L, Ostrowski M, Ferreira DMTP, Rosado EL, Soares-Mota M. Effect of Lactobacillus on body weight and body fat in overweight subjects: a systematic review of randomized controlled clinical trials. Int J Obes. 2017;41(11):1607-1614. doi:10.1038/ijo.2017.161

Cui G, Martin RC, Jin H, et al. Up-regulation of FGF15/19 signaling promotes hepatocellular carcinoma in the background of fatty liver. J Exp Clin Cancer Res. 2018;37(1):136. doi:10.1186/s13046-018-0781-8

d'Avila JC, Siqueira LD, Mazeraud A, et al. Age-related cognitive impairment is associated with long-term neuroinflammation and oxidative stress in a mouse model of episodic systemic inflammation. J Neuroinflammation. 2018;15(1):28. doi:10.1186/s12974-018-1059-y

Dalby MJ, Ross AW, Walker AW, Morgan PJ. Dietary Uncoupling of Gut Microbiota and Energy Harvesting from Obesity and Glucose Tolerance in Mice. Cell Rep. 2017;21(6):1521-1533. doi:10.1016/j.celrep.2017.10.056

Dao MC, Everard A, Aron-Wisnewsky J, et al. Akkermansia muciniphila and improved metabolic health during a dietary intervention in obesity: relationship with gut microbiome richness and ecology. Gut. 2016;65(3):426 LP - 436. doi:10.1136/gutjnl-2014-308778

Davani-Davari D, Negahdaripour M, Karimzadeh I, et al. Prebiotics: Definition, Types, Sources, Mechanisms, and Clinical Applications. Foods (Basel, Switzerland). 2019;8(3). doi:10.3390/foods8030092

De Francesco PN, Cornejo MP, Barrile F, et al. Inter-individual Variability for High Fat Diet Consumption in Inbred C57BL/6 Mice . Front Nutr . 2019;6:67. https://www.frontiersin.org/article/10.3389/fnut.2019.00067

De Gregorio V, Telesco M, Corrado B, et al. Intestine-Liver Axis On-Chip Reveals the Intestinal Protective Role on Hepatic Damage by Emulating Ethanol First-Pass Metabolism. Front Bioeng Biotechnol. 2020;8:163. doi:10.3389/fbioe.2020.00163

De Guzman JM, Ku G, Fahey R, et al. Chronic caloric restriction partially protects against age-related alteration in serum metabolome. Age (Dordr). 2013;35(4):1091-1104. doi:10.1007/s11357-012-9430-x

De Jesus M, Ostroff GR, Levitz SM, Bartling TR, Mantis NJ. A Population of Langerin-Positive Dendritic Cells in Murine Peyer's Patches Involved in Sampling β-Glucan Microparticles. PLoS One. 2014;9(3):e91002. https://doi.org/10.1371/journal.pone.0091002

De Vadder F, Kovatcheva-Datchary P, Zitoun C, Duchampt A, Bäckhed F, Mithieux G. Microbiota-Produced Succinate Improves Glucose Homeostasis via Intestinal Gluconeogenesis. Cell Metab. 2016;24(1):151-157. doi:10.1016/j.cmet.2016.06.013

Del Fabbro S, Calder PC, Childs CE. Microbiota-independent immunological effects of non-digestible oligosaccharides in the context of inflammatory bowel diseases. Proc Nutr Soc. Published online 2020:1-11. doi:DOI: 10.1017/S0029665120006953

Deng Y, Zheng X, Zhang Y, et al. High SPRR1A expression is associated with poor survival in patients with colon cancer. Oncol Lett. 2020;19(5):3417-3424. doi:10.3892/ol.2020.11453

Denson LA, Sturm E, Echevarria W, et al. The orphan nuclear receptor, shp, mediates bile acid-induced inhibition of the rat bile acid transporter, ntcp. Gastroenterology. 2001;121(1):140-147. doi:10.1053/gast.2001.25503

Depommier C, Van Hul M, Everard A, Delzenne NM, De Vos WM, Cani PD. Pasteurized Akkermansia muciniphila increases whole-body energy expenditure and fecal energy excretion in diet-induced obese mice. Gut Microbes. 2020;11(5):1231-1245. doi:10.1080/19490976.2020.1737307

Desai MS, Seekatz AM, Koropatkin NM, et al. A Dietary Fiber-Deprived Gut Microbiota Degrades the Colonic Mucus Barrier and Enhances Pathogen Susceptibility. Cell. 2016;167(5):1339-1353.e21. doi:10.1016/j.cell.2016.10.043

Donaldson GP, Lee SM, Mazmanian SK. Gut biogeography of the bacterial microbiota. Nat Rev Microbiol. 2016;14(1):20-32. doi:10.1038/nrmicro3552

Donohoe DR, Collins LB, Wali A, Bigler R, Sun W, Bultman SJ. The Warburg effect dictates the mechanism of butyrate-mediated histone acetylation and cell proliferation. Mol Cell. 2012;48(4):612-626. doi:10.1016/j.molcel.2012.08.033

Dupont A, Heinbockel L, Brandenburg K, Hornef MW. Antimicrobial peptides and the enteric mucus layer act in concert to protect the intestinal mucosa. Gut Microbes. 2014;5(6):761-765. doi:10.4161/19490976.2014.972238

Duszka K, Picard A, Ellero-Simatos S, et al. Intestinal PPARγ signalling is required for sympathetic nervous system activation in response to caloric restriction. Sci Rep. 2016;6(1):36937. doi:10.1038/srep36937

Edgar RC. UPARSE: highly accurate OTU sequences from microbial amplicon reads. Nat Methods. 2013;10(10):996-998. doi:10.1038/nmeth.2604

Ellacott KLJ, Morton GJ, Woods SC, Tso P, Schwartz MW. Assessment of feeding behavior in laboratory mice. Cell Metab. 2010;12(1):10-17. doi:10.1016/j.cmet.2010.06.001

Ericsson AC, Davis JW, Spollen W, et al. Effects of Vendor and Genetic Background on the Composition of the Fecal Microbiota of Inbred Mice. PLoS One. 2015;10(2):e0116704. https://doi.org/10.1371/journal.pone.0116704

Estes C, Razavi H, Loomba R, Younossi Z, Sanyal AJ. Modeling the epidemic of nonalcoholic fatty liver disease demonstrates an exponential increase in burden of disease. Hepatology. 2018;67(1):123-133. doi:10.1002/hep.29466

Everard A, Belzer C, Geurts L, et al. Cross-talk between Akkermansia muciniphila and intestinal epithelium controls diet-induced obesity. Proc Natl Acad Sci U S A. 2013;110(22):9066-9071. doi:10.1073/pnas.1219451110

Fabbiano S, Suárez-Zamorano N, Chevalier C, et al. Functional Gut Microbiota Remodeling Contributes to the Caloric Restriction-Induced Metabolic Improvements. Cell Metab. 2018;28(6):907-921.e7. doi:https://doi.org/10.1016/j.cmet.2018.08.005

Feinman RD, Pogozelski WK, Astrup A, et al. Dietary carbohydrate restriction as the first approach in diabetes management: critical review and evidence base. Nutrition. 2015;31(1):1-13. doi:10.1016/j.nut.2014.06.011

Feldman AT, Wolfe D. Tissue processing and hematoxylin and eosin staining. Methods Mol Biol. 2014;1180:31-43. doi:10.1007/978-1-4939-1050-2_3

Ferraris RP, Choe J-Y, Patel CR. Intestinal Absorption of Fructose. Annu Rev Nutr. 2018;38:41-67. doi:10.1146/annurev-nutr-082117-051707

Flurkey K, M. Currer J, Harrison DE. Chapter 20 - Mouse Models in Aging Research. In: Fox JG, Davisson MT, Quimby FW, Barthold SW, Newcomer CE, Smith ALBT-TM in BR (Second E, eds. American College of Laboratory Animal Medicine. Academic Press; 2007:637-672. doi:https://doi.org/10.1016/B978-012369454-6/50074-1

Fontana L, Klein S. Aging, adiposity, and calorie restriction. JAMA. 2007;297(9):986-994. doi:10.1001/jama.297.9.986

Fontana L. Modulating human aging and age-associated diseases. Biochim Biophys Acta. 2009;1790(10):1133-1138. doi:10.1016/j.bbagen.2009.02.002

Franco EAN, Sanches-Silva A, Ribeiro-Santos R, de Melo NR. Psyllium (Plantago ovata Forsk): From evidence of health benefits to its food application. Trends Food Sci Technol. 2020;96:166-175. doi:https://doi.org/10.1016/j.tifs.2019.12.006

Franklin CL, Ericsson AC. Microbiota and reproducibility of rodent models. Lab Anim (NY). 2017;46(4):114-122. doi:10.1038/laban.1222

Fraumene C, Manghina V, Cadoni E, et al. Caloric restriction promotes rapid expansion and long-lasting increase of Lactobacillus in the rat fecal microbiota. Gut Microbes. 2018;9(2):104-114. doi:10.1080/19490976.2017.1371894

Fu ZD, Klaassen CD. Increased bile acids in enterohepatic circulation by short-term calorie restriction in male mice. Toxicol Appl Pharmacol. 2013;273(3):680-690. doi:10.1016/j.taap.2013.10.020

Fujii N, Uta S, Kobayashi M, Sato T, Okita N, Higami Y. Impact of aging and caloric restriction on fibroblast growth factor 21 signaling in rat white adipose tissue. Exp Gerontol. 2019;118:55-64. doi:https://doi.org/10.1016/j.exger.2019.01.001

Fujisaka S, Usui I, Nawaz A, et al. Bofutsushosan improves gut barrier function with a bloom of Akkermansia muciniphila and improves glucose metabolism in mice with diet-induced obesity. Sci Rep. 2020;10(1):5544. doi:10.1038/s41598-020-62506-w

Gadaleta RM, Moschetta A. Metabolic Messengers: fibroblast growth factor 15/19. Nat Metab. 2019;1(6):588-594. doi:10.1038/s42255-019-0074-3

Garidou L, Pomié C, Klopp P, et al. The Gut Microbiota Regulates Intestinal CD4 T Cells Expressing RORγt and Controls Metabolic Disease. Cell Metab. 2015;22(1):100-112. doi:10.1016/j.cmet.2015.06.001

Gentile CL, Weir TL. The gut microbiota at the intersection of diet and human health. Science (80-). 2018;362(6416):776 LP - 780. doi:10.1126/science.aau5812

Gerritsen J, Hornung B, Renckens B, et al. Genomic and functional analysis of Romboutsia ilealis CRIB(T) reveals adaptation to the small intestine. PeerJ. 2017;5:e3698-e3698. doi:10.7717/peerj.3698

Gill RG, Pagni PP, Kupfer T, et al. A Preclinical Consortium Approach for Assessing the Efficacy of Combined Anti-CD3 Plus IL-1 Blockade in Reversing New-Onset Autoimmune Diabetes in NOD Mice. Diabetes. 2016;65(5):1310-1316. doi:10.2337/db15-0492

Gong L, Cao W, Chi H, et al. Whole cereal grains and potential health effects: Involvement of the gut microbiota. Food Res Int. 2018;103:84-102. doi:https://doi.org/10.1016/j.foodres.2017.10.025

González-Blázquez R, Alcalá M, Fernández-Alfonso MS, et al. Relevance of control diet choice in metabolic studies: impact in glucose homeostasis and vascular function. Sci Rep. 2020;10(1):2902. doi:10.1038/s41598-020-59674-0

Gonzalo, Hamdan-Pérez N, Tovar AR, et al. Combined high-fat diet and sustained high sucrose consumption promotes NAFLD in a murine model. Ann Hepatol. 2015;14(4):540-546. doi:https://doi.org/10.1016/S1665-2681(19)31176-7

Goodman BE. Insights into digestion and absorption of major nutrients in humans. Adv Physiol Educ. 2010;34(2):44-53. doi:10.1152/advan.00094.2009

Gowd V, Xie L, Zheng X, Chen W. Dietary fibers as emerging nutritional factors against diabetes: focus on the involvement of gut microbiota. Crit Rev Biotechnol. 2019;39(4):524-540. doi:10.1080/07388551.2019.1576025

Green CL, Soltow QA, Mitchell SE, et al. The Effects of Graded Levels of Calorie Restriction: XIII. Global Metabolomics Screen Reveals Graded Changes in Circulating Amino Acids, Vitamins, and Bile Acids in the Plasma of C57BL/6 Mice. Journals Gerontol Ser A. 2019;74(1):16-26. doi:10.1093/gerona/gly058

Grobe JL. Comprehensive Assessments of Energy Balance in Mice. Methods Mol Biol. 2017;1614:123-146. doi:10.1007/978-1-4939-7030-8_10

Grundy MM-L, Edwards CH, Mackie AR, Gidley MJ, Butterworth PJ, Ellis PR. Re-evaluation of the mechanisms of dietary fibre and implications for macronutrient bioaccessibility, digestion and postprandial metabolism. Br J Nutr. 2016;116(5):816-833. doi:10.1017/S0007114516002610

Guevara-Cruz M, Godinez-Salas ET, Sanchez-Tapia M, et al. Genistein stimulates insulin sensitivity through gut microbiota reshaping and skeletal muscle AMPK activation in obese subjects. BMJ open diabetes Res care. 2020;8(1). doi:10.1136/bmjdrc-2019-000948

Guijas C, Montenegro-Burke JR, Cintron-Colon R, et al. Metabolic adaptation to calorie restriction. Sci Signal. 2020;13(648):eabb2490. doi:10.1126/scisignal.abb2490

Gury-Benari M, Thaiss CA, Serafini N, et al. The Spectrum and Regulatory Landscape of Intestinal Innate Lymphoid Cells Are Shaped by the Microbiome. Cell. 2016;166(5):1231-1246.e13. doi:10.1016/j.cell.2016.07.043

Hahn O, Grönke S, Stubbs TM, et al. Dietary restriction protects from age-associated DNA methylation and induces epigenetic reprogramming of lipid metabolism. Genome Biol. 2017;18(1):56. doi:10.1186/s13059-017-1187-1

Hall KD, Ayuketah A, Brychta R, et al. Ultra-Processed Diets Cause Excess Calorie Intake and Weight Gain: An Inpatient Randomized Controlled Trial of Ad Libitum Food Intake. Cell Metab. 2019;30(1):67-77.e3. doi:10.1016/j.cmet.2019.05.008

Hamaker BR, Cantu-Jungles TM. Discrete Fiber Structures Dictate Human Gut Bacteria Outcomes. Trends Endocrinol Metab. Published online May 2020. doi:10.1016/j.tem.2020.05.002

Hannou SA, Haslam DE, McKeown NM, Herman MA. Fructose metabolism and metabolic disease. J Clin Invest. 2018;128(2):545-555. doi:10.1172/JCI96702

Hansen AK, Hansen CHF, Krych L, Nielsen DS. Impact of the gut microbiota on rodent models of human disease. World J Gastroenterol. 2014;20(47):17727-17736. doi:10.3748/wjg.v20.i47.17727

Hepworth MR, Monticelli LA, Fung TC, et al. Innate lymphoid cells regulate CD4+ T-cell responses to intestinal commensal bacteria. Nature. 2013;498(7452):113-117. doi:10.1038/nature12240

Heydari AR, Unnikrishnan A, Lucente LV, Richardson A. Caloric restriction and genomic stability. Nucleic Acids Res. 2007;35(22):7485-7496. doi:10.1093/nar/gkm860

Hilbert T, Steinhagen F, Senzig S, et al. Vendor effects on murine gut microbiota influence experimental abdominal sepsis. J Surg Res. 2017;211:126-136. doi:10.1016/j.jss.2016.12.008

Holland C, Ryden P, Edwards CH, Grundy MM-L. Plant Cell Walls: Impact on Nutrient Bioaccessibility and Digestibility. Foods . 2020;9(2). doi:10.3390/foods9020201

Horackova S, Vesela K, Klojdova I, Bercikova M, Plockova M. Bile salt hydrolase activity, growth characteristics and surface properties in Lactobacillus acidophilus. Eur Food Res Technol. 2020;246(8):1627-1636. doi:10.1007/s00217-020-03518-8

Howcroft TK, Campisi J, Louis GB, et al. The role of inflammation in age-related disease. Aging (Albany NY). 2013;5(1):84-93. doi:10.18632/aging.100531

Howe A, Ringus DL, Williams RJ, et al. Divergent responses of viral and bacterial communities in the gut microbiome to dietary disturbances in mice. ISME J. 2016;10(5):1217-1227. doi:10.1038/ismej.2015.183

Hu D, Yang W, Mao P, Cheng M. Combined Amelioration of Prebiotic Resveratrol and Probiotic Bifidobacteria on Obesity and Nonalcoholic Fatty Liver Disease. Nutr Cancer. Published online May 2020:1-10. doi:10.1080/01635581.2020.1767166

Hufeldt MR, Nielsen DS, Vogensen FK, Midtvedt T, Hansen AK. Variation in the gut microbiota of laboratory mice is related to both genetic and environmental factors. Comp Med. 2010;60(5):336-347. https://pubmed.ncbi.nlm.nih.gov/21262117

Hugenholtz F, de Vos WM. Mouse models for human intestinal microbiota research: a critical evaluation. Cell Mol Life Sci. 2018;75(1):149-160. doi:10.1007/s00018-017-2693-8

Hung T Van, Suzuki T. Dietary Fermentable Fiber Reduces Intestinal Barrier Defects and Inflammation in Colitic Mice. J Nutr. 2016;146(10):1970-1979. doi:10.3945/jn.116.232538

Ibrahim S, Riahi O, Said SM, Sabri MFM, Rozali SBT-RM in MS and ME. Biopolymers From Crop Plants. In: Elsevier; 2019. doi:https://doi.org/10.1016/B978-0-12-803581-8.11573-5

Igarashi M, Guarente L. The unexpected role of mTORC1 in intestinal stem cells during calorie restriction. Cell Cycle. 2017;16(1):1-2. doi:10.1080/15384101.2016.1221210

Ikeda I, Metoki K, Yamahira T, et al. Impact of fasting time on hepatic lipid metabolism in nutritional animal studies. Biosci Biotechnol Biochem. 2014;78(9):1584-1591. doi:10.1080/09168451.2014.923297

Inagaki T, Moschetta A, Lee Y-K, et al. Regulation of antibacterial defense in the small intestine by the nuclear bile acid receptor. Proc Natl Acad Sci U S A. 2006;103(10):3920 LP - 3925. doi:10.1073/pnas.0509592103

Isaacs-Ten A, Echeandia M, Moreno-Gonzalez M, et al. Intestinal microbiome-macrophage crosstalk contributes to cholestatic liver disease by promoting intestinal permeability. Hepatology. 2020;n/a(n/a). doi:10.1002/hep.31228

Ito S, Fujimori T, Furuya A, Satoh J, Nabeshima Y, Nabeshima Y-I. Impaired negative feedback suppression of bile acid synthesis in mice lacking betaKlotho. J Clin Invest. 2005;115(8):2202-2208. doi:10.1172/JCI23076

Ivanov II, Frutos R de L, Manel N, et al. Specific microbiota direct the differentiation of IL-17-producing T-helper cells in the mucosa of the small intestine. Cell Host Microbe. 2008;4(4):337-349. doi:10.1016/j.chom.2008.09.009

Jalili-Firoozinezhad S, Gazzaniga FS, Calamari EL, et al. A complex human gut microbiome cultured in an anaerobic intestine-on-a-chip. Nat Biomed Eng. 2019;3(7):520-531. doi:10.1038/s41551-019-0397-0

Jane M, McKay J, Pal S. Effects of daily consumption of psyllium, oat bran and polyGlycopleX on obesity-related disease risk factors: A critical review. Nutrition. 2019;57:84-91. doi:https://doi.org/10.1016/j.nut.2018.05.036

Jang C, Hui S, Lu W, et al. The Small Intestine Converts Dietary Fructose into Glucose and Organic Acids. Cell Metab. 2018;27(2):351-361.e3. doi:10.1016/j.cmet.2017.12.016

Jegatheesan P, De Bandt J-P. Fructose and NAFLD: The Multifaceted Aspects of Fructose Metabolism. Nutrients. 2017;9(3). doi:10.3390/nu9030230

Jose A, Perez-Jimenez F, Camargo A. The role of diet and intestinal microbiota in the development of metabolic syndrome. J Nutr Biochem. 2019;70:1-27. doi:https://doi.org/10.1016/j.jnutbio.2019.03.017

Kar SK, Jansman AJM, Benis N, et al. Dietary protein sources differentially affect microbiota, mTOR activity and transcription of mTOR signaling pathways in the small intestine. PLoS One. 2017;12(11):e0188282-e0188282. doi:10.1371/journal.pone.0188282

Kastrati I, Canestrari E, Frasor J. PHLDA1 expression is controlled by an estrogen receptor-NFκB-miR-181 regulatory loop and is essential for formation of ER+ mammospheres. Oncogene. 2015;34(18):2309-2316. doi:10.1038/onc.2014.180

Katlinskaya Y V, Katlinski K V, Lasri A, et al. Type I Interferons Control Proliferation and Function of the Intestinal Epithelium. Mol Cell Biol. 2016;36(7):1124 LP - 1135. doi:10.1128/MCB.00988-15

Kawauchi S, Horibe S, Sasaki N, et al. Inhibitory Effects of Sodium Alginate on Hepatic Steatosis in Mice Induced by a Methionine- and Choline-deficient Diet. Mar Drugs. 2019;17(2). doi:10.3390/md17020104

Ke X, Walker A, Haange S-B, et al. Synbiotic-driven improvement of metabolic disturbances is associated with changes in the gut microbiome in diet-induced obese mice. Mol Metab. 2019;22:96-109. doi:https://doi.org/10.1016/j.molmet.2019.01.012

Khotimchenko M. Pectin polymers for colon-targeted antitumor drug delivery. Int J Biol Macromol. 2020;158:1110-1124. doi:https://doi.org/10.1016/j.ijbiomac.2020.05.002

Kim B-R, Shin J, Guevarra R, et al. Deciphering Diversity Indices for a Better Understanding of Microbial Communities. J Microbiol Biotechnol. 2017;27(12):2089-2093. doi:10.4014/jmb.1709.09027

Kim J, Koo B-K, Knoblich JA. Human organoids: model systems for human biology and medicine. Nat Rev Mol Cell Biol. Published online 2020. doi:10.1038/s41580-020-0259-3

Kim KE, Jung Y, Min S, et al. Caloric restriction of db/db mice reverts hepatic steatosis and body weight with divergent hepatic metabolism. Sci Rep. 2016;6:30111. doi:10.1038/srep30111

Kimura I, Ozawa K, Inoue D, et al. The gut microbiota suppresses insulin-mediated fat accumulation via the short-chain fatty acid receptor GPR43. Nat Commun. 2013;4:1829. doi:10.1038/ncomms2852

Kir S, Beddow SA, Samuel VT, et al. FGF19 as a Postprandial, Insulin-Independent Activator of Hepatic Protein and Glycogen Synthesis. Science (80-). 2011;331(6024):1621 LP - 1624. doi:10.1126/science.1198363

Kir S, Zhang Y, Gerard RD, Kliewer SA, Mangelsdorf DJ. Nuclear Receptors HNF4α and LRH-1 Cooperate in Regulating Cyp7a1 in Vivo. J Biol Chem . 2012;287(49):41334-41341. doi:10.1074/jbc.M112.421834

Koh A, De Vadder F, Kovatcheva-Datchary P, Bäckhed F. From dietary fiber to host physiology: Short-chain fatty acids as key bacterial metabolites. Cell. 2016;165(6):1332-1345. doi:10.1016/j.cell.2016.05.041

Kok DEG, Rusli F, van der Lugt B, et al. Lifelong calorie restriction affects indicators of colonic health in aging C57Bl/6J mice. J Nutr Biochem. 2018;56:152-164. doi:https://doi.org/10.1016/j.jnutbio.2018.01.001

Komatsu T, Park S, Hayashi H, Mori R, Yamaza H, Shimokawa I. Mechanisms of Calorie Restriction: A Review of Genes Required for the Life-Extending and Tumor-Inhibiting Effects of Calorie Restriction. Nutrients. 2019;11(12):3068. doi:10.3390/nu11123068

Kordaß T, Osen W, Eichmüller SB. Controlling the Immune Suppressor: Transcription Factors and MicroRNAs Regulating CD73/NT5E. Front Immunol. 2018;9:813. doi:10.3389/fimmu.2018.00813

Korte SW, Dorfmeyer RA, Franklin CL, Ericsson AC. Acute and long-term effects of antibiotics commonly used in laboratory animal medicine on the fecal microbiota. Vet Res. 2020;51:116. doi:10.1186/s13567-020-00839-0

Krag, Elinar; Phillips S. Active and Passive Bile Acid Absorption in Man. Perfusion studies of the Ileum and Jejunum. J Clin Invest. 1974;53(6):1686-1694. doi:10.1017/CBO9781107415324.004

Kraus WE, Bhapkar M, Huffman KM, et al. 2 years of calorie restriction and cardiometabolic risk (CALERIE): exploratory outcomes of a multicentre, phase 2, randomised controlled trial. lancet Diabetes Endocrinol. 2019;7(9):673-683. doi:10.1016/S2213-8587(19)30151-2

Kriegel MA, Sefik E, Hill JA, Wu H-J, Benoist C, Mathis D. Naturally transmitted segmented filamentous bacteria segregate with diabetes protection in nonobese diabetic mice. Proc Natl Acad Sci. 2011;108(28):11548 LP - 11553. doi:10.1073/pnas.1108924108

Křížová L, Dadáková K, Kašparovská J, Kašparovský T. Isoflavones. Molecules. 2019;24(6):1076. doi:10.3390/molecules24061076

Lagkouvardos I, Lesker TR, Hitch TCA, et al. Sequence and cultivation study of Muribaculaceae reveals novel species, host preference, and functional potential of this yet undescribed family. Microbiome. 2019;7(1):28. doi:10.1186/s40168-019-0637-2

Langille MGI, Meehan CJ, Koenig JE, et al. Microbial shifts in the aging mouse gut. Microbiome. 2014;2(1):50. doi:10.1186/s40168-014-0050-9

Laukens D, Brinkman BM, Raes J, De Vos M, Vandenabeele P. Heterogeneity of the gut microbiome in mice: guidelines for optimizing experimental design. FEMS Microbiol Rev. 2016;40(1):117-132. doi:10.1093/femsre/fuv036

Lawrence MA, Baker PI. Ultra-processed food and adverse health outcomes. BMJ. 2019;365:l2289. doi:10.1136/bmj.l2289

Lee C, Franke KB, Kamal SM, et al. Stand-alone ClpG disaggregase confers superior heat tolerance to bacteria. Proc Natl Acad Sci. 2018;115(2):E273 LP-E282. doi:10.1073/pnas.1712051115

Lee H-J, Cha J-Y. Recent insights into the role of ChREBP in intestinal fructose absorption and metabolism. BMB Rep. 2018;51(9):429-436. doi:10.5483/BMBRep.2018.51.9.197

Letexier D, Diraison F, Beylot M. Addition of inulin to a moderately high-carbohydrate diet reduces hepatic lipogenesis and plasma triacylglycerol

concentrations in humans. Am J Clin Nutr. 2003;77(3):559-564. doi:10.1093/ajcn/77.3.559

Li-Hawkins J, Gåfvels M, Olin M, et al. Cholic acid mediates negative feedback regulation of bile acid synthesis in mice. J Clin Invest. 2002;110(8):1191-1200. doi:10.1172/JCI16309

Loomba R, Seguritan V, Li W, et al. Gut Microbiome-Based Metagenomic Signature for Non-invasive Detection of Advanced Fibrosis in Human Nonalcoholic Fatty Liver Disease. Cell Metab. 2017;25(5):1054-1062.e5. doi:10.1016/j.cmet.2017.04.001

López-Collazo E, del Fresno C. Pathophysiology of endotoxin tolerance: mechanisms and clinical consequences. Crit Care. 2013;17(6):242. doi:10.1186/cc13110

Lozupone CA, Stombaugh JI, Gordon JI, Jansson JK, Knight R. Diversity, stability and resilience of the human gut microbiota. Nature. 2012;489(7415):220-230. doi:10.1038/nature11550

Ludwig DS, Hu FB, Tappy L, Brand-Miller J. Dietary carbohydrates: role of quality and quantity in chronic disease. BMJ. 2018;361:k2340. doi:10.1136/bmj.k2340

Luther J, Garber JJ, Khalili H, et al. Hepatic Injury in Nonalcoholic Steatohepatitis Contributes to Altered Intestinal Permeability. Cell Mol Gastroenterol Hepatol. 2015;1(2):222-232. doi:10.1016/j.jcmgh.2015.01.001

Lycke NY, Bemark M. The regulation of gut mucosal IgA B-cell responses: recent developments. Mucosal Immunol. 2017;10(6):1361-1374. doi:10.1038/mi.2017.62

Ma J, Hong Y, Zheng N, et al. Gut microbiota remodeling reverses aging-associated inflammation and dysregulation of systemic bile acid homeostasis in mice sex-specifically. Gut Microbes. 2020;11(5):1450-1474. doi:10.1080/19490976.2020.1763770

Macdonald IA. A review of recent evidence relating to sugars, insulin resistance and diabetes. Eur J Nutr. 2016;55(2):17-23. doi:10.1007/s00394-016-1340-8

Maekawa R, Seino Y, Ogata H, et al. Chronic high-sucrose diet increases fibroblast growth factor 21 production and energy expenditure in mice. J Nutr Biochem. 2017;49:71-79. doi:https://doi.org/10.1016/j.jnutbio.2017.07.010

Magill SS, Edwards JR, Bamberg W, et al. Multistate Point-Prevalence Survey of Health Care–Associated Infections. N Engl J Med. 2014;370(13):1198-1208. doi:10.1056/NEJMoa1306801

Mair W, Dillin A. Aging and Survival: The Genetics of Life Span Extension by Dietary Restriction. Annu Rev Biochem. 2008;77(1):727-754. doi:10.1146/annurev.biochem.77.061206.171059

Makki K, Deehan EC, Walter J, Bäckhed F. The Impact of Dietary Fiber on Gut Microbiota in Host Health and Disease. Cell Host Microbe. 2018;23(6):705-715. doi:10.1016/j.chom.2018.05.012

Mandal RK, Denny JE, Waide ML, et al. Temporospatial shifts within commercial laboratory mouse gut microbiota impact experimental reproducibility. BMC Biol. 2020;18(1):83. doi:10.1186/s12915-020-00810-7

Martinez KB, Leone V, Chang EB. Western diets, gut dysbiosis, and metabolic diseases: Are they linked? Gut Microbes. 2017;8(2):130-142. doi:10.1080/19490976.2016.1270811

Matt SM, Allen JM, Lawson MA, Mailing LJ, Woods JA, Johnson RW. Butyrate and Dietary Soluble Fiber Improve Neuroinflammation Associated With Aging in Mice . Front Immunol . 2018;9:1832. https://www.frontiersin.org/article/10.3389/fimmu.2018.01832

Melo-Gonzalez F, Kammoun H, Evren E, et al. Antigen-presenting ILC3 regulate T cell-dependent IgA responses to colonic mucosal bacteria. J Exp Med. 2019;216(4):728-742. doi:10.1084/jem.20180871

Merino B, Fernández-Díaz CM, Cózar-Castellano I, Perdomo G. Intestinal Fructose and Glucose Metabolism in Health and Disease. Nutr . 2020;12(1). doi:10.3390/nu12010094

Meydani SN, Das SK, Pieper CF, et al. Long-term moderate calorie restriction inhibits inflammation without impairing cell-mediated immunity: a randomized controlled trial in non-obese humans. Aging (Albany NY). 2016;8(7):1416-1431. doi:10.18632/aging.100994

Mihaylova MM, Sabatini DM, Yilmaz ÖH. Dietary and metabolic control of stem cell function in physiology and cancer. Cell Stem Cell. 2014;14(3):292-305. doi:10.1016/j.stem.2014.02.008

Moen B, Henjum K, Måge I, et al. Effect of Dietary Fibers on Cecal Microbiota and Intestinal Tumorigenesis in Azoxymethane Treated A/J Min/+ Mice. PLoS One. 2016;11(5):e0155402-e0155402. doi:10.1371/journal.pone.0155402

Molinaro A, Wahlström A, Marschall H-U. Role of Bile Acids in Metabolic Control. Trends Endocrinol Metab. 2018;29(1):31-41. doi:10.1016/j.tem.2017.11.002

Monteiro CA, Cannon G, Levy RB, et al. Ultra-processed foods: what they are and how to identify them. Public Health Nutr. 2019;22(5):936-941. doi:10.1017/S1368980018003762

Montonye DR, Ericsson AC, Busi SB, Lutz C, Wardwell K, Franklin CL. Acclimation and Institutionalization of the Mouse Microbiota Following Transportation. Front Microbiol. 2018;9:1085. doi:10.3389/fmicb.2018.01085

Most J, Redman LM. Impact of calorie restriction on energy metabolism in humans. Exp Gerontol. 2020;133:110875. doi:https://doi.org/10.1016/j.exger.2020.110875

Most J, Tosti V, Redman LM, Fontana L. Calorie restriction in humans: An update. Ageing Res Rev. 2017;39:36-45. doi:10.1016/j.arr.2016.08.005

Müller M, Canfora EE, Blaak EE. Gastrointestinal Transit Time, Glucose Homeostasis and Metabolic Health: Modulation by Dietary Fibers. Nutrients. 2018;10(3):275. doi:10.3390/nu10030275

Nalapareddy K, Nattamai KJ, Kumar RS, et al. Canonical Wnt Signaling Ameliorates Aging of Intestinal Stem Cells. Cell Rep. 2017;18(11):2608-2621. doi:10.1016/j.celrep.2017.02.056

Neuschwander-Tetri BA, Ford DA, Acharya S, et al. Dietary trans-fatty acid induced NASH is normalized following loss of trans-fatty acids from hepatic lipid pools. Lipids. 2012;47(10):941-950. doi:10.1007/s11745-012-3709-7

Neyrinck AM, Pachikian B, Taminiau B, et al. Intestinal Sucrase as a Novel Target Contributing to the Regulation of Glycemia by Prebiotics. PLoS One. 2016;11(8):e0160488. https://doi.org/10.1371/journal.pone.0160488

Ng KM, Aranda-Díaz A, Tropini C, et al. Recovery of the Gut Microbiota after Antibiotics Depends on Host Diet, Community Context, and Environmental Reservoirs. Cell Host Microbe. 2019;26(5):650-665.e4. doi:10.1016/j.chom.2019.10.011

O'Keefe JH, DiNicolantonio JJ, Sigurdsson AF, Ros E. Evidence, Not Evangelism, for Dietary Recommendations. Mayo Clin Proc. 2018;93(2):138-144. doi:10.1016/j.mayocp.2017.12.001

Odenwald MA, Turner JR. The intestinal epithelial barrier: a therapeutic target? Nat Rev Gastroenterol Hepatol. 2017;14(1):9-21. doi:10.1038/nrgastro.2016.169

Ortega-González M, Ocón B, Romero-Calvo I, et al. Nondigestible oligosaccharides exert nonprebiotic effects on intestinal epithelial cells enhancing the immune response via activation of TLR4-NFκB. Mol Nutr & food Res. 2014;58(2):384—393. doi:10.1002/mnfr.201300296

Palm NW, de Zoete MR, Cullen TW, et al. Immunoglobulin A coating identifies colitogenic bacteria in inflammatory bowel disease. Cell. 2014;158(5):1000-1010. doi:10.1016/j.cell.2014.08.006

Pan H, Finkel T. Key proteins and pathways that regulate lifespan. J Biol Chem. 2017;292(16):6452-6460. doi:10.1074/jbc.R116.771915

Parks EJ, Skokan LE, Timlin MT, Dingfelder CS. Dietary sugars stimulate fatty acid synthesis in adults. J Nutr. 2008;138(6):1039-1046. doi:10.1093/jn/138.6.1039

Pearce SC, Coia HG, Karl JP, Pantoja-Feliciano IG, Zachos NC, Racicot K. Intestinal in vitro and ex vivo Models to Study Host-Microbiome Interactions and Acute Stressors. Front Physiol. 2018;9:1584. doi:10.3389/fphys.2018.01584

Pellizzon MA, Ricci MR. The common use of improper control diets in diet-induced metabolic disease research confounds data interpretation: the fiber factor. Nutr Metab (Lond). 2018;15(1):3. doi:10.1186/s12986-018-0243-5

Peña-Villalobos I, Casanova-Maldonado I, Lois P, Sabat P, Palma V. Adaptive Physiological and Morphological Adjustments Mediated by Intestinal Stem Cells in Response to Food Availability in Mice. Front Physiol. 2019;9:1821. doi:10.3389/fphys.2018.01821

Phillips ML. Gut reaction: environmental effects on the human microbiota. Environ Health Perspect. 2009;117(5):A198-A205. doi:10.1289/ehp.117-a198

Poceviciute R, Ismagilov RF. Human-gut-microbiome on a chip. Nat Biomed Eng. 2019;3(7):500-501. doi:10.1038/s41551-019-0425-0

Postal BG, Ghezzal S, Aguanno D, et al. AhR activation defends gut barrier integrity against damage occurring in obesity. Mol Metab. 2020;39:101007. doi:10.1016/j.molmet.2020.101007

Potthoff MJ, Boney-Montoya J, Choi M, et al. FGF15/19 regulates hepatic glucose metabolism by inhibiting the CREB-PGC-1α pathway. Cell Metab. 2011;13(6):729-738. doi:10.1016/j.cmet.2011.03.019

Prokopidis K, Cervo MM, Gandham A, Scott D. Impact of Protein Intake in Older Adults with Sarcopenia and Obesity: A Gut Microbiota Perspective. Nutrients. 2020;12(8). doi:10.3390/nu12082285

Pyclik M, Srutkova D, Schwarzer M, Górska S. Bifidobacteria cell wall-derived exo-polysaccharides, lipoteichoic acids, peptidoglycans, polar lipids and proteins – their chemical structure and biological attributes. Int J Biol Macromol. 2020;147:333-349. doi:https://doi.org/10.1016/j.ijbiomac.2019.12.227

Qin J, Li Y, Cai Z, et al. A metagenome-wide association study of gut microbiota in type 2 diabetes. Nature. 2012;490(7418):55-60. doi:10.1038/nature11450

Qu B, Halliwell B, Ong CN, Lee BL, Li QT. Caloric restriction prevents oxidative damage induced by the carcinogen clofibrate in mouse liver. FEBS Lett. 2000;473(1):85-88. doi:10.1016/s0014-5793(00)01506-4

Quesada-Vázquez S, Aragonès G, Del Bas JM, Escoté X. Diet, Gut Microbiota and Non-Alcoholic Fatty Liver Disease: Three Parts of the Same Axis. Cells. 2020;9(1):176. doi:10.3390/cells9010176

Raduolovic K, Mak'Anyengo R, Kaya B, Steinert A, Niess JH. Injections of Lipopolysaccharide into Mice to Mimic Entrance of Microbial-derived Products After Intestinal Barrier Breach. J Vis Exp. 2018;(135):57610. doi:10.3791/57610

Rajman L, Chwalek K, Sinclair DA. Therapeutic Potential of NAD-Boosting Molecules: The In Vivo Evidence. Cell Metab. 2018;27(3):529-547. doi:10.1016/j.cmet.2018.02.011

Rampelli S, Soverini M, Turroni S, et al. ViromeScan: a new tool for metagenomic viral community profiling. BMC Genomics. 2016;17(1):165. doi:10.1186/s12864-016-2446-3

Rao M, Sadaphule P, Khembete M, Lunawat H, Thanki K, Gabhe N. Characterization of Psyllium (Plantago ovata) Polysaccharide and its Use as a Binder in Tablets. Indian J Pharm Educ Res. 2013;47:154-159.

Rasmussen TS, de Vries L, Kot W, et al. Mouse Vendor Influence on the Bacterial and Viral Gut Composition Exceeds the Effect of Diet. Viruses. 2019;11(5). doi:10.3390/v11050435

Reynolds A, Mann J, Cummings J, Winter N, Mete E, Te Morenga L. Carbohydrate quality and human health: a series of systematic reviews and meta-analyses. Lancet (London, England). 2019;393(10170):434-445. doi:10.1016/S0140-6736(18)31809-9

Rico-Campà A, Martínez-González MA, Alvarez-Alvarez I, et al. Association between consumption of ultra-processed foods and all cause mortality: SUN prospective cohort study. BMJ. 2019;365:l1949. doi:10.1136/bmj.l1949

Romero-Gómez M, Zelber-Sagi S, Trenell M. Treatment of NAFLD with diet, physical activity and exercise. J Hepatol. 2017;67(4):829-846. doi:10.1016/j.jhep.2017.05.016

Roychowdhury S, Selvakumar PC, Cresci GAM. The Role of the Gut Microbiome in Nonalcoholic Fatty Liver Disease. Med Sci (Basel, Switzerland). 2018;6(2). doi:10.3390/medsci6020047

Rubert J, Schweiger PJ, Mattivi F, Tuohy K, Jensen KB, Lunardi A. Intestinal Organoids: A Tool for Modelling Diet–Microbiome–Host Interactions. Trends Endocrinol Metab. Published online July 20, 2020. doi:10.1016/j.tem.2020.02.004

Rui L. Energy Metabolism in the Liver. Compr Physiol. Published online January 10, 2014:177-197. doi:doi:10.1002/cphy.c130024

Rusli F, Deelen J, Andriyani E, et al. Fibroblast growth factor 21 reflects liver fat accumulation and dysregulation of signalling pathways in the liver of C57BL/6J mice. Sci Rep. 2016;6(1):30484. doi:10.1038/srep30484

Rusli F, Lute C, Boekschoten M V, et al. Intermittent calorie restriction largely counteracts the adverse health effects of a moderate-fat diet in aging C57BL/6J mice. Mol Nutr Food Res. 2017;61(5):1600677. doi:10.1002/mnfr.201600677

Russo M, Fabersani E, Abeijón-Mukdsi MC, et al. Lactobacillus fermentum CRL1446 Ameliorates Oxidative and Metabolic Parameters by Increasing Intestinal Feruloyl Esterase Activity and Modulating Microbiota in Caloric-Restricted Mice. Nutrients. 2016;8(7). doi:10.3390/nu8070415

Sadler R, Singh V, Benakis C, et al. Microbiota differences between commercial breeders impacts the post-stroke immune response. Brain Behav Immun. 2017;66:23-30. doi:10.1016/j.bbi.2017.03.011

Salazar N, Dewulf EM, Neyrinck AM, et al. Inulin-type fructans modulate intestinal Bifidobacterium species populations and decrease fecal short-chain fatty acids in obese women. Clin Nutr. 2015;34(3):501-507. doi:10.1016/j.clnu.2014.06.001

Santos-Marcos JA, Perez-Jimenez F, Camargo A. The role of diet and intestinal microbiota in the development of metabolic syndrome. J Nutr Biochem. 2019;70:1-27. doi:https://doi.org/10.1016/j.jnutbio.2019.03.017

Schanz O, Chijiiwa R, Cengiz SC, et al. Dietary AhR Ligands Regulate AhRR Expression in Intestinal Immune Cells and Intestinal Microbiota Composition. Int J Mol Sci. 2020;21(9). doi:10.3390/ijms21093189

Schnabel L, Buscail C, Sabate J-M, et al. Association Between Ultra-Processed Food Consumption and Functional Gastrointestinal Disorders: Results From the French NutriNet-Santé Cohort. Am J Gastroenterol. 2018;113(8):1217-1228. doi:10.1038/s41395-018-0137-1

Seemann S, Zohles F, Lupp A. Comprehensive comparison of three different animal models for systemic inflammation. J Biomed Sci. 2017;24(1):60. doi:10.1186/s12929-017-0370-8

Seksik P, Landman C. Understanding Microbiome Data: A Primer for Clinicians. Dig Dis. 2015;33(suppl 1(Suppl. 1):11-16. doi:10.1159/000437034

Shan M, Gentile M, Yeiser JR, et al. Mucus enhances gut homeostasis and oral tolerance by delivering immunoregulatory signals. Science. 2013;342(6157):447-453. doi:10.1126/science.1237910

Shtriker MG, Peri I, Taieb E, Nyska A, Tirosh O, Madar Z. Galactomannan More than Pectin Exacerbates Liver Injury in Mice Fed with High-Fat, High-Cholesterol Diet. Mol Nutr Food Res. 2018;62(20):e1800331. doi:10.1002/mnfr.201800331

Singh V, Vijay-Kumar M. Beneficial and detrimental effects of processed dietary fibers on intestinal and liver health: health benefits of refined dietary fibers need to be redefined! Gastroenterol Rep. 2020;8(2):85-89. doi:10.1093/gastro/goz072

Singh V, Yeoh BS, Walker RE, et al. Microbiota fermentation-NLRP3 axis shapes the impact of dietary fibres on intestinal inflammation. Gut. 2019;68(10):1801 LP - 1812. doi:10.1136/gutjnl-2018-316250

Smith AJ, Clutton RE, Lilley E, Hansen KEA, Brattelid T. PREPARE: guidelines for planning animal research and testing. Lab Anim. 2017;52(2):135-141. doi:10.1177/0023677217724823

Soliman GA. Dietary Fiber, Atherosclerosis, and Cardiovascular Disease. Nutrients. 2019;11(5). doi:10.3390/nu11051155

Sonnenburg ED, Smits SA, Tikhonov M, Higginbottom SK, Wingreen NS, Sonnenburg JL. Diet-induced extinctions in the gut microbiota compound over generations. Nature. 2016;529(7585):212-215. doi:10.1038/nature16504

Spencer J, Sollid LM. The human intestinal B-cell response. Mucosal Immunol. 2016;9(5):1113-1124. doi:10.1038/mi.2016.59

Stephen AM, Champ MM-J, Cloran SJ, et al. Dietary fibre in Europe: current state of knowledge on definitions, sources, recommendations, intakes and relationships to health. Nutr Res Rev. 2017;30(2):149-190. doi:DOI: 10.1017/S095442241700004X

Suga T, Yamaguchi H, Sato T, Maekawa M, Goto J, Mano N. Preference of Conjugated Bile Acids over Unconjugated Bile Acids as Substrates for OATP1B1 and OATP1B3. PLoS One. 2017;12(1):e0169719-e0169719. doi:10.1371/journal.pone.0169719

Suh H-J, Yang H-S, Ra K-S, et al. Peyer's patch-mediated intestinal immune system modulating activity of pectic-type polysaccharide from peel of Citrus unshiu. Food Chem. 2013;138(2-3):1079-1086. doi:10.1016/j.foodchem.2012.11.091

Sun J, Buys N. Effects of probiotics consumption on lowering lipids and CVD risk factors: a systematic review and meta-analysis of randomized controlled trials. Ann Med. 2015;47(6):430-440. doi:10.3109/07853890.2015.1071872

Svinka J, Pflügler S, Mair M, et al. Epidermal growth factor signaling protects from cholestatic liver injury and fibrosis. J Mol Med (Berl). 2017;95(1):109-117. doi:10.1007/s00109-016-1462-8

Tatsumi K, Ohashi K, Taminishi S, Okano T, Yoshioka A, Shima M. Reference gene selection for real-time RT-PCR in regenerating mouse livers. Biochem Biophys Res Commun. 2008;374(1):106-110. doi:10.1016/j.bbrc.2008.06.103

Tennoune N, Chan P, Breton J, et al. Bacterial ClpB heat-shock protein, an antigen-mimetic of the anorexigenic peptide α-MSH, at the origin of eating disorders. Transl Psychiatry. 2014;4(10):e458-e458. doi:10.1038/tp.2014.98

Thaiss CA, Levy M, Grosheva I, et al. Hyperglycemia drives intestinal barrier dysfunction and risk for enteric infection. Science (80-). 2018;359(6382):1376 LP - 1383. doi:10.1126/science.aar3318

Thaiss CA, Levy M, Korem T, et al. Microbiota Diurnal Rhythmicity Programs Host Transcriptome Oscillations. Cell. 2016;167(6):1495-1510.e12. doi:10.1016/j.cell.2016.11.003

Ticho AL, Malhotra P, Dudeja PK, Gill RK, Alrefai WA. Intestinal Absorption of Bile Acids in Health and Disease. Compr Physiol. 2019;10(1):21—56. doi:10.1002/cphy.c190007

Tilg H, Zmora N, Adolph TE, Elinav E. The intestinal microbiota fuelling metabolic inflammation. Nat Rev Immunol. 2020;20(1):40-54. doi:10.1038/s41577-019-0198-4

Tiwari UP, Fleming SA, Abdul Rasheed MS, Jha R, Dilger RN. The role of oligosaccharides and polysaccharides of xylan and mannan in gut health of monogastric animals. J Nutr Sci. 2020;9:e21-e21. doi:10.1017/jns.2020.14

Tobin V, Le Gall M, Fioramonti X, et al. Insulin Internalizes GLUT2 in the Enterocytes of Healthy but Not Insulin-Resistant Mice. Diabetes. 2008;57(3):555 LP - 562. doi:10.2337/db07-0928

Todoric J, Di Caro G, Reibe S, et al. Fructose stimulated de novo lipogenesis is promoted by inflammation. Nat Metab. 2020;2(10):1034-1045. doi:10.1038/s42255-020-0261-2

Tran TTT, Corsini S, Kellingray L, et al. APOE genotype influences the gut microbiome structure and function in humans and mice: relevance for Alzheimer's disease pathophysiology. FASEB J. 2019;33(7):8221-8231. doi:10.1096/fj.201900071R

Tremblay S, Côté NML, Grenier G, et al. Ileal antimicrobial peptide expression is dysregulated in old age. Immun Ageing. 2017;14:19. doi:10.1186/s12979-017-0101-8

Van der Sluis M, De Koning BAE, De Bruijn ACJM, et al. Muc2-Deficient Mice Spontaneously Develop Colitis, Indicating That MUC2 Is Critical for Colonic Protection. Gastroenterology. 2006;131(1):117-129. doi:10.1053/j.gastro.2006.04.020

Vancamelbeke M, Vermeire S. The intestinal barrier: a fundamental role in health and disease. Expert Rev Gastroenterol Hepatol. 2017;11(9):821-834. doi:10.1080/17474124.2017.1343143

Varholick JA, Pontiggia A, Murphy E, et al. Social dominance hierarchy type and rank contribute to phenotypic variation within cages of laboratory mice. Sci Rep. 2019;9(1):13650. doi:10.1038/s41598-019-49612-0

Velazquez EM, Nguyen H, Heasley KT, et al. Endogenous Enterobacteriaceae underlie variation in susceptibility to Salmonella infection. Nat Microbiol. 2019;4(6):1057-1064. doi:10.1038/s41564-019-0407-8

Vogt LM, Sahasrabudhe NM, Ramasamy U, et al. The impact of lemon pectin characteristics on TLR activation and T84 intestinal epithelial cell barrier function. J Funct Foods. 2016;22:398-407. doi:https://doi.org/10.1016/j.jff.2016.02.002

Wagner BD, Grunwald GK, Zerbe GO, et al. On the Use of Diversity Measures in Longitudinal Sequencing Studies of Microbial Communities . Front Microbiol . 2018;9:1037. https://www.frontiersin.org/article/10.3389/fmicb.2018.01037

Wang F, Wang J, Liu D, Su Y. Normalizing genes for real-time polymerase chain reaction in epithelial and nonepithelial cells of mouse small intestine. Anal Biochem. 2010;399(2):211-217. doi:10.1016/j.ab.2009.12.029

Wang G, Huang S, Cai S, et al. Lactobacillus reuteri Ameliorates Intestinal Inflammation and Modulates Gut Microbiota and Metabolic Disorders in Dextran Sulfate Sodium-Induced Colitis in Mice. Nutrients. 2020;12(8). doi:10.3390/nu12082298

Wang Z, Litterio MC, Müller M, Vauzour D, Oteiza PI. (-)-Epicatechin and NADPH oxidase inhibitors prevent bile acid-induced Caco-2 monolayer permeabilization through ERK1/2 modulation. Redox Biol. 2020;28:101360. doi:https://doi.org/10.1016/j.redox.2019.101360

Warden CH, Fisler JS. Comparisons of diets used in animal models of high-fat feeding. Cell Metab. 2008;7(4):277. doi:10.1016/j.cmet.2008.03.014

Wong SK, Chin K-Y, Suhaimi FH, Fairus A, Ima-Nirwana S. Animal models of metabolic syndrome: a review. Nutr Metab (Lond). 2016;13(1):65. doi:10.1186/s12986-016-0123-9

Woting A, Blaut M. Small Intestinal Permeability and Gut-Transit Time Determined with Low and High Molecular Weight Fluorescein Isothiocyanate-Dextrans in C3H Mice. Nutrients. 2018;10(6):685. doi:10.3390/nu10060685

Wu RY, Määttänen P, Napper S, et al. Non-digestible oligosaccharides directly regulate host kinome to modulate host inflammatory responses without alterations in the gut microbiota. Microbiome. 2017;5(1):135. doi:10.1186/s40168-017-0357-4

Xu M, Cen M, Shen Y, et al. Deoxycholic Acid-Induced Gut Dysbiosis Disrupts Bile Acid Enterohepatic Circulation and Promotes Intestinal Inflammation. Dig Dis Sci. Published online March 2020. doi:10.1007/s10620-020-06208-3

Yamamuro D, Takahashi M, Nagashima S, et al. Peripheral circadian rhythms in the liver and white adipose tissue of mice are attenuated by constant light and restored by time-restricted feeding. PLoS One. 2020;15(6):e0234439. https://doi.org/10.1371/journal.pone.0234439

Yasser, Alexakis C, Mendall M. Determinants of Weight Loss prior to Diagnosis in Inflammatory Bowel Disease: A Retrospective Observational Study. Gastroenterol Res Pract. 2014;2014:762191. doi:10.1155/2014/762191

Yilmaz ÖH, Katajisto P, Lamming DW, et al. mTORC1 in the Paneth cell niche couples intestinal stem-cell function to calorie intake. Nature. 2012;486(7404):490-495. doi:10.1038/nature11163

Yu C, Wang F, Kan M, et al. Elevated cholesterol metabolism and bile acid synthesis in mice lacking membrane tyrosine kinase receptor FGFR4. J Biol Chem. 2000;275(20):15482-15489. doi:10.1074/jbc.275.20.15482

Zhang C, Li S, Yang L, et al. Structural modulation of gut microbiota in life-long calorie-restricted mice. Nat Commun. 2013;4(1):2163. doi:10.1038/ncomms3163

Zhang D, Tong X, VanDommelen K, et al. Lipogenic transcription factor ChREBP mediates fructose-induced metabolic adaptations to prevent hepatotoxicity. J Clin Invest. 2017;127(7):2855-2867. doi:10.1172/JCI89934

Zhang J, Wen C, Zhang H, Duan Y. Review of isolation, structural properties, chain conformation, and bioactivities of psyllium polysaccharides. Int J Biol Macromol. 2019;139:409-420. doi:https://doi.org/10.1016/j.ijbiomac.2019.08.014

Zhang Q, Yu H, Xiao X, Hu L, Xin F, Yu X. Inulin-type fructan improves diabetic phenotype and gut microbiota profiles in rats. PeerJ. 2018;6:e4446-e4446. doi:10.7717/peerj.4446

Zhang Y, Dong A, Xie K, Yu Y. Dietary Supplementation With High Fiber Alleviates Oxidative Stress and Inflammatory Responses Caused by Severe Sepsis in Mice Without Altering Microbiome Diversity. Front Physiol. 2019;9:1929. https://www.frontiersin.org/article/10.3389/fphys.2018.01929

Zhao S, Jang C, Liu J, et al. Dietary fructose feeds hepatic lipogenesis via microbiota-derived acetate. Nature. 2020;579(7800):586-591. doi:10.1038/s41586-020-2101-7

Zhao Y, Feng Y, Liu M, et al. Single-cell RNA sequencing analysis reveals alginate oligosaccharides preventing chemotherapy-induced mucositis. Mucosal Immunol. 2020;13(3):437-448. doi:10.1038/s41385-019-0248-z

Zhao Y, Tian G, Chen D, et al. Dietary protein levels and amino acid supplementation patterns alter the composition and functions of colonic microbiota in pigs. Anim Nutr (Zhongguo xu mu shou yi xue hui). 2020;6(2):143-151. doi:10.1016/j.aninu.2020.02.005

Zheng X, Wang S, Jia W. Calorie restriction and its impact on gut microbial composition and global metabolism. Front Med. 2018;12(6):634-644. doi:10.1007/s11684-018-0670-8

Zheng Y, Scow JS, Duenes JA, Sarr MG. Mechanisms of glucose uptake in intestinal cell lines: role of GLUT2. Surgery. 2012;151(1):13-25. doi:10.1016/j.surg.2011.07.010

Zhou G, Soufan O, Ewald J, Hancock REW, Basu N, Xia J. NetworkAnalyst 3.0: a visual analytics platform for comprehensive gene expression profiling and meta-analysis. Nucleic Acids Res. 2019;47(W1):W234-W241. doi:10.1093/nar/gkz240

Zinöcker MK, Lindseth IA. The Western Diet-Microbiome-Host Interaction and Its Role in Metabolic Disease. Nutrients. 2018;10(3):365. doi:10.3390/nu10030365

Zmora N, Suez J, Elinav E. You are what you eat: diet, health and the gut microbiota. Nat Rev Gastroenterol Hepatol. 2019;16(1):35-56. doi:10.1038/s41575-018-0061-2

Supplementary data 1

Supplementary Table 1.1 Composition of LF diet (D17060802) and LFCR (D17060803).

Product #		D17060802		D17060803	
%	**gm**	*kcal*	**gm**	*kcal*
Protein	19.2	20	18.8	20
Carbohydrate	67.3	70.0	66.2	70.1
Fat	4	10	4	10
Total		100		100
kcal/gm	3.85		3.77	
Ingredient	**gm**	***kcal***	**gm**	***kcal***
Casein, 80 Mesh	200	*800*	200	*800*
L-Cystine	3	*12*	3	*12*
Corn Starch	452.2	*1809*	452.2	*1809*
Maltodextrin 10	75	*300*	75	*300*
Sucrose	172.8	*691*	172.8	*691*
Cellulose, BW200	50	*0*	50	*0*
Soybean Oil	25	*225*	25	*225*
Lard	0	*0*	0	*0*
Palm Oil	20	*180*	20	*180*
Mineral Mix S10026	10	*0*	14.3	*0*
DiCalcium Phosphate	13	*0*	18.6	*0*
Calcium Carbonate	5.5	*0*	7.9	*0*
Potassium Citrate, 1 H2O	16.5	*0*	23.6	*0*
Vitamin Mix V10001	10	*40*	14.3	*57*
Choline Bitartrate	2	*0*	2.9	*0*
FD&C Yellow Dye #5	0.05	*0*	0	*0*
FD&C Red Dye #40	0	*0*	0.05	*0*
FD&C Blue Dye #1	0	*0*	0	*0*
Total	**1055.05**	***4057***	**1079.56**	***4074***

Supplementary Table 1.2 Composition of LS (LF Low sucrose, D12450J), LS+Inulin (D18012101), LS+Inulin, pectin and psyllium (Comb: D19051003) diets.

D12450J, D18012101, D19051001 - 03

Rodent Diet with 10 kcal% Fat with 50 g Cellulose or
Same with 75 g Added Soluble Fibers

Product #	D12450J		D18012101		D19051001		D19051002		D19051003	
	10 kcal% Fat		Modified w/		Modified w/		Modified w/		Modified w/	
	50 g Cellulose		50 Cell/75 Inulin		50 Cell/75 Psyllium		50 Cell/ 37.5 Inulin/		50 Cell/25 Inulin/	
							37.5 Psyllium		25 Psyllium/25 Pectin	
	gm%	kcal%	gm%	kcal%	gm%	kcal%	gm%	kcal%	gm%	kcal%
Protein	19	20	18	20	18	20	18	20	18	20
Carbohydrate	67	70	62	70	62	68	62	69	62	68
Fat	4	10	4	10	4	10	4	10	4	10
Total		100		100		100		100		100
kcal/gm	3.85		3.68		3.65		3.67		3.67	
Ingredient	gm	kcal	gm	kcal	gm	kcal	gm	kcal	gm	kcal
Casein	200	800	200	800	200	800	200	800	200	800
L-Cystine	3	12	3	12	3	12	3	12	3	12
Corn Starch	506.2	2024.8	478	1912	487.5	1950	482.8	1931	481.3	1925
Maltodextrin 10	125	500	125	500	125	500	125	500	125	500
Sucrose	68.8	275	68.8	275	68.8	275	68.8	275	68.8	275
Cellulose, BW200	50	0	50	0	50	0	50	0	50	0
Inulin, Orafti HP	0	0	75	113	0	0	37.5	56	25	38
Psyllium	0	0	0	0	75	75	37.5	38	25	25
Pectin, Tic Gums 1400	0	0	0	0	0	0	0	0	25	38
Lard	20	180	20	180	20	180	20	180	20	180
Soybean Oil	25	225	25	225	25	225	25	225	25	225
Mineral Mix S10026	10	0	10	0	10	0	10	0	10	0
Dicalcium Phosphate	13	0	13	0	13	0	13	0	13	0
Calcium Carbonate	5.5	0	5.5	0	5.5	0	5.5	0	5.5	0
Potassium Citrate, 1 H2O	16.5	0	16.5	0	16.5	0	16.5	0	16.5	0
Vitamin Mix V10001	10	40	10	40	10	40	10	40	10	40
Choline Bitartrate	2	0	2	0	2	0	2	0	2	0
Yellow Dye #5, FD&C	0.04	0	0.025	0	0	0	0	0	0	0
Red Dye #40, FD&C	0	0	0.025	0	0	0	0	0	0	0
Blue Dye #1, FD&C	0.01	0	0	0	0	0	0	0	0	0
Total	1055.05	4057	1101.85	4057	1111.30	4057	1106.60	4057	1105.10	4057
gm										
Total Fiber	50.0		125.0		125.0		125.0		125.0	
Insoluble Fiber	50.0		50.0		103.6		76.8		67.9	
Soluble Fiber	0.0		75.0		16.5		45.8		55.5	
gm%										
Total Fiber	4.7		11.3		11.2		11.3		11.3	
Insoluble Fiber	4.7		4.5		9.3		6.9		6.1	
Soluble Fiber	0.0		6.8		1.5		4.1		5.0	
mg (considering all sources)										
Calcium	6096.1		6097.2		6222.7		6160.0		6145.6	
Phosphorus	4530.8		4527.1		4571.5		4549.3		4543.6	
Potassium	6023.6		6028.8		6713.3		6371.0		6281.4	
Sodium	1056.9		1058.3		1094.0		1076.2		1418.2	
Magnesium	521.7		520.8		543.7		532.2		529.5	
Manganese	59.1		59.1		60.0		59.5		59.4	
Iron	37.0		37.0		48.3		42.6		41.1	
mg (considering fibers only)										
Calcium	8.1		10.6		135.6		73.1		58.8	
Phosphorus	0.0		0.9		43.8		22.4		16.9	
Potassium	0.0		8.0		691.6		349.8		260.3	
Sodium	10.9		14.2		49.3		31.7		373.9	
Magnesium	2.0		2.0		24.5		13.2		10.5	
Manganese	0.1		0.1		1.0		0.5		0.4	
Iron	0.0		0.0		11.3		5.6		4.1	

Calculated Analysis

Rat and Mouse No.3 Breeding (P)

NUTRIENTS		Total	Supp (9)
Proximate Analysis			
Moisture (1)	%	10.00	
Crude Oil	%	4.20	
Crude Protein	%	22.45	
Crude Fibre	%	4.42	
Ash	%	8.05	
Nitrogen Free Extract	%	50.40	
Digestibility Co-Efficients (7)			
Digestible Crude Oil	%	3.81	
Digestible Crude Protein	%	20.18	
Carbohydrates, Fibre and Non Starch Polysaccharides (NSP)			
Total Dietary Fibre	%	16.15	
Pectin	%	1.53	
Hemicellulose	%	9.61	
Cellulose	%	4.13	
Lignin	%	1.54	
Starch	%	33.88	
Sugar	%	4.37	
Energy (5)			
Gross Energy	MJ/kg	15.11	
Digestible Energy (15)	MJ/kg	12.22	
Metabolisable Energy (15)	MJ/kg	11.18	
Atwater Fuel Energy (AFE) (8)	MJ/kg	13.76	
AFE from Oil	%	11.48	
AFE from Protein	%	27.28	
AFE from Carbohydrate	%	61.24	
Fatty Acids			
Saturated Fatty Acids			
C12:0 Lauric	%	0.05	
C14:0 Myristic	%	0.17	
C16:0 Palmitic	%	0.37	
C18:0 Stearic	%	0.11	
Monounsaturated Fatty Acids			
C14:1 Myristoleic	%	0.01	
C16:1 Palmitoleic	%	0.09	
C18:1 Oleic	%	1.01	
Polyunsaturated Fatty Acids			
C18:2(ω6) Linoleic	%	1.26	
C18:3(ω3) Linolenic	%	0.17	
C20:4(ω6) Arachidonic	%	0.12	
C22:5(ω3) Clupanodonic	%		
Amino Acids			

NUTRIENTS		Total	Supp (9)
Glutamic Acid	%	4.39	
Proline	%	1.56	
Serine	%	1.01	
Hydroxyproline	%		
Hydroxylysine	%		
Alanine	%	0.27	
Macro Minerals			
Calcium	%	1.24	1.11
Total Phosphorus	%	0.83	0.28
Phytate Phosphorus	%	0.26	
Available Phosphorus	%	0.56	0.28
Sodium	%	0.24	0.19
Chloride	%	0.36	0.31
Potassium	%	0.81	
Magnesium	%	0.29	0.04
Micro Minerals			
Iron	mg/kg	163.44	82.50
Copper	mg/kg	20.53	8.75
Manganese	mg/kg	102.71	52.70
Zinc	mg/kg	48.67	8.64
Cobalt	µg/kg	604.44	525.00
Iodine	µg/kg	867.77	775.00
Selenium	µg/kg	388.94	200.00
Fluorine	mg/kg	8.67	
Vitamins			
β-Carotene (2)	mg/kg	1.67	
Retinol (2)	µg/kg	6670.95	5812.50
Vitamin A (2)	iu/kg	22213.06	19375.00
Cholecalciferol (3)	µg/kg	73.70	72.50
Vitamin D (3)	iu/kg	2948.01	2900.00
α-Tocopherol (4)	mg/kg	100.90	81.14
Vitamin E (4)	iu/kg	111.02	89.25
Vitamin B₁ (Thiamine)	mg/kg	28.39	19.11
Vitamin B₂ (Riboflavin)	mg/kg	10.28	7.60
Vitamin B₆ (Pyridoxine)	mg/kg	18.87	14.45
Vitamin B₁₂ (Cyanocobalamine)	µg/kg	19.23	17.75
Vitamin C (Ascorbic Acid)	mg/kg	1.33	
Vitamin K (Menadione)	mg/kg	4.14	3.72
Folic Acid (Vitamin B₉)	mg/kg	2.99	0.49
Nicotinic Acid (Vitamin PP) (6)	mg/kg	85.74	19.11
Pantothenic Acid (Vitamin B₃₅)	mg/kg	40.79	23.80
Choline (Vitamin B₄₇)	mg/kg	1422.37	366.60
Inositol	mg/kg	1839.97	
Biotin (Vitamin H) (6)	µg/kg	316.66	

Amino Acids		Total	Supp (9)
Arginine	%	1.42	
Lysine (6)	%	1.34	0.18
Methionine	%	0.37	0.03
Cystine	%	0.35	
Tryptophan	%	0.27	
Histidine	%	0.55	
Threonine	%	0.88	
Isoleucine	%	0.98	
Leucine	%	1.87	
Phenylalanine	%	1.23	
Valine	%	1.15	
Tyrosine	%	0.87	
Taurine	%		
Glycine	%	1.85	
Aspartic Acid	%	1.40	

Notes
1. All values are calculated using a moisture basis of 10%. Typical moisture levels will range between 9.5 - 11.5%.
2. a. Vitamin A includes Retinol and the Retinol equivalents of β-carotene
   b. Retinol includes the Retinol equivalents of β-Carotene.
   c. 0.48 µg Retinol = 1 µg β-carotene = 1.6 iu Vitamin A activity
   d. 1 µg Retinol = 3.33° iu Vitamin A activity
   e. 1 iu Vitamin A = 0.3 µg Retinol = 0.6 µg β-carotene
   f. The standard analysis for Vitamin A does not detect β-carotene
3. 1 µg Cholecalciferol (D₃) = 40.0 iu Vitamin D
4. 1 mg all-rac-α-tocopherol = 1.1 iu Vitamin E activity
   1 mg all-rac-α-tocopherol acetate = 1.0 iu Vitamin E activity
5. 1 MJ = 239.23 Kcalories = 239.23 Calories = 239,330 calories
6. These nutrients coming from natural raw materials such as cereals may have low availabilities due to the interactions with other compounds.
7. Based on in-vitro digestibility analysis.
8. AF Energy = Atwater Fuel Energy = ((CO%/100)*9000)+ ((CP%/100)*4000)+((NFE%/100)*4000)/239.23
9. Supplemented nutrients from manufactured and mined sources.
15. Calculated.

Supplementary data 2

Bile acid (BA) method and conditions

Each sample (5µl) was analysed using an Agilent 1260 binary HPLC couples to an AB sciex 4000 QTrap triple quadrupole mass spectrometer. HPLC was achieved using a binary gradient of solvent A (Water + 5mM Ammonium Ac + 0.012% Formic Acid) and solvent B (Methanol + 5 mM Ammonium Ac + 0.012% Formic Acid) at a constant flow rate of 600µl/min. Separation was made using a Supelco Ascentis Express C18 150 x 4.6, 2.7µm column maintained at 40°C. Injection was made at 50% B and held for 2 min, ramped to 95%B at 20 min and held until 24 minutes. The column equilibrated to initial conditions for 5 minutes. The mass spectrometer was operated in electrospray negative mode with capillary voltage of -4500V at 550°C. Instrument specific gas flow rates were 25ml/min curtain gas, GS1: 40ml/min and GS2: 50ml/min.

BA standards: d4 Internal standards: Each d4 internal standard is prepared at 1 mg/ml in methanol. Prepare 5 solutions of these all at 40µg/ml by taking 400µl of each stock standard to 10ml in 70% methanol.

INT Std #	Int Std(s)
1	d4-GCA + d4 LCA
2	d4-CA
3	d4-CDCA
4	d4-DCA
5	d4-DCA/CDCA/CA/GCA/LCA

Calibration standards

Each BA is prepared at 1mg/ml in methanol and stored refrigerated.

A 10µg mix of the BAs is prepared in 70% methanol by taking 100µl of each individual BA (at 1mg/ml) into a pooled vial and making to 10ml total volume. Make all to total volume of 500µl with methanol.

Std (ng/ml)	Vol (µl)	Of what std	Make up vol (µl) Methanol	Notes
4000	200	10µg/ml mix	300	
2000	100	10µg/ml mix	400	
1000	50	10µg/ml mix	450	Prep x 2
500	25	10µg/ml mix	475	
200	10	10µg/ml mix	490	
100	50	1000ng/ml mix	450	Prep x 2
25	12.5	1000ng/ml mix	487.5	
15	75	100ng/ml mix	425	
10	50	100ng/ml mix	450	
5	25	100ng/ml mix	475	
0	0	-	500	

Then to each of these, add 25µl of d4-Int Std mix #5 (40µg/ml) to give 2000 ng/ml each.

LC-MS

Conditions

Column: Supelco Ascentis Express C18 150 x 4.6, 2.7µm

Flow: 600µl/min

Mobile phase A: Water + 5mM Amm. Ac + 0.012% Formic acid

Mobile Phase B: Methanol + 5mM Amm. Ac + 0.012% Formic acid

Inj: 5µl

Column: 40°C

Mobile phase preparation

In one litre of methanol or Water:

5 mM Ammonium Acetate = 0.385g

0.012% formic acid = 120µl

LC Gradient

Time	%B
0	50
2	50
20	95
24	95
25	50
29	50

Source Conditions (negative mode)

SOURCE	
CUR:	25
TEM:	550
GS1:	40
GS2:	50
ihe:	ON
CAD:	-2
IS:	-4500
EP	-10
CXP	-9

Multiple reaction monitoring (MRM) settings

ID	Q1	Q3	Dwell	DP	CE	RT
LCA	375.3	375.3	20	-90	-10	22.70
CDCA	391.3	391.3	20	-120	-10	20.85
DCA	391.3	391.31	20	-120	-10	21.17
HDCA	391.3	391.32	20	-120	-10	18.29
MCA	391.3	391.33	20	-120	-10	16.57
UDCA	391.3	391.34	20	-120	-10	17.52
a-MCA	407.3	407.3	20	-120	-10	15.93
b-MCA	407.3	407.31	20	-120	-10	16.29
CA	407.3	407.32	20	-120	-10	18.89
GLCA	432.3	432.3	20	-80	-10	19.77
GCDCA	448.3	448.31	20	-80	-10	17.72
GDCA	448.3	448.32	20	-80	-10	18.28
GCA	464.3	464.3	20	-80	-10	15.70
TLCA	482.2	482.2	20	-130	-10	19.19
TCDCA	498.3	498.3	20	-130	-10	17.10
TDCA	498.3	498.31	20	-130	-10	17.64
T-a-MCA	514.3	514.3	20	-130	-10	10.81
T-b-MCA	514.3	514.31	20	-130	-10	11.06
TCA	514.3	514.32	20	-130	-10	15.08
d4-LCA	379.3	379.3	20	-90	-10	22.70
d4-CDCA	395.3	395.31	20	-120	-10	20.83
d4-DCA	395.3	395.3	20	-120	-10	21.13
d4-CA	411.3	411.3	20	-120	-10	18.86
d4-GCA	468.4	74	20	-80	-40	15.71
P lipid query	153	153	20	-130	-10	

Qualifiers

ID	Q1	Q3	Dwell	DP	CE	RT
GLCA	432.3	74	20	-80	-40	20.59
GCDCA	448.3	74.11	20	-80	-40	18.31
GDCA	448.3	74.12	20	-80	-40	18.93
GCA	464.3	74	20	-80	-40	16.03
TCDCA	498.3	80.1	20	-130	-60	17.33
TDCA	498.3	80.11	20	-130	-60	17.87
T-a-MCA	514.3	80.1	20	-130	-60	10.68
T-b-MCA	514.3	80.11	20	-130	-60	11.02
TCA	514.3	80.12	20	-130	-60	15.12
TLCA	482.2	80	20	-130	-60	19.57

QTrap method file: **Bile salts (MP).dam**
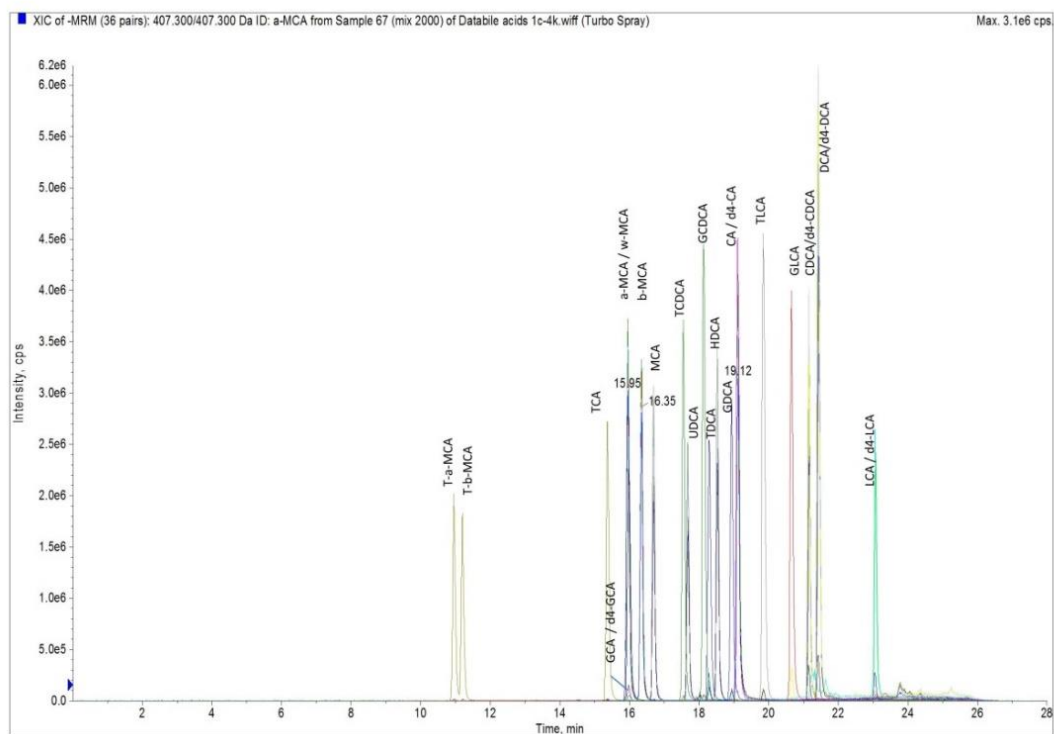
Microbiota analysis at Novogene

Microbial DNA was isolated from approximately 50mg ileal luminal content with the Qiagen DNA mini kit. Additional steps were added to the DNA mini kit protocol to ensure breakage of all bacterial samples. Briefly, the samples were homogenised using silica glass beads for 4x 30 seconds at 6000 rpm in a Precellys®24 (Bertin Technologies, France) and heated to 95°C for 5 minutes. Additionally, samples were incubated with a lysis buffer containing 20mg/ml lysozyme (Lysozyme from chicken egg white, Sigma-Aldrich) after which the homogenising was repeated. The lysozyme was used to help effectively capture usually difficult to lyse taxa, such as gram-positive bacteria. Consequently, DNA was isolated using the Qiagen DNA mini kit following instructions from the manufacturer. DNA quantity was assessed using a Nanodrop 2000 Spectrophotometer (Fisher Scientific, UK).

A minimum of 50ng of DNA was sent to Novogene (Cambridge, UK). Quality assessment was performed by agarose gel electrophoresis to detect DNA integrity, purity, fragment size and concentration. The 16S rRNA amplicon sequencing of the V4 region was performed with an Illumina MiSeq (paired-end 250 bp; San Diego, CA). Paired-end reads was assigned to samples based on their unique barcodes and trimmed by cutting off the barcode and primer sequences. Paired-end reads were merged using FLASH (V1.2.7). Quality filtering on the raw tags were performed using specific filtering conditions to obtain the high-quality clean tags according to the Quantitative Insights into Microbial Ecology (QIIME) (version 1.7.0) quality-controlled process (Caporaso et al., 2011). The tags were compared with the reference database (Gold database) using UCHIME algorithm to detect chimera sequences and then the chimera sequences were removed, and Effective Tags were obtained. Sequences analysis were performed by Uparse software (Uparse v7.0.1001) (Edgar, 2013) using all the effective tags. OTUs were picked with 97% sequence similarity. For each representative sequence, Mothur software was performed against SSUrRNA database of SILVA database. Alpha and beta diversity were calculated by QIIME and displayed with R software (Novogene, Cambridge). Comprehensive statistical and meta-analysis including differential analysis of taxa abundance was completed with the online tool Microbiome Analyst 5.0 (Chong et al., 2020).

Supplementary data 3

Gammaproteobacteria;o__Enterobacteriales;f__Enterobacteriaceae
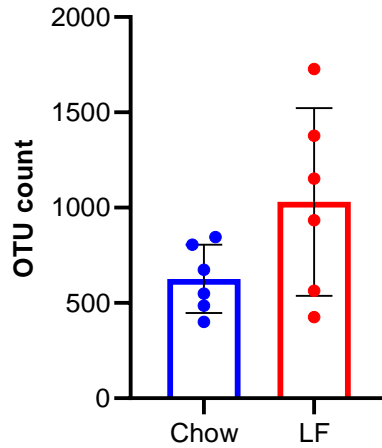
Supplementary figure 3.1 Differences in the abundance of *Enterobacteriaceae* family from the *Gammaproteobacteria* group. Significance was tested by using unpaired T test (***=p<0.001, **= p<0.01, *= p<0.05). LF: Low-fat diet.
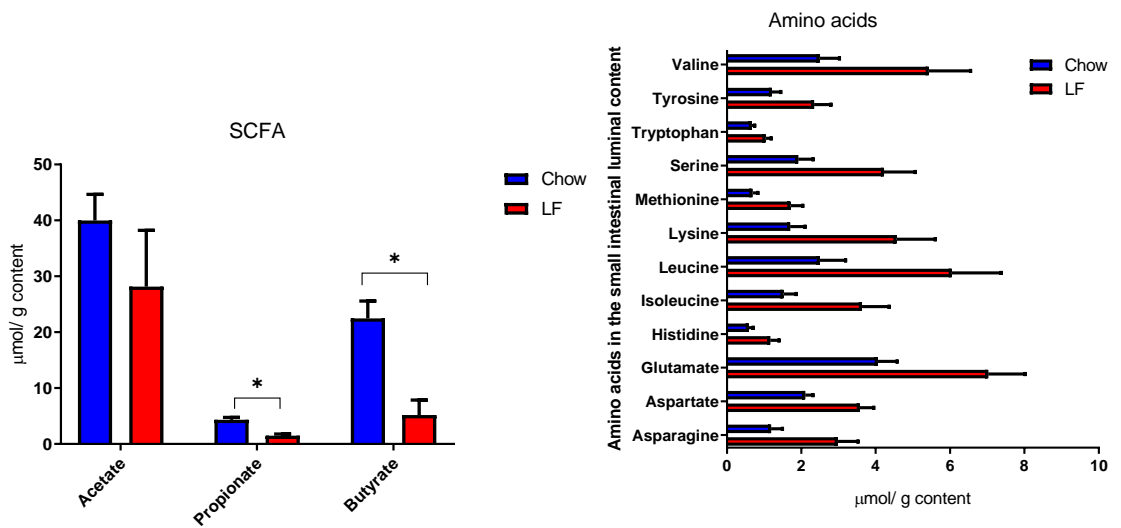
Supplementary figure 3.2 Differential metabolite profiles in the ileal content after 2 weeks feeding with chow and LF diet. Significance was tested by using unpaired T test (***=p<0.001, **= p<0.01, *= p<0.05). LF: Low-fat diet, SCFAs: Short chain fatty acids.

Tlr4
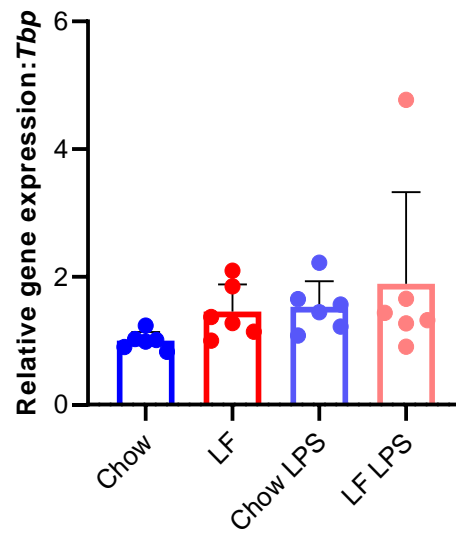
Supplementary figure 3.3 Gene expression of *Tlr4* in response to chow and LF fed mice treated with LPS. LPS: Lipopolysaccharide.
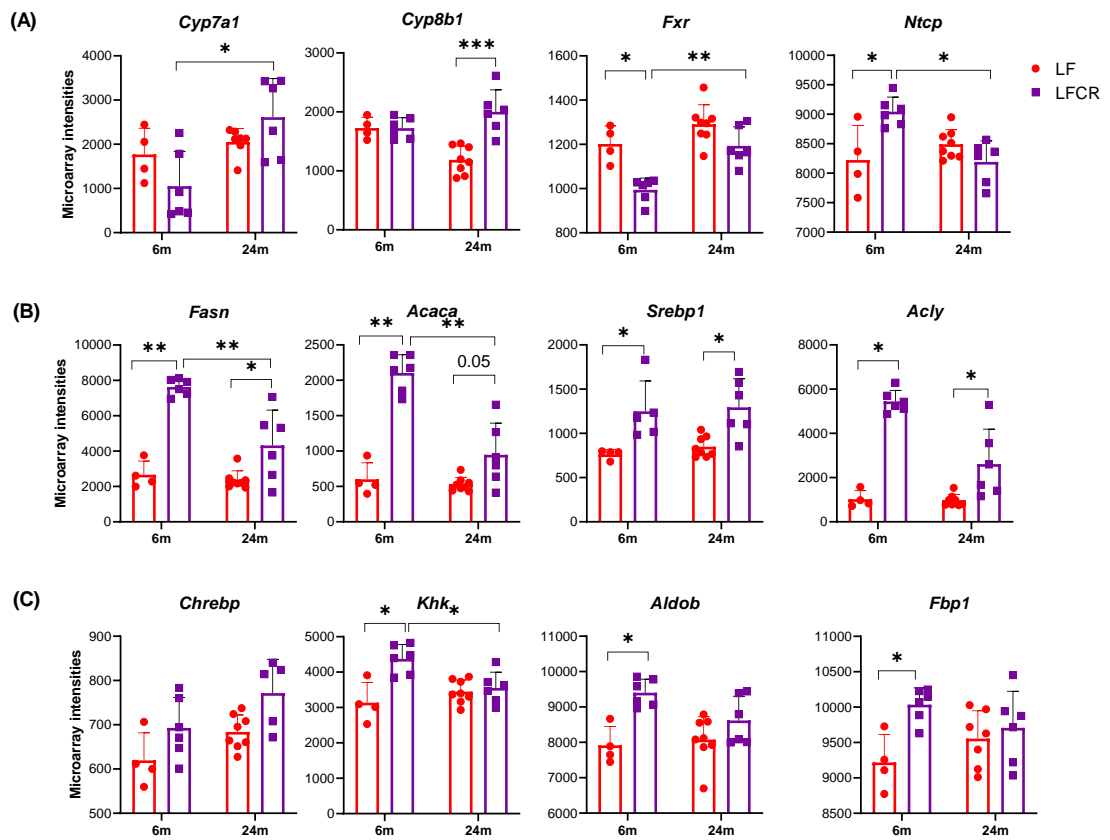
Supplementary figure 3.4 Liver gene expression analysis from adult (6 months) and old mice (24 months) mice exposed to lifelong CR diet. Significance was tested using a 2-way ANOVA with Bonferroni post-hoc test for both diet and time (**= p<0.01, *= p<0.05).

Cyp1a1
Duodenum
4 weeks

(A)

Cyp1a1
Duodenum
10 weeks

(B)
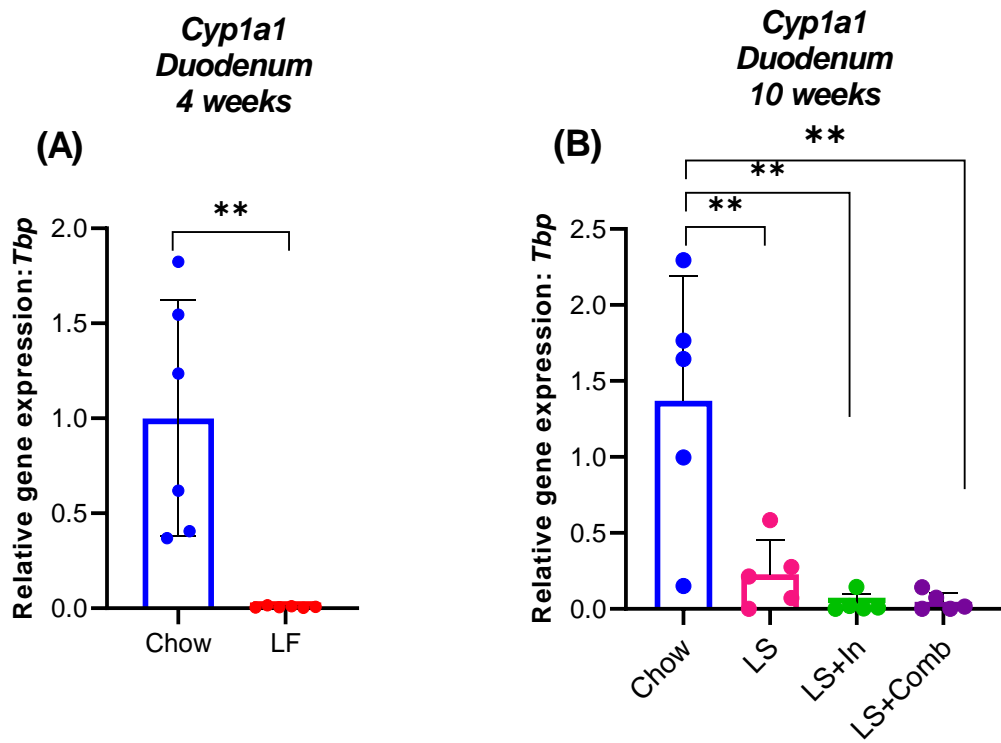
Supplementary figure 3.5 Gene expression of *Cyp1a1* in the duodenum in response to different diets. Significance was tested by using unpaired T test (A) and 1-way ANOVA (B) (***=$p<0.001$, **= $p<0.01$, *= $p<0.05$. LF: Low-fat diet, LS: low sucrose version of the LF diet, LS+In: LS diet enriched with inulin, LS+Comb: LS diet enriched with a combination of inulin, pectin and psyllium.
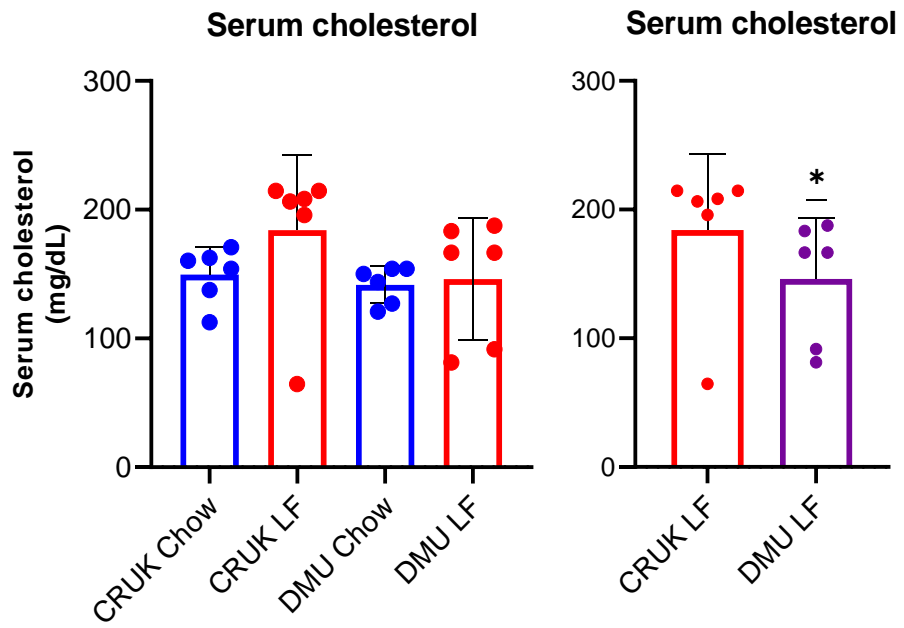
Supplementary figure 3.6 Comparison of serum cholesterol levels in response to the LF diet in mice from different sources; CRUK and DMU. Significance was tested by using 1-way ANOVA and unpaired t test (***=p<0.001, **= p<0.01, *= p<0.05. CRUK: Charles River, UK. DMU: Disease modelling unit at UEA.

Supplementary data 4

		mean diff.	95.00% CI of diff.	P Value
Mptx2	6m:LF vs. 6m:LFCR	41.66	-1154 to 1238	1.00
	6m:LF vs. 24m:LF	1614	322.1 to 2906	0.01
	6m:LFCR vs. 24m:LFCR	336.7	-859.4 to 1533	0.95
	24m:LF vs. 24m:LFCR	-1236	-2527 to 56.21	0.04
Defa-rs1	6m:LF vs. 6m:LFCR	-30.85	-847.0 to 785.3	1.00
	6m:LF vs. 24m:LF	1100	218.8 to 1982	0.01
	6m:LFCR vs. 24m:LFCR	337.7	-478.4 to 1154	0.61
	24m:LF vs. 24m:LFCR	-793.5	-1675 to 88.04	0.04
Defa3	6m:LF vs. 6m:LFCR	307.7	-864.7 to 1480	0.86
	6m:LF vs. 24m:LF	1908	641.9 to 3175	0.00
	6m:LFCR vs. 24m:LFCR	580.9	-591.5 to 1753	0.47
	24m:LF vs. 24m:LFCR	-1020	-2286 to 246.7	0.05
Dmbt1	6m:LF vs. 6m:LFCR	2.475	-426.7 to 431.6	1.00
	6m:LF vs. 24m:LF	465.3	1.746 to 928.9	0.05
	6m:LFCR vs. 24m:LFCR	122.4	-306.8 to 551.6	0.94
	24m:LF vs. 24m:LFCR	-340.4	-804.0 to 123.1	0.05
Cdca3	6m:LF vs. 6m:LFCR	-0.4258	-39.83 to 38.97	1.00
	6m:LF vs. 24m:LF	52.3	9.746 to 94.86	0.02
	6m:LFCR vs. 24m:LFCR	-11.04	-50.44 to 28.36	0.83
	24m:LF vs. 24m:LFCR	-63.77	-106.3 to -21.22	0.00
Cdca8	6m:LF vs. 6m:LFCR	6.973	-13.78 to 27.72	0.75
	6m:LF vs. 24m:LF	30.51	8.101 to 52.92	0.01
	6m:LFCR vs. 24m:LFCR	-0.9638	-21.71 to 19.78	1.00
	24m:LF vs. 24m:LFCR	-24.5	-46.91 to -2.092	0.03
Cenpe	6m:LF vs. 6m:LFCR	10.46	-21.21 to 42.13	0.76
	6m:LF vs. 24m:LF	28.05	-6.162 to 62.25	0.05
	6m:LFCR vs. 24m:LFCR	-11.97	-43.64 to 19.70	0.68
	24m:LF vs. 24m:LFCR	-29.56	-63.77 to 4.649	0.05
Prr1	6m:LF vs. 6m:LFCR	-2.566	-24.87 to 19.74	0.99

	6m:LF vs. 24m:LF	23.7	-0.3931 to 47.79	0.04
	6m:LFCR vs. 24m:LFCR	0.6571	-21.65 to 22.96	1.00
	24m:LF vs. 24m:LFCR	-25.61	-49.70 to -1.516	0.04
Acsl3	6m:LF vs. 6m:LFCR	-176.2	-375.8 to 23.30	0.05
	6m:LF vs. 24m:LF	-0.8748	-216.4 to 214.6	1.00
	6m:LFCR vs. 24m:LFCR	-23.32	-222.9 to 176.2	0.98
	24m:LF vs. 24m:LFCR	-198.7	-414.2 to 16.84	0.05
Scd2	6m:LF vs. 6m:LFCR	-951.6	-1810 to -93.23	0.03
	6m:LF vs. 24m:LF	262.2	-664.9 to 1189	0.95
	6m:LFCR vs. 24m:LFCR	632.9	-225.4 to 1491	0.21
	24m:LF vs. 24m:LFCR	-580.9	-1508 to 346.2	0.16
Lpcat4	6m:LF vs. 6m:LFCR	-251.1	-404.0 to -98.26	0.00
	6m:LF vs. 24m:LF	142.4	-22.67 to 307.5	0.06
	6m:LFCR vs. 24m:LFCR	273.6	120.7 to 426.4	0.00
	24m:LF vs. 24m:LFCR	-120	-285.1 to 45.15	0.06
Elovl6	6m:LF vs. 6m:LFCR	-321.8	-810.3 to 166.6	0.05
	6m:LF vs. 24m:LF	-78.98	-606.6 to 448.6	0.97
	6m:LFCR vs. 24m:LFCR	26.56	-461.9 to 515.0	1.00
	24m:LF vs. 24m:LFCR	-216.3	-743.9 to 311.3	0.62
Chrebp	6m:LF vs. 6m:LFCR	61.02	-180.8 to 302.8	0.87
	6m:LF vs. 24m:LF	-144.3	-405.5 to 116.9	0.39
	6m:LFCR vs. 24m:LFCR	-253.7	-495.5 to -11.84	0.04
	24m:LF vs. 24m:LFCR	-48.33	-309.5 to 212.9	0.94
Mgam	6m:LF vs. 6m:LFCR	-182.5	-1158 to 792.9	0.94
	6m:LF vs. 24m:LF	286.6	-688.8 to 1262	0.82
	6m:LFCR vs. 24m:LFCR	-199.5	-1175 to 775.9	0.93
	24m:LF vs. 24m:LFCR	-668.6	-1644 to 306.8	0.23
Sis	6m:LF vs. 6m:LFCR	-312.8	-969.1 to 343.5	0.51
	6m:LF vs. 24m:LF	212.4	-496.5 to 921.3	0.80
	6m:LFCR vs. 24m:LFCR	-214.4	-870.8 to 441.9	0.76
	24m:LF vs. 24m:LFCR	-739.6	-1449 to -30.73	0.04
Khk	6m:LF vs. 6m:LFCR	11.63	-373.9 to 397.2	1.00
	6m:LF vs. 24m:LF	-413.2	-829.6 to 3.282	0.05
	6m:LFCR vs. 24m:LFCR	-515.9	-901.5 to -130.4	0.01
	24m:LF vs. 24m:LFCR	-91.13	-507.6 to 325.3	0.91

Fbp1	6m:LF vs. 6m:LFCR	-8.73	-89.66 to 72.20	0.99
	6m:LF vs. 24m:LF	-56.57	-144.0 to 30.85	0.26
	6m:LFCR vs. 24m:LFCR	-86.26	-167.2 to -5.331	0.04
	24m:LF vs. 24m:LFCR	-38.43	-125.8 to 48.99	0.57
Sglt1	6m:LF vs. 6m:LFCR	-126.9	-1099 to 844.7	0.98
	6m:LF vs. 24m:LF	-562.5	-1612 to 487.0	0.41
	6m:LFCR vs. 24m:LFCR	-918.1	-1890 to 53.52	0.05
	24m:LF vs. 24m:LFCR	-482.5	-1532 to 566.9	0.53
Glut2	6m:LF vs. 6m:LFCR	-183.9	-1111 to 743.5	0.93
	6m:LF vs. 24m:LF	-860.7	-1862 to 141.0	0.10
	6m:LFCR vs. 24m:LFCR	-1060	-1988 to -132.9	0.02
	24m:LF vs. 24m:LFCR	-383.5	-1385 to 618.2	0.67
Glut5	6m:LF vs. 6m:LFCR	333.7	-184.6 to 852.0	0.27
	6m:LF vs. 24m:LF	92.19	-426.1 to 610.5	0.95
	6m:LFCR vs. 24m:LFCR	-497.5	-1016 to 20.81	0.04
	24m:LF vs. 24m:LFCR	-256	-774.3 to 262.3	0.49
Fgf15	6m:LF vs. 6m:LFCR	-149.6	-473.8 to 174.7	0.53
	6m:LF vs. 24m:LF	-118.7	-468.9 to 231.5	0.74
	6m:LFCR vs. 24m:LFCR	217.6	-106.7 to 541.8	0.24
	24m:LF vs. 24m:LFCR	186.7	-163.5 to 536.9	0.12
Fxr	6m:LF vs. 6m:LFCR	73.58	-295.1 to 442.3	0.93
	6m:LF vs. 24m:LF	267.2	-131.0 to 665.5	0.24
	6m:LFCR vs. 24m:LFCR	193.6	-175.1 to 562.3	0.43
	24m:LF vs. 24m:LFCR	-0.02196	-398.3 to 398.2	1.00
Asbt	6m:LF vs. 6m:LFCR	-400.1	-1282 to 481.5	0.54
	6m:LF vs. 24m:LF	552	-400.3 to 1504	0.35
	6m:LFCR vs. 24m:LFCR	1116	234.2 to 1997	0.01
	24m:LF vs. 24m:LFCR	163.7	-788.5 to 1116	0.95
Osta	6m:LF vs. 6m:LFCR	-47.55	-703.8 to 608.8	1.00
	6m:LF vs. 24m:LF	656.5	-52.38 to 1365	0.05
	6m:LFCR vs. 24m:LFCR	615.4	-40.91 to 1272	0.06
	24m:LF vs. 24m:LFCR	-88.67	-797.6 to 620.2	0.98

Supplement 4.2 Ileal expression profiles of immune and carbohydrate related genes in mice fed with chow, LS, LS+In and LS+Comb. Significance was tested using a 1-way ANOVA with Tukey's multiple comparison test. LS+In: LS diet enriched with inulin, LS+Comb: LS diet enriched with a combination of fibres. LS: Low sucrose version of the LF diet.

		Mean Diff.	95.00% CI of diff.	P Value
Oas1g				
	Chow vs. LS	13.9	2.825 to 24.91	0.01
	Chow vs. LS+In	9.7	-1.322 to 20.77	0.09
	Chow vs. LS+Combination	-1.0	-12.07 to 10.02	0.99
	LS vs. LS+In	-4.1	-15.19 to 6.896	0.71
	LS vs. LS+Combination	-14.9	-25.94 to -3.850	0.01
	LS+In vs. LS+Combination	-10.8	-21.79 to 0.2978	0.06
Oas3				
	Chow vs. LS	26.6	6.019 to 47.16	0.01
	Chow vs. LS+In	22.1	1.496 to 42.64	0.03
	Chow vs. LS+Combination	10.8	-9.731 to 31.41	0.46
	LS vs. LS+In	-4.5	-25.10 to 16.05	0.92
	LS vs. LS+Combination	-15.8	-36.32 to 4.822	0.17
	LS+In vs. LS+Combination	-11.2	-31.80 to 9.346	0.43
Oasl2				
	Chow vs. LS	75.6	-14.79 to 166.0	0.12
	Chow vs. LS+In	66.2	-24.23 to 156.5	0.20
	Chow vs. LS+Combination	0.8	-89.59 to 91.18	1.00
	LS vs. LS+In	-9.4	-99.82 to 80.94	0.99
	LS vs. LS+Combination	-74.8	-165.2 to 15.58	0.04
	LS+In vs. LS+Combination	-65.4	-155.7 to 25.02	0.21
H2-aa				
	Chow vs. LS	866.3	-95.74 to 1828	0.09
	Chow vs. LS+In	456.4	-505.6 to 1418	0.54
	Chow vs. LS+Combination	-254.6	-1217 to 707.4	0.87
	LS vs. LS+In	-409.8	-1372 to 552.2	0.62
	LS vs. LS+Combination	-1121.0	-2083 to -158.9	0.02
	LS+In vs. LS+Combination	-711.1	-1673 to 250.9	0.19
H2-ab1				
	Chow vs. LS	806.7	-132.5 to 1746	0.11
	Chow vs. LS+In	406.7	-532.5 to 1346	0.61
	Chow vs. LS+Combination	-303.1	-1242 to 636.2	0.79
	LS vs. LS+In	-400.0	-1339 to 539.3	0.62
	LS vs. LS+Combination	-1110.0	-2049 to -170.5	0.02
	LS+In vs. LS+Combination	-709.8	-1649 to 229.4	0.18

H2-dmb1				
	Chow vs. LS	45.8	-26.03 to 117.5	0.30
	Chow vs. LS+In	7.8	-63.94 to 79.62	0.99
	Chow vs. LS+Combination	-39.8	-111.6 to 31.97	0.41
	LS vs. LS+In	-37.9	-109.7 to 33.88	0.45
	LS vs. LS+Combination	-85.6	-157.3 to -13.78	0.02
	LS+In vs. LS+Combination	-47.7	-119.4 to 24.13	0.27
Ifit				
	Chow vs. LS	18.0	-2.943 to 38.88	0.11
	Chow vs. LS+In	14.5	-6.460 to 35.36	0.24
	Chow vs. LS+Combination	-3.2	-24.08 to 17.75	0.97
	LS vs. LS+In	-3.5	-24.43 to 17.39	0.96
	LS vs. LS+Combination	-21.1	-42.04 to -0.2224	0.05
	LS+In vs. LS+Combination	-17.6	-38.53 to 3.294	0.12
Ubd				
	Chow vs. LS	88.6	-51.11 to 228.3	0.30
	Chow vs. LS+In	88.6	-51.11 to 228.3	0.30
	Chow vs. LS+Combination	-61.6	-201.3 to 78.10	0.60
	LS vs. LS+In	0.0	-139.7 to 139.7	1.00
	LS vs. LS+Combination	-150.2	-290.0 to -10.51	0.03
	LS+In vs. LS+Combination	-150.2	-290.0 to -10.51	0.03
Tap1				
	Chow vs. LS	27.2	-13.04 to 67.52	0.25
	Chow vs. LS+In	22.2	-18.04 to 62.52	0.42
	Chow vs. LS+Combination	-14.9	-55.18 to 25.38	0.72
	LS vs. LS+In	-5.0	-45.29 to 35.28	0.98
	LS vs. LS+Combination	-42.1	-82.42 to -1.862	0.04
	LS+In vs. LS+Combination	-37.1	-77.42 to 3.143	0.08
Gzmb				
	Chow vs. LS	20.5	0.9119 to 40.04	0.04
	Chow vs. LS+In	17.4	-2.158 to 36.97	0.09
	Chow vs. LS+Combination	6.2	-13.38 to 25.75	0.80
	LS vs. LS+In	-3.1	-22.64 to 16.50	0.97
	LS vs. LS+Combination	-14.3	-33.86 to 5.275	0.20
	LS+In vs. LS+Combination	-11.2	-30.79 to 8.345	0.39
Zbp1				
	Chow vs. LS	28.1	-11.46 to 67.74	0.22
	Chow vs. LS+In	24.8	-14.82 to 64.39	0.31

	Chow vs. LS+Combination	-13.9	-53.46 to 25.74	0.75
	LS vs. LS+In	-3.4	-42.96 to 36.25	0.99
	LS vs. LS+Combination	-42.0	-81.60 to -2.396	0.04
	LS+In vs. LS+Combination	-38.6	-78.25 to 0.9606	0.06
Mgam				
	Chow vs. LS	-520.4	-765.8 to -275.0	0.0001
	Chow vs. LS+In	-1188.0	-1433 to -942.6	0.0001
	Chow vs. LS+Combination	-1197.0	-1442 to -951.4	0.0001
	LS vs. LS+In	-667.5	-912.9 to -422.2	0.0001
	LS vs. LS+Combination	-676.3	-921.7 to -431.0	0.0001
	LS+In vs. LS+Combination	-8.8	-254.2 to 236.6	1.00
Sis				
	Chow vs. LS	-412.4	-836.6 to 11.83	0.05
	Chow vs. LS+In	-1089.0	-1513 to -664.3	0.0001
	Chow vs. LS+Combination	-1103.0	-1528 to -679.3	0.0001
	LS vs. LS+In	-676.2	-1100 to -252.0	0.002
	LS vs. LS+Combination	-691.1	-1115 to -266.9	0.001
	LS+In vs. LS+Combination	-14.9	-439.1 to 409.3	1.00
Khk				
	Chow vs. LS	-216.5	-365.0 to -67.97	0.004
	Chow vs. LS+In	-185.6	-334.1 to -37.10	0.01
	Chow vs. LS+Combination	-102.9	-251.4 to 45.57	0.24
	LS vs. LS+In	30.9	-117.6 to 179.4	0.93
	LS vs. LS+Combination	113.5	-34.95 to 262.0	0.17
	LS+In vs. LS+Combination	82.7	-65.82 to 231.2	0.41
Aldob				
	Chow vs. LS	-232.5	-1020 to 555.6	0.83
	Chow vs. LS+In	-828.5	-1617 to -40.44	0.04
	Chow vs. LS+Combination	-1050.0	-1838 to -262.0	0.01
	LS vs. LS+In	-596.0	-1384 to 192.0	0.18
	LS vs. LS+Combination	-817.6	-1606 to -29.55	0.04
	LS+In vs. LS+Combination	-221.6	-1010 to 566.5	0.85
Fbp1				
	Chow vs. LS	-14.8	-41.93 to 12.43	0.43
	Chow vs. LS+In	-41.9	-69.09 to -14.74	0.002
	Chow vs. LS+Combination	-36.7	-63.86 to -9.501	0.007
	LS vs. LS+In	-27.2	-54.34 to 0.01358	0.05
	LS vs. LS+Combination	-21.9	-49.11 to 5.249	0.14
	LS+In vs. LS+Combination	5.2	-21.94 to 32.41	0.94

Sglt1				
	Chow vs. LS	-601.9	-876.8 to -327.0	0.0001
	Chow vs. LS+In	-542.8	-817.7 to -267.9	0.0002
	Chow vs. LS+Combination	-226.5	-501.4 to 48.38	0.13
	LS vs. LS+In	59.14	-215.8 to 334.0	0.93
	LS vs. LS+Combination	375.4	100.5 to 650.3	0.0062
	LS+In vs. LS+Combination	316.3	41.35 to 591.2	0.02
Glut2				
	Chow vs. LS	-64.0	-114.0 to -13.96	0.010
	Chow vs. LS+In	-75.1	-125.1 to -25.08	0.003
	Chow vs. LS+Combination	-34.5	-84.49 to 15.55	0.24
	LS vs. LS+In	-11.1	-61.14 to 38.91	0.92
	LS vs. LS+Combination	29.5	-20.51 to 79.53	0.36
	LS+In vs. LS+Combination	40.6	-9.396 to 90.65	0.13
Fgf15				
	Chow vs. LS	-52.6	-74.77 to -30.39	0.0001
	Chow vs. LS+In	9.2	-13.02 to 31.36	0.65
	Chow vs. LS+Combination	10.6	-11.55 to 32.83	0.53
	LS vs. LS+In	61.8	39.56 to 83.94	0.0001
	LS vs. LS+Combination	63.2	41.04 to 85.42	0.0001
	LS+In vs. LS+Combination	1.5	-20.71 to 23.67	1.00

The End